UNIVERSITY OF SOUTHERN QUEENSLAND

Modelling Dispersion in Turbulent Boundary Layers Using Centre Manifold Technique

A dissertation submitted by

Fadhel Jasim Mohammed

B. Sc., University of Thi Qar, Iraq, 2001

M. Sc., Al-Mustansiriya University, Iraq, 2005

For the award of the degree of

Doctor of Philosophy

2014

Dedication

To my family

Certification of Dissertation

I certify that the ideas, experimental work, results, analysis and conclusions reported in this dissertation are entirely my own effort, except where otherwise acknowledged. I also certify that the work is original and has not been previously submitted for any other award.

Fadhel Jasim Mohammed, Candidate	Date

ENDORSEMENT

A/Prof. Dmitry V. Strunin, Principal supervisor	Date
Prof. Thanh Tran-Cong, Co-supervisor	Date

Acknowledgments

The research reported in this dissertation was carried out at the School of Agricultural, Faculty of Health, Engineering and Sciences, and the Computational Engineering and Science Research Centre (CESRC), USQ.

Firstly, I would like to thank my principal supervisor A/Prof. Dmitry Strunin for his invaluable guidance and useful suggestions. This dissertation would not have been completed without his continuous support.

I would like to thank my co-supervisor Prof. Thanh Tran-Cong for his instructive discussions during my PhD study.

I would like to thank Dr Duc Ngo-Cong for his cooperation with me especially regarding the experimental work.

Finally, I would like to thank the Iraqi government for giving me the opportunity to complete the PhD Study.

Abstract

The present research is concerned with modelling dispersion of contaminants and substances in turbulent boundary layers based on centre manifold approach. The results of this dissertation are as follows. (i) We derived accurate transport equations involving high-order spatial derivatives to describe the averaged turbulent transport of tracers and contaminants along turbulent channel flows. The central point of the model is the advection-diffusion equation supplemented by no-flux boundary conditions on the bottom and the surface. In all realisations of the flow analysed in this work, the layer has a universal velocity structure and well-defined turbulent diffusion coefficient. The turbulence is assumed well developed, which provides the mechanism of fast cross-flow mixing and thereby justifies the use of the centre manifold method (Mercer and Roberts, 1990). Using the originally two-dimensional transport equations, we derived the one-dimensional model in which the advection, diffusion, dispersion and higher-order coefficients are calculated in terms of the parameters controlling the flow. (ii) We formulated an analytical framework of the averaged transport of contaminants in turbulent boundary layers over smooth and rough substrates; (iii) An advection-diffusion equation is derived for the flow through urban canopies simulated by cubic arrays. (iv) We justified the centre manifold approach by the direct comparison of the numerical solutions of the averaged (1-D) and original (2-D) models using the one-dimensional integrated radial basis network (1D-IRBFN) method.

In the 1D-IRBFN method a Cartesian grid is used to discretise the spatial domain. The method uses the integration instead of conventional differentiation, which provides an effective way to implement derivative boundary conditions. The numerical solutions of the derived 1-D equations obtained by the centre manifolds are in a good agreement with those of the original 2-D advection-diffusion equation. In particular, the models yield practically the same value of the velocity of the point of maximum depth-averaged concentration along the channel.

We also compared the 1D-IRBFN solutions for the 1-D model with the solutions of the original 2-D model by successively adding higher-order derivatives into consideration such as the advection, diffusion and dispersion. A good convergence was observed. The numerical results confirm that the effect of longitudinal diffusion is negligible. We note that our work can be viewed not only as the confirmation of the centre manifold approach by the 1D-IRBFN method but also as a confirmation of the numerical method by the centre manifold theory.

In our analysis we considered two types of the velocity profile across the channel: the classical logarithmic profile and, according to an alternative and more recent

model, power profile. The power profile is based on a different similarity hypothesis (Barenblatt, 2000) compared to the classical logarithmic theory. Arguably the power law better fits experimental measurements of the velocity distribution over the self-similar intermediate region adjacent to the viscous sublayer for a wide variety of boundary layer flows. We separately investigated the dispersion for both the logarithmic and power profile.

Further, we derived even higher-order partial differential equations governing the longitudinal dispersion. From numerical viewpoint, including higher-order spatial derivatives increases the accuracy of the averaged model derived by the centre manifold approach, especially for very large Reynolds numbers.

We also constructed an averaged model of shear dispersion in the turbulent flow above a canopy. The model contains as independent parameters the friction velocity, total thickness of the flow, height of the canopy and frontal area density of the canopy. The model is reduced by the centre manifold procedure to a universal one-dimensional model written in terms of the depth-average concentration of the tracer. The advection and diffusion coefficients, governing the transfer in the averaged model, are found in terms of the independent parameters. The used approach required lengthy derivations and produced quite cumbersome expressions.

However, we emphasize the following important aspect of all the derived one-dimensional centre manifold models: they reveal a hidden property of the transport process, namely the asymptotic one-dimensional law for the averaged concentration. This is a remarkable feature of the originally two-dimensional formulation. Whether such a law exists and what form it might have is not obvious beforehand. At the same time, from practical viewpoint, our results can be used to calculate the distance travelled by the contaminant spill, and the size of the spill; of course those can only serve as a tool for rough estimates.

Papers Resulting from the Research

1. Strunin, D. V. and Mohammed, F. J. (2012). Numerical Analysis of an Averaged Model of Turbulent Transport near a Roughness Layer, *Journal of Australian and New Zealand Industrial and Applied Mathematics*, **53**: C142-C154.

2. Mohammed, F. J., Ngo-Cong, D., Strunin, D. V., Mai-Duy, N. and Tran-Cong, T. (2014). Modelling Dispersion in Laminar and Turbulent Flows in an Open Channel Based on Centre Manifolds Using 1D-IRBFN Method, *Journal of Applied Mathematical Modelling* **38**: 3672-3691.

3. Mohammed, F. J., Strunin, D. V., Ngo-Cong, D. and Tran-Cong, T. (2014). Asymptotics of Averaged Turbulent Transfer in Canopy Flows, Journal of Engineering Mathematics, accepted.

4. Ngo-Cong, D., Mohammed, F. J., Strunin, D. V., Tran-Cong, T. and Mai-Duy, N. (2013). Higher-Order Transport Equations for Turbulent Channel Flows, *Journal of Australian and New Zealand Industrial and Applied Mathematics*, to appear.

Contents

Acronyms & Abbreviations

1D-IRBFN	One-dimensional Indirect/Integrated Radial Basis Function Network
FDM	Finite Different Method
1-D	One-Dimensional
2-D	Two-Dimensional
DRBFN	Direct Radial Basis Function Network
IRBFN	Indirect/Integrated Radial Basis Function Network
MQ	Multiquadric
PDE	Partial Differential Equation
RBF	Radial Basis Function
RBFN	Radial Basis Function Network
RHS	Right Hand Side

List of Tables

List of Figures

Chapter 1

Literature review and motivation

This chapter starts with the literature review of the present study in which we briefly review the dispersion of contaminants in turbulent flows. Then, we review the previous work on the use of the centre manifold approach in the studies of the transport processes in an open channel. We continue with the dispersion of the flow in the urban canopy layer with cube obstacles, followed by the review of the radial basis function networks. Then, we present the motivation for and description of work proposed in the dissertation. Finally, the outline of the dissertation is described.

1.1 Literature review

In the 1950s Taylor proposed the advection-diffusion equation describing the dynamics of the cross-sectional average concentration along a pipe. The equation is valid at large times when spatial variations of the concentration along the pipe become slow. He described the spread of a solute in laminar flow through the pipe under the assumption that the velocity profile across the pipe is primarily responsible for the spreading in the direction of the flow. In 1954, Taylor extended his analysis to turbulent flows. Before the Taylor's work, we present some general concepts of the flow following the book of Fischer et al. (1979).

1.1.1 General description of dispersion in laminar shear flow

We want to derive an equation for longitudinal dispersion following Taylor's analysis and apply it to longitudinal dispersion in an open channel. For this we assume a laminar open channel flow with no-flux boundary conditions, that is, $\partial C/\partial y{=}0$ at the top and bottom of the channel. Let $U(y)$ represents the flow velocity in the direction of x-axis decomposed by $U(y) = u + u'(y)$, where u is the depth aver-

age velocity (constant over the depth) defined by $u = (1/h)\int_0^h U(y)\,dy$ and $u'(y)$ the deviation of the velocity (variable over the depth). The advection-diffusion equation is given by

$$\frac{\partial}{\partial t}(C - c') + (u - u')\frac{\partial}{\partial x}(C - c') = D\left[\frac{\partial^2}{\partial x^2}(C - c') + \frac{\partial^2 c'}{\partial y^2}\right], \tag{1.1}$$

where $c(x, y, t)$ is the contaminant concentration, the average concentration $C = (1/h)\int_0^h c(x, y, t)\,dy$ and the deviation from the average $c(y) = C + c'(y)$. The diffusion coefficient D is assumed to be constant (Fischer et al., 1979).

Let $\xi = x - ut$, $\tau = t$ represents a transformation to a coordinate system whose origin moves at the mean flow velocity. Using the chain rule, the differential operators become

$$\begin{aligned}
\frac{\partial}{\partial x} &= \frac{\partial \xi}{\partial x}\frac{\partial}{\partial \xi} + \frac{\partial \tau}{\partial x}\frac{\partial}{\partial \tau} \\
&= \frac{\partial}{\partial \xi} \\
\frac{\partial}{\partial t} &= \frac{\partial \xi}{\partial t}\frac{\partial}{\partial \xi} + \frac{\partial \tau}{\partial t}\frac{\partial}{\partial \tau} \\
&= -u\frac{\partial}{\partial \xi} + \frac{\partial}{\partial \tau}\,.
\end{aligned}$$

As a result of substituting this transformation, Eq. (1.1) becomes

$$\frac{\partial}{\partial \tau}(C - c') + u'\frac{\partial}{\partial \xi}(C - c') = D\left[\frac{\partial^2}{\partial \xi^2}(C - c') + \frac{\partial^2 c'}{\partial y^2}\right]. \tag{1.2}$$

Since the spreading along the flow direction is assumed to be largely due to the change of the velocity in vertical direction (shear), we neglect the longitudinal diffusion term in Eq. (1.2)

$$\frac{\partial C}{\partial \tau} + \frac{\partial c'}{\partial \tau} + u'\frac{\partial C}{\partial \xi} + u'\frac{\partial c'}{\partial \xi} = D\frac{\partial^2 c'}{\partial y^2}\,. \tag{1.3}$$

A general solution for Eq. (1.3) is not available. Taylor assumed that there exists a balance between the dominant factors, advection and diffusion, so that

$$u'\frac{\partial C}{\partial \xi} = D\frac{\partial^2 c'}{\partial y^2}\,, \tag{1.4}$$

with $\partial c'/\partial y = 0$ at $y = 0,\ h$. This balance can be explained as follows: when

the contaminant is introduced into the fluid flow with a cross-sectional average velocity u along the x-axis, it is advected and distorted by the velocity shear and, at the same time, the diffusion acts to smear out the contaminant cloud to uniform state. After longer time, the contaminant cloud extends over a long distance in the direction of x-axis. As a result of this combined action of the advection and diffusion, the concentration variation becomes slow in x-direction. At this stage, according to Taylor, the balance between the longitudinal advective transport and cross-sectional diffusive transport would be reached. Mathematically, this balance is represented by Eq. (1.4).

The discussion above illustrates that the longitudinal dispersion is due to the gradients of concentration and velocity in the vertical. This means that we remove the non-deviating terms from Eq. (1.3), including the term $\partial C/\partial\tau$ which is the quantity we want to find (Fischer et al., 1979). Taking the depth average ($\frac{1}{h}\int_0^h dy$) will transfer Eq. (1.3) into

$$\frac{\partial C}{\partial \tau} + \overline{u'\frac{\partial c'}{\partial \xi}} = 0\,, \tag{1.5}$$

where $\partial C/\partial\tau = -[\partial c'/\partial\tau + u'(\partial c'/\partial\xi)]$ and the overbar denoting a cross-sectional average. In this result, even if c' is zero, the cross-term $u'\partial c'/\partial\xi$, which become our diffusion term, may not be zero. Subtracting Eq. (1.5) from Eq. (1.4) gives

$$\frac{\partial c'}{\partial \tau} + u'\frac{\partial C}{\partial \xi} + u'\frac{\partial c'}{\partial \xi} - \overline{u'\frac{\partial c'}{\partial \xi}} = D\frac{\partial^2 c'}{\partial y^2}\,, \tag{1.6}$$

which is a governing equation for the concentration deviations c'. If this equation is solvable for c', then we can substitute the solution into (1.5) to obtain the required equation for C. Assume that the concentration is well mixed across the flow and varies slowly, then

$$u'\frac{\partial C}{\partial \xi} \approx -\overline{u'\frac{\partial c'}{\partial \xi}}\,.$$

Now one can neglect the two terms on the left-hand-side of Eq. (1.6), as a result we have

$$\frac{\partial c'}{\partial \tau} + u'\frac{\partial C}{\partial \xi} = D\frac{\partial^2 c'}{\partial y^2}\,. \tag{1.7}$$

Since the average of u' is zero, then the effect of the source term $u'(\partial C/\partial\xi)$ is also zero. The cross-term $D\partial^2 c'/\partial y^2$ represents mass transport due to the fluctuating velocities, while the transport term $u'\partial C/\partial\xi$ represents the action of the shear velocity profile. If the source remains constant for a long time, then the solution to the reduced equation (1.7) is the steady-state solution obtained by solving

Eq. (1.4). This justifies Taylor's discard of the first three terms in Eq. (1.3).

Downstream and after a long time has been elapsed of the dispersion process, the vertical concentration fluctuations will reach a quasi-equilibrium which represents the case of a constant dispersion coefficient. At this steady state (1.7) reduces into

$$u'\frac{\partial C}{\partial \xi} = D\frac{\partial^2 c'}{\partial y^2}\,. \tag{1.8}$$

Solving (1.8) for c' gives

$$c'(y) = \frac{1}{D}\frac{\partial C}{\partial x}\int_0^y \int_0^y u'\,dy\,dy + c'(0)\,. \tag{1.9}$$

In the moving coordinate system, the advection mass flux is

$$\mathbf{M} = u'(C + c')\,. \tag{1.10}$$

Applying the depth average, we obtain the total mass flux

$$\begin{aligned}\mathbf{M} &= \frac{1}{h}\int_0^h u'(C + c')dy \\ &= \frac{1}{h}\int_0^h u'c'dy \\ &= \overline{u'c'}\,.\end{aligned}$$

Note that the depth average of $u'C$ is zero. Substituting the solution for c' from (1.9), the mass transport in the x-direction (using the moving coordinate axis) is given by

$$\mathbf{M}(\tau) = \frac{1}{hD}\int_0^h u'\int_0^y \frac{\partial C}{\partial x}\int_0^y u'\,dy\,dy\,dy\,, \tag{1.11}$$

where $\mathbf{M}(\tau)$ represents the rate of input of mass at time τ and may vary with time (mass units per unit time). The term $\int_0^h u'c'(0)\,dy = 0$ as $\int_0^h u'\,dy = 0$. Since $\partial C/\partial x$ is independent of y, then the depth average mass flux becomes

$$\mathbf{M}(\tau) = -D_L\frac{\partial C}{\partial x}\,, \tag{1.12}$$

where

$$D_L = -\frac{1}{hD}\int_0^h u' \int_0^y \int_0^y u'\, dy\, dy\, dy\,.$$

This is a Fick's law-type mass flux relationship. The expression for D_L above represents an analytical solution for the longitudinal dispersion coefficient, the coefficient is only a function of the depth and the velocity profile. In the moving coordinates system, the one-dimensional diffusion equation (1.5) for the cross-sectional averages becomes

$$\frac{\partial C}{\partial \tau} = D_L \frac{\partial^2 C}{\partial \xi^2}\,. \tag{1.13}$$

In the fixed coordinate system, the corresponding one-dimensional advection dispersion equation to (1.13) is given by

$$\frac{\partial C}{\partial t} + u\frac{\partial C}{\partial x} = D_L \frac{\partial^2 C}{\partial x^2}\,. \tag{1.14}$$

Following the steps (1.1)–(1.13), Taylor (1953) analysed the dispersion of a solute in laminar flow through a pipe. He assumed that the solute has been for long enough time in the pipe so that the concentration is well distributed over the cross section. The velocity profile is

$$u(r) = u_0\left(1 - \frac{r^2}{a^2}\right)\,, \tag{1.15}$$

where a is the radius of the pipe and u_0 the maximum velocity at the centre of the pipe.

In cylindrical coordinates, the advection-diffusion equation governing the mean concentration becomes

$$\frac{\partial C}{\partial t} + u_0\left(1 - \frac{r^2}{a^2}\right)\frac{\partial C}{\partial x} = D\left(\frac{\partial^2 C}{\partial r^2} + \frac{1}{r}\frac{\partial C}{\partial r} + \frac{\partial^2 C}{\partial x}\right)\,. \tag{1.16}$$

Transforming to a coordinate system moving with the mean flow velocity $u_0/2$, neglecting $\partial^2 C/\partial x^2$ and $\partial C/\partial t$ as before and setting $z = r/a$, the deviation in

the concentration C can therefore be calculated from the equation

$$\frac{\partial^2 C}{\partial z^2} + \frac{1}{z}\frac{\partial C}{\partial z} = \frac{a^2 u_0}{D}\left(\frac{1}{2} - z^2\right)\frac{\partial C}{\partial x}\,. \tag{1.17}$$

Solving Eq. (1.17) using the boundary condition $\partial C/\partial z = 0$ at $z = 1$ gives

$$C = A\left(z^2 - \frac{1}{2}z^2\right) + C\,(0)\ , \tag{1.18}$$

where A is a constant (in the moving coordinates, x is stationary) calculated by substituting Eq. (1.18) into Eq. (1.17),

$$A = \frac{a^2 u_0}{8D}\frac{\partial C}{\partial x}.$$

The mass transport of C across the section at x is

$$\mathbf{M} = -2\pi a^2 \int_0^1 u_0\left(\frac{1}{2} - z^2\right) C z\, dz \tag{1.19}$$

and the longitudinal dispersion coefficient is $D_L = a^2 u_0^2/192D$.

The work of Taylor has been followed by extensive research on dispersion: Aris (1956) used "concentration moment" method and built a new basis for Taylor's analysis by ignoring restrictions on the concentration distribution. He also argued that the longitudinal dispersion by molecular diffusion is directly linked to the variations in the velocity profile. The Taylor's or Aris's analysis which based on Reynolds analogy has been extended by Taylor (1954) himself and by Elder (1959) to describe longitudinal diffusion in the turbulent flow in a pipe or an open channel. The analysis above of the dispersion in laminar flow, applies equally well to turbulent flows; turbulent will be treated by allowing u and u' in Eq. (1.1) to represent the ensemble mean and fluctuations, respectively, and replacing D by the cross-sectional turbulent mixing coefficient of the turbulent flow (Fischer et al., 1979). Through this research, the cross-sectional turbulent mixing coefficient $D(y)$ is regarded as a function of the cross-sectional position y. For example, Eqs. (1.4) and (1.13) in the analysis of turbulent flow between parallel plates become

$$u'\frac{\partial C}{\partial \xi} = \frac{\partial}{\partial y}\left[D(y)\frac{\partial c'}{\partial y}\right] \tag{1.20}$$

and

$$D_L = -\frac{1}{h}\int_0^h u' \int_0^y \frac{1}{D(y)} \int_0^y u'\, dy\, dy\, dy\,. \tag{1.21}$$

According to Taylor (1954) the value of $10.06au_*$ is calculated for the longitudinal dispersion coefficient D_L using the 'universal' distribution of velocity in a pipe, $u/u_* = u_0/u_* - f(r/a)$, where a is the pipe radius, r the distance from the central line, f the universal function, provided the flow is fully turbulent, and u_0 the maximum velocity at the centre of the pipe. Elder used the von Karman logarithmic velocity profile, $u = (u_*/\kappa)\,(1 + \ln(y/h))$, where $\kappa = 0.4$ is the von Karman constant, y the distance from the wall and h the channel depth. The longitudinal diffusion coefficient was found to be $5.9u_*h$. Experimental investigations conducted by Syare and Chang (1968) in laboratory channels confirmed that the diffusion coefficient D is not constant, even for two-dimensional flow, and its value varies from 3 to 13. Such a wide variation in the diffusion coefficient is caused by the significant effect of the velocity shear across the flow. Similar approximations to those reported by Sayre were derived by Chatwin (1970, 1971) using an asymptotic series analysis for concentration dispersion based on the assumption that the Fick's law for diffusion is valid.

The study of Taylor and Aris was followed by extensive research on modelling the dispersion in shear flows, with a variety of techniques used. For more details see Gill and Sankarasubramanian (1970), Fischer (1973), Gupta and Bhattacharya (1983), Pagitsas et al. (1986), Smith (1987), Frankel and Brenner (1989), Stokes and Bartonz (1990), Balakotaiah and Chang (1995), and Bryden and Brenner (1996). As can be seen from these studies the longitudinal diffusion is varied as it is sensitive to the distribution of the velocity profile. The authors used various methods such as the integral moments, asymptotic series analysis, multiple time scales analysis, probabilistic approach, and an eigenvalue method employing Laplace transforms and Fourier transforms.

In order to obtain more accurate approximations some authors used two-layer models. Chatwin (1973) divided the flow into a mean stream layer and a viscous layer near bottom. Using a model with equal layers, both well mixed, Thacker (1976) indicated that the bulk concentration satisfies a telegraph function. Smith (1981, 1982) derived a delay-diffusion equation in a similar way to the two-layer model and showed that the results depend on the way the layers are chosen. Chikwendu and Ojiakor (1985) built a two-zone model with a fast zone in the upper part of the flow and a slow one near to the bottom. He averaged the concentration over the fast zone and slow zone separately and described the dynamics in terms of the average concentrations. A system of coupled equations was derived using empirical analysis for the averaged concentrations in each zone. In this model, the Newton's law was used to approximate the diffusion at the interface between the zones. The centre manifold theory, which is our approach of choice in this dissertation, has been used in many different areas of applied mathematics. For example, modelling thermohaline convection (Coullet and Spiegel, 1983),

Couette-Taylor problem for the flow between two concentric rotating (Laure and Demay, 1988; Renardy, 1988), the evolution of slowly varying waves (Lorenz, 1986; Roberts, 1988) and in tearing mode instability in magnetohydrodynamics (Chen and Morrison, 1992).

Coullet and Spiegel (1983) described a general centre manifold procedure to derive ordinary differential equations to predict the solution of a system of partial differential equations when the system is near critical. Roberts (1985) applied the method of Coullet and Spiegel to some simple examples to show the existence of the centre manifold and corresponding evolution equation in terms of the evolution of the amplitudes of some dominant modes. In 1988, Roberts generalised the method of Coullet and Spiegel for finite-dimensional centre manifolds to a case of an infinite-dimensional centre manifold. Subsequently, Mercer and Roberts (1990) applied the theory to describe the dispersion in a channel. In addition to deriving the differential equations for the average concentration, they also showed how to derive initial conditions for the model to achieve fast convergence to solution of the averaged (centre manifold) equations. This model is not only theoretically important because it is firmly supported by the centre manifold theory, but is also practically useful as a tool to estimate the dimensions of patches of emitted substances. In the model, the spreading appears as a combination of advection, diffusion and dispersion as leading factors, expressed by the first, second and third spatial derivatives respectively. In addition to them and unlike the model of Taylor, the model also includes higher-order derivatives.

Watt and Roberts (1995, 1996) designed a one- and two-zone model for an open channel flow using the invariant and centre manifold technique. They designed the appropriate initial conditions for each model based on the given initial conditions of the real physical system using the geometric picture of the invariant manifold theory so that the full and approximate systems are identical after a short time. Using these corrected initial conditions, the authors derived a generalised Taylor description of dispersion. Roberts and Strunin (2004) constructed a two-zone model of contaminant dispersion in Poiseuille channel flow based on the centre manifolds. They validated the analysis by direct computations of the original two-dimensional equations. The authors also formulated modified initial conditions to obtain a better agreement between the manifold solution and the real solution. Yet, this work is best applicable to laminar flows than turbulent flows as the diffusion coefficient was assumed independent of the velocity shear.

Strunin (2011) studied the turbulent dispersion in turbulent boundary layers in an open channel using the centre manifold theory and took into account that the turbulent diffusion coefficient, $D(y)$, depends on the cross-sectional position y, as it is linked to the shear. For the turbulent boundary layer, the author used two velocity profiles, namely logarithmic and power. More details about these two profiles is given in Section 2.1. Mei et al. (2003) and Georgiev et al. (2007) also studied the case of the shear-dependent diffusion based on $k-\epsilon$ and $k-\omega$ turbulent models using centre manifold approach. However, their approach has a drawback of involving a number of empirical coefficients whose values were not precisely known. Also, the boundary conditions in these models are not unique

as pointed out by Strunin (2011).

1.1.2 A brief review of the flow in the urban canopy layer

In the present research, we plan to model shear dispersion of contaminants in an urban canopy layer of cube arrays using centre manifold approach. Modelling shear flow in urban canopies has recently received much attention due to increasing concern worldwide for the health effects of high pollution concentrations in cities (Sabatino et al., 2008). Several models are available to predict the wind distribution within urban areas (Bentham and Britter, 2003; Coceal and Belcher, 2004; Sabatino et al., 2008).

In an equilibrium boundary layer flow the mean wind speed can be expressed in terms of the roughness length, y_0, the displacement height, d, and the surface shear stress, $\tau_0 = \rho u_*^2$, according to the logarithmic velocity profile

$$u(y) = \frac{u_*}{\kappa} \ln\left(\frac{y-d}{y_0}\right) . \tag{1.22}$$

Plate (1995) suggested that the parameters y_0 and d are functions of λ_p and λ_f, respectively. The frontal area density of the obstacle is defined by $\lambda_f = A_f/A_d$, where A_f is the frontal area of each obstacle exposed to the wind and A_d the underlying surface area of an obstacle. The plan area density of the obstacle is defined by $\lambda_p = A_p/A_d$, where A_p is the plan area of an obstacle as viewed from above. For cubical obstacles, $\lambda = \lambda_f = \lambda_p$. Wieringa (1993) pointed out that surface roughness length estimates obtained from wind profile analysis can have large errors due to the method of analysis, best-fit errors and measurements errors, quoted in (Plate, 1995). The displacement height d is defined as the main level of momentum absorption by the rough surface (Thom, 1971; Raupach et al., 1980; Jackson, 1981) at which the neutral wind profile in the inertial sublayer obeys the semi-logarithmic profile (1.22) (Raupach and Thom, 1981).

Macdonald (2000) assumed a linear interpolation of the turbulence length scale at the top of the canopy to the classical Prandtl length scale at the top of the roughness sublayer and obtained a simple model for the velocity profile within and above a canopy of cube obstacle arrays. He showed that for cube arrays with low packing density the predicted exponential velocity profile provides an adequate fit to the average velocity profile within the canopy. Although there exist more sophisticated models which can be used as a base for describing turbulent canopy flow, in the present research we use a more traditional one by Macdonald (2000) to be analysed using centre manifold approach. The model of Macdonald modifies a simple model originally derived by Cionco (1965) for mean wind velocity profiles in vegetative canopy flows to be used for urban-type canopy. The model of Macdonald for the average velocity profile in the urban canopy layer includes three parts: the inertial sublayer, governed by semi-logarithmic profile Wooding

et al. (1973) and defined in Eq. (1.22); the canopy layer in which the velocity profile is exponential of the form

$$u(y) = u_h \exp\left[a(\frac{y}{h} - 1)\right] , \tag{1.23}$$

where u_h is the velocity at the top of the canopy, h the canopy height and the attenuation coefficient a is a constant; and the roughness sublayer (terms like transition layer and interfacial can also be used) located between the lower part of the inertial sublayer and the upper part of the canopy layer. A detailed description of the velocity profile in the roughness sublayer is given in chapter 5. The exponential velocity profile (1.23) was predicted by several investigators for vegetative canopy flows (Cionco, 1965; Raupach and Thom, 1981; Yi, 2008). Macdonald (2000) used the exponential velocity profile above for modelling urban canopy of cube arrays.

The estimation of the roughness height is an initial feature of many meteorological and wind-engineering activities concerned with the dispersion of contaminants and one of the reasons behind the large amounts of scatter in roughness data estimated from velocity measurements (Macdonald et al., 1998). In the following we present several methods that have been developed for estimating surface roughness.

Perry and Joubert (1963) developed graphical procedure for determining y_0 from mean velocity profiles. They reviewed rough-wall boundary layers and showed that the effect of roughness on the flow away from the wall can be accounted for by using an equivalent viscosity depend only on the variables at the wall, such as shear stress, fluid density, viscosity and the roughness size and geometry. Petersen (1997) tested two analytical methods, those due to Lettau (1969) and Counihan (1971), to estimate the surface roughness, y_0, as a function of wind direction at refineries. He measured the velocity profile in the wind tunnel over three refineries and two uniform roughness configurations. The methods are statistically evaluated by comparing their predictions against surface roughness length estimates obtained from wind speed. Based on this evaluation, Petersen argued that these two methods represent true estimates of the surface roughness length for the modelled refineries and roughness configurations. The results also showed that the Lettau method provides a better estimate of the roughness height y_0 for regular arrays of uniform obstacles from

$$y_0 = 0.5h\lambda , \tag{1.24}$$

within a factor of $0.5 - 1.5$ at the 95% confidence interval, of surface roughness length, where h is the obstacle height. The factor 0.5 in (1.24) corresponds to the average drag coefficient of the individual obstacles (Kutzbach, 1961). Lettau suggested that the expression above is limited to canopies with low packing density due to interaction between the obstacles and the development of a finite

displacement height in the velocity profile.

Counihan (1971) derived an analytical expression for estimating the roughness length, y_0, from velocity profiles over regular arrays of cubic obstacles in a wind tunnel, which can be expressed by

$$\frac{y_0}{h} = 1.8\lambda - 0.08\,. \tag{1.25}$$

Counihan argued that this expression is valid for $0.06 < \lambda < 0.15$ and limited to Counihan's type of obstacles. Both Lettau's and Counihan's relation do not account for differences due to varying obstacle geometries and also for the nonlinear reduction of y_0/h with increasing area density of the obstacles.

Theurer, quoted in (Macdonald et al., 1998; Shao and Yang, 2005), approximated y_0 by the expression

$$\frac{y_0}{h} = 1.6\lambda\,(1 - 1.67\lambda)\ . \tag{1.26}$$

He suggested that this relation is limited to $\lambda < 0.25$. Bottema (1996, 1997) presented an analytical model for estimating y_0 and d regular building groups

$$\frac{y_0}{h} = \frac{y_{ref} - d}{h} \exp\left(\frac{\kappa}{\sqrt{0.5\lambda p}}\right)\ , \tag{1.27}$$

where y_{ref} is a reference height, p the drag coefficient. The displacement height d is estimated from the circulation zone volume. The roughness model proposed by Bottema suggests a large sensitivity to obstacle pattern type and drag coefficient p.

Recently, Macdonald et al. (1998) derived Lettau's relation for estimating the roughness height y_0 from basic principles by assuming that the logarithmic velocity profile (1.22) is accurate down to the height of the obstacles with a displacement height d. He proposed the following relationship:

$$\frac{y_0}{h} = \left(1 - \frac{d}{h}\right) \exp\left[-\left(0.5\frac{p}{\kappa^2}\beta\left(1 - \frac{d}{h}\right)\lambda\right)^{-0.5}\right], \tag{1.28}$$

where the displacement height d is given by $d/h = 1 + A_1^{-\lambda}\,(\lambda - 1)$. The numerical factor 0.5 under the exponential in (1.28) was based on a combination of many experiments, and corresponds to the average drag coefficient of the individual obstacles (Macdonald et al., 1998). The best fit to wind-tunnel data is provided

by the values of $A_1 = 4.43$ and $\beta = 1$ for staggered arrays and $A_1 = 3.59$ and $\beta = 0.55$ for the square arrays of roughness obstacles. Macdonald obtained the correct qualitative behaviour of the roughness height over the entire range of area density. He suggested that the explicit appearance of the drag coefficient p in Eq. (1.28) and the inclusion of the effect of the displacement height d which account for the reduction of y_0 with increasing obstacle density above a certain maximum are the main improvements of correlation presented in his model over previous models. The reduction of the roughness height y_0 occurs at a packing density of about $\lambda = 0.20$ (Macdonald, 2000).

Shao and Yang (2005) compared the estimated y_0 and d with several wind data sets, e.g., (O'Loughlin and Macdonald, 1964; Lettau, 1969; Counihan, 1971; Theurer, 1973; Raupach et al., 1980; Liedtke, 1992; Hall et al., 1996), and found that there is a reasonable agreement among the estimates of the relationships and measurements for $\lambda < 0.15$. The relations of Lettau (1969) and that of Theurer (1973) predict a monotonic increase of y_0/h with λ and overestimate y_0/h when λ exceeds about 0.2. The model of Macdonald et al. (1998) fits well to the observations and reproduces the trend that y_0/h drops off after peaking at about $\lambda = 0.15$. In the proposed research we adopt the model of Macdonald et al. (1998) to estimate the roughness height y_0 and the displacement d in the semi-logarithmic law (1.22).

1.1.3 A brief review on the numerical method of radial basis function networks

In this dissertation, we use the 1D-IRBFN method for modelling dispersion in a turbulent open channel flow based on centre manifold theory (see Chapter 5). Kansa (1990a,b) investigated a collocation scheme based on multiquadric (MQ) radial basis functions (RBF) for the numerical solution of partial differential equations (PDEs). Their numerical results showed that: (i) the MQ is an extremely accurate approximation scheme for interpolation and partial derivative estimates for a variety of two-dimensional functions over both gridded and scattered data; (ii) the MQ is more efficient than finite difference schemes which require many operations to achieve the same degree of accuracy. The Kansa's approach is referred to as the conventional differentiated radial basis function network (DRBFN). Radial basis function networks (RBFN) are broad enough for universal approximation based on meshfree discretisation (Park and Sandberg, 1991).

As an alternative to the (DRBFN), Mai-Duy and Tran-Cong (2001a) used the integration instead of conventional differentiation to construct the RBF approximations (the IRBFN method) as a better accuracy procedure than the conventional differentiated radial basis function network (DRBFN) method for the approximation of a function and its derivatives and for the solution of PDEs. Numerical results showed that IRBFN achieves superior accuracy compared to DRBFN in the approximation of both function and especially its derivatives (Mai-Duy and

Tran-Cong, 2001a, 2003).

Mai-Duy and Tanner (2007) presented a one-dimensional integrated radial basis function network (1D-IRBFN) collocation method for the solution of second- and fourth-order PDEs. The 1D-IRBFN method is constructed to satisfy the governing DEs together with boundary conditions in an exact manner based on a Cartesian grid. This method is much more efficient than the original IRBFN method reported by Mai-Duy and Tran-Cong (2001a) and was further developed for the simulation of fluid flow problems. Ngo-Cong et al. (2011) proposed the one-dimensional integrated radial basis function network (1D-IRBFN) collocation method for an accurate and efficient solution to fluid mechanics problems. The significant high level of accuracy and efficiency has been achieved in terms of several characteristics: (i) the Radial Basis Function network (RBFN) is a high-order approximation; (ii) the use of integration instead of conventional differentiation to construct the RBF approximations significantly improves the stability and accuracy of the numerical solution as the integration is a smoothing operation and is more numerically stable; (iii) Cartesian grids are used to discretise the problem domains as generating a Cartesian grid is much simpler and easier than generating a finite element mesh.

1.2 Motivation

An asymptotic evolution equation governing the cross-flow averaged concentration C of contaminants and other substances

$$\frac{\partial C}{\partial t} = g_1 \frac{\partial C}{\partial x} + g_2 \frac{\partial^2 C}{\partial x^2} + g_3 \frac{\partial^3 C}{\partial x^3} + \dots \tag{1.29}$$

can be effectively used for prediction of the spreading of the substances in environmental and industrial flows. We plan to analytically derive the coefficients g_1, g_2 and g_3 responsible for the advection, diffusion and dispersion respectively. Sometimes all the coefficients $n = 2, 3, ...$ are called dispersion coefficients in the sense that they lead to stretching the signal in space. However, one can distinguish between the diffusion mechanism (g_2) and dispersion mechanism as such (g_3) in a more strict sense, according to the dissipation of Fourier modes of the signal (via g_2) and their propagation with different speeds (via g_3). The coefficients are deduced from the original non-averaged transfer equation as functions of parameters controlling the flow such as the Reynolds number R and von Karman constant κ. Once deduced, the model (1.29) can be solved to get the information about the size of clouds of contaminants. Even without solving it one can quickly estimate the size just based on the values of the coefficients g_1, g_2 and g_3. The characteristic distance over which the substance propagates during some time T

is

$$\begin{aligned} L_1 &= g_1 T \qquad \text{due to the advection,} \\ L_2 &= (g_2 T)^{1/2} \quad \text{due to the diffusion,} \\ &\ldots \\ L_n &= (g_n T)^{1/n} \quad \text{due to the } n^{th} - \text{order transfer process.} \end{aligned} \tag{1.30}$$

One of the first attempts to construct such an equation was made by Taylor (1953, 1954). He designed an advection-diffusion equation for the averaged concentration along the channel using semi-empirical arguments. The equation was applicable for large times when spatial variations of the concentration along the channel become slow.

A more accurate method of constructing such an equation, based on centre manifold theory, was proposed in a series of works originated by Roberts. In one of the first papers, Mercer and Roberts (1990) applied the centre manifold theory to describe the dispersion in a laminar flow in a channel.

Roberts (1989) showed how to derive appropriate initial conditions for the centre manifold model, so that the motion on the centre manifold and the motion along the actual trajectory converge to each other at the fastest rate. We will discuss this issue later in the present research.

Because of the viscosity, the flow near the channel bottom is slower. This led some authors to an idea to divide the flow into two zones in order to obtain more accurate description. In doing so, Chatwin (1973) divided the flow into the mean stream layer and the viscous layer near the bottom. Smith (1981) derived a delay-diffusion equation similarly to the two-zone model and showed that the results depend on the way the zones are chosen. Chikwendu and Ojiakor (1985) built a two-zone model with the fast zone in the upper part of the flow and a slow zone near the bottom. They averaged the concentration over each zone separately and described the dynamics in terms of the average concentration in each zone. A system of coupled equations was derived using approximate arguments about how coupling occurs. Namely, the Newton's law was chosen to approximated the diffusion through the interface between the zones. Watt and Roberts (1995) designed zonal models using techniques closely related to the centre manifold approach. Roberts and Strunin (2004) derived a two-zone model based on the centre manifolds. They validated the analysis using direct computations of the original two-dimensional equations.

Turbulent flows are more difficult to model than laminar flows because, firstly, the turbulent diffusion coefficient depends on the velocity shear and, secondly, the boundary conditions at the bottom may not be easy to formulate. Strunin (2011) analyzed the transport of contaminants in turbulent boundary layers of

two types. He considered the classical logarithmic velocity profile and, according to an alternative, more recent model, power velocity profile. The flow was assumed steady and variations of the contaminant concentration in space and time were supposed slow. The dynamical structure of turbulence was taken into account through the connection between the turbulent diffusion coefficient and the velocity shear.

The ensemble-averaged concentration (see Fig. 1.1) of a passive substance, $c(x, y, t)$, is subject to the 2-D advection-diffusion equation

$$\frac{\partial c}{\partial t} + u(y)\frac{\partial c}{\partial x} = \frac{\partial}{\partial y}\left[D(y)\frac{\partial c}{\partial y}\right], \tag{1.31}$$

where $u(y)$ is the mean velocity of the flow in the channel as a function of y and $D(y)$ the coefficient responsible for the turbulent diffusion across the channel. The boundary conditions describe non-penetration through the bottom ($y = 0$) and surface ($y = h$, the channel height),

$$D\frac{\partial c}{\partial y}\bigg|_{y=0} = D\frac{\partial c}{\partial y}\bigg|_{y=h} = 0\,. \tag{1.32}$$

We do not include the along-the-flow component of the diffusion, $D_L\partial c^2/\partial x^2$, although this can be done without difficulty. Further in the research we show that this term does not affect the averaged model. The diffusion coefficient can be determined by taking into account that the turbulent momentum flux, u_*^2, is constant across the flow and proportional to the momentum gradient,

$$u_*^2 = D_m(y)\frac{\partial u}{\partial y}\,, \tag{1.33}$$

where $D_m(y)$ is the turbulent diffusion coefficient. Following Barenblatt (2003), the diffusion coefficient is represented by the Prandtl formula for the stress

$$D(y) = KD_m(y)\,, \tag{1.34}$$

where the proportionality coefficient $K(Sc)$ may generally depend on the Schmidt number. By using Eqs. (1.33) and (1.34) we obtain

$$D(y) = K\frac{u_*^2}{\partial_y u}\,. \tag{1.35}$$

We will adopt different models for $u(y)$ to be used in Eqs. (1.31) and (1.35). Equations (1.31)–(1.35) form a self-consistent model which we will convert into the equation for the depth-averaged concentration of contaminant, C, using centre manifolds. We plan to analytically derive the coefficients g_1, g_2, g_3 and some higher-order coefficients responsible for the advection, diffusion, dispersion etc. respectively.

In this research we focus on two types of turbulent flow: an open channel flow over a smooth bottom and a flow above substantial roughness such as canopies, either natural or artificial. In both cases, the flow has two dimensions: vertical and horizontal (downstream). Everything is uniform in lateral direction (z-direction). The contaminant is released into the flow instantaneously, and after a long time the contaminant concentration varies slowly in space and time. Thus, all the derivatives $\partial^m/\partial x^n$ are supposed small.

As we said, for the channel flow, we consider the classical logarithmic velocity profile and power velocity profile. For the canopy flows, we propose a theoretical framework of the dispersion near non-smooth objects with agglomerations of bluff parts sitting on a relatively smooth surface. Examples of such flows can be the flows through roughness in channels, near surfaces of aircrafts or ships, where roughness is caused by attached devices, or through urban canopies.

Strunin (2011) used this approach to study the flow near a smooth substrate, now we extend it to a more complex canopy flow. Using the centre manifold approach, we transfer the original 2–D equation (1.31) to a 1–D ordinary differential equation resulting in some benefits. Firstly, we simplified the problem by reducing the number of independent variables. Secondly, we gained a valuable knowledge: we revealed a universal law, which governs the behaviour of solutions evolving from different initial conditions (the universality can be proved).

The outcome of this model provides an accurate description of the cross-flow averaged dispersion along the turbulent boundary layer. We also derive some higher-order coefficients describing the averaged dispersion in a smooth channel. Furthermore, we compare the actual solutions for the average concentration following from the averaged (1-D) model and the original (2-D) model.

1.2.1 Objectives of the present research

In the present research, (1) use the centre manifold approach to (a) derive an advection, diffusion, dispersion–and higher-order coefficients for the equation governing the averaged transport in a smooth channel, (b) formulate an analytical framework of the averaged transport of contaminants in turbulent boundary layers near smooth and rough substrates, (c) derive an advection-diffusion equation for the flow through canopies, and we (2) Justify the centre manifold approach directly by comparing the numerical solutions of the averaged (1-D) and original (2-D) models using the numerical one-dimensional integrated radial basis

network(1D-IRBFN) method.

1.2.2 Outline of the present dissertation

In this study, each chapter is structured in a self-contend manner as follows.

Chapter 1 presents the literature review and motivation of the present study. Here, we give a brief review on the transport of contaminants in an open channel flow, and the use of centre manifold. Also, we discuss the canopy flow and the numerical method of radial basis function network. We also outline the objectives of the present research.

Chapter 2 includes some important concepts from fluid mechanics that we use in the present research such as an advection-diffusion equation for the depth-averaged concentration along an open channel, the classical logarithmic law and the power law. Then, we describe the method for modelling of the shear dispersion using centre manifolds.

Chapter 3 presents modeling dispersion for turbulent flows in an open channel based on centre manifolds using 1D-IRBFN method. A direct numerical verification of the 1D-IRBFN method with examples of the dispersion in laminar and turbulent flows in an open channel with a smooth bottom are given. The shear dispersion of contaminant based on centre manifold theory is successfully simulated by using the 1D-IRBFN method. The numerical solution of the derived model obtained by centre manifolds for both laminar and turbulent flows are in a good agreement with that of the original advection-diffusion equation.

Chapter 4 reports higher-order transport equations for turbulent channel flows. The derived partial differential equations governs the longitudinal dispersion of contaminants in a turbulent open channel flow. As a velocity profile we used the classical logarithmic profile and power profile and a recent alternative model.

Chapter 5 presents an averaged model of shear dispersion in the turbulent flow above the canopy using centre manifold method. We derive an advection-diffusion equation for the averaged concentration, involving first and second derivatives with respect to spatial coordinate. The coefficients of the equation are derived and analysed against the parameters characterising the turbulent flow. In the limit of large flow depths, the values of the coefficients coincide with those obtained earlier for the flow over a smooth bottom.

Chapter 6 gives some concluding remarks from the present research.

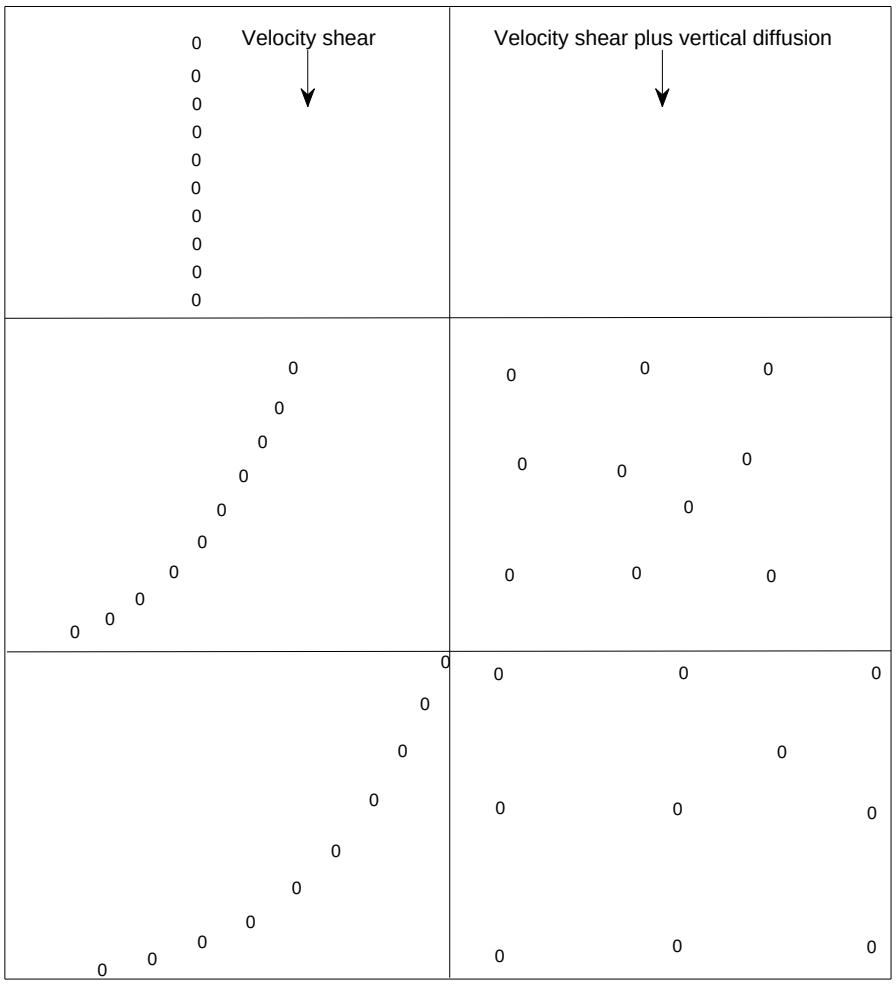

Figure 1.1 A sketch of the spreading of contaminant along the channel: under the velocity shear (left) and under the shear plus cross-flow diffusion (right). The two factors make the picture look as if there is the along-the-flow diffusion.

Chapter 2

Basic concepts: fluid mechanics and centre manifold theory

In the present chapter we describe some important concepts from fluid mechanics that we use in the present research. For example, an advection-diffusion equation for the depth-averaged concentration along an open channel, the classical logarithmic law and the power law. Then, we give a framework of modelling the shear dispersion using centre manifold theory.

2.1 Concepts from fluid mechanics

In the following subsections, the transport using diffusion and dispersion processes in an open channel are described (Fischer et al., 1979). We also separately analyse the dispersion for the logarithmic and power velocity profiles (Tennekes and Lumley, 1972; Monin and Yaglom, 1975; Landau and Lifshitz, 1981; Barenblatt, 2000); of our particular interest is the case of very large Reynolds number.

2.1.1 Transport via diffusion

Consider an open channel flow in which the flow is assumed steady and the contaminant concentration is transferred by diffusion alone, in the direction of x-axis. Fick's law states that the mass flux of a contaminant passing through a cross-sectional area in a given direction is proportional to the gradient of the contaminant concentration in that direction. Mathematically, the Fick's law can be expressed by (Fischer et al., 1979)

$$M = -D\frac{\partial c}{\partial x}\,, \tag{2.1}$$

where M is the contaminant mass flux, D the diffusion coefficient (hereafter assumed constant) and $c(x,t)$ the concentration of diffusing contaminant. In addition to the Fick's law, conservation of mass leads to a second relation between the mass flux $M(x,t)$ and concentration $c(x,t)$,

$$\frac{\partial c}{\partial t} + \frac{\partial M}{\partial x} = 0\,. \tag{2.2}$$

Substituting Eq. (2.1) into Eq. (2.2) gives

$$\frac{\partial c}{\partial t} = D\left(\frac{\partial^2 c}{\partial x^2}\right)\,. \tag{2.3}$$

Eq. (2.3) is known as diffusion equation and describes how mass is transferred by Fickian diffusion processes. Higher order diffusion equations can also be derived for some processes. Consider an arbitrary control volume, V, located entirely within the fluid. The fluid moves in or out of this volume through its surface, S. The concentration flux of contaminant in the volume can be related to the mass flux $\mathbf{M}$ across the surface by

$$\frac{\partial}{\partial t}\int_V c(x,t)\,dV + \int_S \mathbf{M}(x,t)\cdot\mathbf{n}\,dS = 0\,, \tag{2.4}$$

where $c(x,t)$ is the contaminant concentration per unit volume at the point x at time t, $\mathbf{M}(x,t)$ the mass flux across the unit surface located at x and $\mathbf{n}$ the unit vector normal to the surface element dS. Applying Green's theorem to Eq. (2.4) gives

$$\int_V \left(\frac{\partial c}{\partial t} + \nabla\cdot\mathbf{M}\right)\,dV = 0\,. \tag{2.5}$$

Since the volume is arbitrary Eq. (2.5) becomes

$$\frac{\partial c}{\partial t} = -\nabla\cdot\mathbf{M}\,. \tag{2.6}$$

Eq. (2.6) is called the continuity equation. Substituting Eq. (2.1) into Eq. (2.6) gives

$$\frac{\partial c}{\partial t} = D\nabla^2 c\,. \tag{2.7}$$

In cartesian coordinates, Eq. (2.7) can be written as

$$\frac{\partial c}{\partial t} = D\left(\frac{\partial^2 c}{\partial x^2} + \frac{\partial^2 c}{\partial y^2} + \frac{\partial^2 c}{\partial z^2}\right) . \tag{2.8}$$

2.1.2 Transport via both advection and diffusion

Now suppose that the fluid itself moves with an average velocity u in the x direction (the transport by the mean motion of the fluid is called advection) and consider the transport via the advection and diffusion. The total rate of mass transport is

$$M = uc + \left(-D\frac{\partial c}{\partial x}\right) , \tag{2.9}$$

where M is the mass flux, uc the advective flux and $-D(\partial c/\partial x)$ the diffusive flux. Substituting Eq. (2.9) into Eq. (2.2), we have

$$\frac{\partial c}{\partial t} + \frac{\partial}{\partial x}(uc) = D\frac{\partial^2 c}{\partial x^2} . \tag{2.10}$$

In three dimensions the equation takes the form

$$\frac{\partial c}{\partial t} + \nabla \cdot (c\mathbf{u}) = D\nabla^2 c . \tag{2.11}$$

Using the conservation of mass $\nabla \cdot \mathbf{u} = 0$, Eq. (2.11) becomes

$$\frac{\partial c}{\partial t} + \mathbf{u}\nabla c = D\nabla^2 c . \tag{2.12}$$

In cartesian coordinates, Eq. (2.12) is written as

$$\frac{\partial c}{\partial t} + u\frac{\partial c}{\partial x} + v\frac{\partial c}{\partial y} + w\frac{\partial c}{\partial z} = D\left[\frac{\partial^2 c}{\partial x^2} + \frac{\partial^2 c}{\partial y^2} + \frac{\partial^2 c}{\partial z^2}\right] , \tag{2.13}$$

where u, v and w are the components of $\mathbf{u}$ in the x, y and z directions. The advection-diffusion equation in the x direction is simply

$$\frac{\partial c}{\partial t} + u\frac{\partial c}{\partial x} = D\frac{\partial^2 c}{\partial x^2}\,. \tag{2.14}$$

Eq. (2.14) means that there is an advection transport in the same direction as the diffusion and differs from (2.10) as the fluid is moving with a constant velocity u in the x direction only (the gradients in the y direction are small). If the diffusive transport in the x direction is smaller than the advection transport, then Eq. (2.14) can be written as

$$\frac{\partial c}{\partial t} + u\frac{\partial c}{\partial x} = D\frac{\partial^2 c}{\partial y^2}\,, \tag{2.15}$$

where y is a transverse direction.

2.1.3 Illustrative example on an advection-diffusion equation

In the following, Burger's equation is analytically solved as an example on an advection-diffusion equation.

2.1.4 Analytical solution of Burger's equation

Burger's equation is a nonlinear advection-diffusion equation which has the form (Logan, 1994)

$$\frac{\partial u}{\partial t} + u\frac{\partial u}{\partial x} = D\frac{\partial}{\partial x}\left(\frac{\partial u}{\partial x}\right)\,, \tag{2.16}$$

where the term $u\partial u/\partial x$ represents a nonlinear advection which is responsible about the transport process and $D\partial/\partial x(\partial u/\partial x)$ represents the diffusion or a dissipative term that tends to smear out concentrations. Eq. (2.16) is analysed as an illustrative example on solving an advection-diffusion equation. This equation incorporates an advection and diffusion in the same direction. Consider

$$u(x,t) = U(y) \quad \text{such that} \quad y = x - ct \tag{2.17}$$

as twice continuously differentiable solutions of Eq. (2.16), where c is to be determined. Substituting (2.17) into (2.16) gives an ordinary differential equation for $u = U(y)$ of the form

$$-c\frac{dU}{dy} + U\frac{dU}{dy} - D\frac{d}{dy}\left(\frac{dU}{dy}\right) = 0\,. \tag{2.18}$$

Integrating Eq. (2.18), one obtains

$$-cU + \frac{U^2}{2} - D\frac{dU}{dy} = A\,, \tag{2.19}$$

where A is a constant of integration. Rewriting Eq. (2.19) as

$$\frac{dU}{dy} = D^{-1}\left(\frac{1}{2}U^2 - cU - A\right)\,. \tag{2.20}$$

The constants A and c can be evaluated using the continuity of dU/dy. As a result,

$$A = -\frac{u_1 u_2}{2} \quad \text{and} \quad c = \frac{u_1 + u_2}{2}\,. \tag{2.21}$$

Eq. (2.20) therefore becomes

$$-2D\frac{dU}{dy} = (U - u_1)\,(u_2 - U)\,. \tag{2.22}$$

Integrating (2.22) gives

$$\frac{y}{D} = \frac{2}{u_2 - u_1}\ln\left(\frac{u_2 - U}{U - u_1}\right)\,, \tag{2.23}$$

where the constant of integration was chosen so that $U(0) = c$. Solving (2.23) for U, one has

$$U(y) = u_1 + \frac{u_2 - u_1}{1 + \exp[(u_2 - u_1)\,y/2D]}\,. \tag{2.24}$$

This is a traveling wave solution of Burger's equation.

2.1.5 Initial value problem for Burger's equation

The initial value problem for Burger's equation (Logan, 1994) can be written as

$$\frac{\partial u}{\partial t} + u\frac{\partial u}{\partial x} - D\frac{\partial}{\partial x}\left(\frac{\partial u}{\partial x}\right) = 0, \quad x \in R,\ t > 0, \tag{2.25}$$

$$u(x,0) = u_0(x), \quad x \in R\,. \tag{2.26}$$

Using Cole-Hopf transformation, this problem can be reduced to the initial value problem for the linear diffusion equation and then can be solved analytically. Substituting $u = dw/dx$ into (2.25) and integrating once, one obtains

$$\frac{\partial w}{\partial t} + \frac{1}{2}\left(\frac{\partial w}{\partial x}\right) - D\frac{\partial^2 w}{\partial x^2} = 0\,. \tag{2.27}$$

By substituting $w = -2D\ln v$, where v is a function, into (2.27), one deduces the Cole-Hopf transformation

$$u = -\frac{2D}{v}\left(\frac{\partial v}{\partial x}\right)\,. \tag{2.28}$$

Using Cole-Hopf transformation, Eq. (2.25) can be reduced into

$$\frac{\partial v}{\partial t} - D\frac{\partial^2 v}{\partial x^2} = 0\,. \tag{2.29}$$

Also, using (2.28) the initial condition (2.26) can be rewritten as

$$u(x,0) = u_0(x) = -\frac{2D}{v(x,0)}\left(\frac{\partial v(x,0)}{\partial x}\right)\,.$$

Integrating yields

$$v(x,0) = v_0(x) = -\exp\left(-\frac{1}{2D}\int_0^x u_0(y)dy\right)\,. \tag{2.30}$$

The initial value problem (2.29)–(2.30) has the solution

$$v(x,t) = \left(\frac{1}{4\Pi Dt}\right)^{1/2}\int_R v_0(\xi)\exp\left[-\frac{(x-\xi)^2}{4Dt}\right]d\xi\,. \tag{2.31}$$

Substituting (2.31) into (2.28), one gets

$$u(x,t) = \frac{\int_R [(x-\xi)/t] \exp[-G(\xi,x,t)/2D]\, d\xi}{\int_R \exp[-G(\xi,x,t)/2D]\, d\xi}\,, \tag{2.32}$$

where

$$G(\xi,x,t) = \frac{(x-\xi)^2}{2t} + \int_0^\xi u_0(y)dy\,.$$

Equation (2.32) represents the solution of the initial value problem (2.25)–(2.26) associated with Burger's equation.

2.1.6 Logarithmic velocity profile

Consider a steady turbulent flow in an open channel flow of depth h, driven by horizontal pressure gradient. The coordinates x and y are directed along and across the channel respectively. The y-component of the mean velocity is zero everywhere if it is zero at both walls. Corresponding equations of motion for the mean flow are

$$0 = -\frac{1}{\rho}\frac{\partial P}{\partial x} - \frac{d}{dy}\overline{v_1 v_2} + \nu\frac{d^2u}{dy^2}, \tag{2.33}$$

$$0 = -\frac{1}{\rho}\frac{\partial P}{\partial y} - \frac{d}{dy}\overline{v_2^2}\,. \tag{2.34}$$

In Eq. (2.33) and Eq. (2.34), ρ is the fluid density, v_1 and v_2 are the longitudinal and vertical components of the velocity fluctuations respectively, ν is the kinematic viscosity, overbar means ensemble-averaging, and u is the x-component of the mean velocity. Integrating Eq. (2.34), we get

$$\frac{P}{\rho} + \overline{v_2^2} = \frac{P_0}{\rho}, \tag{2.35}$$

where P_0 is a function of x only. By assumption, $\overline{v_2^2}$ is independent of x, that is, $\partial P/\partial x$ is equal to dP_0/dx. These gradients should be independent of x. Then, integrating Eq. (2.33) from $y = 0$ to infinity, we obtain

$$0 = -\frac{y}{\rho}\frac{dP_0}{dx} - \overline{v_1 v_2} + \nu\frac{du}{dy} - u_*^2\,, \tag{2.36}$$

where ρu_*^2 is the stress at the surface and u_* is the friction velocity. On the surface $y = h$, the shear stress is zero: $-\rho\overline{v_1 v_2} + \mu(du/dy) = 0$. Hence, when $y = h$, Eq. (2.36) becomes

$$u_*^2 = -\frac{h}{\rho}\left(\frac{dP_0}{dx}\right) . \tag{2.37}$$

Substituting the value of dP_0/dx from Eq. (2.37) into Eq. (2.36), we obtain

$$-\overline{v_1 v_2} + \nu\frac{du}{dy} = u_*^2\left(1 - \frac{y}{h}\right) . \tag{2.38}$$

Now, we non-dimensionalise Eq. (2.38) using h/u_* as the time scale and h as the length scale. Therefore, we have

$$-\frac{\overline{v_1 v_2}}{u_*^2} + \frac{\nu}{hu_*}\frac{d(u/u_*)}{d(y/h)} = 1 - \frac{y}{h} . \tag{2.39}$$

Re-write Eq. (2.39) as

$$-\frac{\overline{v_1 v_2}}{u_*^2} + \frac{d(u/u_*)}{d(yu_*/\nu)} = 1 - \frac{\nu}{hu_*}\frac{yu_*}{\nu} . \tag{2.40}$$

Let $y_+ \equiv yu_*/\nu$, $\eta = y/h$. Equations (2.39) and (2.40) become

$$-\frac{\overline{v_1 v_2}}{u_*^2} + R_*^{-1}\frac{d}{d\eta}\left(\frac{u}{u_*}\right) = 1 - \eta , \tag{2.41}$$

$$-\frac{\overline{v_1 v_2}}{u_*^2} + \frac{d}{dy_+}\left(\frac{u}{u_*}\right) = 1 - R_*^{-1}y_+ , \tag{2.42}$$

where $R_* = hu_*/\nu$. When $R_* \to \infty$, Eq. (2.41) reduces to

$$-\frac{\overline{v_1 v_2}}{u_*^2} = 1 - \eta . \tag{2.43}$$

The flow governed by Eq. (2.43) is called the core region (outer layer). As $R_* \to \infty$, but with y_+ of order one, (2.42) becomes

$$-\frac{\overline{v_1 v_2}}{u_*^2} + \frac{d(u/u_*)}{d(yu_*/\nu)} = 1 . \tag{2.44}$$

The flow governed by Eq. (2.44) is called the surface layer. Denote

$$\frac{u}{u_*} = f(y_+) \tag{2.45}$$

and

$$-\frac{\overline{v_1 v_2}}{u_*^2} = g(y_+)\,. \tag{2.46}$$

The relations above are called the law of the wall. The system Eq. (2.44)-Eq. (2.46) completed with the boundary conditions $f(0) = 0$ and $g(0) = 0$. In the core region, we use the turbulent energy budget, which is

$$-\overline{v_1 v_2}\frac{du}{dy} = \epsilon + \frac{d}{dy}\left(-\frac{\overline{Pv_2}}{\rho} + \frac{1}{2}\overline{q^2 v_2}\right)\,, \tag{2.47}$$

where ϵ is the viscous dissipation of the turbulent energy $\overline{q^2}$, q is the mean energy flux density. Under the flow circumstances considered the viscous transport of $\overline{q^2}$ is neglected. Referring back to Eq. (2.43), $-\overline{v_1 v_2} = u_*^2$ for all finite values of η and q^2 and P/ρ are of order u_*^2, too. Then the right-hand side of Eq. (2.47) must be of order u_*^3/h, that is $du/dy = u_*/h$, since the Reynolds stress is of order u_*^2. If we stay above the surface layer to ensure that no other characteristic lengths can complicate the picture, without any loss of generality, we state that

$$\frac{du}{dy} = \frac{u_*}{h}\left(\frac{dF}{d\eta}\right)\,, \tag{2.48}$$

where $dF/d\eta$ is the derivative of some unknown function of order one (Tennekes and Lumley, 1972). Integrating Eq. (2.48) from $\eta = 1$ toward the wall, we have

$$\frac{u - u_0}{u_*} = F(\eta)\,, \tag{2.49}$$

where u_0 is the velocity of the main stream at infinity. Equation Eq. (2.49) is not applicable at $\eta \to 0$. We assume that the surface layer and the wall layer can be matched. According to Eq. (2.45), the velocity gradient in the surface layer is

$$\frac{du}{dy} = \frac{u_*^2}{\nu}\left(\frac{df}{dy_+}\right)\,. \tag{2.50}$$

Equating Eq. (2.48) and Eq. (2.50), and considering $y_+ \to 0$ and $\eta \to 0$, we get

$$\frac{u_*}{h}\left(\frac{dF}{d\eta}\right) = \frac{u_*^2}{\nu}\left(\frac{df}{dy_+}\right) . \tag{2.51}$$

Multiplying the above equation by y/h, we have

$$\eta\left(\frac{dF}{d\eta}\right) = y_+\left(\frac{df}{dy_+}\right) = \frac{1}{\kappa}\,, \tag{2.52}$$

where κ is the von Karman constant. The inertial sublayer represents the part of the flow where Eq. (2.52) is satisfied, since the left-hand side is a function of η and the (RHS) is a function of y_+. Thus, Eq. (2.52) can be integrated as

$$F(\eta) = \frac{1}{\kappa}\ln\eta + const\,, \tag{2.53}$$

$$f(y_+) = \frac{1}{\kappa}\ln y_+ + const\,, \tag{2.54}$$

such that the equations above are valid only if $\eta \ll 1$ and $y_+ \gg 1$. Substituting Eq. (2.45) into Eq. (2.54), one obtains the classical logarithmic profile (Tennekes and Lumley, 1972; Monin and Yaglom, 1975)

$$\frac{u}{u_*} = \frac{1}{\kappa}\ln y_+ + B\,. \tag{2.55}$$

The logarithmic law (2.55) is not applicable at very short distances from the wall and gives negative infinity on the wall, $y = 0$, since the effect of the viscosity then becomes important, and cannot be neglected (Landau and Lifshitz, 1981).

In our analysis, we adopt a modelling assumption that, the entire flow from the bottom to the surface is one inertial boundary layer. Using $B = 5.5$ and $\kappa = 0.4$ provides an agreement between the inner and outer regions of the developed boundary flow and ensures that the layer has universal velocity structure (Nikuradse, 1932; Keulegan, 1938). The constants $B = 5.5$ and $\kappa = 0.4$ were firstly established by Nikuradse (1932) for hydraulically smooth pipe flow. Keulegan (1938) adopted the same values of the constants for smooth open channels. Coles (1956) showed that the law of the wall is well represented by equation (2.55) when using $\kappa = 0.4$ and $B = 5.1$. Huffman and Bradshaw (1972) used the values $B = 5.0$ and $\kappa = 0.41$. More recently, Steffler et al. (1985) adopted the values $B = 5.5$ and $\kappa = 0.4$ and presented some turbulence measurements for uniform flow in a smooth rectangular channel. They found that the velocity measurements in the viscous sublayer agree well with the linear form of the law of the wall.

2.1.7 Power velocity profile

Barenblatt (1993, 2000, 2003) put forward an alternative theory of the boundary layer. Again, consider stationary homogeneous shear in the direction of the mean flow bounded by a rigid wall, e.g. channel flow. The mean velocity gradient, $\partial u/\partial y$, in the inertial layer, suggested by dimensional analysis, is $\partial u/\partial y = u_*/y\,\Phi(y_+, \mathrm{Re})$, where Re is the Reynolds number, $y_+ = u_* y/\nu$ the dimensionless coordinate, y the distance from the bottom, u_* the friction velocity, ν the kinematic molecular viscosity and Φ the dimensionless function. In the 1930s, von Karman neglected the viscous sub-layer by assuming that at $y_+ \to \infty$ and $\mathrm{Re} \to \infty$, the function Φ tends to a finite limit, so that $\Phi(y_+, \mathrm{Re}) = 1/\kappa$. This assumption leads to the classical logarithmic law of the form (2.55). This law is Reynolds-number independent for the mean velocity over the cross-section of a channel. Barenblatt argued that the assumption of von Karman is inadequate and showed that the influence of the viscosity and the Reynolds number should be taken into account in the inertial layer. Hereby, an alternative theory can be put forward based on the assumption that at large y_+, the finite limit of the function Φ does not exist. Instead, the function can be written in the form $\Phi = \gamma(\mathrm{Re}) y_+^{\alpha(\mathrm{Re})}$. For the functions $\gamma(\mathrm{Re})$ and $\alpha(\mathrm{Re})$, Barenblatt (2000) obtained the Reynolds-number-dependent scaling law

$$\Phi = \frac{u}{u_*} = (\gamma_0 \ln \mathrm{Re} + \gamma_1)\, y_+^{\frac{\zeta}{\ln \mathrm{Re}}}\,, \tag{2.56}$$

where the constants γ_0, γ_1, and α are universal. By comparing Eq. (2.56) with the most reliable data for turbulent pipe flows, he found

$$\zeta = \frac{3}{2}, \qquad \gamma_0 = \frac{1}{\sqrt{3}}, \qquad \gamma_1 = \frac{5}{2}\,, \tag{2.57}$$

with the Reynolds number defined as

$$\mathrm{Re} = \frac{\overline{u} d}{\nu}\,. \tag{2.58}$$

Here $\overline{u}$ is the average velocity across the pipe and d the pipe diameter. Substituting Eq. (2.57) and Eq. (2.58) into Eq. (2.56), we have

$$\Phi = \left(\frac{1}{\sqrt{3}} \ln \mathrm{Re} + \frac{5}{2}\right) y_+^{\frac{3}{2 \ln \mathrm{Re}}}\,.$$

Subsequently he extended this theory to turbulent boundary layers near walls or other forms of rigid boundaries.

2.2 Centre manifold theory

This section describes the basics of the centre manifold approach and mainly follows Roberts (1989) and Mercer and Roberts (1990).

2.2.1 An introduction to centre manifolds

In this section we elaborate in more detail on the mathematical concept of centre manifold and the associated approach to dynamical systems in general as described in Carr (1981). In our dissertation it will be coupled with the theories of turbulent boundary layer to study dispersion. Let

$$\begin{aligned} dx/dt &= Ax + f(x,y)\,, \\ dy/dt &= By + g(x,y)\,, \end{aligned} \tag{2.59}$$

be a dynamical system, where $x \in R^n$; $y \in R^m$; A and B are constant matrices; and f and g are sufficiently smooth. Note that the notations in this section are independent of those in other sections, for example, x and y have nothing to do with the coordinates x and y in a channel.

Definition 1 *A curve $y = h(x)$, defined for $|x|$ small, is called an invariant manifold for the system Eq. (2.59) , if the solution $x(t)$ of Eq. (2.59) evaluated at x_0 belongs to $h(x)$, that is, $y(t) = h(x(t))$.*

Definition 2 *A smooth invariant manifold $y = h(x)$ of the system above is said to be a centre manifold of the origin, $h(0) = 0$ ($h'(0) = 0$), and the requirement that the spectrum of A is pure imaginary and the spectrum of B has real-part negative and bounded away from zero.*

The smooth functions, f and g, satisfy $f(0,0) = 0$, $f'(0,0) = 0$, $g(0,0) = 0$ and $g'(0,0) = 0$, where g' is defined to be the Jacobian matrix of g. In case that f and g are both zero, the system Eq. (2.59) has two invariant manifolds, stable manifold, $x = 0$, and centre manifold, $y = 0$. As $t \to \infty$, the solutions of the system tend exponentially fast to solutions of $dx/dt = Ax$. This illustrates how the centre manifold reduces the dimension of the dynamical system, that is, we only need to study the evolution of a first order equation on an invariant manifold. The situation is more complex, if f and g are non-zero. Below we present some results of the centre manifold theory (Carr, 1981; Watt and Roberts, 1995) which enable us to solve the system for the centre manifold.

Theorem 1 *The system Eq. (2.59) has a centre manifold $y = h(x)$ such that $|x|$ is small, h is C^2, and the evolution on the centre manifold is governed by the n-dimensional system*

$$du/dt = Au + f(u, h(u))\,, \tag{2.60}$$

where u is a new variable to parameterise the location of the system on the centre manifold. The following result includes what is needed to determine the asymptotic behaviour of small solutions of (2.59).

Theorem 2 *(1) If the zero solution of Eq. (2.60) is stable, asymptotically stable, or unstable, then the zero solution of Eq. (2.59) is stable, asymptotically stable, or unstable.*

(2) If the zero solution of Eq. (2.60) is stable and Eq. (2.59) has the solution $(x(t), y(t))$ with small $(x(0), y(0))$, then as $t \to \infty$, there exists a solution $u(t)$ of Eq. (2.60) such that

$x(t) = u(t) + \mathrm{O}(exp(-\gamma t))$ *and* $y(t) = h\left(u(t)\right) + \mathrm{O}(exp(-\gamma t))\,,$ *where $\gamma > 0$ is a constant.*

Now, we substitute $y(t) = h(x(t))$ into the second equation in Eq. (2.59), to get

$$h'(x)[Ax + f(x, h(x))] = Bh(x) + g(x, h(x))\,. \tag{2.61}$$

The equation Eq. (2.61) together with the conditions $h(0) = 0$, $h'(0) = 0$ form a system to solve. Define $M(\phi(x)) = \phi'(x)[Ax + f(x, \phi(x))] - B\phi(x) - g(x, \phi(x))$ in a neighborhood of the origin for C^1-functions, $\phi : R^n \to R^m$. The centre manifold can be approximated to any degree of accuracy according to the next result.

Theorem 3 *Let ϕ be a C^1-function defined in a neighborhood of the origin R^n into R^m such that $\phi(0) = 0$ and $\phi'(0) = 0$. If $M(\phi(x)) = \mathrm{O}(|x|^q)$, as $x \to 0$ and $q > 1$, then $|h(x) - \phi(x)| = \mathrm{O}(|x|^q)$, as $x \to 0$.*

As an illustration of the theorems above, consider the following example (Carr, 1981).

$$\begin{aligned} dx/dt &= xy + ax^3 + by^2x\,, \\ dy/dt &= -y + cx^2 + dx^2y\,. \end{aligned} \tag{2.62}$$

The system Eq. (2.62) has a centre manifold $y = h(x)$ [by theorem(1)]. Using the second equation of the system above we have

$$M(\phi(x)) = \phi'(x)[x\phi(x) + ax^3 + bx\phi^2(x)] + \phi(x) - cx^2 - dx^2\phi(x)\,.$$

If $\phi(x) = cx^2$ and $M(\phi(x)) = O(x^4)$, then $h(x) = cx^2 + O(x^4)$, [by theorem (3)]. Therefore, the equation which governs the flow [by theorem (2)] is

$$du/dt = uh(u) + au^3 + buh^2(u) = (a + c)u^3 + O(u^5)\,.$$

Then the zero solution of Eq. (2.62) is asymptotically stable if $a + c < 0$ and unstable if $a+c > 0$. If $a+c = 0$, then we have to find a better approximation to h. Let $a+c = 0$. Put $\phi(x) = cx^2+\psi(x)$, where $\psi(x) = O(x^4)$. Thus, $M(\phi(x)) = \psi(x) - cdx^4 + O(x^6)$. Therefore, $\phi(x) = cx^2 + cdx^4$, then $M(\phi(x)) = O(x^6)$. Hence, $h(x) = cx^2 + cdx^4 + O(x^6)$, [by theorem (3)]. The solution on the centre manifold is governed by

$$du/dt = uh(u) + au^3 + buh^2(u) = (cd + bc^2)u^5 + O(u^7)\,.$$

The zero solution of Eq. (2.62) is asymptotically stable if $cd+bc^2 < 0$, and unstable if $cd + bc^2 > 0$. If $cd + bc^2 = 0$, then we have to obtain a better approximation to h and so on.

2.2.2 Initial conditions for the averaged centre manifold model

The centre manifold theory states that if the linearised state of a continuous-time dynamical system has n zero eigenvalues and m eigenvalues with negative real parts only, then there is a locally defined smooth n-dimensional invariant manifold such that all nearby trajectories of the system are exponentially quickly attracted to the manifold. The theory applies in the locale of a fixed point, when linearised about the fixed point. This manifold is called the centre manifold. We refer to the book of Carr (1981) for a detailed description. Below is a simple illustrative example of a centre manifold. Let $c_0(x, y)$ be a given initial concentration, we want to find out the appropriate initial values of the depth-averaged concentration C for the centre manifold model (1.29) in order to ensure a long term agreement between the manifold model and the physical system. We consider the following dynamical system from Roberts (1989) to explain the mechanism of the centre manifolds and to demonstrate how the initial conditions for the centre manifold

are derived.

$$\begin{aligned} dx/dt &= -xy\,, \\ dy/dt &= -y + x^2 - 2y^2\,. \end{aligned} \tag{2.63}$$

The linearised state of the system (2.63), $dx/dt = 0$, $dy/dt = -y$, is characterised by the zero eigenvalue for the slow variable x and the negative eigenvalue, -1, for the fast variable y. It can be shown (Mercer and Roberts, 1990) that all trajectories of (2.63) are attracted to the parabola

$$y = x^2 \tag{2.64}$$

called the centre manifold (see Fig. 2.1). If it was not for the nonlinear perturbative terms $x^2 - 2y^2$, the variable y would quickly fall onto the equilibrium state $y = 0$ (the analogue to quickly decaying vertical non-uniformities under diffusion) while x would stay in the neutral state $x =$const (analogue of the neutral state of constant concentration). For the full system (2.63) the trajectories drop onto the manifold or attractor, (2.64), on which the perturbation, $x^2 - 2y^2$, is comparable to the linear term, $-y$. On the manifold the motion is slow and described by $dx/dt = -xy$, where

$$y = x^2 \tag{2.65}$$

so that

$$dx/dt = -x^3\,. \tag{2.66}$$

On the manifold the variable y depends on t via x to which it is connected by (2.64).

For the dynamical system (2.63), Roberts (1989) described a procedure to estimate the starting point on the manifold to best match the long term behavior of a trajectory of the system (2.63) which is initially at the point (x_0, y_0) off the centre manifold. Following Roberts, the evolution on a particular trajectory may be written as

$$x = \left[1/x_0^2 + 2(t+\tau) - \tau e^{-t}/x_0^2\right]^{-1/2} + O(\psi^2)\,, \tag{2.67}$$

where $\tau = (y_0/x_0^2 - 1)\exp(y_0/x_0^2 - 1)$ and ψ has a constant value, which characterises the trajectory. Following Roberts (1985), the equations for the trajectories can be written in the form

$$\psi(x,y) = \left(\frac{y}{x^2} - 1\right)\exp\left(\frac{1+2y}{2x^2}\right)\,, \tag{2.68}$$

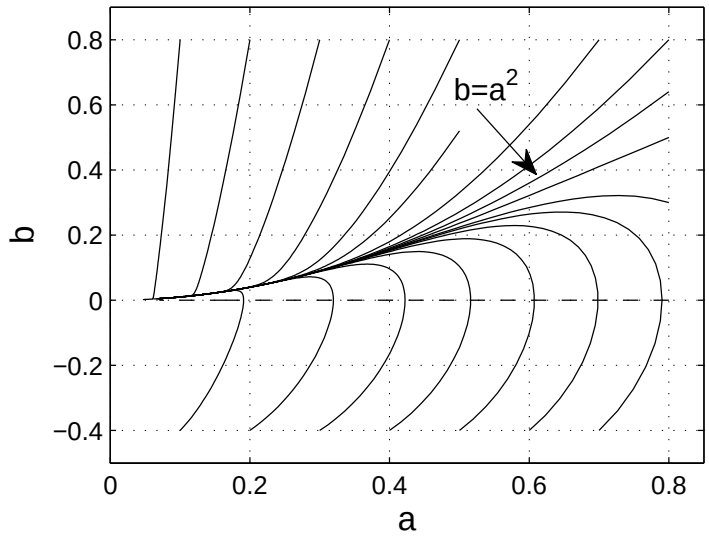

Figure 2.1 Attraction of the trajectories to parabola $b = a^2$ is system (2.63) (Strunin, 2011).

where ψ has a constant value, which characterizes the trajectory. The trajectories off the centre manifold, ψ is small, are given as

$$y = x^2 + \psi x^2 \exp\left[-\left(\frac{1}{2x^2} + 1\right)\right] + O(\psi^2)\,,$$

such that the evolution of the system on this trajectory is governed by

$$x = \left[C + 2t - 2\psi \exp\left(-1 - C - t\right)\right]^{-1/2} + O(\psi^2)\,, \tag{2.69}$$

where C is a constant. The constant C is found to be $C = 1/x^2 + 2\tau$ where $\tau = (y_0/x_0^2 - 1)\exp(y_0/x_0^2 - 1)$, taking into account that the system is initially at the point (x_0, y_0) with $t = 0$. Eq. (2.67) is found by substituting the value of C into Eq. (2.69). If the trajectory is on the centre manifold, that is $y_0 = x_0^2$, then $\tau = 0$ and $\psi = 0$ and the evolution on the real trajectory, $x = [1/x_0^2 + 2t]^{-1/2}$, is identical to the centre manifold solution. If the trajectory (2.67) is initially off the centre manifold, then there are two effects on the long term evolution of the system: the effect of the exponential term $-\tau e^{-t}/x_0^2$, which is negligible as time increases, and the effect of the time shift τ. Roberts argues that the time shift τ is a significant long term effect of initially being off the centre manifold. In order to obtain quick convergence, he calculated an initial point different to x_0, say s_0, on the centre manifold which best corresponds to the full system initially being at a point (x_0, y_0) off the centre manifold. Since the values of x_0 and y_0 are small

then $\tau \approx (y_0/x_0^2 - 1)$. Eq. (2.67) can be rewritten

$$x \approx \left[1/x_0^2 + 2t + 2\tau\right]^{-1/2} + O(\psi^2)\,. \tag{2.70}$$

Now denote $1/x_0^2 + 2\tau$ as $1/s_0^2$. This defines the point on the centre manifold, which is initially at $x = s_0$ and moves so that the actual motion approaches it exponentially quickly. As a result, the solution on the centre manifold, $x \approx [1/s_0^2 + 2t]^{-1/2}$, converges exponentially quickly to a solution off the centre manifold $x = [1/x_0^2 + 2t - \tau e^{-t}/x_0^2]^{-1/2} + O(\psi^2)$, where $s_0 = x_0 - x_0(y_0 - x_0^2) + O(\psi^2)$.

If the trajectory off the centre manifold starts at (x_0, y_0), then the x-solution will converge to the x-solution for the trajectory that starts at $y = x_0^2$ on the manifold after a sufficiently large time. Rewrite Eq. (2.70)

$$x \approx \frac{1}{\sqrt{2t}}\left[1 + \frac{2\tau + 1/x_0^2}{2t}\right]^{-1/2} + O(\psi^2)$$

and expand into the Taylor's series

$$x \approx \frac{1}{\sqrt{2t}}\left[1 - \frac{2\tau + 1/x_0^2}{4t} + \ldots\right] + O(\psi^2)\,. \tag{2.71}$$

In the limit $t \to \infty$, $x \to 1/\sqrt{2t}$ asymptotically. See that $(2\tau + 1/x_0^2)/t$ is the relative discrepancy between $1/\sqrt{2t}$ and the (RHS) of Eq. (2.71); it decreases with time. Therefore, the long term evolution of the system (2.63) started off the centre manifold still converges to the centre manifold only not as fast as when it started from $x = s_0$. It is a matter of how long we are willing to wait until the motion approaches the centre manifold. In our problem of dispersion we wait for long enough time for the approach to occur. Thus, we choose not to construct a special initial condition that is similar to $x = s_0$ in the example above, although it undoubtedly makes the convergence faster. Note that Chatwin (1970) and more recently Roberts and Strunin (2004) did construct such an initial condition in their dispersion problem.

In the next sub-section, the mechanism of centre manifolds is formalized in the case of dispersion.

2.2.3 Dispersion in shear flows with longitudinal diffusion neglected

Consider the flow in a channel. There are two competing factors that govern the distribution of contaminants: (i) the cross-flow diffusion which tends to quickly spread the contaminant in the vertical direction and ensure smooth distribution

in this direction; and (ii) the velocity shear which creates non-uniformity of the concentration across the channel, thus acting as an opposite factor to the diffusion. As a result of simultaneous action of these competing factors, the contaminant evolves relatively slowly in space and time reaching a regime when the centre manifold approach can be applied. Let us show, following Mercer and Roberts (1990), how this problem is formulated mathematically. Performing the Fourier transformation of Eq. (1.31) one gets

$$\frac{\partial \hat{c}}{\partial t} = L[\hat{c}] - iku(y)\hat{c}\,, \tag{2.72}$$

where $\hat{c}(y,k,t)$ is the Fourier transform defined by $\hat{c} = \frac{1}{2\pi}\int_{-\infty}^{\infty} \exp(-ikx)c\,dx$. The linear operator $L[\hat{c}] = \frac{\partial}{\partial y}[D(y)\frac{\partial \hat{c}}{\partial y}]$ expresses the cross-flow turbulent diffusion and has a discrete spectrum of eigenvalues. One of the eigenvalues is equal to zero; it corresponds to the neutral eigenmode $\hat{c} = const$, that is an arbitrary constant level of concentration across the channel. All the other eigenvalues are negative; they correspond to decaying non-uniformities of the concentration across the channel due to the diffusion provided that there is no flux through the boundaries. Consider a simple case for which the diffusion coefficient $D(y)$ is constant (Strunin, 2011). The diffusion equation for this case, $\partial\hat{c}/\partial t = D(\partial^2\hat{c}/\partial y)$, complemented by the boundary conditions (1.32) gives $\hat{c} = e^{\lambda t}\cos(ky)$, where the spectrum of eigenvalues λ_m is discrete, $\lambda_m = -Dk_m^2$, $k_m = \pi m/h$, $m = 0, 1, ...$. All λ_m are negative except for $\lambda_0 = 0$ corresponding to the neutral eigenmode $\hat{c} = \text{const}$. The negative eigenvalues, λ_m, correspond to decaying non-uniformities of the concentration across the channel due to the diffusion. The case of non-constant diffusion coefficient, $D(y)$, is just a generalization of this case. After sufficiently long time, variations of the concentration along the channel, that is in x direction, become slow; accordingly we suppose that the wave number k is small. We add to Eq. (2.72) the trivial equation $\partial_t k = 0$, just in order to pretend that k is a variable and, consequently, the shear-associated advection term $-iku(y)\hat{c}$ in Eq. (2.72) is nonlinear. This is just a little trick aimed at treating the advection term as a nonlinear perturbation in similarity to $x^2 - 2y^2$ in Eq. (2.63). Then the dynamics exponentially quickly evolve to a low-dimensional state, where each of the fast modes depends on t via the slow neutral mode.

Now, we need to explain how slow the variations should be (in other words, how small the wave number "k" should be, as "k" is the inverse of the typical length of the variation). Let us treat the advection (shear) term in the basic equation (2.72) as a perturbation with respect to the vertical diffusion. formally, we can even treat the wave number k as a variable satisfying the trivial equation $\partial_t k = 0$. Thus, formally the term $k\hat{c}$ becomes "nonlinear perturbation". We suppose that it is small compared to the vertical diffusion, giving $kU \ll D/h^2$, where U is the characteristic mean velocity of the flow. From here we evaluate how small the wave number should be: $k \ll D/(h^2U)$. One can obtain the same relation realising that the characteristic time of vertical mixing, h^2/D, should be much smaller than the characteristic time required for the substance particles to pass the horizontal distance $1/k$ with the velocity U, that is the time $1/(Uk)$. This

yields $h^2/D \ll 1/(Uk)$, from where $k \ll D/(h^2U)$ as before.

As a measure of the "amplitude" of the neutral mode we choose the depth-averaged concentration, $\hat{C}$. As a result, we have

$$\hat{c} = \hat{c}(\hat{C}, k, y) \quad \text{such that} \quad \frac{\partial \hat{C}}{\partial t} = G(\hat{C}, k)\,. \tag{2.73}$$

The first part of Eq. (2.73) is analogous to (2.65) and the second part analogous to (2.66). With Eq. (2.73) taken into account, equation (2.72) becomes

$$L[\hat{c}] = \frac{\partial \hat{c}}{\partial \hat{C}} G + iku\hat{c}\,. \tag{2.74}$$

Taking into account that the original problem is linear in $\hat{c}$, we assume asymptotic expansion for $\hat{c}$ and G which is also linear in $\hat{C}$, that is,

$$\hat{c} = \sum_{n=0}^{\infty} c_n(y)(ik)^n \hat{C}\,, \quad G = \sum_{n=1}^{\infty} g_n (ik)^n \hat{C}\,. \tag{2.75}$$

The definition of $\hat{C}$ as the depth-averaged implies the conditions

$$\frac{1}{h}\int_0^h c_0\, dy = 1\,, \quad \int_0^h c_n\, dy = 0 \quad \text{for } n = 1, 2, \ldots \tag{2.76}$$

Substituting Eq. (2.75) into Eq. (2.74) and collecting similar terms in powers of the small parameter k we obtain a sequence of equations for the unknown functions $c_n(y)$ and coefficients g_n,

$$L[c_0] = 0\,, \tag{2.77}$$

$$L[c_n] = \sum_{m=1}^{n} c_{n-m} g_m + u(y) c_{n-1} \quad \text{for } n = 1, 2, \ldots \tag{2.78}$$

Integrating Eq. (2.78) over the depth we get $D\frac{\partial c}{\partial y}\Big|_{y=h} - D\frac{\partial c}{\partial y}\Big|_{y=0} = g_n + \overline{u(y)c_{n-1}}$, where the over-line means depth-averaged. Once the fluxes through the boundaries are zero, $D\frac{\partial c}{\partial y}\Big|_{y=h} = D\frac{\partial c}{\partial y}\Big|_{y=0} = 0$, then

$$g_n = -\overline{u(y)c_{n-1}} \quad \text{for } n = 1, 2, \ldots \tag{2.79}$$

Successively we can calculate g_n and c_n for any desired n. Considering only three

leading terms in the G series in Eq. (2.75) gives a relatively short approximate version of the averaged model

$$\frac{\partial \hat{C}}{\partial t} = g_1(ik)\hat{C} + g_2(ik)^2\hat{C} + g_3(ik)^3\hat{C} + \dots \tag{2.80}$$

Now, applying the inverse Fourier transform to (2.80), we obtain the (1-D) advection-diffusion equation (1.29) for the averaged concentration. In applying the inverse Fourier transform to Eq. (2.80), we are band-limited to small enough wave number for which the centre manifold approach is useful. Further terms in this equation will also be of interest to us in the proposed research.

Chapter 3

Modeling dispersion in laminar and turbulent flows in an open channel based on centre manifolds using 1D-IRBFN method

This chapter presents a direct numerical verification of the centre manifold method with examples of the dispersion in laminar and turbulent flows in an open channel with a smooth bottom. The one-dimensional integrated radial basis function network (1D-IRBFN) method is used as a numerical approach to compute solution of the original two-dimensional (2-D) advection-diffusion equation. The 2-D solution is depth-averaged and compared with the solution of the 1-D equation derived using the centre manifolds. The numerical results will show that the 2-D and 1-D solutions are in good agreement both for the laminar flow and turbulent flow. The maximum depth-averaged concentrations for the 1-D and 2-D models gradually converge to each other, with their velocities becoming practically equal. The obtained numerical results also demonstrate that the longitudinal diffusion is relatively small compared to the advection.

3.1 Introduction

An asymptotic evolution equation governing the cross-flow averaged concentration of contaminants and other substances can be effectively used for prediction of the spreading of the substances in environmental and industrial flows. As was mentioned in Chapter 2, Taylor (1953, 1954) constructed an advection-diffusion equation describing the averaged concentration along a channel using half-empirical arguments. The equation was proposed for both laminar and turbulent pipe flows and it is applicable asymptotically at large times when spatial

variations of the concentration along the channel become slow. The work of Taylor was followed by an extensive research on modelling the dispersion in shear flows, with a variety of techniques used (Aris, 1956; Elder, 1959; Smith, 1987).

Such an equation can be analytically constructed using a more accurate method based on centre manifold theory. The method was proposed in a series of works originated by Roberts. In 1985, Roberts applied the method of Coullet and Spiegel (1983) to some simple examples to show the existence of the centre manifold and corresponding evolution equation in terms of the evolution of the amplitudes of some dominant modes. The centre manifold theory has been applied to describe the dispersion in a laminar channel flow and showed how to derive appropriate initial conditions for the asymptotic model (Mercer and Roberts, 1990).

Roberts and Strunin (2004) used two-zone model of contaminant dispersion in Poiseuille channel flow based on the centre manifolds in order to obtain more accurate approximations. They validated the analysis by direct computations of the original two-dimensional equations; and formulated modified initial conditions to obtain a better agreement between the manifold solution and the real solution. Strunin (2011) analysed the transport of contaminants in turbulent boundary layers of two types, namely the classical logarithmic velocity profile and according to an alternative model, power velocity profile. Strunin assumed steady flow with slow variation in the contaminant concentration in space and time.

In this chapter, by following Mohammed, Ngo-Cong, Strunin, Mai-Duy and Tran-Cong (2014), the one-dimensional integrated radial basis function network (1D-IRBFN) is used as numerical method for modelling dispersion of contaminants in an open channel. This numerical method with the use of integration instead of conventional differentiation to construct the RBF approximations significantly improved the accuracy and stability of numerical solution. The method was developed by Mai-Duy and Tanner (2007) and applied to several engineering problems such as structural analysis (Le et al., 2010; Ngo-Cong et al., 2011), viscous and viscoelastic flows (Ngo-Cong et al., 2012b; Ho-Minh et al., 2012; Tran et al., 2012), and fluid-structure interaction (Ngo-Cong et al., 2012a).

The chapter is organised as follows. In Section 3.2, we briefly describe the modelling of dispersion based on centre manifold theory, followed by a discussion of the numerical approach in Section 4.4. Section 3.4 discusses the modelling of turbulent dispersion in an open channel. In section 3.5, the numerical approach is verified, followed by the discussion on numerical results in Section 4.5. Section 3.7 concludes the chapter.

In the next section, the mechanism of centre manifolds is formalized in the case of shear dispersion.

3.2 Modelling dispersion based on centre manifold theory

We consider the 2-D advection-diffusion equation

$$\partial_t c + u(y)\partial_x c = \partial_y[D(y)\partial_y c]\,, \tag{3.1}$$

where $u(y)$ is the velocity of the flow in the channel supposed known; c the contaminant concentration; and $D(y)$ the diffusion coefficient which is responsible for the turbulent diffusion across the channel and defined by

$$D(y) = K\frac{u_*^2}{\partial_y u}\,, \tag{3.2}$$

in which u_* is the friction velocity and the (non-dimensional and positive) proportionality coefficient K may generally depend on the Schmidt number (Barenblatt, 2003). The boundary conditions describe non-penetration through the bottom ($y = 0$) and surface ($y = h$, h is the channel height),

$$D\partial_y c|_{y=0} = D\partial_y c|_{y=h} = 0\,. \tag{3.3}$$

We then convert the model (3.1)–(3.3) into the equation for the averaged concentration C_1 using the centre manifolds (Section 2.2),

$$\partial_t C_1 = g_1\partial_x C_1 + g_2\partial_x^2 C_1 + g_3\partial_x^3 C_1 \ldots\,. \tag{3.4}$$

The coefficients g_1, g_2 and g_3 are responsible for the advection, diffusion and dispersion, respectively, and are analytically derived as shown in Section 2.2. We do not include the along-the-flow component of the diffusion, $D_L\partial_x^2 c$, although this can be done without difficulty. In Sub-section 3.6.3, we show that this term does not significantly affect the averaged model.

Our plan is to solve the original (2-D) transport equation (3.1) with some initial conditions to determine $c(x, y, t)$ after a long elapsed time, then compute the averaged concentration as $C_2(x, t) = \frac{1}{h}\int_0^h c(x, y, t)\,dy$ and compare it with the solution $C_1(x, t)$ obtained from (3.4). We expect that the two solutions converge to each other, which confirms the correctness of the averaged model. Several numerical examples on dispersion modelling using the centre manifolds are investigated and reported in Section 4.5.

3.3 Numerical approach: one-dimensional integrated radial basis function networks (1D-IRBFN)

In this section, we briefly describe the 1D-IRBFN methods developed by Mai-Duy and Tanner (2007) including 1D-IRBFN-2 and 1D-IRBFN-4 schemes, with the full details given in Appendix B. The domain of interest is discretised using a Cartesian grid, i.e. an array of straight lines that run parallel to the x- and y-axes as shown in Fig. 3.1. The dependent variable u and its derivatives on each grid line are approximated using an IRBFN interpolation scheme as described in the remainder of this section.

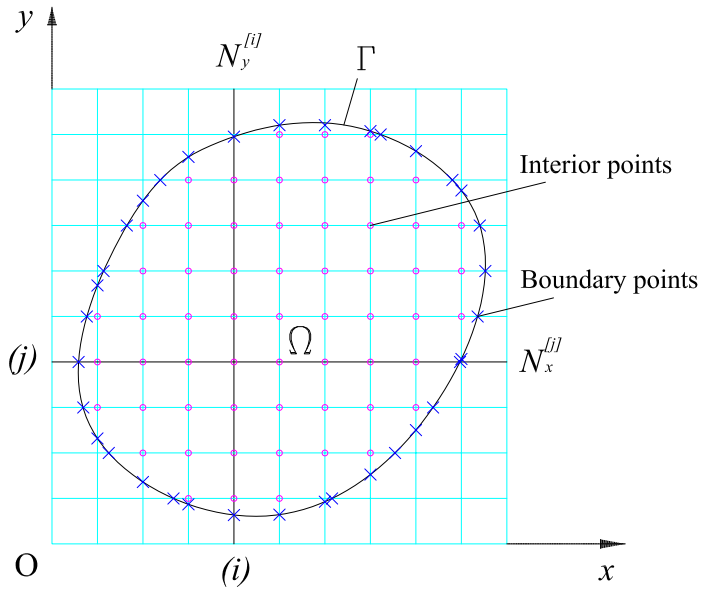

Figure 3.1 Cartesian grid.

3.3.1 Second-order 1D-IRBFN (1D-IRBFN-2 scheme)

Consider an x-grid line, e.g. $[j]$ (Fig. 3.1). The variation of u along this line is sought in the IRBF form. The second-order derivative of u is decomposed into RBFs; the RBF network is then integrated once and twice to obtain the expressions for the first-order derivative of u and the solution u itself,

$$\frac{\partial^2 u(x)}{\partial x^2} = \sum_{i=1}^{N_x^{[j]}} w^{(i)} G^{(i)}(x) = \sum_{i=1}^{N_x^{[j]}} w^{(i)} H_{[2]}^{(i)}(x)\,, \tag{3.5}$$

$$\frac{\partial u(x)}{\partial x} = \sum_{i=1}^{N_x^{[j]}} w^{(i)} H_{[1]}^{(i)}(x) + p_1\,, \tag{3.6}$$

$$u(x) = \sum_{i=1}^{N_x^{[j]}} w^{(i)} H_{[0]}^{(i)}(x) + p_1 x + p_2 \,, \tag{3.7}$$

where $N_x^{[j]}$ is the number of nodes on the grid line $[j]$; $\{w^{(i)}\}_{i=1}^{N_x^{[j]}}$ RBF weights to be determined; $\left\{G^{(i)}(x)\right\}_{i=1}^{N_x^{[j]}} = \left\{H_{[2]}^{(i)}(x)\right\}_{i=1}^{N_x^{[j]}}$ known non-local RBFs; $H_{[1]}^{(i)}(x) = \int H_{[2]}^{(i)}(x)dx$; $H_{[0]}^{(i)}(x) = \int H_{[1]}^{(i)}(x)dx$; and p_1 and p_2 integration constants which are also unknown. An example of RBF, used in this work, is the multiquadrics $G^{(i)}(x) = \sqrt{(x - x^{(i)})^2 + a^{(i)2}}$, $a^{(i)}$ - the RBF width determined as $a^{(i)} = \beta d^{(i)}$, β a positive factor, and $d^{(i)}$ the distance from the i^{th} centre to its nearest neighbour. The new basis functions $H_{[1]}^{(i)}(x)$ and $H_{[0]}^{(i)}(x)$ obtained from integrating the multiquadrics $G^{(i)}(x)$ are as follows.

$$H_{[1]}^{(i)}(x) = \frac{r}{2}A + \frac{\left(a^{(i)}\right)^2}{2}B, \tag{3.8}$$

$$H_{[0]}^{(i)}(x) = \left(\frac{r^2}{6} - \frac{\left(a^{(i)}\right)^2}{3}\right)A + \frac{\left(a^{(i)}\right)^2 r}{2}B, \tag{3.9}$$

in which $r = x - x^{(i)}$, $A = \sqrt{r^2 + a^{(i)2}}$, and $B = \ln(r + A)$.

3.3.2 Fourth-order 1D-IRBFN (1D-IRBFN-4 scheme)

The 1D-IRBFN-4 scheme is used to solve 1-D third- and fourth-order differential equations (Eqs. (3.27) and (3.45)). Consider a 1-D computational domain (a line) with N_x points. The variation of u along this line is sought in the IRBF form. The fourth-order derivative is decomposed into RBFs. The RBF networks are then integrated to obtain the lower-order derivatives and the function itself,

$$\frac{\partial^4 u(x)}{\partial x^4} = \sum_{i=1}^{N_x} w^{(i)} G^{(i)}(x) = \sum_{i=1}^{N_x} w^{(i)} H_{[4]}^{(i)}(x) \,, \tag{3.10}$$

$$\frac{\partial^3 u(x)}{\partial x^3} = \sum_{i=1}^{N_x} w^{(i)} H_{[3]}^{(i)}(x) + p_1 \,, \tag{3.11}$$

$$\frac{\partial^2 u(x)}{\partial x^2} = \sum_{i=1}^{N_x} w^{(i)} H_{[2]}^{(i)}(x) + p_1 x + p_2 \,, \tag{3.12}$$

$$\frac{\partial u(x)}{\partial x} = \sum_{i=1}^{N_x} w^{(i)} H_{[1]}^{(i)}(x) + \frac{p_1}{2}x^2 + p_2 x + p_3 \,, \tag{3.13}$$

$$u(x) = \sum_{i=1}^{N_x} w^{(i)} H_{[0]}^{(i)}(x) + \frac{p_1}{6}x^3 + \frac{p_2}{2}x^2 + p_3 x + p_4 \,, \tag{3.14}$$

where $\left\{G^{(i)}(x)\right\}_{i=1}^{N_x} = \left\{H_{[4]}^{(i)}(x)\right\}_{i=1}^{N_x}$ are known RBFs; $H_{[3]}^{(i)}(x) = \int H_{[4]}^{(i)}(x)dx$; $H_{[2]}^{(i)}(x) = \int H_{[3]}^{(i)}(x)dx$; $H_{[1]}^{(i)}(x) = \int H_{[2]}^{(i)}(x)dx$; $H_{[0]}^{(i)}(x) = \int H_{[1]}^{(i)}(x)dx$; $\{w^{(i)}\}_{i=1}^{N_x}$ are RBF weights to be determined; and p_1, p_2, p_3 and p_4 integration constants which are also unknown. The new basis functions $H_{[3]}^{(i)}(x)$, $H_{[2]}^{(i)}(x)$, $H_{[1]}^{(i)}(x)$ and $H_{[0]}^{(i)}(x)$ obtained from integrating the multiquadrics $G^{(i)}(x)$ are as follows.

$$H_{[3]}^{(i)}(x) = \frac{r}{2}A + \frac{\left(a^{(i)}\right)^2}{2}B, \tag{3.15}$$

$$H_{[2]}^{(i)}(x) = \left(\frac{r^2}{6} - \frac{\left(a^{(i)}\right)^2}{3}\right)A + \frac{\left(a^{(i)}\right)^2 r}{2}B, \tag{3.16}$$

$$H_{[1]}^{(i)}(x) = \left(-\frac{13\left(a^{(i)}\right)^2 r}{48} + \frac{r^3}{24}\right)A + \left(-\frac{\left(a^{(i)}\right)^4}{16} + \frac{\left(a^{(i)}\right)^2 r^2}{4}\right)B, \tag{3.17}$$

$$H_{[0]}^{(i)}(x) = \left(\frac{\left(a^{(i)}\right)^4}{45} - \frac{83\left(a^{(i)}\right)^2 r^2}{720} + \frac{r^4}{120}\right)A + \left(-\frac{3\left(a^{(i)}\right)^4 r}{48} + \frac{4\left(a^{(i)}\right)^2 r^3}{48}\right)B. \tag{3.18}$$

3.4 Application to turbulent dispersion in an open channel

Original 2-D model: Consider a turbulent shear flow in an open channel as presented in Strunin (2011). The concentration of contaminant is described by the 2-D advection-diffusion equation (3.1), (hereafter all quantities are non-dimensional)

$$\frac{\partial c}{\partial t} + u(y)\frac{\partial c}{\partial x} = \frac{\partial}{\partial y}\left(D(y)\frac{\partial c}{\partial y}\right), \tag{3.19}$$

where the diffusion coefficient $D(y)$ is represented by (3.2), and the velocity obeys the classical logarithmic law,

$$u(y) = (1/\kappa)\ln(Ry) + B\,. \tag{3.20}$$

where $R = 6000$, *and* $B = 5.5$, $\kappa = 0.4$ and $K = 1$.

The logarithmic law (3.20) is a classical model for turbulent boundary layer described in many books, e.g., Monin and Yaglom (1975). This law is valid in the region $\epsilon < y < 1$ ($\epsilon = 50/R \gg 5/R = h_1/h$, where h_1 is the width of the viscous sublayer). At large Reynolds numbers the value of ϵ is small. Actually, in the present computations we use $\epsilon = 5/R$ but the large Reynolds number $R = 6000$

ensures that both $5/R$ and $50/R$ are small. We note that Eq. (3.4) was derived under the assumption of smallness of ϵ.

We use $B = 5.5$ and $\kappa = 0.4$ because of the following reason: In our analysis, it is convenient that the entire flow from the bottom to the surface is one inertial boundary layer. Using $B = 5.5$ and $\kappa = 0.4$ provides an agreement between the inner and outer regions of the developed boundary flow and ensures that the layer has universal velocity structure (Nikuradse, 1932; Keulegan, 1938). Nikuradse (1932) first found the constants $B = 5.5$ and $\kappa = 0.4$ for hydraulically smooth pipe flow. In 1938, Keulegan assumed that the same values for these constants can be adopted for smooth open channels. In the literature, these empirical constants can have different values. An extensive survey of mean velocity profile measurements in various 2-D turbulent boundary layer flows by Coles (1956) showed that the law of the wall is well represented by equation (3.20) when using $\kappa = 0.4$ and $B = 5.1$. Huffman and Bradshaw (1972) used the values $B = 5.0$ and $\kappa = 0.41$. More recently, Steffler et al. (1985) adopted the values $B = 5.5$ and $\kappa = 0.4$ and presented some turbulence measurements for uniform flow in a smooth rectangular channel. They found that the velocity measurements in the viscous sublayer agree well with the linear form of the law of the wall.

We consider Eq. (3.19) in a rectangular domain $x_A \leq x \leq x_B, \epsilon \leq y \leq 1$ as shown in Fig. 3.2, subject to the boundary conditions:

$$c = 0 \text{ on } x = x_A \,, \tag{3.21}$$

$$c = 0 \text{ on } x = x_B \,, \tag{3.22}$$

$$\frac{\partial c}{\partial y} = 0 \text{ on } y = \epsilon \,, \tag{3.23}$$

$$\frac{\partial c}{\partial y} = 0 \text{ on } y = 1 \,. \tag{3.24}$$

The initial condition is taken in the form of a cloud of the contaminant arbitrarily centered at $x_0 = -11.5$, $y_0 = 1$ (note that $x_A < x_0 < x_B$, and x_A and x_B are set to -100 and 100 at the initial moment, respectively),

$$c(x, y, 0) = \exp\left[-\left(0.1\,(x - x_0)\right)^4 - \left(7(y - y_0)\right)^4\right] \,. \tag{3.25}$$

The domains of interest are represented by Cartesian grids. Applying the Crank-Nicolson scheme to Eq. (3.19) in conjunction with the use of the 1D-IRBFN method for spatial discretisation leads to

$$\frac{c^{(n+1)} - c^{(n)}}{\Delta t} = \frac{F^{(n)}(x, y, t)}{2} + \frac{F^{(n+1)}(x, y, t)}{2} \,, \tag{3.26}$$

where $F(x, y, t) = -u(y)\partial c/\partial x + \kappa K \partial \left(y \partial c/\partial y\right)/\partial y$.

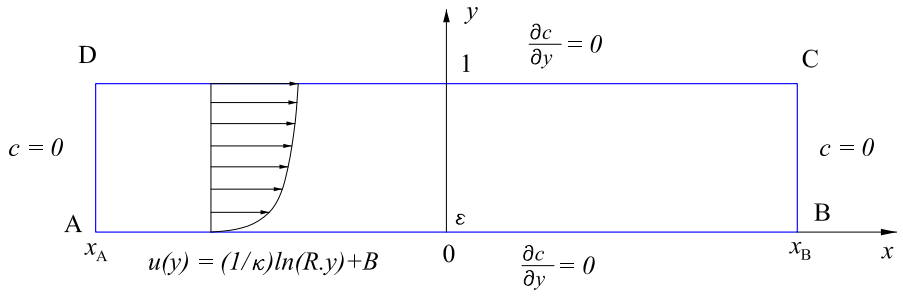

Figure 3.2 The shear flow in an open channel: the problem geometry and boundary conditions.

Low-dimensional depth-averaged 1-D one-zone model: In the present simulation, we take into account the first four derivatives in the RHS of (3.4) and ignore the higher-order derivatives, leading to the following equation

$$\frac{\partial C_1}{\partial t} \approx g_1 \frac{\partial C_1}{\partial x} + g_2 \frac{\partial^2 C_1}{\partial x^2} + g_3 \frac{\partial^3 C_1}{\partial x^3} + g_4 \frac{\partial^4 C_1}{\partial x^4}\,, \tag{3.27}$$

where as shown in Strunin (2011) $g_1 \approx -(1/\kappa)(\ln R - 1) + B$; $g_2 \approx 1/(4\kappa^3 K)$; and $g_3 \approx 17/(216\kappa^5 K^2)$ for the case of logarithmic velocity profile. Note that, the coefficients $g_i, i = 1, 2, 3$ are obtained at the limit of $\epsilon \to 0$ with assuming a very large Reynolds number R. In the present chapter we also calculate the next coefficient, g_4, through Eqs. (2.76)–(2.79) as follows: Substitution of $n = 3$ into Eq. (2.78) leads to

$$L\left[c_3\right] = \sum_{m=1}^{3} c_{3-m} g_m + u\left(y\right) c_{3-1} = c_1 g_2 + c_0 g_3 + c_2[g_1 + u\left(y\right)]\,, \tag{3.28}$$

where $u\left(y\right) = 1/\kappa \ln\left(R.y\right) + A/u_*$, $c_0 = 1$; and c_1 and c_2 were respectively defined by Strunin (2011) as follows.

$$c_1 = [\frac{1}{K\kappa^2}\left(y \ln y - y\right)],$$
$$c_2 = \frac{1}{4K^2\kappa^4}\left(-2y + \frac{y^2}{2} + 3y \ln y - 2y^2 \ln y + y^2 \ln^2 y + \frac{139}{108}\right).$$

Substituting these functions and coefficients into (3.28), we have

$$\begin{aligned}\frac{\partial}{\partial y}\left(y\frac{\partial c_3}{\partial y}\right) = \frac{1}{4K^3\kappa^6}\Bigg(&\frac{254}{108} - 3y + \frac{1}{2}y^2 + \frac{139}{108}\ln y + 2y \ln y \\ &-\frac{3}{2}y^2 \ln y + 3y \ln^2 y - y^2 \ln^2 y + y^2 \ln^3 y\Bigg)\,.\end{aligned} \tag{3.29}$$

Integrating Eq. (3.29) once, we get

$$y\frac{\partial c_3}{\partial y} = \frac{1}{4K^3\kappa^6}\left(\frac{115}{108}y - \frac{5}{4}y^2 + \frac{5}{27}y^3 + \frac{139}{108}y\ln y \right.$$
$$\left. -\frac{1}{2}y^2\ln y - \frac{1}{18}y^3\ln y + \frac{3}{2}y^2\ln^2 y - \frac{2}{3}y^3\ln^2 y + \frac{1}{3}y^3\ln^3 y\right) + B_1. \tag{3.30}$$

Applying the boundary conditions $y\frac{\partial c}{\partial y}|_{y=\epsilon} = y\frac{\partial c}{\partial y}|_{y=1} = 0$ to (3.30), we get $B_1 = 0$. Integrating Eq. (3.30) again, we get

$$c_3 = \frac{1}{4K^3\kappa^6}\left(-\frac{2}{9}y - \frac{1}{8}y^2 - \frac{1}{162}y^3 + \frac{139}{108}y\ln y - y^2\ln y \right.$$
$$\left. +\frac{11}{54}y^3\ln y + \frac{3}{4}y^2\ln^2 y - \frac{1}{3}y^3\ln^2 y + \frac{1}{9}y^3\ln^3 y\right) + B_2. \tag{3.31}$$

Applying the averages $\int_\epsilon^1 c_n\, dy = 0$ for $n = 1, 2, ...$ to Eq. (3.31), we obtain

$$\frac{1}{4K^3\kappa^6}\left(-\frac{187}{432}y^2 + \frac{1}{8}y^3 - \frac{283}{10368}y^4 + \frac{139}{216}y^2\ln y - \frac{1}{2}y^3\ln y \right.$$
$$\left. +\frac{89}{864}y^4\ln y + \frac{1}{4}y^3\ln^2 y - \frac{5}{48}y^4\ln^2 y + \frac{1}{36}y^4\ln^3 y\right)_\epsilon^1 + B_2 y|_\epsilon^1 = 0. \tag{3.32}$$

Taking the limit $\epsilon \to 0$, we get

$$B_2 = \frac{3475}{41472K^3\kappa^6}.$$

Substitution of the value of B_2 into Eq. (3.31) yields

$$c_3 = \frac{1}{4K^3\kappa^6}\left(\frac{3475}{10368} - \frac{2}{9}y - \frac{1}{8}y^2 - \frac{1}{162}y^3 + \frac{139}{108}y\ln y \right.$$
$$\left. -y^2\ln y + \frac{11}{54}y^3\ln y + \frac{3}{4}y^2\ln^2 y - \frac{1}{3}y^3\ln^2 y + \frac{1}{9}y^3\ln^3 y\right). \tag{3.33}$$

The value of g_4 is then calculated through Eq. (2.79) (see Sub-section 2.2.3)

$$g_4 = -\overline{u\,(y)\,c_3\,(y)} = -\int_\epsilon^1 \left[\frac{1}{\kappa}\ln\left(R\,y\right) + \frac{A}{u_*}\right] c_3\, dy$$
$$= -\int_\epsilon^1 \left[\frac{1}{\kappa}\ln R + \frac{1}{\kappa}\ln y + \frac{A}{u_*}\right] c_3\, dy = -\frac{1}{\kappa}\int_\epsilon^1 c_3\ln y\, dy,$$

or

$$g_4 = -\frac{1}{1-\epsilon}\frac{1}{4K^3\kappa^7}\left(-\frac{3475}{10368}y + \frac{163}{432}y^2 - \frac{25}{216}y^3 + \frac{89}{5184}y^4 + \frac{3475}{10368}y\ln y \right.$$
$$-\frac{163}{216}y^2\ln y + \frac{25}{72}y^3\ln y - \frac{89}{1296}y^4\ln y + \frac{139}{216}y^2\ln^2 y$$
$$\left.-\frac{7}{12}y^3\ln^2 y + \frac{29}{216}y^4\ln^2 y + \frac{1}{4}y^3\ln^3 y - \frac{1}{9}y^4\ln^3 y + \frac{1}{36}y^4\ln^4 y\right)_{\epsilon}^{1}.$$

Taking the limit $\epsilon \to 0$, we obtain

$$g_4 = -\frac{65}{4608K^3\kappa^7}\,.$$

Eq. (3.27) is subject to the boundary conditions

$$C_1 = 0,\ \frac{\partial C_1}{\partial x} = 0, \quad \text{at } x = x_A,\ x = x_B\,. \tag{3.34}$$

An initial condition (at $t = t_0$) for Eq. (3.27) is taken to be

$$C_1(x, t_0) = C_2(x, t_0), \tag{3.35}$$

where $C_2(x, t_0) = \frac{1}{(1-\varepsilon)}\int_{\varepsilon}^{1} c\,(x, y, t_0)\,dy$.

The spatial discretisation of first-order and second-order derivatives in Eq. (3.19) is carried out by using (3.5)–(3.7), while the first-order, second-order, third-order and fourth-order derivatives in Eq. (3.27) are discretised through (3.10)−−(3.14).

Note that the peak of depth-averaged concentration C (C can be C_1 or C_2) moves along the positive x-axis as time t goes on and the concentration on the inlet and outlet boundaries of the computational domain is assumed to be zero. In order to reduce the computational effort, the computational domain is regularly shifted along the x-axis after a period of time $\Delta\tau$. The strategy to shift the computational domain from time $t = \tau^{(k)}$ to time $t = \tau^{(k)} + \Delta\tau$ is described in Fig. 3.3. When creating a new computational domain, the inlet boundary is set at the position $x_{A'}$ where $C = \epsilon_C$, presently $\epsilon_C = 10^{-4}$. The concentration in the new region BB'C'C is assigned to be zero at the initial time $t = \tau^{(k)} + \Delta\tau$. The flowchart of numerical procedure is presented in Fig. 3.4.

3.5 Verification of the 1D-IRBFN method

Before computing the 1-D and 2-D models using the 1D-IRBFN method and comparing results, we need to verify the method. We consider an artificially constructed advection-diffusion equation with a source function,

$$\frac{\partial c}{\partial t} + u(y)\frac{\partial c}{\partial x} - \frac{\partial^2 c}{\partial y^2} = f(x, y, t)\,, \tag{3.36}$$

where $f(x, y, t) = 2\left(-t/(t^2+1) - xu(y) - 2y^2 + 1\right) e^{-(x^2+y^2)}/(t^2+1)$; and $u(y)$ is given by (3.20). It is easy to check that (3.36) has the analytical solution,

$$c(x, y, t) = e^{-(x^2+y^2)}/(t^2+1). \tag{3.37}$$

We solve Eq. (3.36) numerically in a rectangular domain $-0.5 \le x \le 0.5, \epsilon \le y \le 1$ with $\epsilon = 5/R$ using two cases of boundary conditions:

- Case 1: Dirichlet boundary conditions imposed along all four edges of the rectangular domain.
- Case 2: Dirichlet boundary conditions imposed along two horizontal edges, and Neumann boundary conditions imposed along two vertical edges.

We intend to demonstrate that the numerical solution by the 1D-IRBFN method well agrees with the analytical solution (3.37); this will justify the numerical method.

The boundary and initial conditions must be consistent with (3.37). The initial time moment is taken at $t_0 = 0$. Table 3.1 and Fig. 3.6 present the numerical results, namely, the relative error norms (Ne) of the present numerical method for Case 1 and Case 2. The relative error norm is calculated as

$$Ne = \sqrt{\frac{\sum_{i=1}^{N}\left(c^{(i)} - c_a^{(i)}\right)^2}{\sum_{i=1}^{N}\left(c_a^{(i)}\right)^2}}\,, \tag{3.38}$$

where the subscript "a" denotes the analytical solution; and N is the total number of unknown nodal values in the computational domain. Assuming that the solution is convergent with respect to the grid refinement, the behaviour of the error of the solution is assumed to be $Ne \approx \alpha h^{\lambda} = O(h^{\lambda})$, in which h is the grid spacing; and α and λ the parameters of the exponential model ($\lambda > 0$ is

the convergence rate). The convergence behaviour for Case 1 and Case 2 are $O(h^{3.54})$ and $O(h^{2.13})$, respectively. Fig. 3.7 shows a good agreement between the 1D-IRBFN results of y-average value of the variable c along the x-axis and the analytical solution at several times $t = 1.0, 2.0$ and 3.0.

Table 3.1 Two-dimensional advection-diffusion equation with source: Grid convergence study for 1D-IRBFN method at time t = 2.0, using a time step $\Delta t = 5.10^{-3}$.

Grid	Ne	
	Case 1	Case 2
21x21	9.01E-06	1.15E-03
31x31	2.58E-06	4.96E-04
41x41	9.82E-07	2.70E-04
51x51	4.14E-07	1.66E-04
61x61	1.75E-07	1.09E-04

3.6 Comparison of 1-D and 2-D dispersion models

3.6.1 Laminar shear flow in an open channel

Consider a shear flow in an open channel Fig. 3.5. Note that the direction of the y-axis is opposite to that in Fig. 3.2 so that the bottom is at $y = 1$, we follow Roberts and Strunin (2004). The concentration of contaminant obeys the 2-D non-dimensional advection-diffusion equation

$$\frac{\partial c}{\partial t} + u(y)\frac{\partial c}{\partial x} = \frac{\partial^2 c}{\partial y^2}\,, \tag{3.39}$$

where $u(y) = (3/2)Pe(1 - y^2)$; $Pe = Uh/D$ is the Peclet number, presently set to be 60; U the constant average downstream velocity; h the channel height; and D the constant coefficient of diffusion.

Roberts and Strunin (2004) considered two versions of the 2-D model. In the first version, they studied (3.39) in the entire channel domain $x_A \leq x \leq x_B, 0 \leq y \leq 1$. They called it a one-zone version. The boundary conditions are

$$c = 0, \text{ on } x = x_A\,, \tag{3.40}$$

$$c = 0, \text{ on } x = x_B\,, \tag{3.41}$$

$$\frac{\partial c}{\partial y} = 0, \text{ on } y = 0\,, \tag{3.42}$$

$$\frac{\partial c}{\partial y} = 0, \text{ on } y = 1\,. \tag{3.43}$$

As in Roberts and Strunin (2004), the initial condition is taken in the form

$$c(x,y,0) = 10\exp\left[-\left(0.1\,(x-x_0)\right)^4 - \left(7(y-y_0)\right)^4\right]\,, \tag{3.44}$$

with $x_0 = -11.5$, and $y_0 = 0$. The centre manifold theory leads to the following 1-D one-zone model for the flow

$$\frac{\partial C_1}{\partial t} = g_1\frac{\partial C_1}{\partial x} + g_2\frac{\partial^2 C_1}{\partial x^2} + g_3\frac{\partial^3 C_1}{\partial x^3}\,, \tag{3.45}$$

where $g_1 = -Pe,\ g_2 = Pe^2/30$ and $g_3 = -Pe^3/1575$ (Roberts and Strunin, 2004).

The boundary conditions and the initial condition for (3.45) are taken as (3.34) and (3.35), respectively, in which $c(x,y,t_0)$ is the 2-D concentration from the problem (3.39)–(5.62) at $t = t_0$.

In the second version, Roberts and Strunin (2004) subdivided the channel into two zones – slow near the bottom ($\alpha < y \le 1$) and fast near the surface ($0 \le y \le \alpha$), with $\alpha = 0.55$ as shown in Fig. 3.5. For the cross-zone averaged concentrations in the fast and slow zones, $C_{1f}(x,t)$ and $C_{1s}(x,t)$ respectively, they derived the equations

$$\frac{\partial C_{1f}}{\partial t} = a_1 C_{1f} + a_2 C_{1s} + a_3\frac{\partial C_{1f}}{\partial x} + a_4\frac{\partial C_{1s}}{\partial x} + a_5\frac{\partial^2 C_{1f}}{\partial x^2} + a_6\frac{\partial^2 C_{1s}}{\partial x^2}\,, \tag{3.46}$$

$$\frac{\partial C_{1s}}{\partial t} = b_1 C_{1f} + b_2 C_{1s} + b_3\frac{\partial C_{1f}}{\partial x} + b_4\frac{\partial C_{1s}}{\partial x} + b_5\frac{\partial^2 C_{1f}}{\partial x^2} + b_6\frac{\partial^2 C_{1s}}{\partial x^2}\,, \tag{3.47}$$

where $a_1 = -4.441,\ a_2 = 4.441,\ a_3 = -1.397Pe,\ a_4 = 0.0478Pe,\ a_5 = 9.68\times10^{-4}Pe^2,\ a_6 = -1.85\times10^{-3}Pe^2$; and $b_1 = 5.428,\ b_2 = -5.428,\ b_3 = -0.0461Pe,\ b_4 = -0.527Pe,\ b_5 = -1.78\times10^{-3}Pe^2,\ b_6 = 3.34\times10^{-3}Pe^2$. The depth-averaged concentration for the whole channel is

$$C_1(x,t) = \alpha C_{1f}(x,t) + (1-\alpha)C_{1s}(x,t)\,. \tag{3.48}$$

The system of Eqs. (3.46) and (3.47) is subject to the boundary conditions

$$C_{1f} = 0,\ \frac{\partial C_{1f}}{\partial x} = 0, \quad \text{at } x = x_A,\ x = x_B\,, \tag{3.49}$$

$$C_{1s} = 0,\ \frac{\partial C_{1s}}{\partial x} = 0, \quad \text{at } x = x_A,\ x = x_B\,. \tag{3.50}$$

In order to achieve the fastest (exponential) convergence of the 1-D and 2-D models, Roberts and Strunin derived the following initial conditions (Roberts and Strunin, 2004) for details. A similar derivation is discussed in a simple example

in Section 2.2).

$$
\begin{aligned}
C_{1f}(x,t_0) \approx & \int_0^1 \left(2.159 - 5.720y^2 + 4.705y^4 - 1.548y^6\right) c\,(x,y,t_0)\,dy \\
& + Pe \int_0^1 \left(-0.010 + 0.174y^2 - 0.482y^4 + 0.494y^6\right) \frac{\partial c\,(x,y,t_0)}{\partial x} dy\,, \\
C_{1s}(x,t_0) \approx & \int_0^1 \left(-0.417 + 6.991y^2 - 5.750y^4 + 1.892y^6\right) c\,(x,y,t_0)\,dy \\
& + Pe \int_0^1 \left(0.020 - 0.333y^2 + 0.867y^4 - 0.786y^6\right) \frac{\partial c\,(x,y,t_0)}{\partial x} dy\,,
\end{aligned}
\tag{3.51}
$$

where $c(x, y, t_0)$ is, by our choice, the 2-D concentration from the problem (3.39)–(5.62) at $t = t_0$.

In the following we discuss the numerical results. Fig. 3.8 shows the concentration in the channel at times $t = 0.00$ and 0.09, obtained using the 1D-IRBFN method applied to Eqs. (3.1) and (3.4); they are close to those obtained in Roberts and Strunin (2004) by finite different method (FDM). A good agreement is also demonstrated in Fig. 3.9 showing our 1D-IRBFN results and FDM results of Roberts and Strunin (2004) for the original (2-D) model and the centre manifold (1-D) models in the one-zone and two-zone versions. The 1D-IRBFN and FDM results correlate well for the slow zone and slightly differ for the fast zone.

Figs. 3.10 and 3.11 present the grid convergence study for 2-D analysis of the position of the maximum depth-averaged concentration (x_{max}) and the maximum depth-averaged concentration (C_{max}) with respect to time t. The figures show that the numerical results obtained are indistinguishable for grids denser than or equal to 81×47.

Figs. 3.12 and 3.13 present the corresponding grid convergence study for the 1-D one-zone analysis and the converged solution compared with the 2-D and 1-D two-zone results. Fig. 3.13 demonstrates that the 1-D two-zone solution agrees well with the 2-D model solution while the 1-D one-zone solution is not in very good agreement with the 2-D solution. This is because only three terms (the first-order, second-order and third-order derivatives) are considered in the governing equation of 1-D one-zone model. One can improve the accuracy by including higher-order terms. The maximum depth-averaged concentrations for the 1-D one-zone and 2-D models converge to each other and their advection velocities along the x-axis are almost the same as the two curves in Fig. 3.12 nearly coincide as time increases. The present numerical solutions are obtained at very large times up to $t = 7.0$, rather than at short times around $t = 0.09$, as reported in the work by Roberts and Strunin (2004).

3.6.2 Turbulent shear flow in an open channel

In this example we investigate a shear flow in an open channel governed by Eq. (3.19). Four cases for the 1-D one-zone model are considered here as follows.

- Case 1: Only the advection term ($g_1\partial C_1/\partial x$) on the RHS of (3.27) is taken into account.
- Case 2: The advection and diffusion terms ($g_1\partial C_1/\partial x, g_2\partial^2 C_1/\partial x^2$) on the RHS of (3.27) are taken into account.
- Case 3: The first three leading terms–advection, diffusion and dispersion terms ($g_1\partial C_1/\partial x, g_2\partial^2 C_1/\partial x^2, g_3\partial^3 C_1/\partial x^3$) on the RHS of (3.27) are taken into account.
- Case 4: The first four leading terms–advection, diffusion and dispersion, and fourth-order dissipation ($g_1\partial C_1/\partial x$, $g_2\partial^2 C_1/\partial x^2$, $g_3\partial^3 C_1/\partial x^3$, $g_4\partial^4 C_1/\partial x^4$) on the RHS of (3.27) are taken into account.

Figs. 3.14–3.16 compare the distribution of the depth-averaged concentration along the channel between the 2-D model and the 1-D model for the four cases at times $t = 10.0, 20.0$ and 30.0. It appears that the 1-D Case 1 results are very different from those of the 2-D model while the results of the 1-D Case 2, Case 3 and Case 4 are in good agreement with those of the 2-D model.

Figs. 3.17 and 3.18 show the grid convergence study for the 2-D analysis of x_{max} and C_{max} respectively against t. The numerical results are convergent with increasing grid density. The corresponding grid convergence study for the 1-D (Case 4) analysis is also conducted. We compare the converged 1-D solution with the 2-D solution on a 101×201 grid as shown in Figs. 3.19 and 3.20. Observe that the values of x_{max} are almost the same, and the values of C_{max} for both the 1-D and 2-D models converge to each other as time increases.

3.6.3 Effect of longitudinal diffusion

It is straightforward to investigate how the longitudinal (along-the-channel) diffusion affects the centre manifold model of Eqs. (2.79), see Sub-section 2.2.3, and (3.27). In place of (3.19) we have

$$\frac{\partial c}{\partial t} + u(y)\frac{\partial c}{\partial x} = \frac{\partial}{\partial y}\left(D(y)\frac{\partial c}{\partial y}\right) + D_L\frac{\partial^2 c}{\partial x^2}\,, \tag{3.52}$$

where D_L is the diffusion coefficient along the channel assumed constant. Instead of (2.72), we now get

$$\partial_t \hat{c} = L[\hat{c}] - iku(y)\hat{c} + (ik)^2 D_L \hat{c}\,. \tag{3.53}$$

Performing the same procedure as in Sub-section (2.2.3), we obtain

$$L[\hat{c}] = \frac{\partial \hat{c}}{\partial \hat{C}_1} G + iku\hat{c} - (ik)^2 \hat{C}_1\,, \tag{3.54}$$

and, further, upon substitution of (2.75) into (3.54), we get

$$L[\hat{c}] = \sum_{n=1}^{\infty}\sum_{m=1}^{n} c_{n-m} g_m (ik)^n \hat{C}_1 + u(y)\sum_{n=0}^{\infty} c_n (ik)^{n+1}\hat{C}_1 - D_L \sum_{n=0}^{\infty} c_n (ik)^{n+2}\hat{C}_1\,,$$

and, collecting similar terms,

$$L[c_n] = \sum_{m=1}^{n} c_{n-m} g_m + u(y)c_{n-1} - D_L c_{n-2} \quad \text{for } n = 2, 3, ... \tag{3.55}$$

When $n = 1$, Eq. (3.55) coincides with (2.78). Integrating (3.55) over the depth, we obtain

$$D(y)\partial_y c|_{y=h} - D(y)\partial_y c|_{y=0} = g_n + \overline{u(y)c_{n-1}} - D_L \overline{c_{n-2}}\,,$$

where, as before, the overbar means depth-averaged. Since the fluxes through the boundaries are zero, we have

$$g_n = -\overline{u(y)c_{n-1}} + D_L \overline{c_{n-2}} \quad \text{for } n = 2, 3, ...$$

Note that the only effect of D_L is the addition to the diffusion coefficient g_2, because $\overline{c_{n-2}} = 0$ for all n except $n = 2$ for which $\overline{c_0} = 1$. For the logarithmic velocity profile $g_2 \approx 1/(4\kappa^3 K) + D_L$. Using $K = 1$, $\kappa = 0.4$ and $D_L = 0.05$, according to Taylor (1954), we estimate the ratio between the longitudinal diffusion coefficient and the diffusion coefficient due to the shear $D_L/(1/4\kappa^3 K) = 0.0128$.

The small influence of D_L on the concentration dynamics is illustrated by Figs. 3.21 and 3.22, showing the maximum concentration C_{max} and its position x_{max} versus time for the 1-D and 2-D models. Observe that the effect of the turbulent longitudinal dispersion is indeed small compared to the role of the shear. This supports the modelling of Roberts and Strunin (2004) and Strunin (2011) who ignored the longitudinal diffusion from the very beginning.

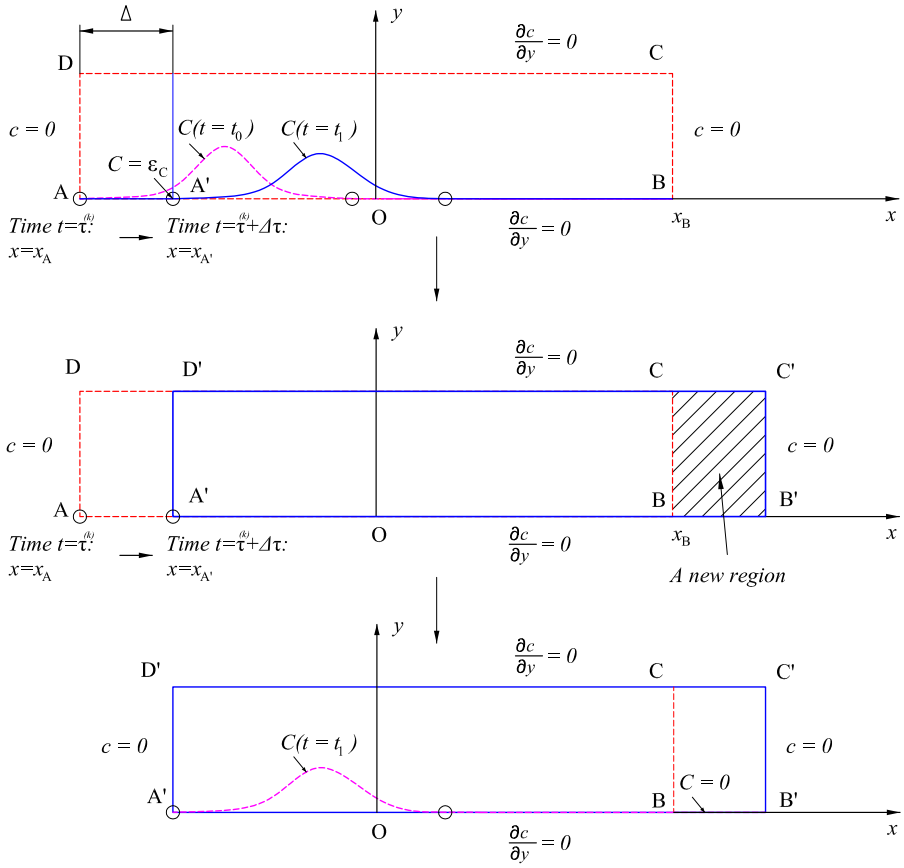

Figure 3.3 Shear flow in an open channel: The computational domain is shifted along the x-axis from time $t = \tau^{(k)}$ to time $t = \tau^{(k)} + \Delta\tau$.

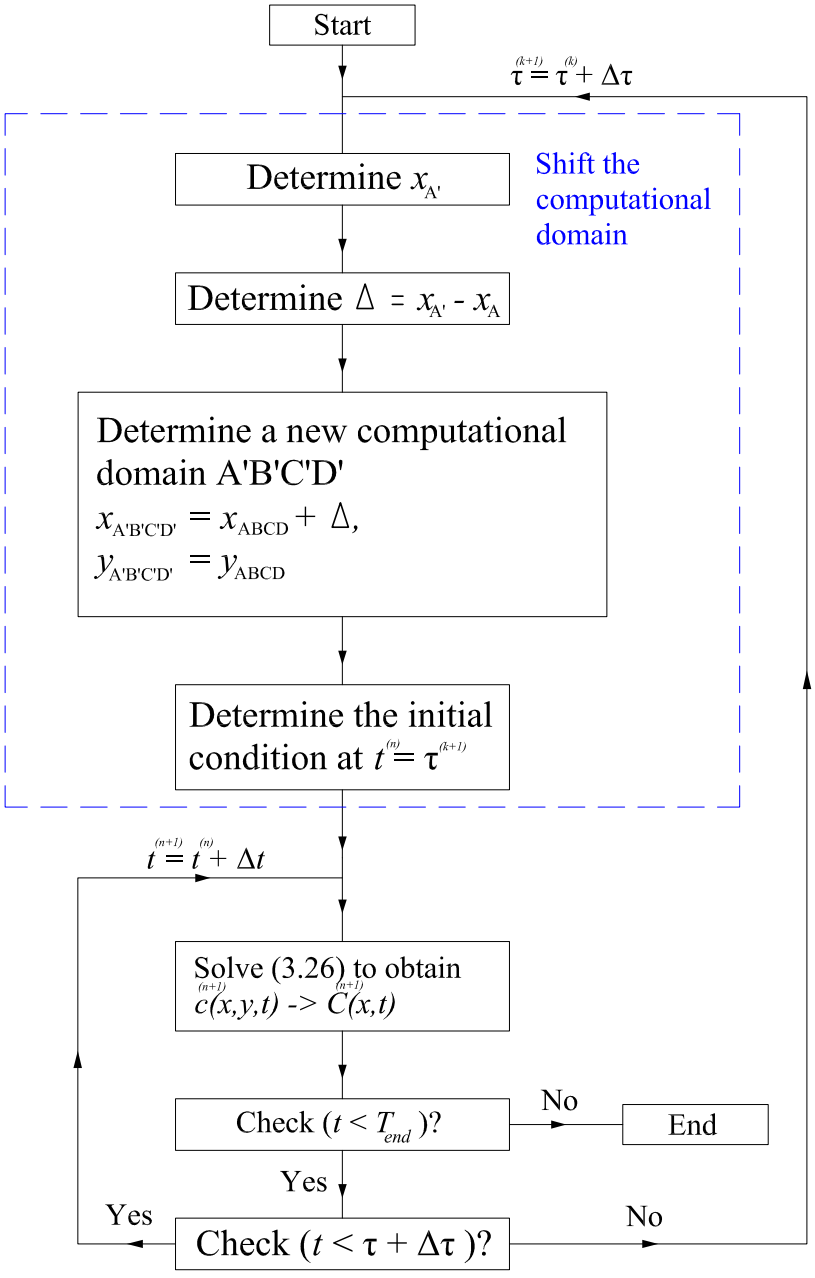

Figure 3.4 Flowchart of the numerical analysis.

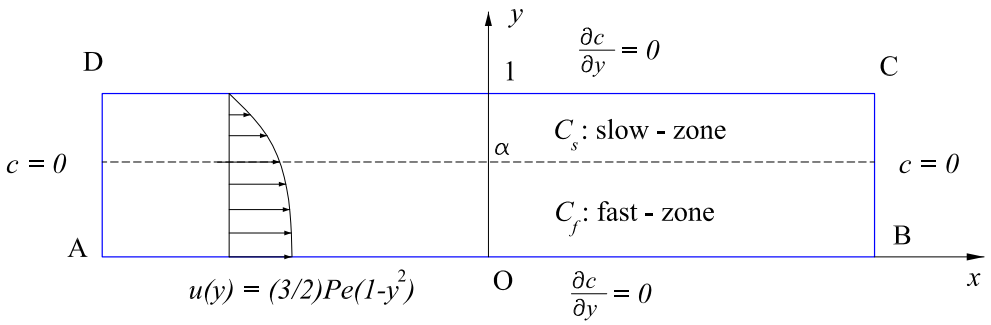

Figure 3.5 Laminar shear flow in an open channel: Problem geometry and boundary conditions.

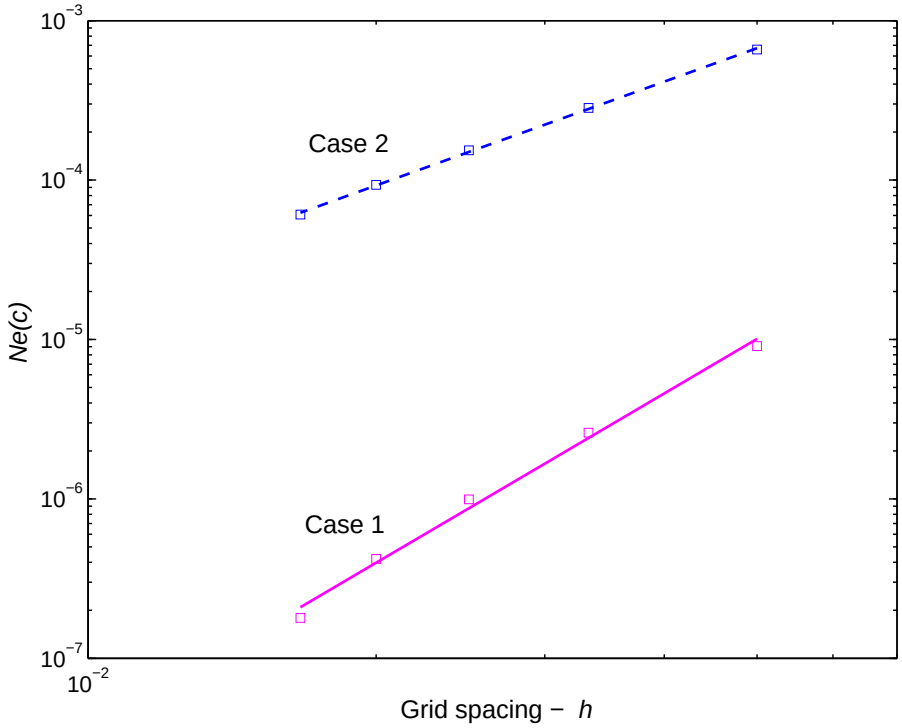

Figure 3.6 2-D advection-diffusion equation with source: Convergence study for 1D-IRBFN method, using a time step $\Delta t = 5.10^{-3}$. The convergence behaviour of 1D-IRBFN for Case 1 and Case 2 are $O(h^{3.54})$ and $O(h^{2.13})$, respectively .

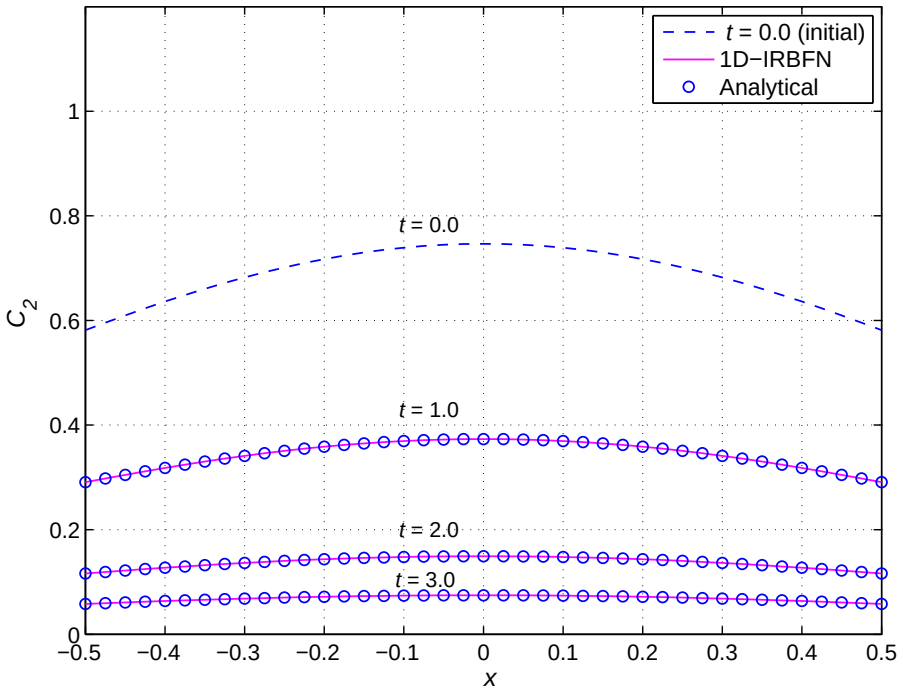

Figure 3.7 2-D advection-diffusion equation with source (Case 2): Comparison of the y-average value of the variable c (C_2) along the x-axis between the analytical solution and 1D-IRBFN result at several times $t = 1, 2.0$ and 3.0, using a time step $\Delta t = 5.10^{-3}$ and a grid of 41×41.

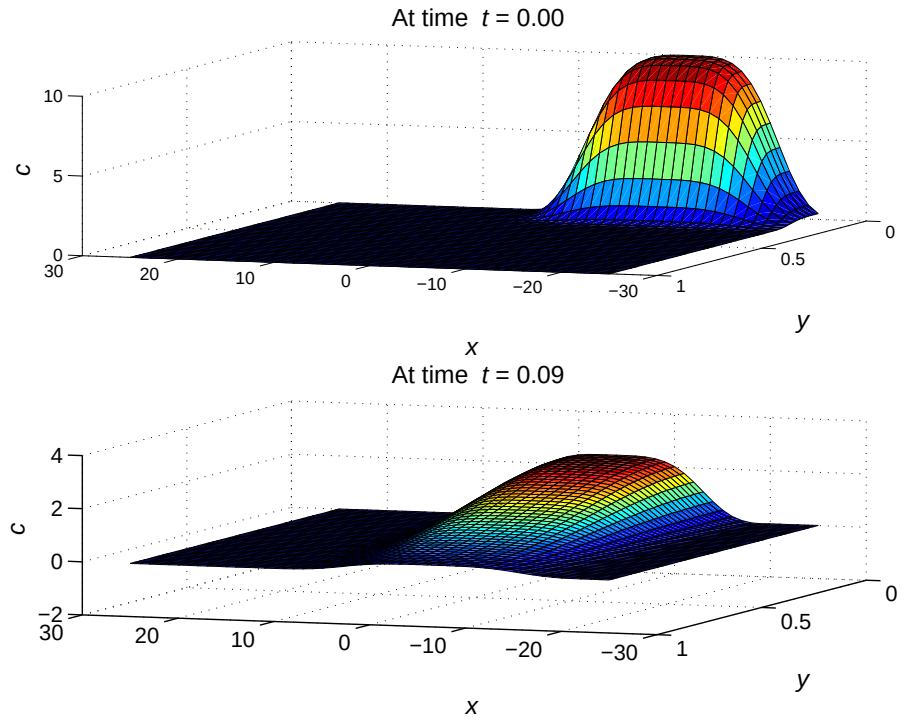

Figure 3.8 Laminar shear flow in an open channel: Concentration field in the channel at times $t = 0.00$ and 0.09, using a time step $\Delta t = 0.005$.

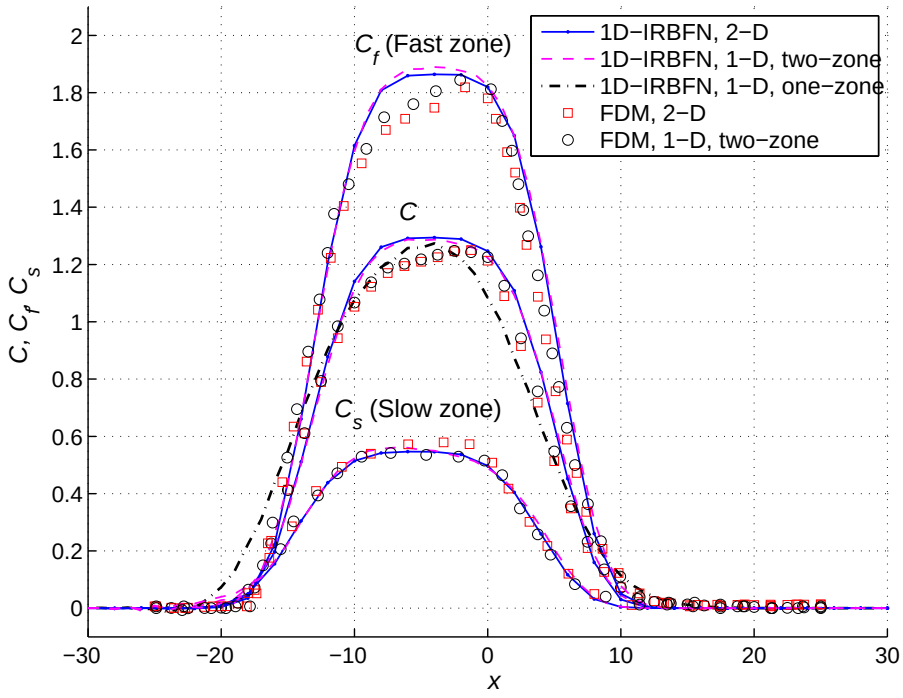

Figure 3.9 Laminar shear flow in an open channel: Comparison between 1D-IRBFN and FDM Roberts and Strunin (2004) results of the original (2-D) model, the 1-D two-zone model and the 1-D one-zone model at time $t = 0.09$, using a time step $\Delta t = 0.005$. Note that the initial condition is taken at time $t = 0.0$ for both 1-D and 2-D analyses.

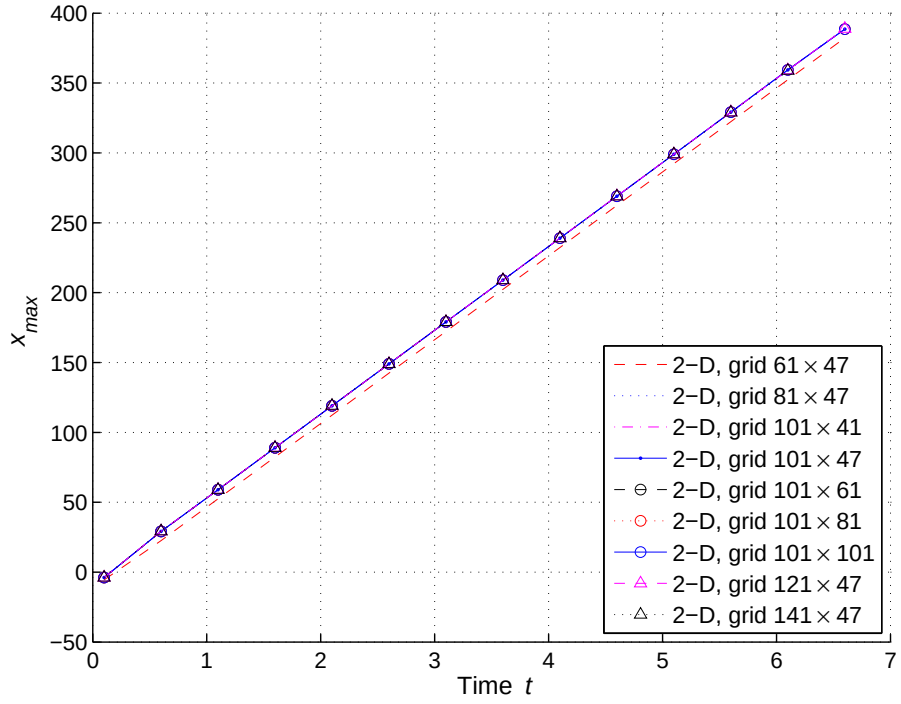

Figure 3.10 Laminar shear flow in an open channel: The grid convergence study for 2-D analysis of the position x of the maximum depth-averaged concentration with respect to time t, using the 1D-IRBFN method and a time step $\Delta t = 0.005$.

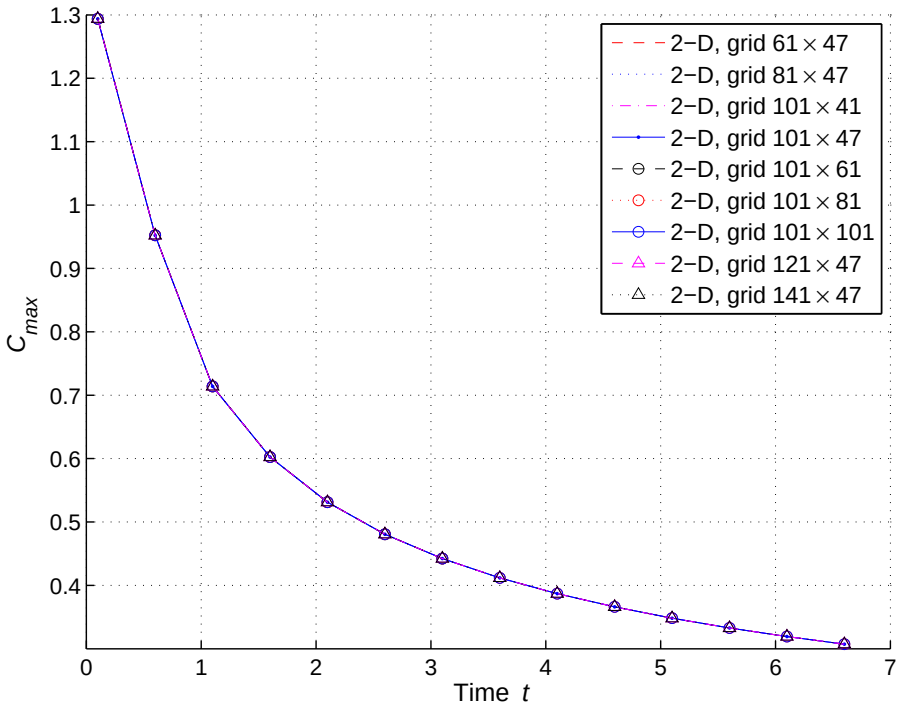

Figure 3.11 Laminar shear flow in an open channel: The grid convergence study for 2-D analysis of the maximum depth-averaged concentration with respect to time t, using the 1D-IRBFN method and a time step $\Delta t = 0.005$.

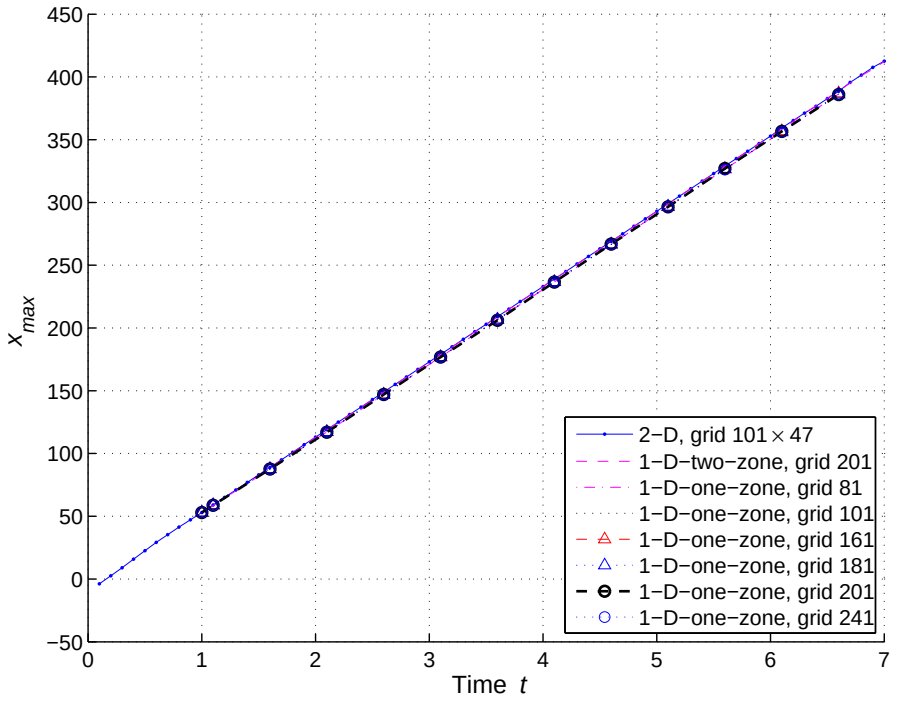

Figure 3.12 Laminar shear flow in an open channel: The grid convergence study for 1-D one-zone analysis of the position of the maximum depth-averaged concentration (x_{max}) with respect to time t in comparison with the original (2-D) model and the 1-D two-zone model, using the 1D-IRBFN method and a time step $\Delta t = 0.005$. Note that the initial condition is taken at time $t = 1.0$ for 1-D analyses.

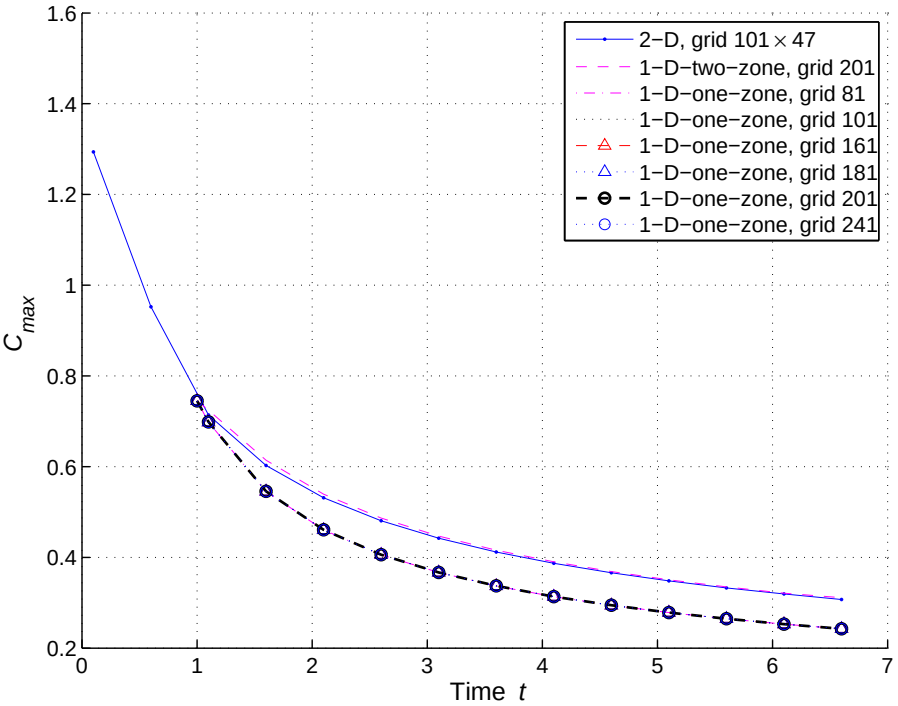

Figure 3.13 Laminar shear flow in an open channel: The grid convergence study for 1-D one-zone analysis of the maximum depth-averaged concentration with respect to time t in comparison with the original (2-D) model and the 1-D two-zone model, using the 1D-IRBFN method and a time step $\Delta t = 0.005$. Note that the initial condition is taken at time $t = 1.0$ for 1-D analyses.

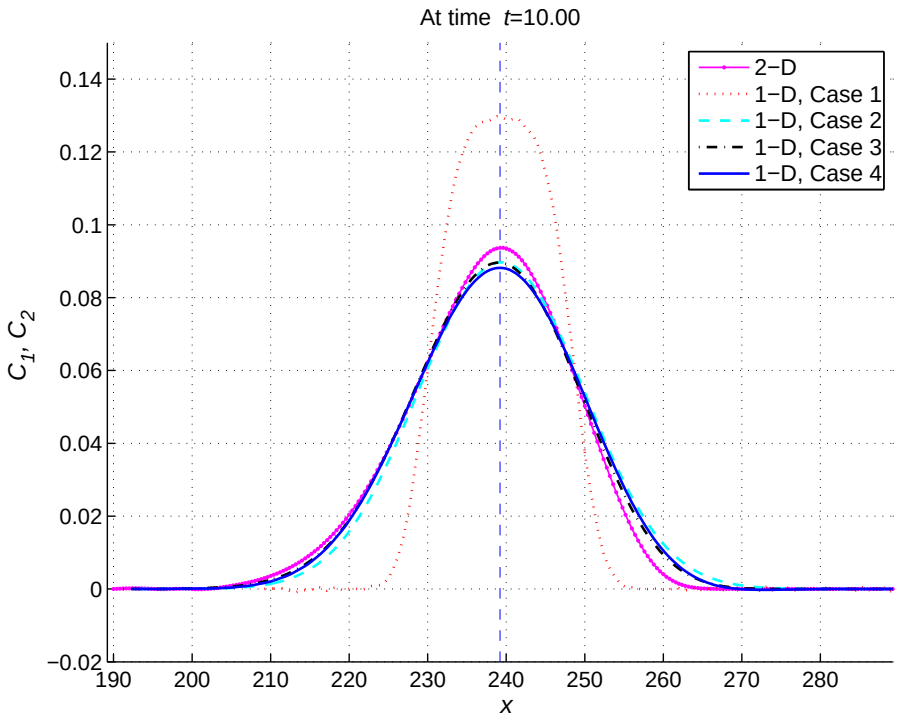

Figure 3.14 Turbulent shear flow in an open channel: Comparison of the depth-averaged concentration along the channel among the results of the 2-D and 1-D models for Case 1, Case 2, Case 3 and Case 4 at time $t = 10.00$, using a time step $\Delta t = 5.10^{-3}$ and grids of 101×201 and 201 for 2-D and 1-D analyses, respectively.

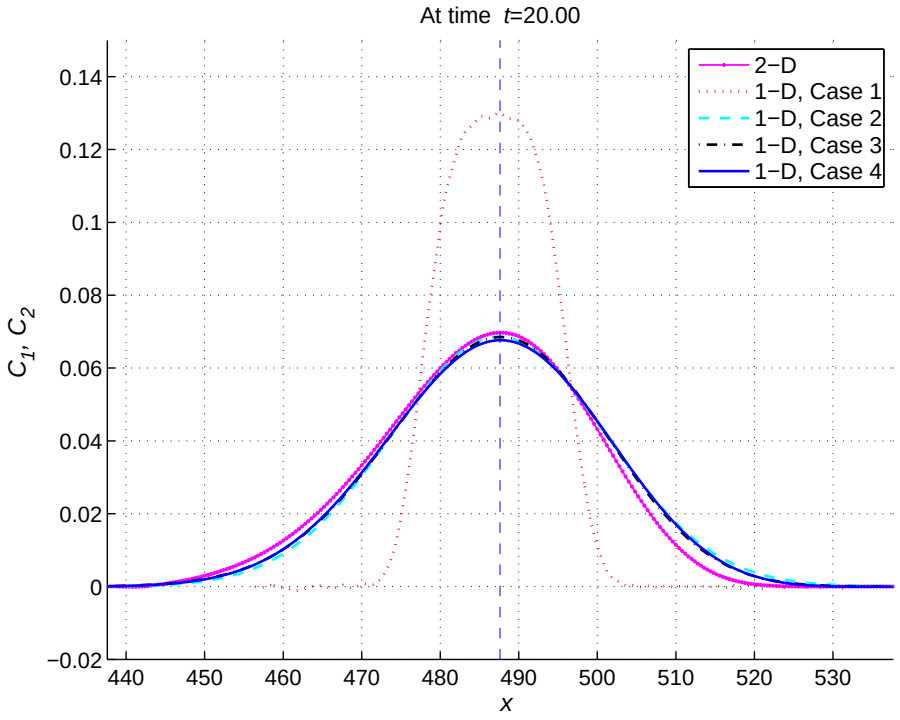

Figure 3.15 Turbulent shear flow in an open channel: Comparison of the depth-averaged concentration along the channel among the results of the 2-D and 1-D models for Case 1, Case 2 and Case 3 at time $t = 20.00$, using a time step $\Delta t = 5.10^{-3}$ and grids of 101×201 and 201 for 2-D and 1-D analyses, respectively.

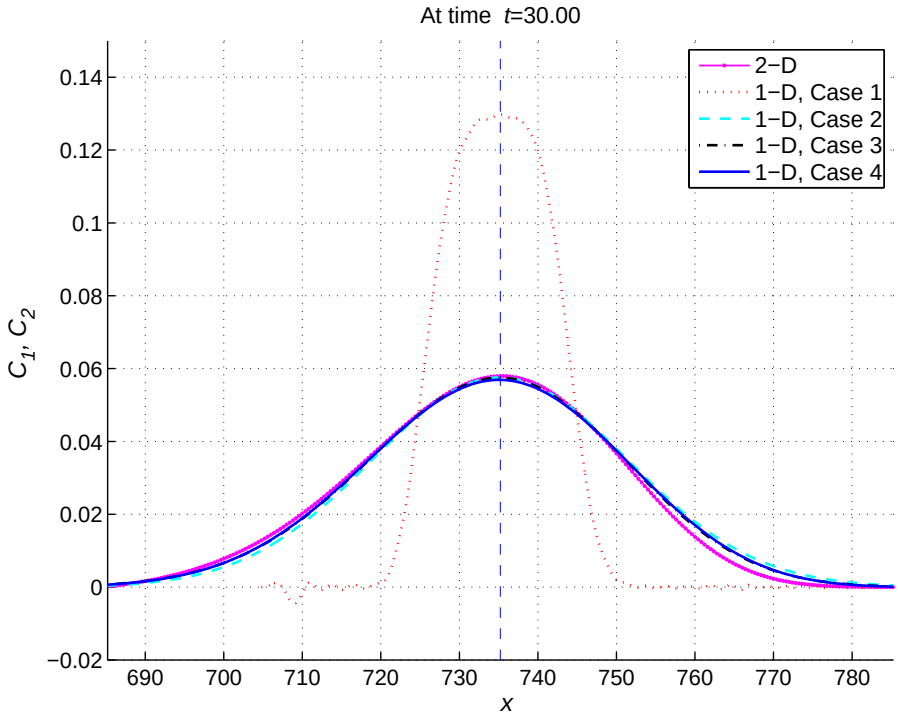

Figure 3.16 Turbulent shear flow in an open channel: Comparison of the depth-averaged concentration along the channel among the results of the 2-D and 1-D models for Case 1, Case 2 and Case 3 at time $t = 30.00$, using a time step $\Delta t = 5.10^{-3}$ and grids of 101×201 and 201 for 2-D and 1-D analyses, respectively.

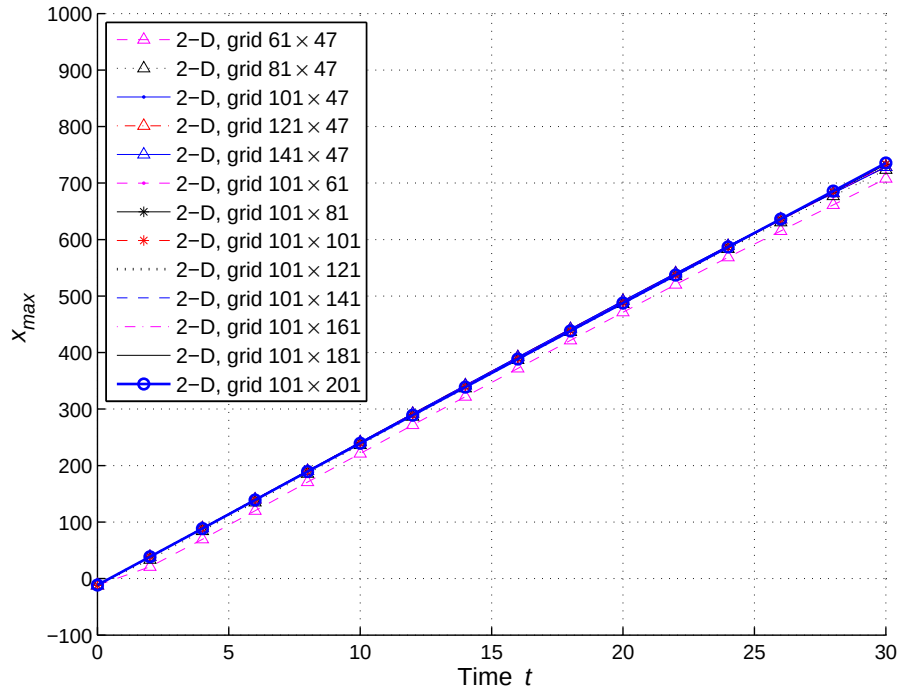

Figure 3.17 Turbulent shear flow in an open channel: The grid convergence study for 2-D analysis of the position x of the maximum depth-averaged concentration with respect to time t.

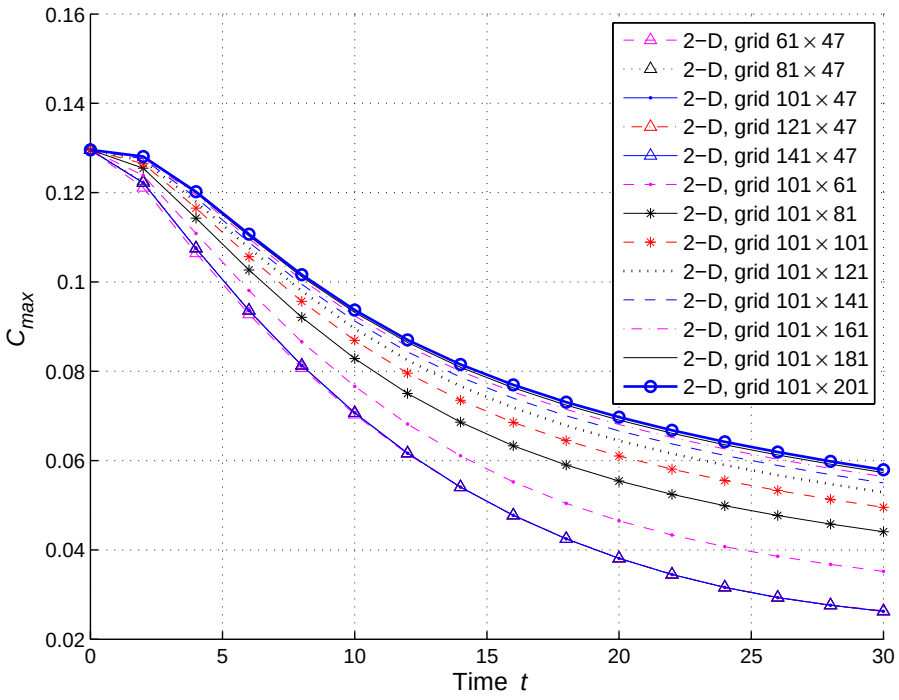

Figure 3.18 Turbulent shear flow in an open channel: The grid convergence study for 2-D analysis of the maximum depth-averaged concentration with respect to time t.

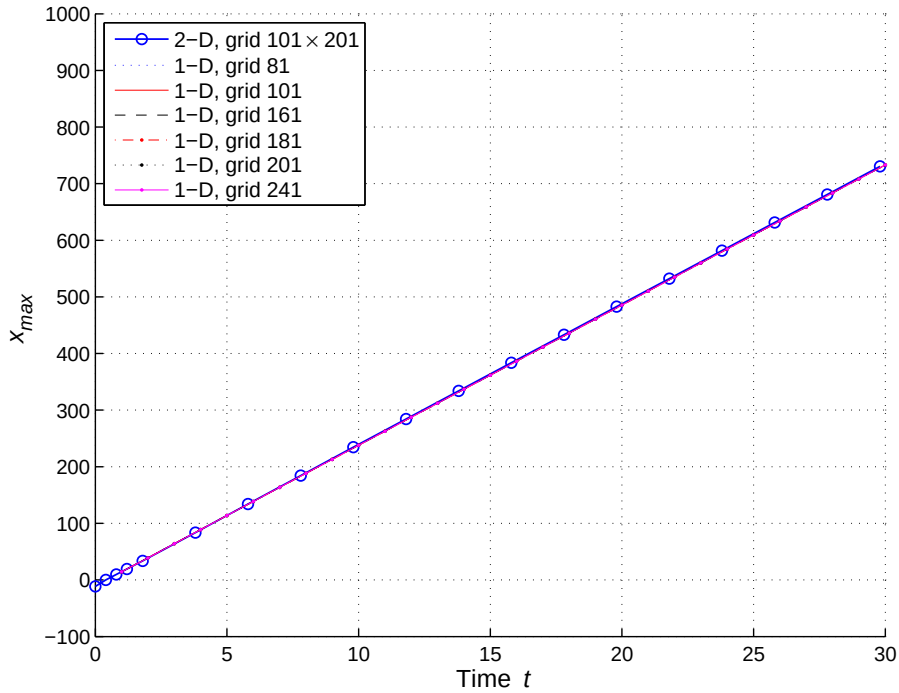

Figure 3.19 Turbulent shear flow in an open channel: The grid convergence study for 1-D (Case 4) analysis of the position of the maximum depth-averaged concentration with respect to time t in comparison with the 2-D result. Note that the initial condition is taken at the time $t = 1.0$.

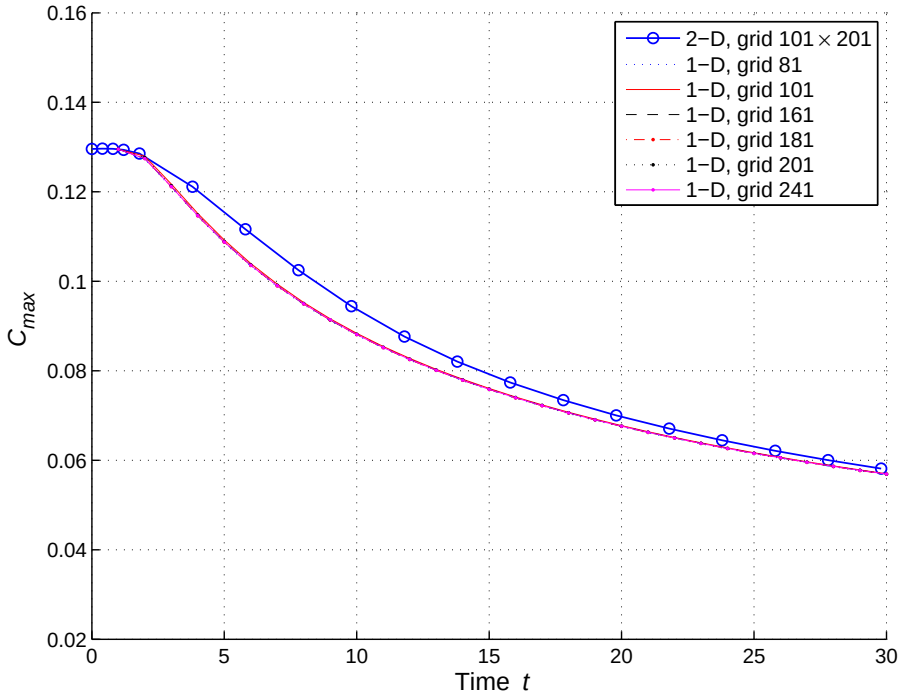

Figure 3.20 Turbulent shear flow in an open channel: The grid convergence study for 1-D (Case 4) analysis of the maximum depth-averaged concentration with respect to time t in comparison with the 2-D result. Note that the initial condition is taken at the time $t = 1.0$ for 1-D analysis.

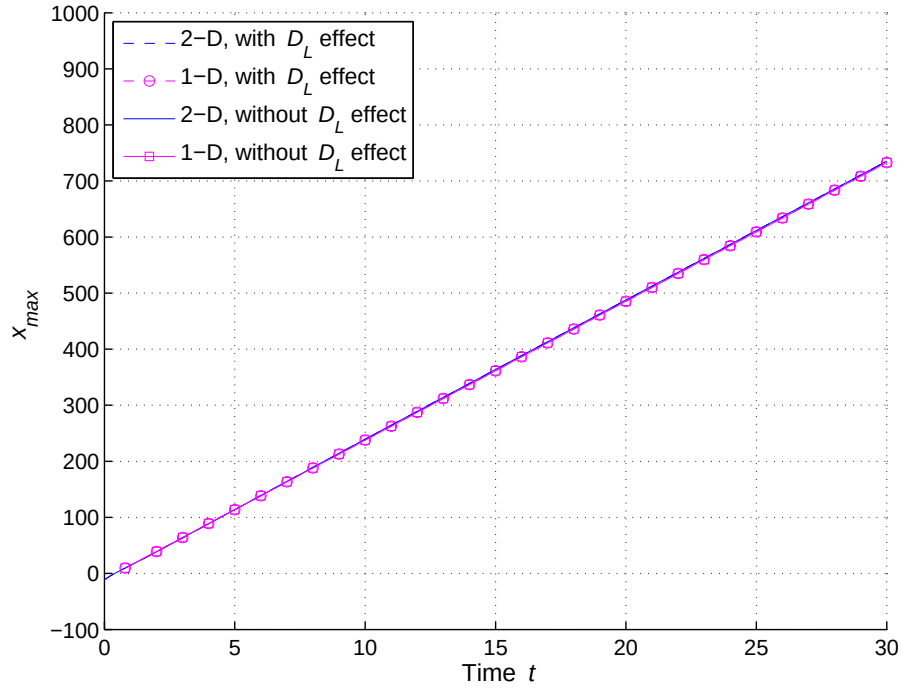

Figure 3.21 Turbulent shear flow in an open channel: The influence of longitudinal diffusion on the position x of the maximum depth-averaged concentration with respect to time t, using a time step $\Delta t = 5.10^{-3}$ and grids of 101×201 and 201 for 2-D and 1-D analyses, respectively.

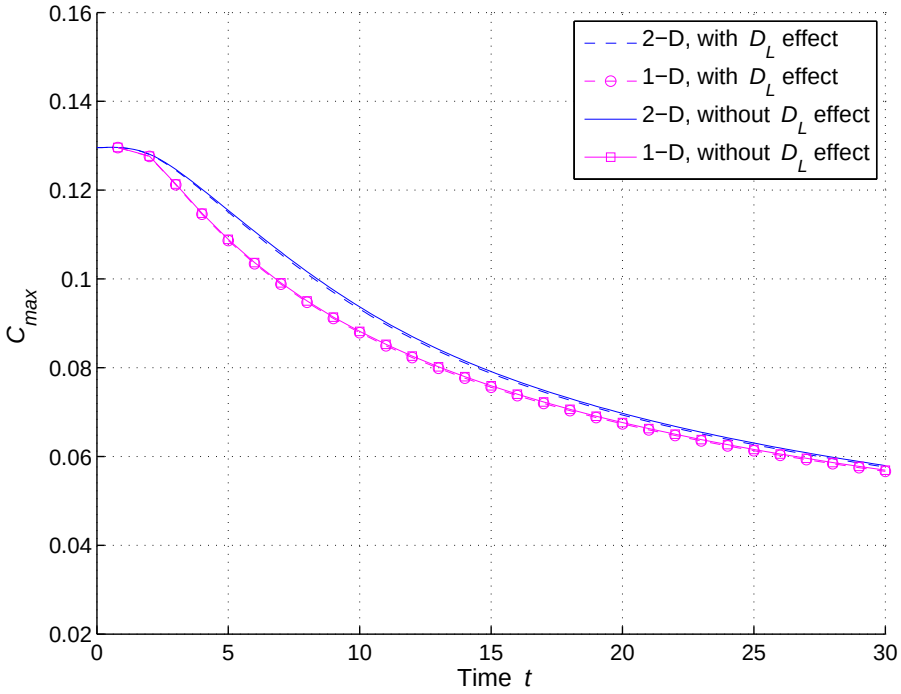

Figure 3.22 Turbulent shear flow in an open channel: The influence of longitudinal diffusion on the maximum depth-averaged concentration with respect to time t, using a time step $\Delta t = 5.10^{-3}$ and grids of 101×201 and 201 for 2-D and 1-D analyses, respectively.

3.7 Concluding remarks

The shear dispersion of contaminant based on centre manifold theory is successfully simulated by using the 1D-IRBFN method. The numerical solution of the derived 1-D (one-zone and two-zone) model equations obtained by centre manifolds for both laminar and turbulent flows are in a good agreement with that of the original 2-D advection-diffusion equation. These models yield almost the same velocities for the point of the maximum depth-averaged concentration along the channel. We obtain the 1D-IRBFN solution for the maximum depth-averaged concentration for the 1-D one-zone model taking into account several leading terms including advection, diffusion and dispersion. The solution converges to that of the original 2-D model. A small gap between the solutions exists, however, the accuracy of the centre manifold equation can be improved by including higher-order derivatives. The numerical results confirm that the effect of longitudinal diffusion is negligible. Note that our work can be viewed not only as the confirmation of the centre manifold approach by the 1D-IRBFN technique but also as another confirmation of the numerical technique by the centre manifolds. Our results demonstrate that convergence takes place even for unmodified initial condition as discussed in Sub-section 2.2.2. The convergence in this case is algebraic, not exponential.

Chapter 4

Higher-order transport equations for turbulent open channel flows

We derive high-order partial differential equations governing the longitudinal dispersion of contaminants in a turbulent open channel flow and numerically investigate the convergence of these high-order equations. The derivation is based on the centre manifold theory, which provides an accurate approach for modelling the transport of the depth-averaged concentration of the contaminant. Two types of the average velocity profile are considered: logarithmic and power. We use the one-dimensional integrated radial basis function network (1D-IRBFN) method as a numerical approach to obtain the numerical solutions to both the original 2–D equation and the approximate 1–D equations. We compare the original models with their centre manifolds approximations for contaminant transport in an open channel at very large Reynolds numbers. The numerical results obtained from the approximate 1–D models are in good agreement with those of the original 2–D model for both the logarithmic and power velocity profiles.

4.1 Introduction

When a cloud of contaminant is introduced into a fluid flow it is stretched by the velocity shear and at the same time smeared by the vertical diffusion. After a longer time, the contaminant cloud extends over a long distance along the channel (in x-direction) and the concentration variation becomes slow. The contaminant transport is governed by the two-dimensional advection-diffusion equation (Taylor, 1954)

$$\frac{\partial c}{\partial t} + u(y)\frac{\partial c}{\partial x} = \frac{\partial}{\partial y}\left[D(y)\frac{\partial c}{\partial y}\right], \tag{4.1}$$

in which we neglected the diffusion in x-direction. Here, c is the contaminant concentration and $D(y)$ the diffusion coefficient which is responsible for the turbulent

diffusion across the channel (in y-direction) and defined by

$$D(y) = K\frac{u_*^2}{\partial_y u}\,, \tag{4.2}$$

where K is the non-dimensional coefficient of proportionality and u_* the friction velocity. The expression (4.2) for the diffusion coefficient $D(y)$ is deduced from the Prandtl formula for the stress (Strunin, 2011). The velocity $u(y)$ is supposed known. Eq. (4.1) is complemented by the boundary conditions described as

$$D\frac{\partial c}{\partial y}|_{y=0} = D\frac{\partial c}{\partial y}|_{y=h} = 0\,. \tag{4.3}$$

An accurate method to derive an equation for the depth-averaged concentration, C, is supported by centre manifold theory. Roberts and Strunin (2004) and Mercer and Roberts (1990) used the method to derive a high-order equation governing the depth-averaged concentration in laminar open channel flow. They also derived a corrected initial conditions allowing fast convergence of the original model to the asymptotic one. Strunin (2011) constructed a similar equation for a turbulent open channel flow. He used two forms of the velocity profile, namely logarithmic and power. For a steady two dimensional flow of an incompressible fluid, the logarithmic velocity profile takes the form (Coles, 1956)

$$u = \frac{u_*}{\kappa}\ln\left(\frac{u_* y}{\nu}\right) + A\,, \tag{4.4}$$

where $\kappa = 0.4$ the von karman constant, ν the kinematic molecular viscosity and A the empirical constant. The logarithmic law (4.4) is Reynolds number independent. Alternatively, Barenblatt (1993) took into account the effect of the viscosity and the Reynolds number in the inertial layer and deduced the power velocity profile

$$u(y) = u_*\left(\frac{1}{\sqrt{3}}\ln \mathrm{Re} + \frac{5}{2}\right) y_+^{\frac{3}{2\ln \mathrm{Re}}}\,, \tag{4.5}$$

where Re is the Reynolds number and $y_+ = u_* y/\nu$ the dimensionless coordinate. Barenblatt (2000) introduced experimental data in support of the power law (4.5). He showed that the scaling law (4.5) gives an accurate description of the mean velocity distribution over the self-similar intermediate region adjacent to the viscous sublayer for a wide variety of boundary layer flows. The accuracy of the scaling law depends on how the Reynolds number is defined properly. Barenblatt (2003) studied the universality of the power velocity profile in modelling dispersion using three different configurations of sources located on the bottom. A self-similar

asymptotic solutions are obtained describing the concentration transfer at small times in the lower part of the turbulent boundary layer far from the flow surface. Barenblatt (2000) emphasized that these solutions clearly demonstrate Reynolds number dependence. In the present study, we separately investigate the dispersion of contaminants for the logarithmic and power velocity profiles, over the entire cross section of the flow at large times using very large Reynolds number.

In the present research, we assume a steady turbulent flow and fully developed of the inertial layer in order to ensure fast distribution of contaminants across the flow. This assumption should be made for the flow to be treated by the centre manifold approach. The flow is considered in an open channel in which the shear stress is constant measured by the squared friction velocity u_*^2. The mean velocity profile is taken to be either (4.4) or (4.5) and the flow is investigated over the entire cross section of the channel from the bottom, except the narrow viscous sublayer, to the surface with neglecting waves.

Based on the centre manifold theory, the depth-averaged concentration, C, is governed by the following equation.

$$\frac{\partial C}{\partial t} = g_1 \frac{\partial C}{\partial x} + g_2 \frac{\partial^2 C}{\partial x^2} + g_3 \frac{\partial^3 C}{\partial x^3} + g_4 \frac{\partial^4 C}{\partial x^4} + g_5 \frac{\partial^5 C}{\partial x^5} + g_6 \frac{\partial^6 C}{\partial x^6} + \dots . \tag{4.6}$$

Throughout the present chapter, we analytically calculate the coefficients g_4, g_5 and g_6 for the power velocity profile, and g_5 and g_6 for the logarithmic velocity profile. Similar analysis of the coefficients g_4 (for the power velocity profile) and g_5 (for the logarithmic velocity profile) can be found in Ngo-Cong et al. (2013). The rest of the coefficients are previously derived (Strunin, 2011; Mohammed, Ngo-Cong, Strunin, Mai-Duy and Tran-Cong, 2014). In Eq. (4.6), the coefficients g_n for any n are analytically calculated from the formula

$$g_n = -\overline{u(y)c_{n-1}} \quad \text{for } n = 1, 2, \dots , \tag{4.7}$$

where the overline means depth-averaging. For Eq. (4.7), we use $c_0 = 1$ and calculate c_n for any n as follows:

$$L[c_n] = \sum_{m=1}^{n} c_{n-m} g_m + u(y) c_{n-1} \quad \text{for } n = 1, 2, \dots . \tag{4.8}$$

A detailed derivation for Eqs. (4.7) and (4.8) is found in Chapter 2. We ignore the longitudinal diffusion as it does not significantly affect the averaged model (Mohammed, Ngo-Cong, Strunin, Mai-Duy and Tran-Cong, 2014).

The chapter is organised as follows. Sections 4.2 and 4.3 include applying the centre manifold theory to derive higher-order coefficients for the logarithmic and power velocity profiles. Section 4.4 presents the numerical approach, followed by the discussion on numerical results in Section 4.5. Section 4.6 concludes the chapter.

4.2 Higher-order coefficients for the logarithmic velocity profile

Consider the logarithmic velocity profile defined in (4.4). Substituting (4.4) into (4.2) gives the following form for the diffusion coefficient.

$$D(y) = \kappa K u_* y \,.$$

The velocity profile (4.4) is not applicable at very short distance from the bottom $y = 0$ (Monin and Yaglom, 1975; Landau and Lifshitz, 1981). It is valid in the region $\epsilon < y < 1$ ($\epsilon = 50/R = h_1/h$, where h is the channel height and h_1 the width of the viscous sublayer). We assume that the Reynolds number is large so that the value of ϵ is small. In the present computations we use $\epsilon = 5/R$ but the large Reynolds number ensures that both $5/R$ and $50/R$ are small. The non-dimensional form of Eq. (4.1) is

$$\frac{\partial c}{\partial t} + u(y)\frac{\partial c}{\partial x} = \frac{\partial}{\partial y}\left(D(y)\frac{\partial c}{\partial y}\right) , \tag{4.9}$$

in which $u(y) = (1/\kappa)\ln(Ry) + B$ and $D(y) = \kappa K y$, where $B = 5.5$. In Eq. (4.9), we keep the old notations for convenience. The associated non-dimensional form of the boundary conditions (4.3) are given by

$$y\frac{\partial c}{\partial y}|_{y=\epsilon} = y\frac{\partial c}{\partial y}|_{y=1} = 0 \,.$$

In the following, we calculate the coefficient g_5 for the logarithmic velocity profile based on $c_0 = 1$, c_1, c_2, g_1, g_2, g_3 and g_4 (Strunin, 2011; Mohammed, Ngo-Cong, Strunin, Mai-Duy and Tran-Cong, 2014). Substituting $n = 4$ into (4.8) leads to

$$\begin{aligned}\frac{\partial}{\partial y}\left(y\frac{\partial c_4}{\partial y}\right) = \frac{1}{4K^4\kappa^8}\Bigg(&\frac{4337}{5184} - \frac{28}{27}y - \frac{1}{162}y^3 + \frac{3475}{10368}\ln y + \frac{230}{108}y\ln y \\ &- \frac{13}{8}y^2\ln y + \frac{16}{81}y^3\ln y \\ &+ \frac{139}{108}y\ln^2 y - \frac{7}{54}y^3\ln^2 y + \frac{3}{4}y^2\ln^3 y - \frac{2}{9}y^3\ln^3 y + \frac{1}{9}y^3\ln^4 y\Bigg) \,.\end{aligned} \tag{4.10}$$

Integrating (4.10) twice gives

$$c_4 = \frac{1}{4K^4\kappa^8}\left(\frac{431}{2592}y - \frac{89}{288}y^2 + \frac{5}{108}y^3 - \frac{47}{41472}y^4 + \frac{3475}{10368}y\ln y \right.$$
$$+\frac{1}{9}y^2\ln y - \frac{1}{72}y^3\ln y - \frac{29}{5184}y^4\ln y + \frac{139}{432}y^2\ln^2 y \qquad (4.11)$$
$$\left. -\frac{1}{6}y^3\ln^2 y + \frac{49}{1728}y^4\ln^2 y + \frac{1}{12}y^3\ln^3 y - \frac{1}{36}y^4\ln^3 y + \frac{1}{144}y^4\ln^4 y\right) + B_4\,.$$

The integration constant B_4 is found via the condition $\int_\epsilon^1 c_4 dy = 0$, then

$$\frac{1}{4K^4\kappa^8}\left(-\frac{1}{1536}y^2 - \frac{4677}{69984}y^3 + \frac{73}{13824}y^4 + \frac{33299}{43200000}y^5 + \frac{3475}{20736}y^2\ln y \right.$$
$$-\frac{211}{1944}y^3\ln y + \frac{29}{1152}y^4\ln y - \frac{16159}{3240000}y^5\ln y + \frac{139}{1296}y^3\ln^2 y - \frac{11}{192}y^4\ln^2 y$$
$$\left. +\frac{2089}{216000}y^5\ln^2 y + \frac{1}{48}y^4\ln^3 y - \frac{1}{150}y^5\ln^3 y + \frac{1}{720}y^5\ln^4 y\right)_\epsilon^1 + B_4 y|_\epsilon^1 = 0\,.$$

Taking the limit $\epsilon \to 0$, we have all the terms involving products $\epsilon^m \ln^\ell \epsilon$ vanish and obtain

$B_4 = \dfrac{1433}{93312K^4\kappa^8}$. As a result

$$c_4 = \frac{1}{4K^4\kappa^8}\left(\frac{1433}{23328} + \frac{431}{2592}y - \frac{89}{288}y^2 + \frac{5}{108}y^3 - \frac{47}{41472}y^4 + \frac{3475}{10368}y\ln y \right.$$
$$+\frac{1}{9}y^2\ln y - \frac{1}{72}y^3\ln y - \frac{29}{5184}y^4\ln y + \frac{139}{432}y^2\ln^2 y \qquad (4.12)$$
$$\left. -\frac{1}{6}y^3\ln^2 y + \frac{49}{1728}y^4\ln^2 y + \frac{1}{12}y^3\ln^3 y - \frac{1}{36}y^4\ln^3 y + \frac{1}{144}y^4\ln^4 y\right)\,.$$

Now we calculate g_5, based on (4.7) for n=5, we obtain

$$\begin{aligned} g_5 = -\frac{1}{4K^4\kappa^9}\Bigg(&-\frac{1433}{23328}y+\frac{1751}{41472}y^2+\frac{53}{23328}y^3+\frac{105}{41472}y^4-\frac{15113}{25920000}y^5 \\ &+\frac{1433}{23328}y\ln y-\frac{1751}{20736}y^2\ln y-\frac{53}{7776}y^3\ln y-\frac{35}{3456}y^4\ln y \\ &+\frac{15113}{5184000}y^5\ln y+\frac{3475}{20736}y^2\ln^2 y \\ &-\frac{187}{1296}y^3\ln^2 y+\frac{25}{576}y^4\ln^2 y-\frac{509}{64800}y^5\ln^2 y+\frac{139}{1296}y^3\ln^3 y \\ &-\frac{1}{16}y^4\ln^3 y+\frac{97}{8640}y^5\ln^3 y+\frac{1}{48}y^4\ln^4 y-\frac{1}{144}y^5\ln^4 y+\frac{1}{720}y^5\ln^5 y\Bigg)_{\epsilon}^{1}. \end{aligned} \tag{4.13}$$

Taking the limit $\epsilon \to 0$, we get

$$g_5 = \frac{1165339}{311040000K^4\kappa^9}\,.$$

Similar derivation for g_6 can be found in Appendix A.

4.3 Higher-order coefficients for the power velocity profile

Power velocity profile follows from an alternative theory to the logarithmic model. The mean velocity gradient, $\partial u/\partial y$, in the inertial layer, suggested by dimensional analysis, is

$$\frac{\partial u}{\partial y} = \frac{u_*}{y}\,\Phi(y_+, \mathrm{Re})\,,$$

where Φ is the dimensionless function. In the 1930s, von Karman neglected the viscous sub-layer by assuming that at $y_+ \to \infty$ and $\mathrm{Re} \to \infty$, the function Φ tends to a finite limit, we have $\Phi(y_+, \mathrm{Re}) = 1/\kappa$. This assumption leads to the classical logarithmic law of the form (4.4). This law is Reynolds-number independent for the mean velocity over the cross-section of a channel. Barenblatt (1993, 2000, 2003) argued that the assumption of von Karman is inadequate and showed that the influence of the viscosity and the Reynolds number should be taken into account in the inertial layer. Hereby, an alternative theory can be put forward based on the assumption that at large y_+, the finite limit of the function Φ does not exist. Instead, the function can be written in the form $\Phi = \gamma(\mathrm{Re})y_+^{\alpha(\mathrm{Re})}$. For the functions $\gamma(\mathrm{Re})$ and $\alpha(\mathrm{Re})$, he obtained (Barenblatt, 2000) the Reynolds-

number-dependent scaling law

$$\Phi = \frac{u}{u_*} = (\gamma_0 \ln \mathrm{Re} + \gamma_1)\, y_+^{\frac{\zeta}{\ln \mathrm{Re}}}\,, \tag{4.14}$$

where the constants γ_0, γ_1, and α are universal. By comparing (4.14) with the most reliable data for turbulent pipe flows, he found

$$\zeta = \frac{3}{2}, \qquad \gamma_0 = \frac{1}{\sqrt{3}}, \qquad \gamma_1 = \frac{5}{2}\,, \tag{4.15}$$

with the Reynolds number defined as $\mathrm{Re} = \overline{u}\, d/\nu$ in which $\overline{u}$ is the average velocity across the pipe and d the pipe diameter. Substituting (4.15) into (4.14), we have

$$u(y) = u_* \left(\frac{1}{\sqrt{3}} \ln \mathrm{Re} + \frac{5}{2} \right) y_+^{\alpha}\,,$$

where $\alpha = 3/(2ln\mathrm{Re})$. Similar theory applies to wall turbulence in channels (Barenblatt, 2000). The Reynolds number Re is based on the maximal velocity, which is the velocity at the surface, $u(h)$, and defined by

$$\mathrm{Re} = \frac{u(h)\ell}{\nu}\,, \tag{4.16}$$

in which ℓ has the same order of magnitude as the depth of the channel. As a simple assumption, we adopt that the length of turbulence equals a fixed portion of the total depth, $\ell = \beta h$ where β is the empirical constant. Substituting (4.14) into (4.2) gives the following expression for the diffusion coefficient

$$D(y) = \frac{u^{1-\alpha} K \nu^{\alpha}}{\left(\frac{1}{\sqrt{3}} \ln \mathrm{Re} + \frac{5}{2} \right) \alpha} y^{1-\alpha}\,. \tag{4.17}$$

Hereafter, all the quantities are non-dimensional. The 2–D advection-diffusion equation (4.1) becomes

$$\frac{\partial c}{\partial t} + q y^{\alpha} \frac{\partial c}{\partial x} = \frac{K}{q\alpha} \frac{\partial}{\partial y} [y^{1-\alpha} \frac{\partial c}{\partial y}]\,, \tag{4.18}$$

where $u(y) = qy^{\alpha}$ and $q = R^{\alpha}(1/\sqrt{3} \ln \mathrm{Re} + 5/2)$ in which R is defined by

$$R = \left(\frac{\mathrm{Re}}{\beta(\frac{\sqrt{3}}{2\alpha} + \frac{5}{2})} \right)^{\frac{1}{\alpha+1}}\,. \tag{4.19}$$

The boundary conditions associated with (4.18) are

$$y^{1-\alpha}\frac{\partial c}{\partial y}|_{y=\epsilon} = y^{1-\alpha}\frac{\partial c}{\partial y}|_{y=1} = 0\,.$$

The coefficient g_4 for the power velocity peofile is calculated as follows. Substituting $n = 3$ into (4.8) leads to

$$L\left[c_3\right] = \sum_{m=1}^{3} c_{3-m}g_m + u\left(y\right)c_{3-1} = c_1g_2 + c_0g_3 + c_2[g_1 + u\left(y\right)]\,, \tag{4.20}$$

where $c_0 = 1$ and g_1, c_1, b, g_2, c_2, m and g_3 are calculated from Eqs. (4.8), (4.10), (4.11), (4.12), (4.16), (4.17) and (4.18), respectively, found in Strunin (2011). Substituting these coefficients and functions into (4.20) gives

$$\begin{aligned}\frac{\partial}{\partial y}\left(y^{1-\alpha}\frac{\partial c_3}{\partial y}\right) &= \frac{\alpha r q^3}{2\kappa(2\alpha+1)}y^{5\alpha+2} + \frac{\alpha r q^2 g_1(4\alpha+3)}{2\kappa(2\alpha+1)}y^{4\alpha+2}\\ &+\frac{\alpha q g_1^2\left(2r+qs\right)}{2\kappa}y^{3\alpha+2} + \frac{\alpha^2 b q^4}{\kappa^2(\alpha+1)(2\alpha+1)}y^{3\alpha+1}\\ &+\frac{\alpha s q g_1^3}{2\kappa}y^{2\alpha+2} + \frac{2\alpha^2 q^3\left(g_2+bg_1\right)}{\kappa^2(2\alpha+1)}y^{2\alpha+1}\\ &+\frac{\alpha^2 q^2\left(2g_1g_2+bg_1^2\right)}{\kappa(\alpha+1)}y^{\alpha+1} + \frac{\alpha m q^2}{\kappa}y^{\alpha} + \frac{\alpha q}{\kappa}\left(g_3+bg_2+mg_1\right)\,,\end{aligned} \tag{4.21}$$

where s and r are defined by

$$s = \frac{\alpha^2 q^2}{K^2(\alpha+1)^2(\alpha+2)}\,,$$

$$r = \frac{\alpha^2 q^3}{K^2(\alpha+1)(2\alpha+1)(3\alpha+2)}\,.$$

Integrating (4.21) twice, we obtain

$$\begin{aligned}c_3 &= \frac{\alpha r q^3}{6\kappa(2\alpha+1)^2(5\alpha+3)}y^{6\alpha+3} + \frac{\alpha r q^2 g_1}{2\kappa(2\alpha+1)(5\alpha+3)}y^{5\alpha+3}\\ &+\frac{\alpha q g_1^2\left(2r+qs\right)}{6\kappa(\alpha+1)(4\alpha+3)}y^{4\alpha+3} + \frac{rbq}{2(2\alpha+1)}y^{4\alpha+2} + \frac{\alpha s q g_1^3}{6\kappa(\alpha+1)(2\alpha+3)}y^{3\alpha+3}\\ &+r\left(g_2+bg_1\right)y^{3\alpha+2} + \frac{s}{2}\left(2g_1g_2+bg_1^2\right)y^{2\alpha+2}\\ &+\frac{\alpha m q^2}{\kappa(\alpha+1)(2\alpha+1)}y^{2\alpha+1} + \frac{\alpha q}{\kappa(\alpha+1)}\left(g_3+bg_2+mg_1\right)y^{\alpha+1} + A_2\,.\end{aligned} \tag{4.22}$$

The integration constant A_2 can be found from the condition $\int_\epsilon^1 c_3 dy = 0$.

$$\begin{aligned} A_2 = &-\frac{\alpha r q^3}{12\kappa(2\alpha+1)^2(3\alpha+2)(5\alpha+3)} - \frac{\alpha r q^2 g_1}{2\kappa(2\alpha+1)(5\alpha+3)(5\alpha+4)} \\ &-\frac{\alpha q g_1^2\,(2r+qs)}{24\kappa(\alpha+1)^2(4\alpha+3)} - \frac{rqb}{2(2\alpha+1)(4\alpha+3)} \\ &-\frac{\alpha s q g_1^3}{6\kappa(\alpha+1)(2\alpha+3)(3\alpha+4)} - \frac{r\,(g_2+bg_1)}{3(\alpha+1)} - \frac{s\,(2g_1g_2+bg_1^2)}{2(2\alpha+3)} \\ &-\frac{\alpha m q^2}{2\kappa(\alpha+1)^2(2\alpha+1)} - \frac{\alpha q\,(g_3+bg_2+mg_1)}{\kappa(\alpha+1)(\alpha+2)}\,. \end{aligned} \tag{4.23}$$

Using (4.22) and (4.7) for n=4, we get

$$\begin{aligned} g_4 = &-\frac{\alpha r q^4}{6\kappa(2\alpha+1)^2(5\alpha+3)(7\alpha+4)} - \frac{\alpha r q^3 g_1}{4\kappa(2\alpha+1)(3\alpha+2)(5\alpha+3)} \\ &-\frac{\alpha q^2 g_1^2\,(2r+qs)}{6\kappa(\alpha+1)(4\alpha+3)(5\alpha+4)} - \frac{rbq^2}{2(2\alpha+1)(5\alpha+3)} \\ &-\frac{\alpha s q^2 g_1^3}{24\kappa(\alpha+1)^2(2\alpha+3)} - \frac{rq\,(g_2+bg_1)}{(4\alpha+3)} - \frac{sq\,(2g_1g_2+bg_1^2)}{6(\alpha+1)} \\ &-\frac{\alpha m q^3}{\kappa(\alpha+1)(2\alpha+1)(3\alpha+2)} - \frac{\alpha q^2\,(g_3+bg_2+mg_1)}{2\kappa(\alpha+1)^2} - \frac{A_2 q}{\alpha+1}\,. \end{aligned} \tag{4.24}$$

Similar derivation for g_5 and g_6 can be found in Appendix A.

4.4 Numerical approach: one-dimensional radial basis function networks

In this section, the 1D-IRBFN method (Mai-Duy and Tanner, 2007) is briefly described with the full details given in Appendix B.1. We extend the method to calculate function derivatives up to 6^{th}-order. The domain of interest is discretised using a Cartesian grid, i.e. an array of straight lines that run parallel to the x- and y-axes. The dependent variable u and its derivatives on each grid line are approximated using an IRBFN interpolation scheme. Consider an x-grid line with N_x points. The variation of u along this line is sought in the IRBF form. The highest-order derivative (order n) is decomposed into RBFs. The RBF networks are then integrated to obtain the lower-order derivatives and the function itself,

$$\frac{\partial^n u(x)}{\partial x^n} = \sum_{i=1}^{N_x} w^{(i)} G^{(i)}(x) = \sum_{i=1}^{N_x} w^{(i)} H^{(i)}_{[n]}(x), \tag{4.25}$$

$$\frac{\partial^{n-1} u(x)}{\partial x^{n-1}} = \sum_{i=1}^{N_x} w^{(i)} H^{(i)}_{[n-1]}(x) + p_1, \tag{4.26}$$

$$\frac{\partial^{n-2} u(x)}{\partial x^{n-2}} = \sum_{i=1}^{N_x} w^{(i)} H^{(i)}_{[n-2]}(x) + p_1 x + p_2, \tag{4.27}$$

... ...

$$\frac{\partial u(x)}{\partial x} = \sum_{i=1}^{N_x} w^{(i)} H^{(i)}_{[1]}(x) + p_1 \frac{x^{n-2}}{(n-2)!} + p_2 \frac{x^{n-3}}{(n-3)!} + ... + p_{n-2} x + p_{n-1}, \tag{4.28}$$

$$u(x) = \sum_{i=1}^{N_x} w^{(i)} H^{(i)}_{[0]}(x) + p_1 \frac{x^{n-1}}{(n-1)!} + p_2 \frac{x^{n-2}}{(n-2)!} + ... + p_{n-2} \frac{x^2}{2} + p_{n-1} x + p_n, \tag{4.29}$$

where $\left\{G^{(i)}(x)\right\}_{i=1}^{N_x} = \left\{H^{(i)}_{[n]}(x)\right\}_{i=1}^{N_x}$ are known RBFs; $H^{(i)}_{[n-1]}(x) = \int H^{(i)}_{[n]}(x)dx$; $H^{(i)}_{[n-2]}(x) = \int H^{(i)}_{[n-1]}(x)dx$; ...; $H^{(i)}_{[1]}(x) = \int H^{(i)}_{[2]}(x)dx$; $H^{(i)}_{[0]}(x) = \int H^{(i)}_{[1]}(x)dx$; $\{w^{(i)}\}_{i=1}^{N_x}$ are RBF weights to be determined; and p_1, p_2, ..., and p_n integration constants which are also unknown. An example of RBF, used in this work, is the multiquadrics $G^{(i)}(x) = \sqrt{(x - x^{(i)})^2 + a^{(i)2}}$, $a^{(i)}$ - the RBF width determined as $a^{(i)} = \beta d^{(i)}$, β a positive factor, and $d^{(i)}$ the distance from the i^{th} centre to its nearest neighbour. In the present study, the highest order of derivative is 6^{th}-order ($n = 6$). The new basis functions $H^{(i)}_{[5]}(x)$, $H^{(i)}_{[4]}(x)$, ..., $H^{(i)}_{[1]}(x)$ and $H^{(i)}_{[0]}(x)$ obtained from integrating the multiquadrics $G^{(i)}(x)$ are as follows.

$$H^{(i)}_{[5]}(x) = \frac{r}{2} A + \frac{a^2}{2} B, \tag{4.30}$$

$$H^{(i)}_{[4]}(x) = \left(\frac{r^2}{6} - \frac{a^2}{3}\right) A + \frac{a^2 r}{2} B, \tag{4.31}$$

$$H^{(i)}_{[3]}(x) = \left(-\frac{13a^2 r}{48} + \frac{r^3}{24}\right) A + \left(-\frac{a^4}{16} + \frac{a^2 r^2}{4}\right) B, \tag{4.32}$$

$$H^{(i)}_{[2]}(x) = \left(\frac{a^4}{45} - \frac{83a^2 r^2}{720} + \frac{r^4}{120}\right) A + \left(-\frac{a^4 r}{16} + \frac{1a^2 r^3}{12}\right) B, \tag{4.33}$$

$$H^{(i)}_{[1]}(x) = \frac{113a^4 r - 194a^2 r^3 + 8r^5}{5760} A + \frac{15a^6 + 60a^2 r^2(-3a^2 + 2r^2)}{5760} B, \tag{4.34}$$

$$H^{(i)}_{[0]}(x) = \frac{-128a^6 + 1779a^4 r^2 - 1518a^2 r^4 + 40r^6}{201600} A + \frac{5a^6 r - 20a^4 r^3 + 8a^2 r^5}{1920} B. \tag{4.35}$$

in which $r = x - x^{(i)}$, $A = \sqrt{r^2 + a^{(i)2}}$, and $B = \ln(r + A)$.

The discretisation of spatial derivatives in Eqs. (4.1) and (4.6) is carried out by using (4.25)–(4.28). Note that the peak of depth-averaged concentration C moves along the positive x-axis as time increases and the concentration on the inlet and outlet boundaries of the computational domain is assumed to be zero. In order to reduce the computational effort, an algorithm to regularly shift the computational domain along the x-axis after a period of time $\Delta\tau$ is applied (Mohammed, Ngo-Cong, Strunin, Mai-Duy and Tran-Cong, 2014). In this algorithm, the computational domain is chosen large enough to make sure the value of C on the inlet and outlet boundaries equal to or less than $\epsilon_C = 10^{-4}$ during the computation.

4.5 Numerical results and discussion

In this section, we investigate the performance of the 1–D and 2–D models for both power and logarithmic velocity profiles using the 1D-IRBFN method in a simulation of turbulent shear flow in an open channel. The comparison of numerical solutions between both velocity profiles are also presented.

4.5.1 Power velocity profile

We conduct a grid convergence study of C_{max} and x_{max} (the maximum depth-averaged concentration and its position along the channel, respectively) for the 2–D model at $\mathrm{Re} = 10^5$ as shown in Fig. 4.1. The converged solution is obtained for grids equal or denser than 151×151. The corresponding study for the 1–D model is described in Fig. 4.2 in comparison with the converged 2–D solution. The grid convergence behaviour is also observed for the 1–D model as the solutions are indistinguishable when refining the grid. A good agreement between the 1–D and 2–D models is demonstrated in Fig. 4.2 showing that the 1–D and 2–D solutions of C_{max} and x_{max} are coincide at large times.

Fig. 4.3 compares the solutions of C_{max} and x_{max} w.r.t. time among the 2-D model and the 1-D models with different orders (from 2^{nd}-order to 6^{th}-order). It appears that there is a small gap of C_{max} among the 1-D models with different orders and the 2-D model at the beginning time, however all solutions become coincide as time increases. The same trend is also demonstrated in Fig. 4.4 showing the variation of C_{max} along the channel at different times $t = 20.0,\ 30.0$ and 150.0. Note that the $3^{rd} - 6^{th}$-order 1-D models yield more accurate solutions to that of the 2-D model than the 2^{nd}-order 1-D model at the beginning time ($t = 20.0$ and 30.0).

4.5.2 Comparison between logarithmic and power 1–D models

We compare the performance of the 1-D models associated with the power and logarithmic velocity profiles. For the purpose of comparison, we need to choose the value of R for the logarithmic velocity model so that the advection velocity for both models are the same (i.e., $g_1^{log} = g_1^{power}$). For the case of the power velocity model in Section 4.5.1, we have $Re = 10^5$ and $g_1 = -23.6392$. For the case of the logarithmic velocity model, the variation of g_1 w.r.t. R is described in Fig. 4.5. Based on this figure, we take $R = 3850.04$ in order to satisfy the condition $g_1^{log} = g_1^{power} = -23.6392$. The obtained logarithmic and power velocity profiles are depicted in Fig. 4.6.

We conduct a grid convergence study of C_{max} and x_{max} for the 2–D model at $R = 3850.04$ (Fig. 4.7). The converged solution is obtained for grids equal or denser than 151×151. The corresponding study for the 1–D model is described in Fig. 4.8 in comparison with the converged 2–D solution on a grid of 151×201. The grid convergence behaviour is also achieved as the solutions are almost coincide when increasing the grid number. A good agreement between the 1–D and 2–D models is demonstrated in Fig. 4.8 showing the 1–D and 2–D solutions of C_{max} and x_{max} w.r.t. time. Fig. 4.9 compares the solutions of C_{max} and x_{max} w.r.t. time among the 2-D model and the 1-D models with different orders (from 2^{nd}-order to 6^{th}-order). It can be seen that there is a small gap of C_{max} among the 1-D models with different orders and the 2-D model at the beginning time, however, all solutions become coincide with increasing time.

In Eq. (4.6), the coefficients g_n are analytically derived and responsible for the effects of advection, diffusion and dispersion. The coefficients are defined as functions of parameters characterising the flow such as Reynolds number and von Karman constant κ. Even without solving the equation (4.6), we can quickly estimate the size of the contaminant based on its coefficients g_n. The characteristic distances over which the substance propagates during a period of time T are defined by (see Chapter 1, Eq. (1.30))

$$L_1 = g_1 T \qquad \text{due to the advection,} \tag{4.36}$$

$$L_2 = (g_2 T)^{1/2} \quad \text{due to the diffusion,} \tag{4.37}$$

$$L_3 = (g_3 T)^{1/3} \quad \text{due to the dispersion.} \tag{4.38}$$

From (4.36)-(4.38), we have $g_2/g_1 = L_2^2/L_1$ and $g_3/g_1 = L_2^3/L_1$. Therefore, with the same advection effect, the bigger the ratio g_2/g_1 and g_3/g_1 are, the larger the effects of diffusion and dispersion happen.

We study a shear flow in an open channel with the logarithmic velocity profile for the 2–D model and 1–D model including high-order terms for $R = 3742.64$. For both the logarithmic and power velocity profiles, the results of C_{max} and x_{max} for $3^{rd} - 6^{th}$–order 1–D models are almost the same and in good agreement with those of the 2–D model. Table 4.1 gives the ratios of power coefficients to

logarithmic coefficients for the case of $g_1^{log} = g_1^{power}$. The ratios demonstrate that the effects of diffusion and dispersion for the power model are larger than those for the logarithmic model as confirmed by the following numerical results.

Fig. 4.10 presents the results of x_{max} and C_{max} with respect to time, respectively, for the 1–D and 2–D models and the logarithmic and power velocity profiles. For both velocity profiles, the 1–D and 2–D solutions converge to each other with increasing time. The figure also shows that the power model has larger diffusion and dispersion effects than the logarithmic model since the values of C_{max} obtained by the power model is less than those by the logarithmic model. This agrees well with the analytic results obtained from the centre manifolds theory where the ratios of g_2/g_1 and g_3/g_1 of the power theory are larger than those of the logarithmic theory (Table 4.1). Fig. 4.11 describes the relative error $(\delta/\Delta = (C_{max}^{2D} - C_{max}^{1D})/C_{max}^{2D})$ between the 1–D and 2–D solutions reduces as the time goes on for both profiles. The figure demonstrates that the logarithmic–1–D model performs better than the power–1–D model at the beginning time, however, the latter is superior to the former at large times.

Table 4.1 Comparison of coefficients between the power velocity model ($Re = 10^5$) and the logarithmic velocity model ($R = 3850.04$) when $g_1^{log} = g_1^{power}$, and $\kappa = 0.4$.

	g_1	g_2	g_3	g_4	g_5	g_6
Power	-23.6392	5.7362	11.5455	-74.6714	76.0521	343.9028
Logarithmic	-23.6392	3.9538	2.9509	-8.6096	14.2921	-10.6065
Power/Logarithmic	1.00	1.45	3.91	8.67	5.32	-32.42

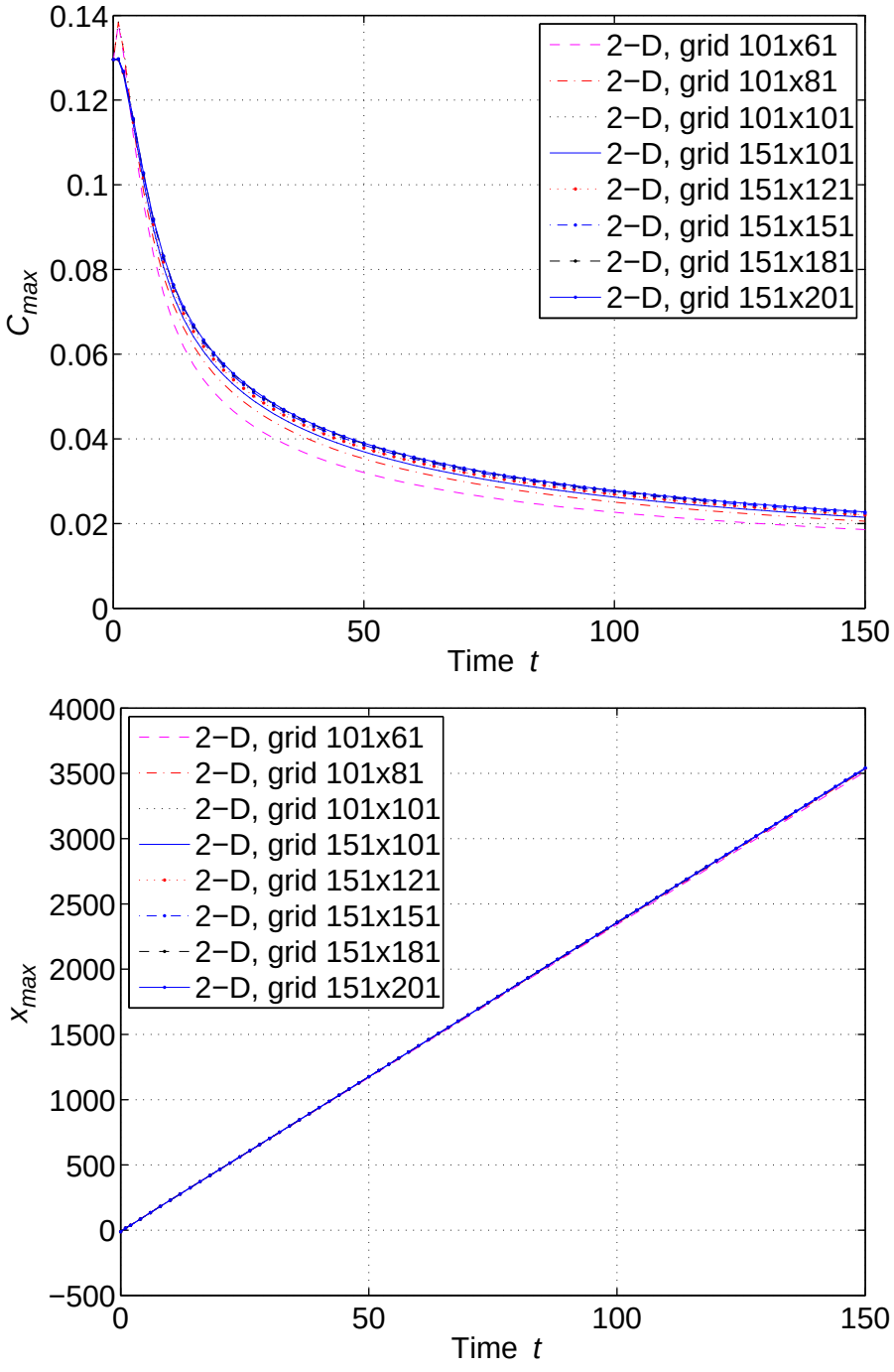

Figure 4.1 Turbulent shear flow in an open channel with power velocity profile: grid convergence study for 2–D analysis of C_{max} and x_{max} with respect to time t, for $\mathrm{Re} = 10^5$ and $\beta = 1.0$.

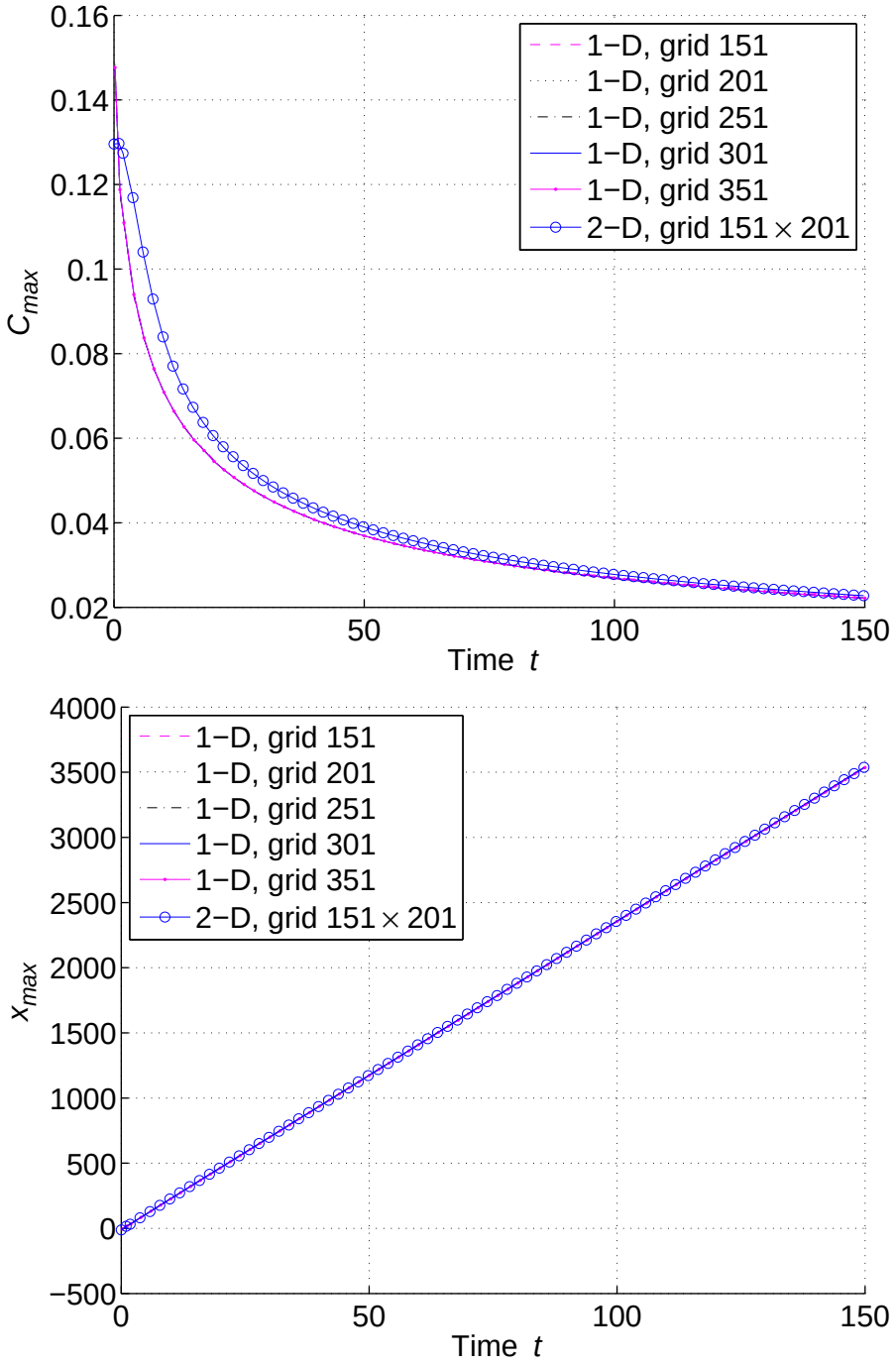

Figure 4.2 Turbulent shear flow in an open channel with power velocity profile: grid convergence study for 1–D analysis of C_{max} and x_{max} with respect to time t, for $\mathrm{Re} = 10^5$ and $\beta = 1.0$.

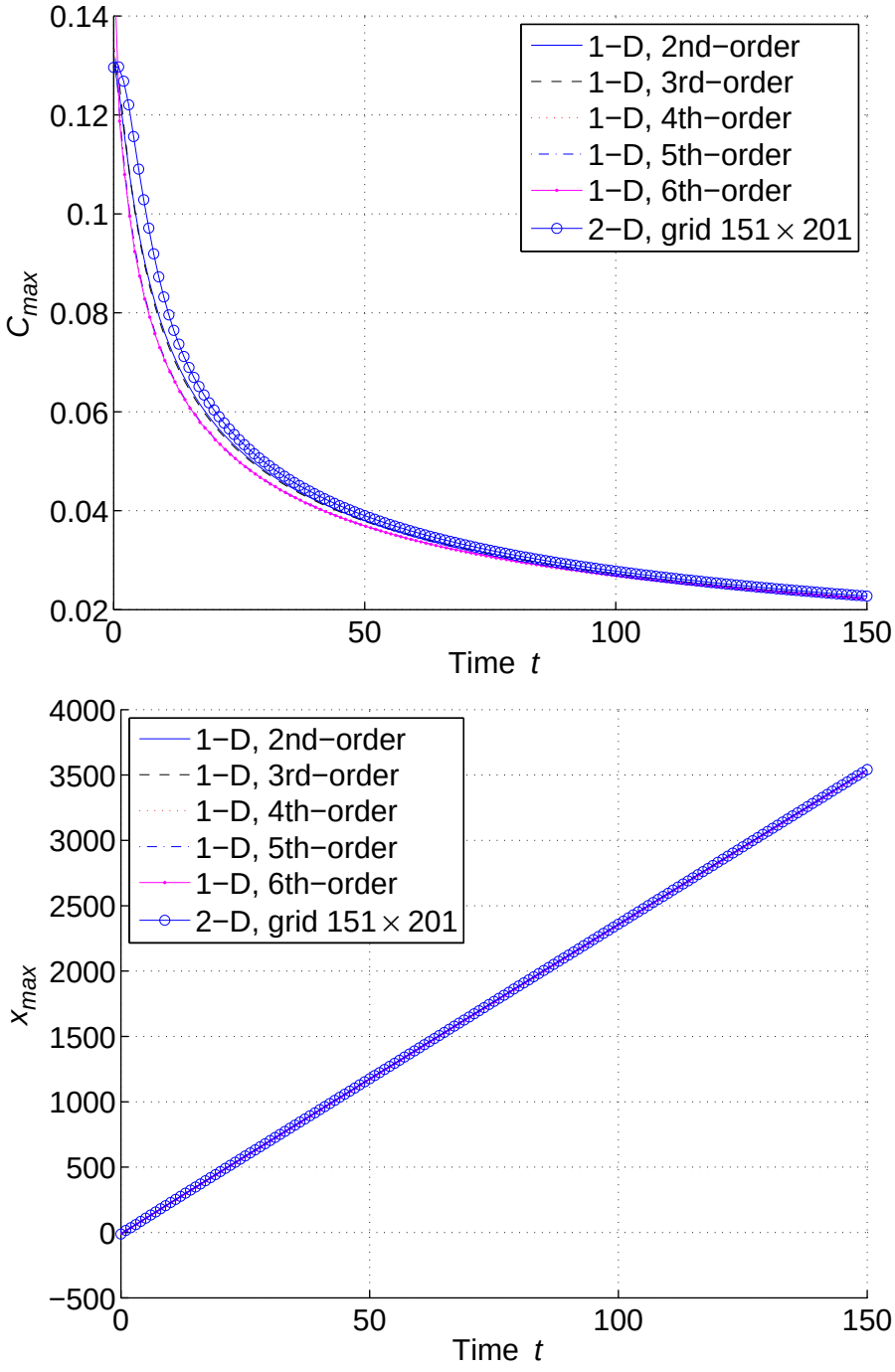

Figure 4.3 Turbulent shear flow in an open channel with power velocity profile: comparison of C_{max} and x_{max} among the 2–D and 1–D models with different orders, using grids of 151×201 for 2–D analysis and 301 for 1–D analysis, for $\mathrm{Re} = 10^5$ and $\beta = 1.0$.

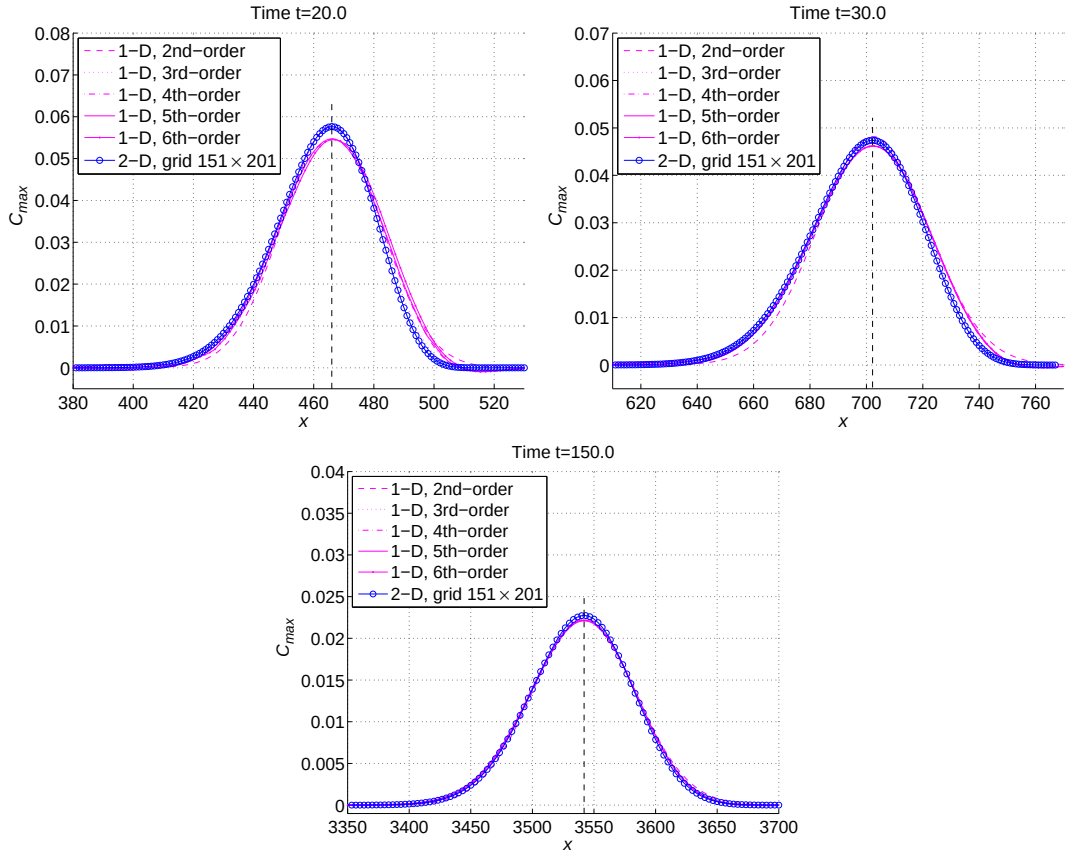

Figure 4.4 Turbulent shear flow in an open channel with power velocity profile: comparison of depth-averaged concentration along the channel among the 2–D and 1–D models with different orders, using grids of 151×201 for 2–D analysis and 301 for 1–D analysis, $\mathrm{Re} = 10^5$, $\beta = 1.0$ and $R = 3742.64$.

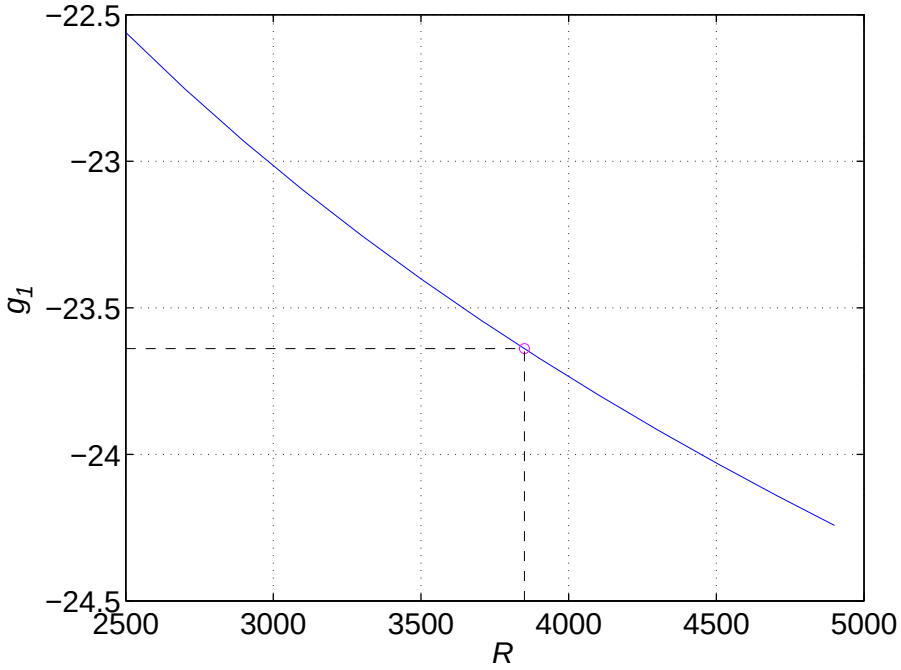

Figure 4.5 Variation of g_1 w.r.t. R for the logarithmic velocity profile. Note that at $R = 3850.04$, $g_1^{logarithmic} = g_1^{power} = -23.6392$ (corresponding to the power velocity profile with $Re = 10^5$ and $\beta = 1.0$).

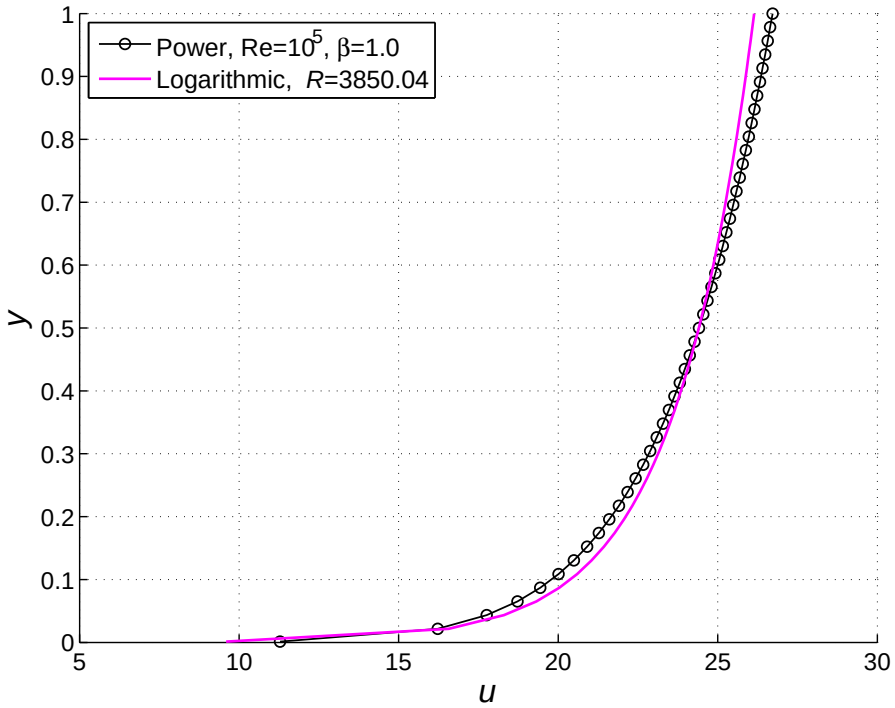

Figure 4.6 Comparison between the logarithmic velocity profile (for $R = 3850.04$) and power velocity profile (for $\mathrm{Re} = 10^5,\ \beta = 1.0$). Note that both profiles yield the same averaged velocity ($g_1^{logarithmic} = g_1^{power}$).

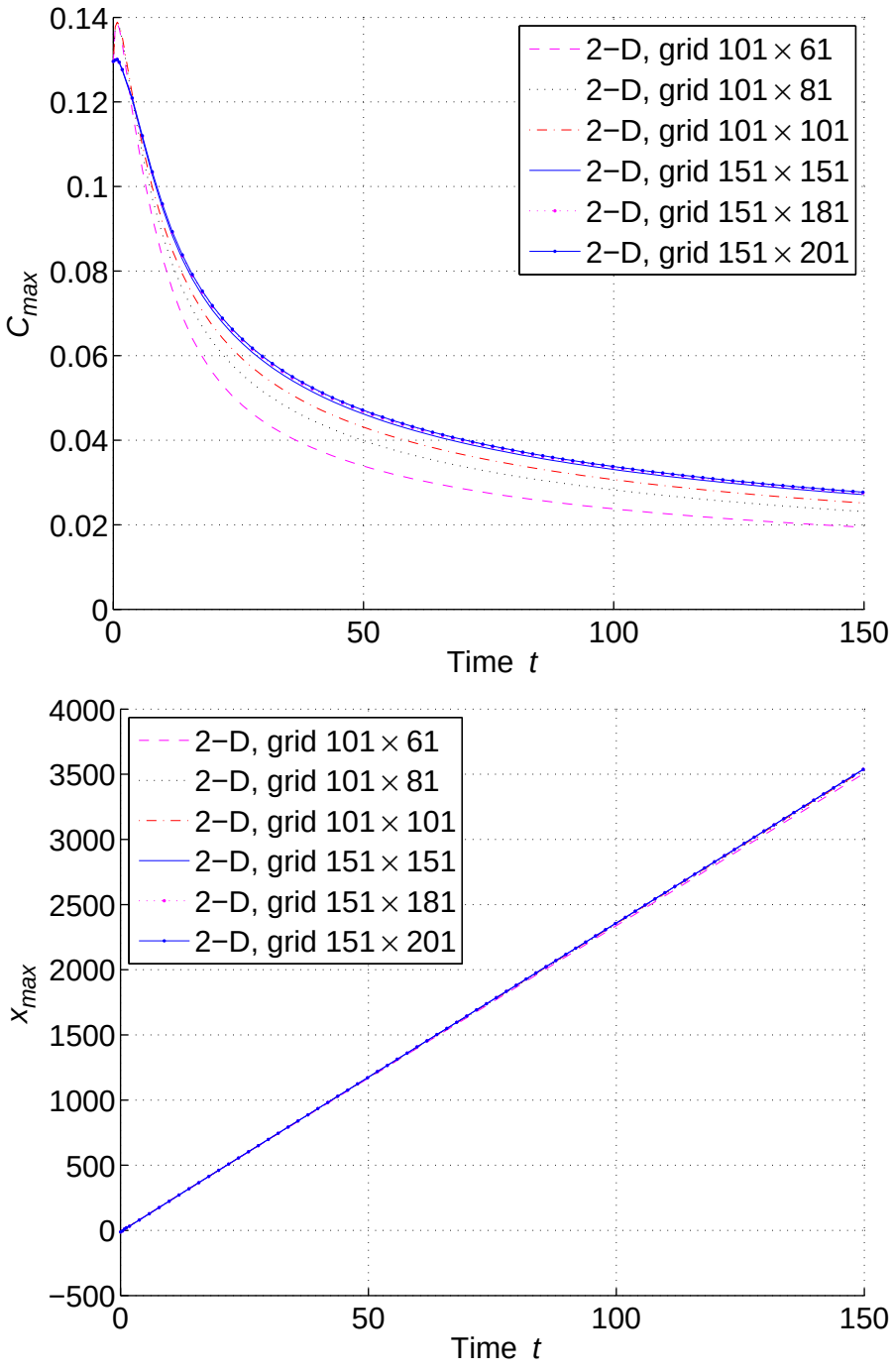

Figure 4.7 Turbulent shear flow in an open channel with logarithmic velocity profile: grid convergence study for 2–D analysis of C_{max} and x_{max} with respect to time t, for $R = 3850.04$.

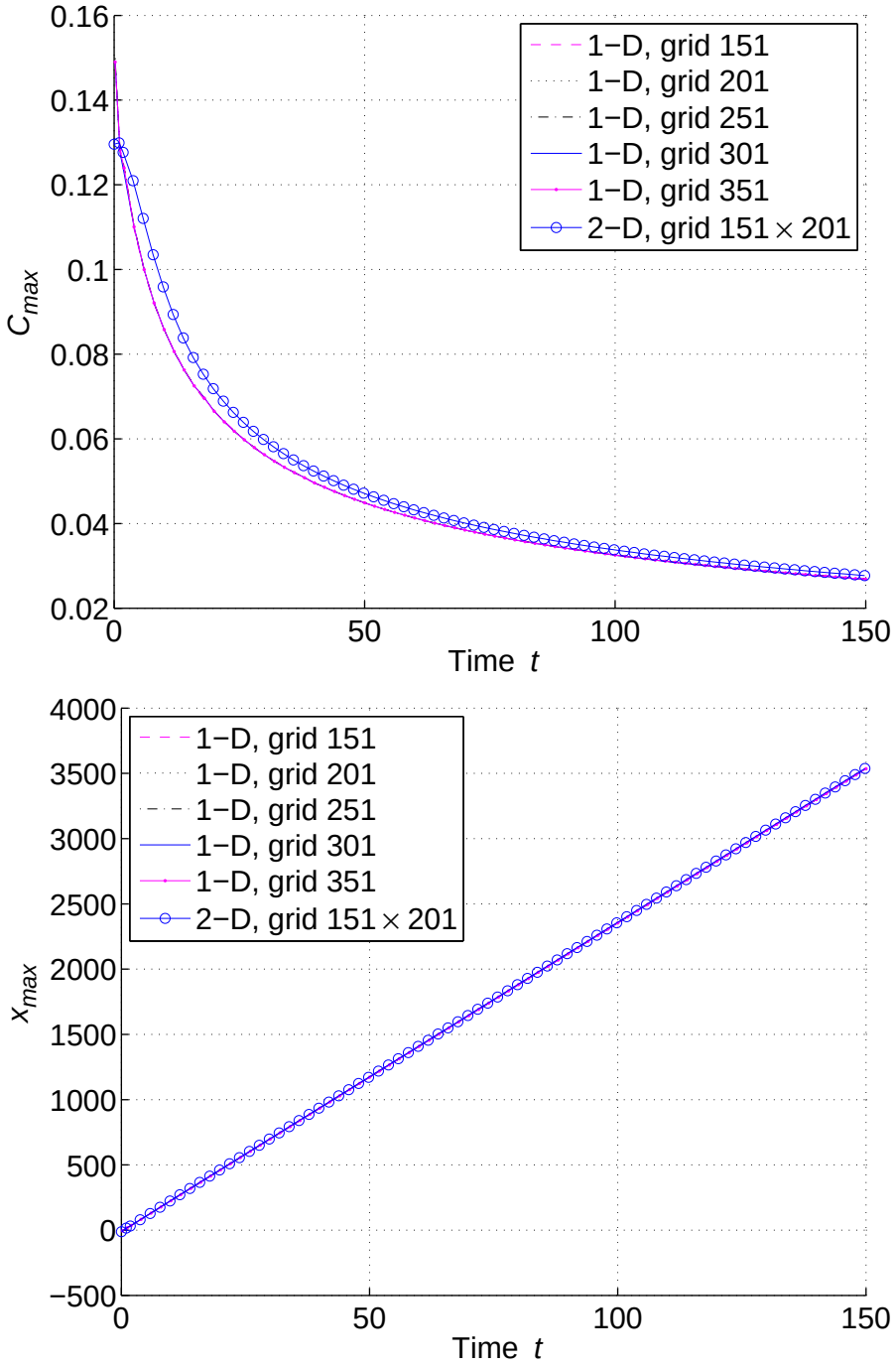

Figure 4.8 Turbulent shear flow in an open channel with logarithmic velocity profile: grid convergence study for 1–D analysis of C_{max} and x_{max} with respect to time t, for $R = 3850.04$.

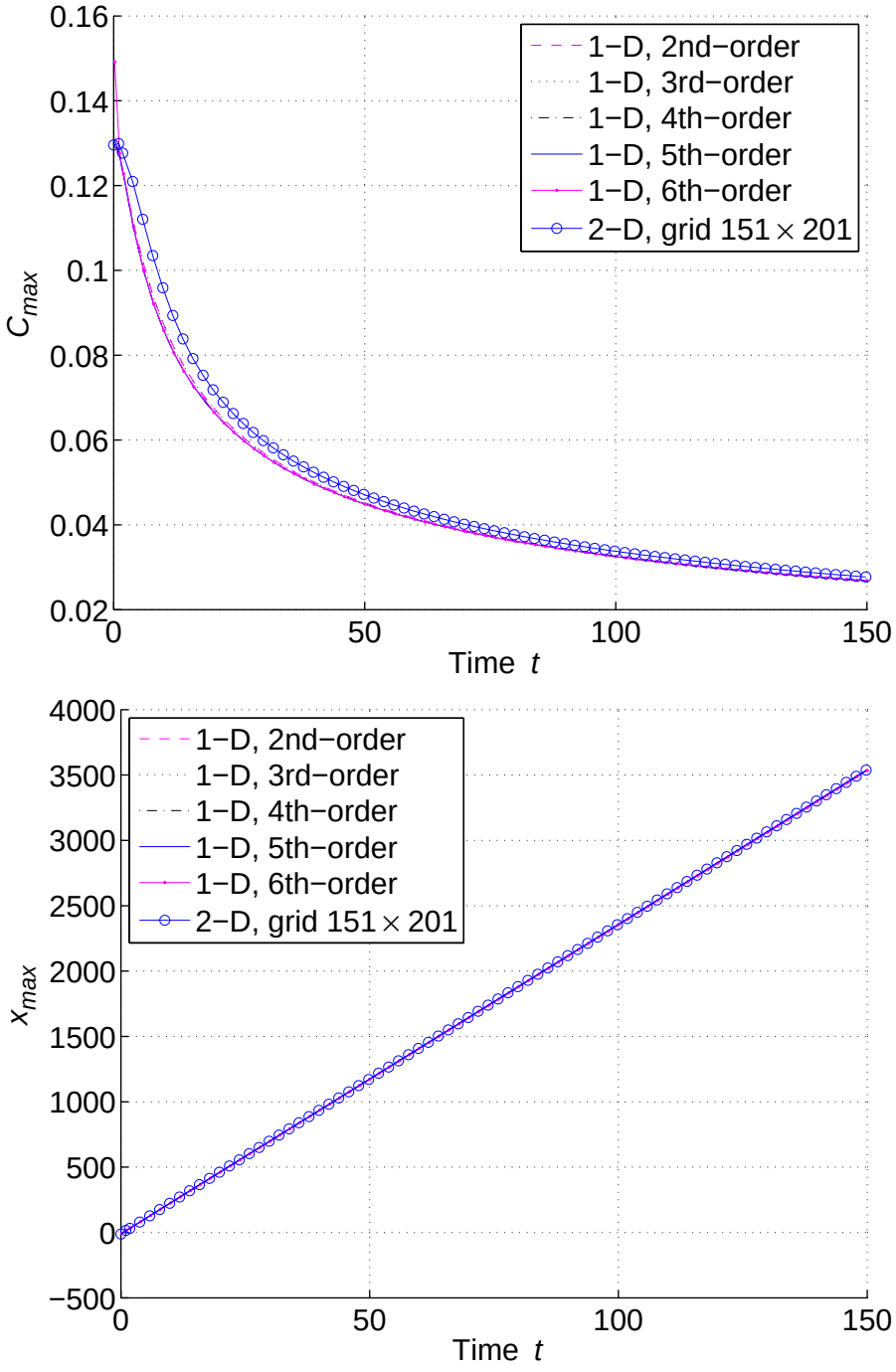

Figure 4.9 Turbulent shear flow in an open channel with logarithmic velocity profile: comparison of C_{max} and x_{max} among the 2–D and 1–D models with different orders, using grids of 151×201 for 2–D analysis and 301 for 1–D analysis, for $R = 3850.04$.

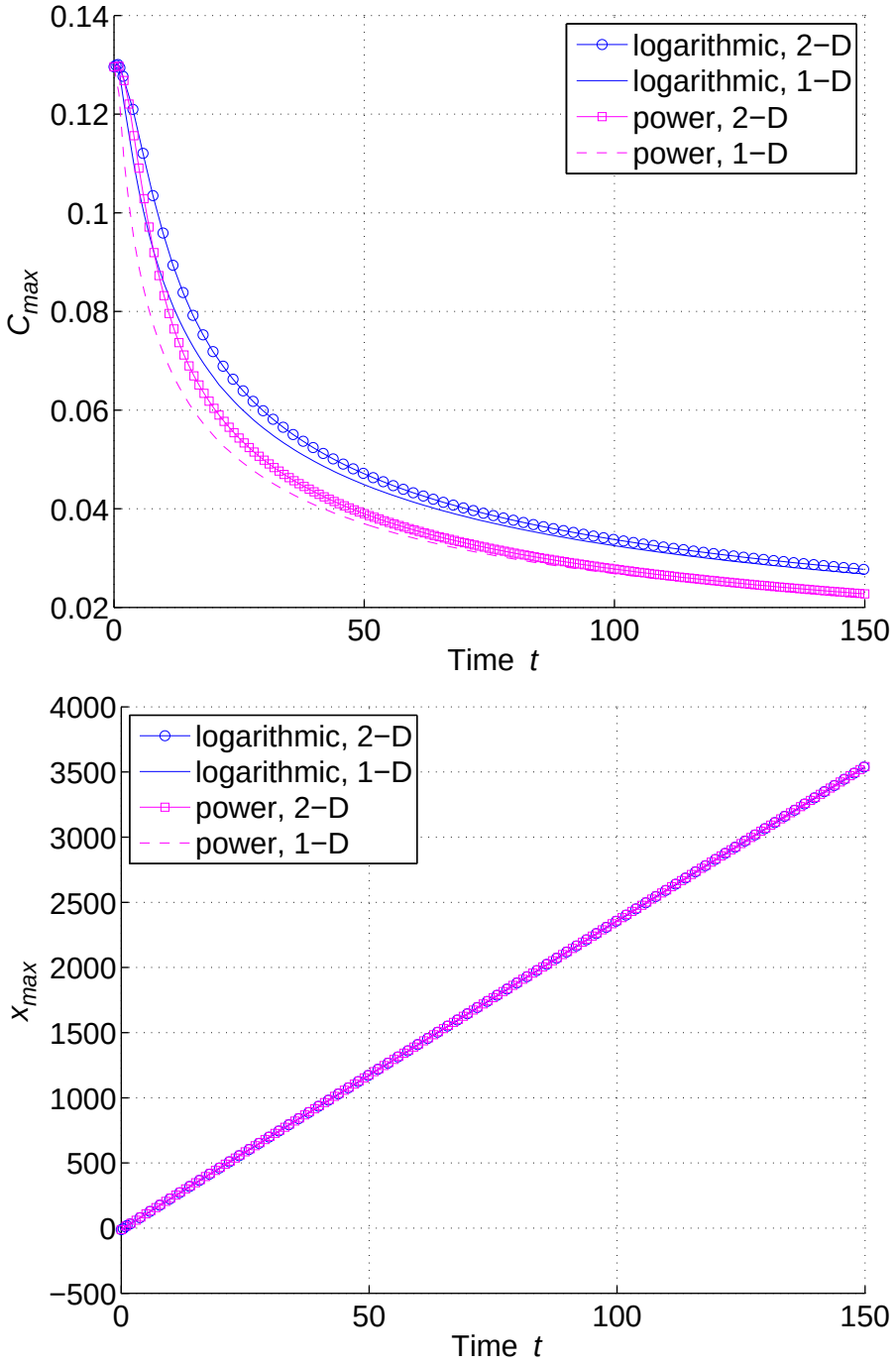

Figure 4.10 Comparison among the 1–D and 2–D results (C_{max} and x_{max} with respect to t) of the power velocity model ($Re = 10^5$) and the logarithmic velocity model ($R = 3850.04$) when $g_1^{log} = g_1^{power}$.

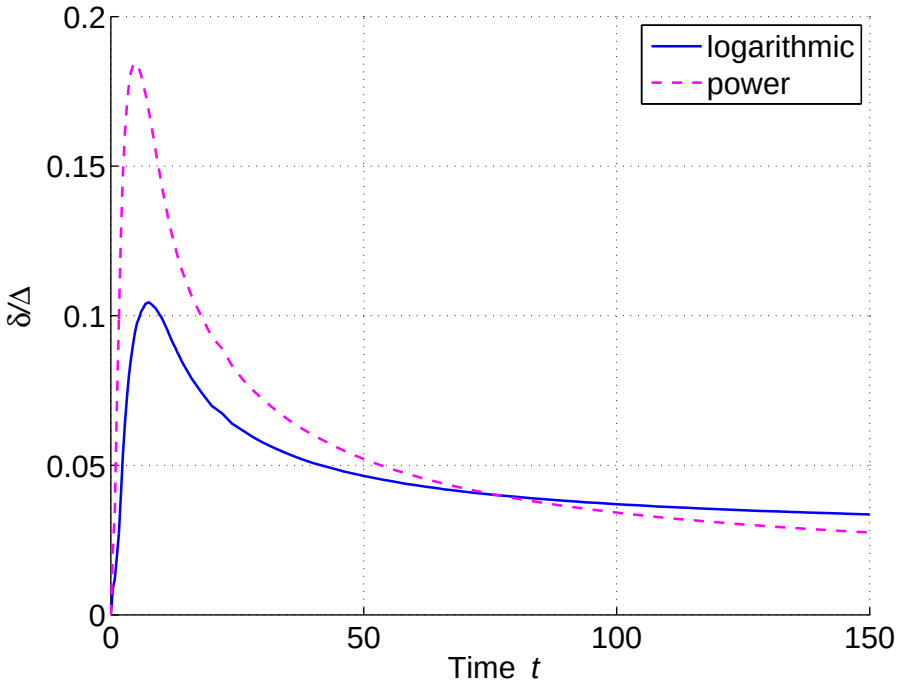

Figure 4.11 Comparison of δ/Δ between the power velocity model ($Re = 10^5$) and the logarithmic velocity model ($R = 3850.04$) when $g_1^{log} = g_1^{power}$.

4.6 Conclusion

The centre manifolds theory is applied to derive 1–D the high-order partial differential equation governing the dispersion of contaminant in turbulent channel flows based on both the power and logarithmic velocity profiles. The high-order equations (up to sixth-order) are then successfully verified through the solution of the original 2–D equation using the 1D-IRBFN method as a numerical approach. The numerical solution of 1–D models are in good agreement with that of the 2–D model for both the power and logarithmic velocity profiles. It is noted that the solutions of $3^{rd} - 6^{th}$-order 1–D equations are almost coincide and more accurate than that of the 2^{nd}-order 1–D equation, compared to the 2–D solution. For the same advection velocity ($g_1^{log} = g_1^{power}$), both 1–D and 2–D results show that the power model produces larger diffusion and dispersion effects than the logarithmic model. It is worth pointing out that one can estimate the advection, diffusion and dispersion of contaminants in a channel flow based on the analytically derived coefficients without the need of solving the 1–D or 2–D governing equations.

Chapter 5

Asymptotics of averaged turbulent transfer in urban canopy flows

We formulate and analyse a long-time asymptotic model of dispersion in turbulent canopy flows, of urban or industrial nature. The model is formulated in terms of the concentration averaged across the flow, for example over the river depth. The general approach laying a firm base into the averaging procedure was proposed by Roberts and co-authors in the late 1980s. We derive an evolution partial differential equation for the averaged concentration, involving first, second and higher derivatives with respect to spatial coordinate. The coefficients of the equation are derived and analysed against the parameters characterising the turbulent flow. In particular we show that, in the limit of large flow depths, the values of the coefficients coincide with those obtained earlier for the flow over a smooth bottom.

5.1 Introduction

Centre manifold approach developed in a series of works originated by Roberts (Mercer and Roberts, 1990) allows to derive a relatively simple one-dimensional partial differential equation describing the spreading of the depth-averaged amount of tracer, such as heat or concentration of a contaminant, in environmental and industrial flows,

$$\partial_t C = \sum_{i=1}^{\infty} g_i \partial_x^i C \approx g_1 \partial_x C + g_2 \partial_x^2 C \,, \tag{5.1}$$

where $C(x,t)$ is the depth-averaged concentration of the tracer, axis x is directed along the flow, for example, along the river or atmospheric wind. In the model (5.1) the spreading results from the advection, diffusion and dispersion, expressed by the first, second and third x-derivatives respectively. It is assumed that sufficiently long time has passed since the tracer had been discharged into the flow. As a result, the x-variations of the concentration are assumed slow. Further below we show how the coefficients g_i of the model are deduced using the original non-averaged transfer equation. In the end, they emerge as combinations of fundamental input parameters such as the Reynolds number. It is important to note that the model is not only theoretically sound because it is supported by the centre manifold theory, but can also provide, using the coefficients g_i, simple practical estimates of the sizes of clouds of emitted tracers. For example, the typical distance travelled by the tracer during the time T is

$$\begin{aligned} &L_1 = g_1 T \text{ due to the advection,} \\ &L_2 = (g_2 T)^{1/2} \text{ due to the diffusion.} \end{aligned} \tag{5.2}$$

Once g_i are tabulated against the physical parameters characterizing the canopy and the flow, one can use (5.2) to calculate how far the patch of the substance has drifted and what its size approximately became. The use of (5.2) is a simple alternative (of course at the expense of accuracy) to numerically solving equation (5.1) or solving the original advection-diffusion equation, from which (5.1) is derived.

Previously, equations of the type (5.1) were derived by different approaches in application to flows, both laminar and turbulent, near smooth substrates. In his pioneering paper published several decades ago Taylor (1953) constructed an approximate advection-diffusion equation which controls the long term evolution of the average concentration of a contaminant in a straight channel or pipe. Initially the equation was intended for laminar flows, but later it was extended in straightforward manner to describe turbulent flows as well (Taylor, 1954; Aris, 1956). Researchers used a variety of techniques analysing the downstream transport of tracers in channels. For example, Aris (1956) analysed the concentration moment, Pagitsas et al. (1986) considered multiple time scales, and Chatwin (1970) resorted to the asymptotic series approach. Roberts and co-authors (Mercer and Roberts, 1990; Roberts and Strunin, 2004; Strunin and Roberts, 2009; Strunin, 2011) based their analysis on a rigorous procedure supported by the centre manifold theory. In brief, if the normalised state of the system has a number of zero eigenvalues, say n, and that if all the other eigenvalues are negative, then the system evolves exponentially quickly towards an n-dimensional centre manifold. On the centre manifold, the system then evolves slowly according to the evolution of n amplitude functions reaching a relatively constant state for which differential equations can be derived. Based on the centre manifold theory and its generalisation for finite dimensions by Coullet and Spiegel (1983), Roberts (1988) developed a procedure to calculate a sequence of successively more accurate approximations to the evolution of the concentration in space and time. Strunin

and Roberts (2009); Strunin (2011) used the centre manifolds to derive asymptotic models of shear dispersion in log- and power- turbulent flows in smooth open channels. The flows near rough surfaces, such as agricultural fields or urban canopies, are not less important and can be treated with the same approach.

The canopy flows are extremely complicated, and any transfer model would inevitably depend on adopted approximations for turbulence through the canopy and adjacent roughness layer (using the terminology of Raupach et al. (1980)). The roughness layer is the layer above the canopy and beneath the lower edge of the inertial layer. We call it matching layer in Section 5.3, we also refer to Fig. 5.2. We consider the layered model described in Macdonald (2000). There are different models based on various versions of the flow structure, particularly for agricultural canopies, e.g. (Harman and Finnigan, 2007). We analyse a steady *inertial* turbulent layer of constant width H above the canopy turbulent layer of width h. It can be, for example, a flow in an open channel subject to a constant shear stress applied to the fluid surface and measured by the friction velocity u_*^2. Hereafter we refer to the channel flow, however, our analysis can be generalised to the cases of turbulent boundary layers of varying depth, for example near a semi-plane. The ensemble-averaged concentration, assumed to be passive, $c(x, y, t)$, is subject to the advection-diffusion equation

$$\partial_t c + u(y)\partial_x c = \partial_y[D(y)\partial_y c]\,, \tag{5.3}$$

where $D(y)$ is the turbulent diffusion coefficient across the flow. The model (5.3) is more applicable to channel fluid flows than atmospheric flows because atmospheric wind may rapidly change direction and strength (Legg, 1983; Flesh et al., 1995; Arya, 1999). Similarly to Mercer and Roberts (1990) we neglect the downstream turbulent diffusion to explore the situation, where the downstream diffusion and dispersion emerge in the averaged equation (5.1) as "pure" effects of the cross-flow diffusion and advection in the original equation (5.3). Yet, our analysis can be generalised to include the downstream diffusion in (5.3) without difficulty. The boundary conditions express non-penetration through the surface, $y = H$, and the bottom, $y = 0$,

$$D\partial_y c|_{y=0} = D\partial_y c|_{y=H} = 0\,. \tag{5.4}$$

Turbulent diffusion tends to spread the substance uniformly over the depth of the channel. The concentration would quickly become constant along vertical if it was not for the velocity shear. Because of it, near the bottom the substance particles move slowly, while the particles near the surface move fast. This effect creates non-uniformity in vertical direction and acts against the diffusion. An ongoing competition of the two factors – advection and diffusion – controls the distribution of the substances in the flow. Such a competition can be effectively modelled using the centre manifold theory, a tool frequently used in nonlinear science. We utilise this approach in our work.

The present chapter is structured as follows. In Section 5.2 we explain the basic principles of the centre manifolds. Then, in Section 5.3 we specify the velocity $u(y)$ and turbulent diffusion coefficient $D(y)$; we need them to derive equation (5.1)– our ultimate goal. Clearly, $u(y)$ and $D(y)$ depend on the structure of turbulence in the flow. This structure is viewed as three-layered, namely, canopy layer, matching layer (roughness layer) and inertial layer. In Section 5.4 the mathematical method described in the introduction is applied to the structure described in Section 5.3 and, as a result, equation (5.1) is derived (the leading coefficients g_i are numerically calculated). Section 5.5 presents the verification of the derived 1–D model by direct computations using the original 2–D model. Section 5.6 summarizes the chapter.

5.2 Centre manifold approach

In the following we briefly describe the 1–D model based on the centre manifold theory. Taking the Fourier transform to (5.3), we obtain

$$\partial_t \hat{c} = L[\hat{c}] - iku(y)\hat{c}\,, \tag{5.5}$$

where $\hat{c}(y,k,t)$ is the Fourier transform defined by $1/(2\pi)\int_{-\infty}^{\infty}\exp(-ikx)c\,dx$. The linear operator $L[\hat{c}] = \partial_y[D(y)\partial_y\hat{c}]$ expresses the cross-flow turbulent diffusion and has a discrete spectrum of eigenvalues. One of the eigenvalues is equal to zero; it corresponds to the neutral eigenmode $\hat{c}$ =const that is an arbitrary constant level of concentration across the channel. Based on centre manifold theory, see Chapter 2 for more details, we assume that the concentration field is dependent only on the neutral mode $\hat{c}$ =const and how it evolves. As a result, we have

$$\hat{c} = \hat{c}(\hat{C},k,y) \quad \text{such that} \quad \partial_t\hat{C} = G(\hat{C},k)\,, \tag{5.6}$$

where $\hat{C}$ is the depth-average of $\hat{c}$ chosen as a measure of the "amplitude" of the neutral mode. Equation (5.6) effectively says that the concentration $\hat{c}(y,k,t)$ depends on the time through $\hat{C}$.

With (5.6) taken into account, equation (5.5) becomes

$$L[\hat{c}] = \frac{\partial\hat{c}}{\partial\hat{C}}G + iku\hat{c}\,. \tag{5.7}$$

Since the original problem (5.5) is linear in $\hat{c}$, we assume asymptotic expansion

for $\hat{c}$ and G which is also linear in $\hat{C}$, that is,

$$\hat{c} = \sum_{n=0}^{\infty} c_n(y)(ik)^n \hat{C}\,, \quad G = \sum_{n=1}^{\infty} g_n (ik)^n \hat{C}\,. \tag{5.8}$$

The definition of $\hat{C}$ as the depth-averaged implies the conditions

$$\frac{1}{h}\int_0^h c_0\, dy = 1\,, \quad \int_0^h c_n\, dy = 0 \quad \text{for } n = 1, 2, \ldots\,. \tag{5.9}$$

Substituting (5.8) into (5.7) and collecting similar terms in powers of the small parameter k we obtain a sequence of equations for the unknown functions $c_n(y)$ and coefficients g_n,

$$L[c_0] = 0\,, \tag{5.10}$$

$$L[c_n] = \sum_{m=1}^{n} c_{n-m} g_m + u(y) c_{n-1} \quad \text{for } n = 1, 2, \ldots\,. \tag{5.11}$$

Integrating (5.11) over the depth we get

$$D\partial_y c|_{y=H} - D\partial_y c|_{y=0} = g_n \overline{c_0} + \overline{u(y)c_{n-1}} = g_n + \overline{u(y)c_{n-1}}\,,$$

where the overline means depth-averaging. Once the fluxes through the boundaries are zero, $D\partial_y c|_{y=H} = D\partial_y c|_{y=0} = 0$, then

$$g_n = -\overline{u(y)c_{n-1}} \quad \text{for } n = 1, 2, \ldots\,. \tag{5.12}$$

Successively we can calculate g_n and c_n for any n. Considering only two leading terms in the G series in (5.8) gives

$$\partial_t \hat{C} = g_1 (ik)\hat{C} + g_2 (ik)^2 \hat{C} + \ldots\,. \tag{5.13}$$

Applying the inverse Fourier transform to (5.13), we obtain the advection-diffusion-dispersion equation for the averaged concentration in the form,

$$\frac{\partial C}{\partial t} = g_1 \frac{\partial C}{\partial x} + g_2 \frac{\partial^2 C}{\partial x^2} + \ldots\,. \tag{5.14}$$

Applying the inverse Fourier transform is band-limited to a low wave number for

which the centre manifold theory is applicable.

5.3 Layered structure of canopy turbulence

The aim of this section is to specify the velocity $u(y)$ and diffusion coefficient $D(y)$. They are part of the original transport equation (5.3), which we intend to treat with the centre manifold technique in the next section.

The inertial layer is described by the classical semi-logarithmic velocity profile (Tennekes and Lumley, 1972),

$$\frac{u(y)}{u_*} = \frac{1}{\kappa} \ln\left(\frac{y-d}{y_0}\right) , \tag{5.15}$$

where y_0 is the roughness height, d is the displacement height and κ is the von Karman constant. Eq. (5.15) is for the range $y_w < y < H$, where y_w is the matching layer height and H the inertial layer height. They are written out further in this section.

For the canopy layer, we adopt the model of Macdonald (2000). A parameter that characterizes geometry of obstacles is the frontal area density $\lambda = A_f/A_d$, where A_f is the frontal area of an obstacle exposed to the flow and A_d is the total surface area per obstacle (total area divided by the number of obstacles). Following Cionco (1965), Macdonald considered cylindrically shaped obstacles and assumed that within the canopy layer there is a balance between the local shear stress and obstacle drag force. This assumption leads to the exponential velocity profile

$$u(y) = u_h \exp\left[a\left(\frac{y}{h} - 1\right)\right] , \tag{5.16}$$

where a is the so-called attenuation coefficient and u_h is the velocity at $y = h$. Macdonald (2000) showed that for cube arrays with low packing density the predicted exponential velocity profile (5.16) provides an adequate fit to the average velocity profile within the canopy.

Typically $2 < a < 3$ (Cionco, 1972). Note that the exponential profile (5.16) does not give precisely zero at $y = 0$, however, the velocity there is small so it is regarded as a virtual zero. Thus, Eq. (5.16) is for the range $0 < y < h$, where h is the canopy height. The analysis of Macdonald (2000) showed that the parameter a linearly depends on the frontal area density as

$$a = m\lambda ,$$

with $m = 9.6$. Although this flow model is intended for the urban canopy or fluid flows with roughness in the first place, we will also consider the velocity profile (5.16) in application to vegetation canopies. Of course, we realise that vegetation is not a set of cylindrically shaped obstacles. However, there are certain physical arguments to support the same formula in application to plants (Yi et al., 2005; Yi, 2008). In this case the attenuation coefficient is written as

$$a = \mathrm{LAI}/2\,,$$

where LAI stands for the so-called leaf area index. Accordingly, on our plots we will indicate the both values of λ and LAI, corresponding to the same value of the attenuation coefficient.

For the mixing length ℓ_c in the canopy the following expression in terms of λ, a and h, was obtained

$$\frac{\ell_c}{h} = \sqrt{\frac{p\lambda(1-e^{-2a})}{4a^3}}\,, \tag{5.17}$$

where $p = 1.2$. At the top of the canopy the shear stress must be continuous (Fig. 5.2). Using the Prandtl expression for the shear stress, $\ell^2(\partial u/\partial y)^2$, substituting in it the velocity Eq. (5.16) and equating to the shear stress in the inertial layer u_*^2, gives

$$\frac{u_*}{u_h} = \frac{a\ell_c}{h}\,. \tag{5.18}$$

The two velocity profiles the semi-logarithmic one expressed by Eq. (5.15) and the canopy one expressed by Eq. (5.16) must match each other. Macdonald (2000) achieved this by assuming that the mixing length ℓ changes linearly against y when moving from the top of the canopy to some yet-to-be-determined contact point with the semi-logarithmic layer, $y = y_w$. At this point the length ℓ must coincide with the mixing length on the lower edge of the semi- logarithmic law. The latter one equals

$$\ell = \kappa(y-d)\,, \tag{5.19}$$

(this is precisely the expression that eventually leads to Eq. (5.15)). At the point $y = y_w$ formula (5.19) becomes $\ell_w = \kappa(y_w - d)$. Macdonald adopted the following linear interpolation of the length connecting the point $\ell = \ell_c$ at $y = h$ with the

point $\ell = \ell_w$ at $y = y_w$,

$$\ell(y) = \ell_c + \frac{y-h}{y_w - h}\left[\kappa\,(y_w - d) - \ell_c\right] = A + By\,, \tag{5.20}$$

where A and B are introduced for convenience and defined by the left-hand side of Eq. (5.20),

$$A = \ell_c - \frac{h}{y_w - h}\left(\kappa\,(y_w - d) - \ell_c\right),\; B = \frac{1}{y_w - h}\left(\kappa\,(y_w - d) - \ell_c\right)\,.$$

Further, it was assumed that within the layer connecting the canopy and inertial layer, the friction velocity is constant, giving

$$\frac{\partial u}{\partial y} = \frac{u_*}{\ell}\,, \tag{5.21}$$

where ℓ is represented by Eq. (5.20). Integrating (5.21) gives the velocity in the connecting layer of the form

$$u(y) = \frac{u_*}{B}\ln\left(\frac{A+By}{A+Bh}\right) + u_h\,. \tag{5.22}$$

Here the constant of integration is chosen such that the boundary condition $u = u_h$ at $y = h$ are met. At the matching point $y = y_w$ formula (5.22) should give the same value as the semi-logarithmic law (5.15), that is

$$\frac{u_*/u_h}{B}\ln\left(\frac{A+By_w}{A+Bh}\right) + 1 = \frac{u_*/u_h}{\kappa}\ln\left(\frac{y_w - d}{y_0}\right)\,. \tag{5.23}$$

Relation (5.23) presents an implicit equation with respect to the coordinate y_w to be found. Calculations of Macdonald (2000) based on available experimental data showed that roughly $y_w/h \approx 2$.

Lastly, we adopted the following empirical expressions for the ratios d/h and y_0/h as functions of λ (Macdonald et al., 1998),

$$\frac{d}{h} = 1 + A_1^{-\lambda}\left(\lambda - 1\right)\,, \tag{5.24}$$

where A_1 is an empirical parameter. $A_1 = 3.59$ is used for the square arrays and

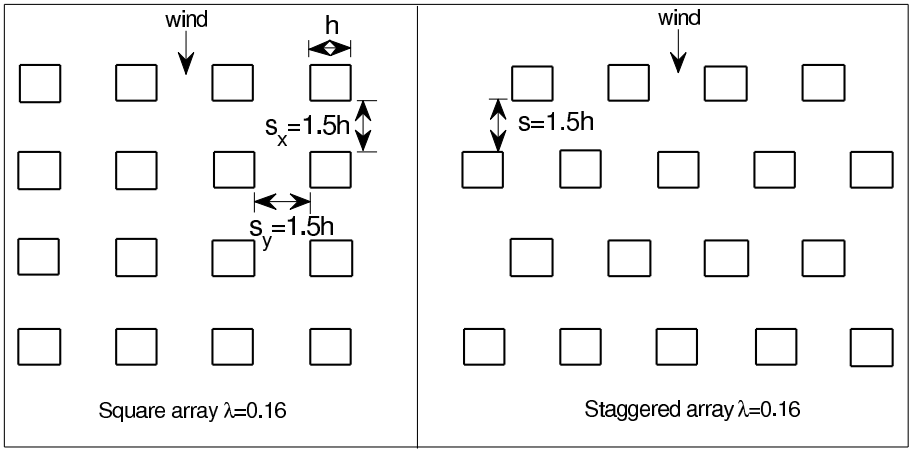

Figure 5.1 The square (left) and staggered (right) cube arrays (the packing density is 0.16 (s/h=1.5)), these patterns have been tested in the hydraulic flume by Macdonald et al. (2002).

$A_1 = 4.43$ for the staggered arrays. The square and staggered patterns are shown in Fig. 5.1.

$$\frac{y_0}{h} = \left(1 - \frac{d}{h}\right) \exp\left[-\left(0.5\frac{p}{\kappa^2}\beta\left(1 - \frac{d}{h}\right)\lambda\right)^{-0.5}\right], \tag{5.25}$$

where β is a constant introduced for higher precision; we use $\beta = 0.55$ for square obstacles and $\beta = 1$ for staggered obstacles. Note that the ratio of the mixing length to the canopy height, ℓ_c/h, is a function of λ as well, via Eq. (5.17).

As for the ratio u_h/u_*, we need to make a few comments on how it is determined. At the top of the canopy the velocity variation is large, which makes this task difficult. Macdonald (2000) determined u_h using the velocity measurements at a fixed point at the top of the canopy. The mean velocity profile was determined as an average of five measured profiles for each kind of obstacles. As can be seen from Table 2 in Macdonald (2000), the shear stress u_h/u_* at the top of the canopy is roughly constant for all $\lambda \geq 0.16$. With this in mind we used $u_h/u_* = 4.2$ for square obstacles and $u_h/u_* = 3.05$ for staggered ones. We calculated these values as the average of those with $\lambda \geq 0.16$ (Table 2 in Macdonald (2000)). Bentham and Britter (2003) argued that this range of packing densities is useful for practical applications. The layered structure of the canopy is illustrated in Fig. 5.2. Regarding the surface of the canopy shown in Fig. 5.2, we emphasize that the surface as such exists only for a fluid flow. As for the atmospheric flow, the top boundary is roughly where the intensive turbulence, generated by the friction against land, significantly decays. The release is supposed to be of a fixed amount of substance. However, continuous release is also acceptable by the model, but in this case we need to go sufficiently far downstream from the discharge point to ensure that particles have travelled for long time.

The above model identifies the velocity profiles in the three successive layers of interest: canopy layer Eq. (5.16), connecting layer Eq. (5.22) and inertial

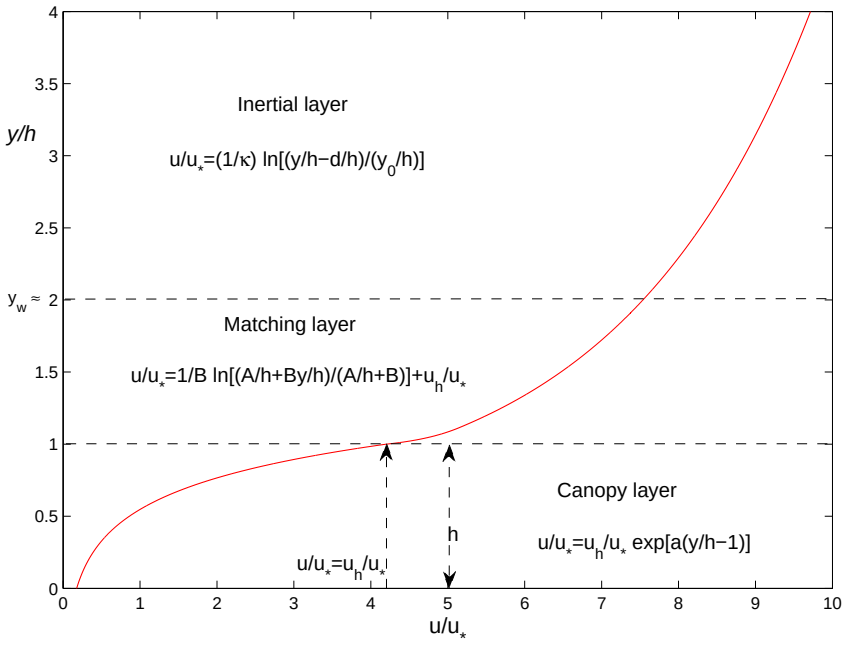

Figure 5.2 A wind profile within and above a canopy. The profile is plotted for square cubes of 0.16 packing density or using $LAI = 3.072$.

(semi-logarithmic) layer Eq. (5.15). The same model is used by Strunin and Mohammed (2012) and Mohammed, Strunin, Ngo-Cong and Tran-Cong (2014). Using the profiles, it is easy to get expressions for the turbulent diffusion coefficient for momentum in each layer. Re-arranging the Prandtl formula for the stress, $\ell^2(\partial u/\partial y)^2$ as $(\ell^2 \partial u/\partial y)\partial u/\partial y = D_{mom}\partial u/\partial y$, we have

$$D_{mom} = \ell^2 \frac{\partial u}{\partial y}\,. \tag{5.26}$$

Finally, we assume that the diffusion coefficient for the passive substance in each layer is proportional to D_{mom} (Barenblatt, 2003),

$$D = K\, D_{mom}\,. \tag{5.27}$$

where K is the coefficient of proportionality between the turbulent diffusion coefficient for momentum and the one for passive substance; strictly speaking it is not exactly 1 and may vary (Monin and Yaglom, 1975). The diffusion coefficient is continuous through the layers.

Coupled with the diffusion equations Eq. (5.3) and boundary conditions Eq. (5.4) the diffusion coefficient represented by Eq. (5.27) constitute a self-consistent model with the following independent dimensional parameters: the friction velocity u_*, width of the inertial layer H, height of the canopy h and frontal area density of the canopy λ. Choosing the canopy height, h, as the length scale and the friction velocity, u_*, as the velocity scale, we come to a short list of just

two non-dimensional input parameters: H/h and λ. Of course, implicitly the model also depends on the shape of obstacles – square or staggered. The model is reducible to the averaged form (5.1) by the centre manifold procedure similar to Strunin (2011). This will lead to the advection, diffusion and other coefficients, g_n, of the averaged model as functions of the independent parameters.

5.4 Analysis and numerical results

Now that we specified the velocity field $u(y)$, we are practically ready to apply the centre manifold technique and calculate the leading coefficients g_i of the transport equation (5.1) of interest. This is the aim of the present section. Yet, before doing so, we need to write down the diffusion coefficient $D(y)$ in each layer, using the respective velocity $u(y)$. Also, it is useful to convert the problem into non-dimensional form.

Substituting the velocity in each layer of the canopy flow into the expression for the diffusion coefficient (5.26)–(5.27), we get

(1) For the canopy layer,

$$D(y) = Ku_*\ell_c \exp\left[a\left(\frac{y}{h} - 1\right)\right].$$

(2) For the matching layer,

$$D(y) = Ku_*\left(A + By\right).$$

(3) For the inertial layer,

$$D(y) = K\kappa u_*\left(y - d\right).$$

Now we insert the velocity and corresponding diffusion coefficient in each layer into the advection-diffusion equation (5.3) and non-dimensionalyze it using h/u_* as the time scale and h as the length scale. Thus, we transfer to the non-dimensional variables via $x = x_1 h$, $u = u_1 u_*$, $t = t_1 h/u_*$, $y = y_1 h$, $D = D_1 h u_*$. As a result, equation (5.3) assumes the non-dimensional form given below.

(1) For the canopy layer,

$$\partial_{t_1} c + u_1(y_1)\partial_{x_1} c = K\partial_{y_1}\left[\frac{\ell_c}{h} e^{[a(y_1-1)]}\partial_{y_1} c\right], \tag{5.28}$$

where

$$u_1(y_1) = \frac{u_h}{u_*}\exp\left[a\left(y_1 - 1\right)\right]. \tag{5.29}$$

(2) For the matching layer,

$$\partial_{t_1} c + u_1(y_1)\partial_{x_1} c = K\partial_{y_1}\left[\frac{A+Bhy_1}{h}\partial_{y_1} c\right], \tag{5.30}$$

where

$$u_1(y_1) = \frac{1}{B}\ln\left(\frac{A+Bhy_1}{A+Bh}\right) + \frac{u_h}{u_*}. \tag{5.31}$$

(3) For the inertial layer,

$$\partial_{t_1} c + u_1(y_1)\partial_{x_1} c = K\partial_{y_1}\left[\kappa\frac{hy_1-d}{h}\partial_{y_1} c\right], \tag{5.32}$$

where

$$u_1(y_1) = \frac{1}{\kappa}\ln\left(\frac{hy_1-d}{y_0}\right). \tag{5.33}$$

As we now work with non-dimensional quantities, we also need to transform the transport equation for the average concentration, which is our target, from the dimensional form (5.14) into the following non-dimensional form,

$$\frac{\partial C}{\partial t} = \frac{g_1}{u_*}\frac{\partial C}{\partial x} + \frac{g_2}{hu_*}\frac{\partial^2 C}{\partial x^2} + \frac{g_3}{h^2 u_*}\frac{\partial^3 C}{\partial x^3} + \dots .$$

As we see, the non-dimensional advection coefficient equals g_1/u_*, the diffusion coefficient equals $g_2/(hu_*)$ and the dispersion coefficient equals $g_3/(h^2u_*)$. Hereafter, we denote these three non-dimensional coefficients just by g_1, g_2 and g_3 for convenience remembering the connection between the dimensional and non-dimensional representations.

Firstly, we calculate c_0 using (5.10) and the boundary conditions

$$\frac{\partial c}{\partial y_1}|_{y_1=0} = \frac{\partial c}{\partial y_1}|_{y_1=H/h} = 0.$$

This leads to

$$\frac{h}{H}\int_0^{\frac{H}{h}} c_0\, dy_1 = 1 \text{ and } c_0 = 1. \tag{5.34}$$

Now we can calculate g_1 using (5.34) and (5.12) at $n = 1$,

$$g_1 = -\overline{u_1(y_1)c_0} = -\frac{h}{H}\int_0^{\frac{H}{h}} u_1(y_1)\, dy_1 \,.$$

Breaking down the integral into three according to the layered structure of the flow and using the velocity expressions for the layers, (5.29), (5.31) and (5.33), gives

$$\begin{aligned} g_1 &= -\frac{h}{H}\left\{\int_0^1 \frac{u_h}{u_*} e^{[a(y_1-1)]}\, dy_1 + \int_1^{\frac{y_w}{h}} \left[\frac{1}{B}\ln\left(\frac{A+Bhy_1}{A+Bh}\right) + \frac{u_h}{u_*}\right] dy_1 \right. \\ &\quad \left. + \int_{\frac{y_w}{h}}^{\frac{H}{h}} \frac{1}{\kappa}\ln\left(\frac{hy_1-d}{y_0}\right)\, dy_1\right\}, \\ &= -\frac{h}{H}\left\{\frac{u_h}{u_*}\left(\frac{1-e^{-a}}{a}-1\right) + \frac{A}{hB^2}\ln\left(\frac{A+By_w}{A+Bh}\right)\right. \\ &\quad \left. + \frac{H-d}{h\kappa}\ln\left(\frac{H-d}{y_0}\right) + \frac{d}{h\kappa}\ln\left(\frac{y_w-d}{y_0}\right) - \frac{y_w(\kappa-B)}{h\kappa B} - \frac{H}{h\kappa} + \frac{1}{B}\right\}. \end{aligned} \tag{5.35}$$

In order to determine c_1, we use (5.34), (5.35) and (5.11) at $n = 1$, that is

$$L[c_1] = c_0 g_1 + u(y_1)c_0\,, \tag{5.36}$$

which is an ordinary differential equation

$$\frac{\partial}{\partial y_1}\left[D(y_1)\frac{\partial c_1}{\partial y_1}\right] = g_1 + u_1(y_1)\,. \tag{5.37}$$

For each layer, we calculate c_1 using (5.35), (5.37) and the respective expression for the velocity. The concentration in each layer will be labeled by a respective subscript: "c" will mean canopy, "m" – matching and "i" – inertial. For the canopy layer,

$$\frac{\partial}{\partial y_1}\left[K\frac{\ell_c}{h}\, e^{[a(y_1-1)]}\frac{\partial c_{1c}}{\partial y_1}\right] = g_1 + \frac{u_h}{u_*}e^{[a(y_1-1)]}\,.$$

Integrating this equation once, we get

$$\frac{\partial c_{1c}}{\partial y_1} = \frac{h}{K\ell_c}\left\{g_1 y_1\, e^{[-a(y_1-1)]} + r_{1c}\, e^{[-a(y_1-1)]} + \frac{u_h}{au_*}\right\},$$

and

$$c_{1c} = \frac{h}{K\ell_c}\left\{-\frac{g_1}{a}y_1 e^{[-a(y_1-1)]} - \frac{g_1}{a^2}e^{[-a(y_1-1)]} - \frac{r_{1c}}{a}e^{[-a(y_1-1)]} + \frac{u_h y_1}{a u_*}\right\} + r_{2c}\,. \tag{5.38}$$

For the matching layer,

$$\frac{\partial}{\partial y_1}\left[K\frac{A+Bhy_1}{h}\frac{\partial c_{1m}}{\partial y_1}\right] = g_1 + \frac{1}{B}\ln\left(\frac{A+Bhy_1}{A+Bh}\right) + \frac{u_h}{u_*}\,.$$

Integrating once, we get

$$\frac{\partial c_{1m}}{\partial y_1} = \frac{1}{K}\left[g_1\frac{h}{A+Bhy_1}y_1 + \left(\frac{1}{B}\right)^2\ln\left(\frac{A+Bhy_1}{A+Bh}\right) + \frac{u_h}{a u_*}\frac{h}{A+Bhy_1}y_1 + r_{1m}\frac{h}{A+Bhy_1} - \left(\frac{1}{B}\right)^2\right]. \tag{5.39}$$

and

$$c_{1m} = \frac{1}{K}\left\{\frac{g_1 u_* + u_h}{B^2 u_*}\left[\frac{A+Bhy_1}{h} - \frac{A}{h}\ln\left(\frac{A+Bhy_1}{h}\right)\right] + \frac{A+Bhy_1}{hB^3}\left[\ln\left(\frac{A+Bhy_1}{A+Bh}\right) - 1\right] - \left(\frac{1}{B}\right)^2 y_1 + \frac{r_{1m}}{B}\ln\left(\frac{A+Bhy_1}{h}\right)\right\} + r_{2m}\,. \tag{5.40}$$

For the inertial layer,

$$\frac{\partial}{\partial y_1}\left[K\kappa\frac{hy_1-d}{h}\frac{\partial c_{1i}}{\partial y_1}\right] = g_1 + \frac{1}{\kappa}\ln\left(\frac{hy_1-d}{y_0}\right)\,.$$

Integrating, we get

$$\frac{\partial c_{1i}}{\partial y_1} = \frac{1}{K\kappa}\left\{g_1\frac{h}{hy_1-d}y_1 + \frac{1}{\kappa}\left[\ln\left(\frac{hy_1-d}{y_0}\right) - 1\right] + r_{1i}\frac{h}{hy_1-d}\right\}\,.$$

and

$$c_{1i} = \frac{1}{K\kappa}\left\{ g_1 \left[\frac{hy_1 - d}{h} + \frac{d}{h} \ln\left(\frac{hy_1 - d}{h} \right) \right] + \frac{hy_1 - d}{h\kappa} \left[\ln\left(\frac{hy_1 - d}{y_0} \right) - 1 \right] + r_{1i} \ln\left(\frac{hy_1 - d}{h} \right) - \frac{y_1}{\kappa} \right\} + r_{2i} \,, \tag{5.41}$$

where the value of $K = 1$ is used for the computations in Section 5.5. The integration constants r_{1c}, r_{1m}, and r_{1i} can be determined by using the continuity of flux through the boundaries. From the boundary condition $\frac{\partial c_{1c}}{\partial y_1}|_{y_1=0} = 0$ we find

$$r_{1m} = \frac{u_h}{u_*} \left(\frac{1 - e^{-a}}{a} - 1 \right) + \frac{A + Bh}{h} \left(\frac{1}{B} \right)^2 . \tag{5.42}$$

From the boundary condition $D_{1c} \frac{\partial c_{1c}}{\partial y_1}|_{y_1=1} = D_{1m} \frac{\partial c_{1m}}{\partial y_1}|_{y_1=1}$ we get

$$r_{1m} = \frac{u_h}{u_*} \left(\frac{1}{a} - 1 \right) + \frac{A + Bh}{h} \left(\frac{1}{B} \right)^2 . \tag{5.43}$$

The constant r_{1i} can be calculated in two ways: first, from the condition

$$\frac{\partial c_{1i}}{\partial y_1}|_{y_1=H/h} = 0 \,,$$

giving

$$r_{1i} = -\frac{H}{h} g_1 - \frac{H - d}{h\kappa} \left[\ln\left(\frac{H - d}{y_0} \right) - 1 \right] , \tag{5.44}$$

and, second, from the condition

$$D_{1m} \frac{\partial c_{1m}}{\partial y_1}|_{y_1=y_w/h} = D_{1i} \frac{\partial c_{1i}}{\partial y_1}|_{y_1=y_w/h} \,,$$

Using (5.35) it can be easily shown that the second way leads to the same answer. In order to find the integration constants r_{2c}, r_{2m}, and r_{2i}, we use the continuity condition for the concentration between the layers and normalising (5.9) for $n = 1$. As a result, we come to the linear system of three equations with respect to the three unknown constants, In order to simplify the form of the system, let us

introduce some notations,

$$s_1 = -\frac{1}{K}\left[\frac{u_h g_1}{u_*}\left(\frac{1}{a}+1\right) - \left(\frac{u_h}{u_*}\right)^2\right].$$

$$s_2 = \frac{1}{K}\left\{\frac{u_* g_1 + u_h}{B^2 u_*}\left[\frac{A+Bh}{h} - \frac{A}{h}\ln\left(\frac{A+Bh}{h}\right)\right]\right.$$
$$\left. -\frac{A+Bh}{hB^3} + \frac{r_{1m}}{B}\ln\left(\frac{A+Bh}{h}\right) - \left(\frac{1}{B}\right)^2\right\}.$$

$$s_3 = \frac{1}{K}\left\{\frac{u_* g_1 + u_h}{B^2 u_*}\left[\frac{A+By_w}{h} - \frac{A}{h}\ln\left(\frac{A+By_w}{h}\right)\right]\right.$$
$$\left. +\frac{A+By_w}{hB^3}\left[\ln\left(\frac{A+By_w}{A+Bh}\right) - 1\right] - \frac{y_w}{hB^2} + \frac{r_{1m}}{B}\ln\left(\frac{A+By_w}{h}\right)\right\}.$$

$$s_4 = \frac{1}{K\kappa}\left\{g_1\left[\frac{y_w-d}{h} + \frac{d}{h}\ln\left(\frac{y_w-d}{h}\right)\right] + \frac{y_w-d}{h\kappa}\left[\ln\left(\frac{y_w-d}{y_0}\right) - 1\right]\right.$$
$$\left. -\frac{y_w}{h\kappa} + r_{1i}\ln\left(\frac{y_w-d}{h}\right)\right\}.$$

$$s_5 = \frac{1}{K}\left\{\frac{g_1 u_h}{a u_*} + \frac{2u_h g_1 + a r_{1c} u_h}{u_* a^2}\left(1-e^a\right) + \frac{u_h^2}{2u_*^2} + \frac{Bg_1 u_* + Bu_h - u_*}{B^3 u_*}\right.$$
$$\times\left[\frac{A}{h}\left(\frac{y_w}{h}-1\right) + \frac{B}{2}\left(\left(\frac{y_w}{h}\right)^2 - 1\right)\right] - \frac{A(u_* g_1 - u_h) - h u_* r_{1m}}{hB^3 u_*}$$
$$\times\left[\frac{A+By_w}{h}\left(\ln\left(\frac{A+By_w}{h}\right) - 1\right) - \frac{A+Bh}{h}\left(\ln\left(\frac{A+B}{h}\right) - 1\right)\right]$$
$$+\frac{1}{2B^4}\left[\left(\frac{A+By_w}{h}\right)^2\left(\ln\left(\frac{A+By_w}{A+Bh}\right) - \frac{1}{2}\right) + \frac{1}{2}\left(\frac{A+Bh}{h}\right)^2\right]$$
$$\left. -\frac{1}{2B^2}\left(\left(\frac{y_w}{h}\right)^2 - 1\right)\right\}$$
$$+\frac{1}{K\kappa}\left\{\left(g_1 - \frac{1}{\kappa}\right)\left[\frac{1}{2}\left(\frac{H}{h}\right)^2 - \frac{dH}{h^2} - \frac{1}{2}\left(\frac{y_w}{h}\right)^2 + \frac{dy_w}{h^2}\right]\right.$$
$$+\frac{g_1 d + h r_{1i}}{h}\left[\frac{H-d}{h}\left(\ln\left(\frac{H-d}{h}\right) - 1\right) - \frac{y_w-d}{h}\left(\ln\left(\frac{y_w-d}{h}\right) - 1\right)\right]$$
$$+\frac{1}{2\kappa}\left[\left(\frac{H-d}{h}\right)^2\left(\ln\left(\frac{H-d}{y_0}\right) - \frac{1}{2}\right) - \left(\frac{y_w-d}{h}\right)^2\left(\ln\left(\frac{y_w-d}{y_0}\right) - \frac{1}{2}\right)\right.$$
$$\left.\left. -\left(\left(\frac{H}{h}\right)^2 - \left(\frac{y_w}{h}\right)^2\right)\right]\right\}.$$

In the new notations the system has the form

$$\begin{aligned} s_1 + r_{2c} &= s_2 + r_{2m}\,, \\ s_3 + r_{2m} &= s_4 + r_{2i}\,, \\ -s_5 &= r_{2c} + r_{2m}\left(\frac{y_w}{h} - 1\right) + r_{2i}\left(\frac{H}{h} - \frac{y_w}{h}\right)\,, \end{aligned}$$

from where

$$\begin{aligned} r_{2i} &= \frac{h}{H}\left\{s_1 - s_2 - s_5 + \frac{y_w}{h}s_3 - \frac{y_w}{h}s_4\right\}\,. \\ r_{2m} &= -s_3 + s_4 + r_{2i}\,, \\ r_{2c} &= -s_1 + s_2 + r_{2m}\,. \end{aligned} \tag{5.45}$$

System (5.45) was solved numerically and then the concentrations were computed in each layer, using (5.38), (5.40) and (5.41). We discuss the results further in the present section.

Now, we use (5.12) for $n = 2$ to calculate g_2,

$$g_2 = -\frac{h}{H}\int_0^{H/h} u_1(y_1)c_1 dy_1\,.$$

According to the three-layer structure, we have

$$\begin{aligned} g_2 &= -\frac{h}{H}\left\{\int_0^1 u_{1c}(y_1)c_{1c}dy_1 + \int_1^{\frac{y_w}{h}} u_{1m}(y_1)c_{1m}dy_1 + \int_{\frac{y_w}{h}}^{\frac{H}{h}} u_{1i}(y_1)c_{1i}dy_1\right\} \\ &= -\frac{h}{H}\left\{\int_0^1 \left[\frac{u_h}{u_*}\,e^{a(y_1-1)}\right]\left[\frac{u_h}{Ku_*}\left(-g_1\,e^{-a(y_1-1)}\left(y_1 + \frac{1}{a}\right) + \frac{u_h}{u_*}y_1\right) + r_{2c}\right]dy_1\right. \\ &\quad + \int_1^{\frac{y_w}{h}}\left[\frac{1}{B}\ln\left(\frac{A+Bhy_1}{A+Bh}\right) + \frac{u_h}{u_*}\right]\left[\frac{1}{K}\left[\left(\frac{u_*g_1 + u_h}{B^2u_*}\right)\right.\right. \\ &\quad \times\left(\frac{A+Bhy_1}{h} - \frac{A}{h}\ln\left(\frac{A+Bhy_1}{h}\right)\right) + \left(\frac{1}{B}\right)^3\left(\frac{A+Bhy_1}{h}\right) \\ &\quad \times\left(\ln\left(\frac{A+Bhy_1}{A+Bh}\right) - 1\right) - \left(\frac{1}{B}\right)^2 y_1 + \frac{r_{1m}}{B}\ln\left(\frac{A+Bhy_1}{h}\right)\Big] + r_{2m}\Big]\,dy_1 \\ &\quad + \int_{\frac{y_w}{h}}^{\frac{H}{h}}\left[\frac{1}{\kappa}\ln\left(\frac{hy_1 - d}{y_0}\right)\right]\left[\frac{1}{K\kappa}\left(\frac{g_1\,(hy_1 - d)}{h} + \frac{g_1 d}{h}\ln\left(\frac{hy_1 - d}{h}\right)\right.\right. \\ &\quad \left.\left.\left. + \frac{hy_1 - d}{\kappa h}\left(\ln\left(\frac{hy_1 - d}{y_0}\right) - 1\right) + r_{1i}\ln\left(\frac{hy_1 - d}{h}\right)\right) - \frac{y_1}{\kappa} + r_{1i}\right]dy_1\right\} \end{aligned}$$

and further,

$$
\begin{aligned}
g_2 = -\frac{h}{HK}\Bigg\{ & -\frac{u_h^2 u_* g_1\left(a^2+2a\right)-2u_h^3\left(e^{-a}+a-1\right)+2a^2u_h^2u_*r_{1c}}{2a^2u_*^3} \\
& +\frac{2au_hu_*^2r_{2c}\left(1-e^{-a}\right)K}{2a^2u_*^3}+\frac{Bu_*g_1+2Bu_h-3u_*}{B^5u_*}\left[\left(\frac{A+By_w}{h\sqrt{2}}\right)^2\right. \\
& \left.\times\left(\ln\left(\frac{A+By_w}{A+Bh}\right)-\frac{1}{2}\right)+\left(\frac{A+Bh}{2}\right)^2\right]+\frac{A\left(u_*g_1-Bu_*r_{1m}+u_h\right)}{hB^4u_*} \\
& \times\left[\frac{A+Bh}{h}\left(\ln\left(\frac{A+Bh}{h}\right)\right)^2-\frac{A+By_w}{h}\left(\ln\left(\frac{A+By_w}{h}\right)\right)^2\right] \\
& +\left[\frac{A\left(u_*g_1+u_h\right)}{hB^4u_*}\left(2+\ln\left(\frac{A+Bh}{h}\right)\right)-\frac{r_{1m}}{B^3}\left(2+\ln\left(\frac{A+Bh}{h}\right)\right)\right. \\
& \left.-\frac{Au_h}{hB^3u_*}\left(g_1+\frac{u_h}{u_*}\right)+\frac{r_{1m}u_h}{B^2u_*}\right]\left[\frac{A+By_w}{h}\left(\ln\left(\frac{A+By_w}{h}\right)-1\right)\right. \\
& \left.-\frac{A+Bh}{h}\left(\ln\left(\frac{A+Bh}{h}\right)-1\right)\right]+\frac{\left(A+By_w\right)^2}{2h^2B^5}\left(\ln\left(\frac{A+By_w}{A+Bh}\right)\right)^2 \\
& +\frac{A+hKB^3r_{2m}}{hB^5}\left[\frac{A+By_w}{h}\left(\ln\left(\frac{A+By_w}{A+Bh}\right)-1\right)+\frac{A+Bh}{h}\right] \\
& +\frac{Au_h}{hu_*B^2}\left(\frac{Bg_1-1}{B}+\frac{u_h}{u_*}+\frac{Kr_{2m}B^2h}{A}\right)\left(\frac{y_w}{h}-1\right) \\
& +\frac{u_h\left(Bu_*g_1+Bu_h-2u_*\right)}{2B^2u_*^2}\left(\left(\frac{y_w}{h}\right)^2-1\right)+\frac{g_1\kappa-3}{2\kappa^3}\left[\left(\frac{H-d}{h}\right)^2\right. \\
& \left.\times\left(\ln\left(\frac{H-d}{y_0}\right)-\frac{1}{2}\right)-\left(\frac{y_w-d}{h}\right)^2\left(\ln\left(\frac{y_w-d}{y_0}\right)-\frac{1}{2}\right)\right] \\
& +\frac{g_1d+hr_{1i}}{h\kappa^2}\left[\frac{H-d}{h}\left(\ln\left(\frac{H-d}{h}\right)\right)^2-\frac{y_w-d}{h}\left(\ln\left(\frac{y_w-d}{h}\right)\right)^2\right] \\
& +\frac{1}{2\kappa^3}\left[\left(\frac{H-d}{h}\right)^2\left(\ln\left(\frac{H-d}{y_0}\right)\right)^2-\left(\frac{y_w-d}{h}\right)^2\left(\ln\left(\frac{y_w-d}{y_0}\right)\right)^2\right] \\
& +\left[\frac{d-hr_{2i}\kappa^2}{h\kappa^3}+\frac{g_1d+hr_{1i}}{h\kappa^2}\left(2+\ln\left(\frac{y_0}{h}\right)\right)\right] \\
& \times\left[\frac{y_w-d}{h}\left(\ln\left(\frac{y_w-d}{y_0}\right)-1\right)-\frac{H-d}{h}\left(\ln\left(\frac{H-d}{y_0}\right)-1\right)\right]\Bigg\}\,.
\end{aligned}
\tag{5.46}
$$

Computing g_3 for the canopy flow requires very extensive algebra (through the research project, we only managed to calculate g_3 and high-order coefficients for the channel flow). Note, however, that g_3 gives just a correction to the effect of the diffusion expressed through g_2. It is the diffusion coefficient g_2 that carries the main responsibility for the stretching of the contaminant cloud along the channel. Numerically, we have obtained a good agreement between the 2–D and 1–D solutions for the canopy flow (see Section 5.5) based only on the first two derivatives, g_1 and g_2. In addition and according to our experience with the channel flow (see Chapter 4), adding higher-order derivatives to the 1–D

equation (5.1) will improve the solution only a little. Fig. 5.3 shows some velocity profiles using data of Macdonald (2000) for square and staggered cube arrays at various packing densities. Below the level $y/h = 1$ lies the canopy layer, the semi-logarithmic layer is located above $y = y_w$ and the matching profile lies between them.

It is interesting to compare the results for the transfer coefficients g_1 and g_2 with those for the flow in a smooth channel analysed by Strunin (2011). In the limit of very large Reynolds numbers he obtained

$$g_1 \to -\frac{1}{\kappa}\ln R = -\frac{1}{\kappa}\ln\left(\frac{u_* H}{\nu}\right),$$

where the Reynolds number was based on the total depth of the channel, $R = u_* H/\nu$ with u_* being the friction velocity and ν kinematic viscosity. The Reynolds number R is different to R_h defined in (5.53). R is based on the inertial layer height, while R_h is based on the canopy height. Taking the limit in our answer (5.35) as $H \to \infty$, we get

$$g_1 \to -\frac{h}{H}\left\{\frac{H-d}{h\kappa}\ln\left(\frac{H-d}{y_0}\right) - \frac{H}{h\kappa}\right\} \to -\frac{1}{\kappa}\ln\frac{H}{y_0} = -\frac{1}{\kappa}\ln\left(\frac{u_* H}{\nu}\cdot\frac{\nu}{u_* y_0}\right)$$

$$= -\frac{1}{\kappa}\left[\ln\left(\frac{u_* H}{\nu}\right) + \ln\left(\frac{\nu}{u_* y_0}\right)\right] \to -\frac{1}{\kappa}\ln\left(\frac{u_* H}{\nu}\right), \tag{5.47}$$

which is exactly the result above (Strunin and Mohammed, 2012; Mohammed, Strunin, Ngo-Cong and Tran-Cong, 2014). From (5.47) we see that the advection coefficient for the canopy flow is less than that for the smooth channel flow, because the second term in the square brackets is negative (it is, the inverse Reynolds number based on the roughness height, y_0; despite y_0 is small, the velocity is large enough to make such Reynolds number large). From physical viewpoint, the canopy just slows down the flow relative to the smooth flow with the same shear stress (friction velocity). The advection coefficient g_1 is the depth-averaged velocity, accordingly, for the canopy flow, it is smaller in absolute value. Analysing formula for the diffusion coefficient g_2, (5.46), in the limit $H \to \infty$, we find

$$\lim_{H\to\infty} g_2 = \frac{1}{4K\kappa^3}\frac{H}{h}. \tag{5.48}$$

This result also agrees with the result by Strunin (2011).

In the following, we want to compare the obtained values of g_1 and g_2 with those by Strunin (2011) for the one-layer flow that is the flow entirely consisting of the inertial layer. We need to re-scale the formulae by Strunin using the new spatial scale, which is h. By contrast, Strunin used as a scale the entire width of the flow that is H. In what follows we re-do the manipulations from Strunin (2011)

using the new scale, h. Consider the classical – logarithmic – velocity profile,

$$u = \frac{u_*}{\kappa} \ln\left(\frac{u_* y}{\nu}\right) + A\,. \tag{5.49}$$

Substituting (5.49) into the expression for the diffusion coefficient (recall that the shear stress is constant and proportional to u_*^2)

$$D = K u_*^2/(\partial u/\partial y)\,,$$

we get

$$D(y) = \kappa K u_* y\,. \tag{5.50}$$

Now substitute (5.49) and (5.50) into the advection-diffusion equation (5.3) and non-dimensionalise using h/u_* as the time scale and h as the length scale. This leads to the non-dimensional equation, in which we keep the old notations for convenience,

$$\frac{\partial c}{\partial t} + u(y)\frac{\partial c}{\partial x} = \kappa K \frac{\partial}{\partial y}\left(y\frac{\partial c}{\partial y}\right)\,, \tag{5.51}$$

where

$$u(y) = \frac{1}{\kappa}\ln(R_h y) + \frac{A}{u_*} \quad \text{for } \varepsilon < y < 1\,,\ \varepsilon = h_1/h\,, \tag{5.52}$$

where

$$R_h = \frac{u_* h}{\nu} \tag{5.53}$$

is the Reynolds number based on the canopy height h. Near the bottom lies the narrow viscous sub-layer,

$$\varepsilon = h_1/h\,, \tag{5.54}$$

which is small at large Reynolds numbers. Later on in our derivation we will take the limit $\varepsilon \to 0$. In non-dimensional form the boundary conditions become

$$y\frac{\partial c}{\partial y}\bigg|_{y=\varepsilon} = y\frac{\partial c}{\partial y}\bigg|_{y=H/h} = 0\,. \tag{5.55}$$

Calculating c_0 from (5.10) under the boundary conditions (5.55) and satisfying (5.9) in non-dimensional form, we readily find

$$c_0 = 1\,. \tag{5.56}$$

Using (5.12) for $n = 1$, (5.52) and (5.56) and taking the limit $\varepsilon \to 0$ we get

$$g_1 = -\frac{1}{\kappa}(\ln R - 1) - A/u_* \tag{5.57}$$

with

$$R = \frac{u_* H}{\nu}\,.$$

Using (5.57) and (5.56), we can determine c_1 from (5.11) at $n = 1$, that is

$$L[c_1] = c_0 g_1 + u(y) c_0\,, \tag{5.58}$$

or

$$\frac{\partial}{\partial y}(y\frac{\partial c_1}{\partial y}) = -\frac{1}{K\kappa^2}\left[\ln\left(\frac{u_* H}{\nu}\right) - 1 - \ln\left(\frac{u_* h y}{\nu}\right)\right]\,. \tag{5.59}$$

Integrating (5.59) once under the boundary conditions

$$y\frac{\partial c}{\partial y}\bigg|_{y=\varepsilon} = y\frac{\partial c}{\partial y}\bigg|_{y=H/h} = 0\,,$$

we get

$$\frac{\partial c_1}{\partial y} = -\frac{1}{K\kappa^2}\left[\ln\left(\frac{u_* H}{\nu}\right) - \ln\left(\frac{u_* h y}{\nu}\right)\right]\,,$$

and further

$$c_1 = -\frac{1}{K\kappa^2}\left[\ln\left(\frac{u_* H}{\nu}\right) - (y\ln y + y)\right] + B_1\,.$$

The integration constant B_1 is determined from the condition

$$\int_\varepsilon^{H/h} c_1\, dy = 0\,.$$

As a result,

$$c_1 = -\frac{1}{K\kappa^2}\left[\ln\left(\frac{u_* H}{\nu}\right) - (y\ln y + y)\right] + \frac{3H}{4hK\kappa^2}\,. \tag{5.60}$$

Now we can determine g_2,

$$g_2 = -\overline{u(y)c_1(y)} = -\frac{h}{H}\int_\varepsilon^{H/h}\left[\frac{1}{\kappa}\ln(Ry) + A/u_*\right]$$

$$\times \left[-\frac{1}{K\kappa^2} \left(\ln\left(\frac{u_* H}{\nu}\right) - (y \ln y + y) \right) + \frac{3H}{4hK\kappa^2} \right] dy$$

$$= \frac{h}{H} \left\{ \frac{1}{K\kappa^3} \left[\ln\left(\frac{u_* H}{\nu}\right) \left(\frac{y^2}{2} \ln(Ry) - \frac{y^2}{4} \right) - \frac{y^2}{2} \left((\ln(Ry))^2 - \ln(Ry) + \frac{1}{2} \right) \right.\right.$$

$$\left.\left. + \frac{y^2}{2} \left(\ln(Ry) - \frac{1}{2} \right) - \frac{3H}{4h} \left(\ln(Ry) - y \right) \right] \right.$$

$$\left. + \frac{A/u_*}{K\kappa^2} \left[\frac{y^2}{2} \ln\left(\frac{u_* H}{\nu}\right) - \frac{y^2}{2} \left(\ln(Ry) - \frac{1}{2} \right) + \frac{y^2}{2} - \frac{3y^2}{4} \right] \right\}_{\varepsilon}^{\frac{H}{h}} \tag{5.61}$$

Taking the limit $\varepsilon \to 0$ in (5.61), we get the answer

$$g_2 = \frac{H}{4hK\kappa^3} \,.$$

This differs from the corresponding expression for g_2 obtained in Strunin (2011) by the factor H/h due to the new scaling.

From Fig. 5.4 we see that the diffusion coefficient for the canopy flow is larger than that for the smooth flow. The reason is the slower velocity through the canopy itself. Strunin showed that the concentration component c_1 is a decreasing function of y, which is positive near the bottom and negative in the rest of the flow, with the total integral $\int_0^{H/h} c_1 \, dy$ being zero. Now, the value g_2 is represented by the integral $-(h/H) \int_0^{H/h} u(y) c_1(y) \, dy$; its value depends on the shape of the velocity profile. The canopy flow has lower velocity near the bottom because of the canopy resistance. Consequently, the contribution of the bottom part of the integral, which makes *negative* contribution into the value of g_2 due to the negative sign in front of the integral, is reduced. The result is that the value of g_2 for the canopy flow is larger. Comparison of the advection and diffusion coefficients versus total thickness for different densities of square and staggered obstacles are demonstrated in Figs. 5.5–5.8.

Lastly, we analysed the dependence of the advection and diffusion coefficients against the obstacle packing densities for their range that is typical for urban canopies. Figs. 5.9–5.10 refer to the case when the thickness of the entire flow is equal to the height of the canopy. Fig. 5.9 shows the decreasing advection (in absolute value) due to slowing down of the flow caused by denser set of obstacles; this seems a natural result. The diffusion coefficient increases with the density as more densely packed obstacles make larger resistance to the flow and, consequently, create steeper velocity profiles. The latter in turn lead to the larger diffusion coefficients because the latter is created by the velocity shear. At the same time there is a relatively short interval of λ where g_2 is nearly constant and even slightly decreases against the density; this should due to fine peculiarities of the velocity profile. This effect is weak and we leave it for further investigation. The case when the total thickness is 10 times larger than the canopy height is illustrated in Fig. 5.11 and Fig. 5.12. We see that the advection coefficient after an interval of decrease in absolute value goes up (in absolute value) versus density. This latter effect may be loosely interpreted as a faster slide of the flow above the

canopy. The behaviour of the diffusion coefficient looks usual as can be explained as above for the case $H/h = 1$.

5.5 Comparison of 2–D and 1–D models using 1D-IRBFN method

In this section, we applied the one-dimensional integrated radial basis function (1D-IRBF) method to simulate the canopy flow governed by the original 2–D advection-diffusion equations (5.28)–(5.32) and the low-dimensional 1–D equation (5.1). The 1D-IRBF and IRBF-based methods have been successfully developed and verified through several engineering problems such as turbulent flows in an open channel (Mohammed, Ngo-Cong, Strunin, Mai-Duy and Tran-Cong, 2014), viscous flows (Mai-Duy and Tran-Cong, 2001b; Mai-Duy and Tanner, 2007; Ngo-Cong et al., 2012b), and structural analysis (Ngo-Cong et al., 2011), and fluid-structure interaction (Ngo-Cong et al., 2012a).

We consider a case of square cube array, $\lambda = 0.16$ and $H = 4$. Based on Eqs. (5.35) and (5.46), we obtain $g_1 = -6.4203$ and $g_2 = 41.6907$. In the numerical experiments we analyse the 2–D equations in a rectangular domain with the length $L = 1000$ and the height $H = 4$, subject to the boundary conditions: $c = 0$ on the left and right boundaries, and $\partial c/\partial y = 0$ on the top and bottom boundaries. The domain of interest is discretised using uniform Cartesian grids. The Crank-Nicolson scheme is employed for temporal discretisation. As in Mohammed, Ngo-Cong, Strunin, Mai-Duy and Tran-Cong (2014), we adopt the initial condition in the form

$$c(x, y, 0) = \exp\left[-\left(0.1\left(x - x_0\right)\right)^4 - \left(0.7(y - y_0)\right)^4\right], \tag{5.62}$$

with $x_0 = -11.5$ and $y_0 = 0$. We refer the reader to a similar study (Mohammed, Ngo-Cong, Strunin, Mai-Duy and Tran-Cong, 2014) for technical details.

Figs. 5.13 and 5.14 present the grid convergence study for the 2–D model in terms of the maximum depth–averaged concentration (C_{max}) and its position, (x_{max}), versus time, respectively. The depth–averaged concentration is calculated as $C(x,t) = \frac{1}{H}\int_0^H c\,(x, y, t)\,dy$, where $c(x, y, t)$ is the 2–D solution. The converged solution is obtained for grids denser than or equal to 201×81. The grid convergence behaviour is also established for the 1D model as shown in Figs. 5.15 and 5.16.

The main purpose of Figs. 5.15 and 5.16 is to compare indicative characteristics of the concentration field under the 1–D and 2–D models, namely: (a) the motion of the position of the maximum depth-averaged concentration along the flow, and (b) the decay of the maximum averaged concentration in time. The motion of the maximum concentration reflects the role of the advection coefficient g_1, while the decay of the maximum concentration reflects the dissipative effect of the diffusion

coefficient g_2. Interestingly, as seen in Figs. 5.17 and 5.18, the evolution of the concentration field may bring about two local maxima. Their evolution causes a sudden change in the position of the global maximum, x_{max}, at early times as visible in Figs. 5.13 and 5.15. But eventually the 2–D and 1–D curves go in parallel, which indicates that the 1–D and 2–D models yield the same advection velocities. The 1–D and 2–D concentration profiles as such, although different at early stages of the dynamics (Figs. 5.16 and 5.17), get very close to each other at large times. It is important to remind that it is the large time limit when the centre manifold approach becomes applicable. These comparisons support the derived 1–D model.

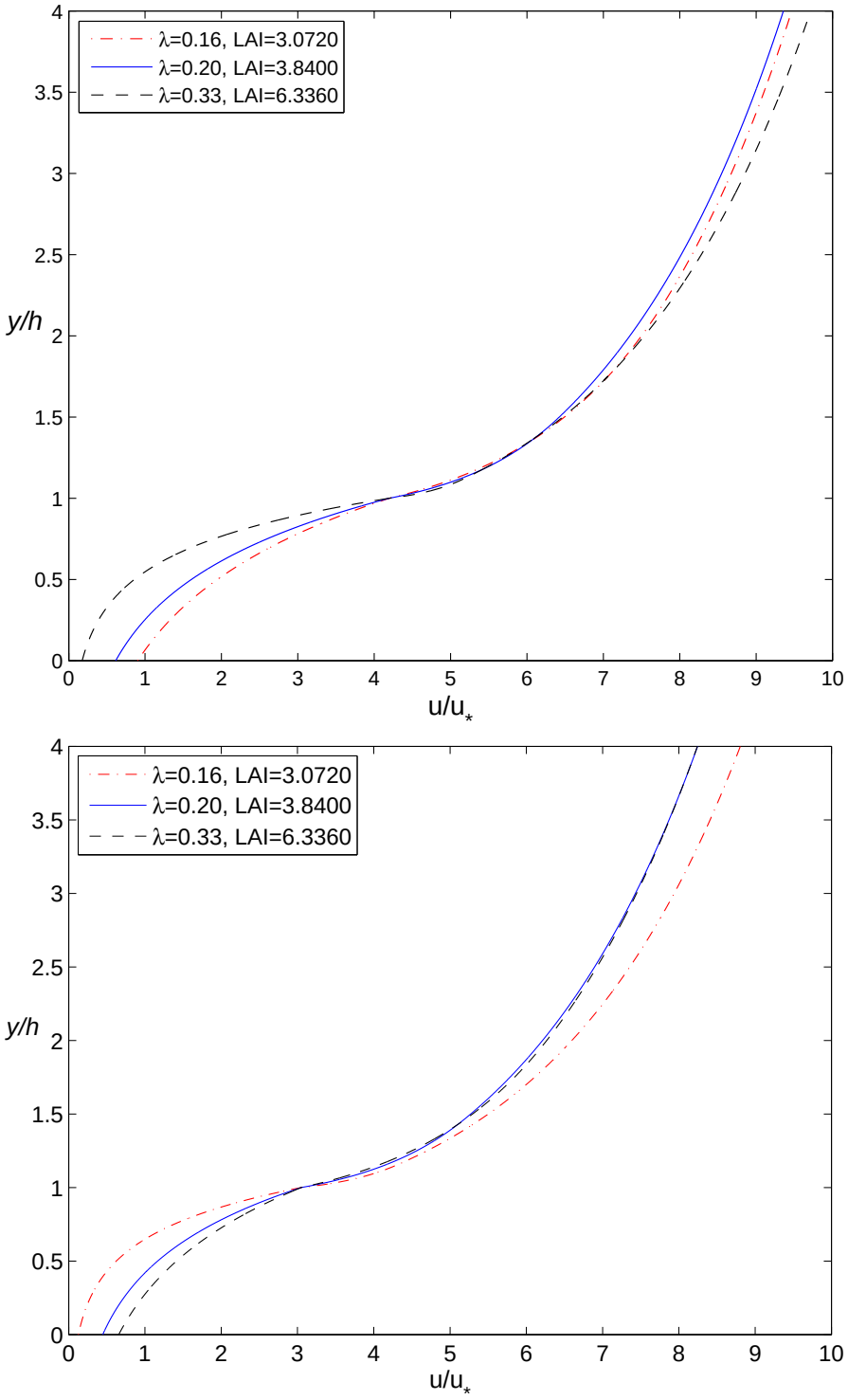

Figure 5.3 Mean velocity profiles for different λ for the square cube arrays (top) and the staggered cube arrays (bottom). The parameters $A_1 = 3.59$, $\beta = 0.55$, $u_h/u_* = 4.2$ are used for the square cubes and the values $A_1 = 4.43$, $\beta = 1$, $u_h/u_* = 3.05$ are used for the staggered cubes.

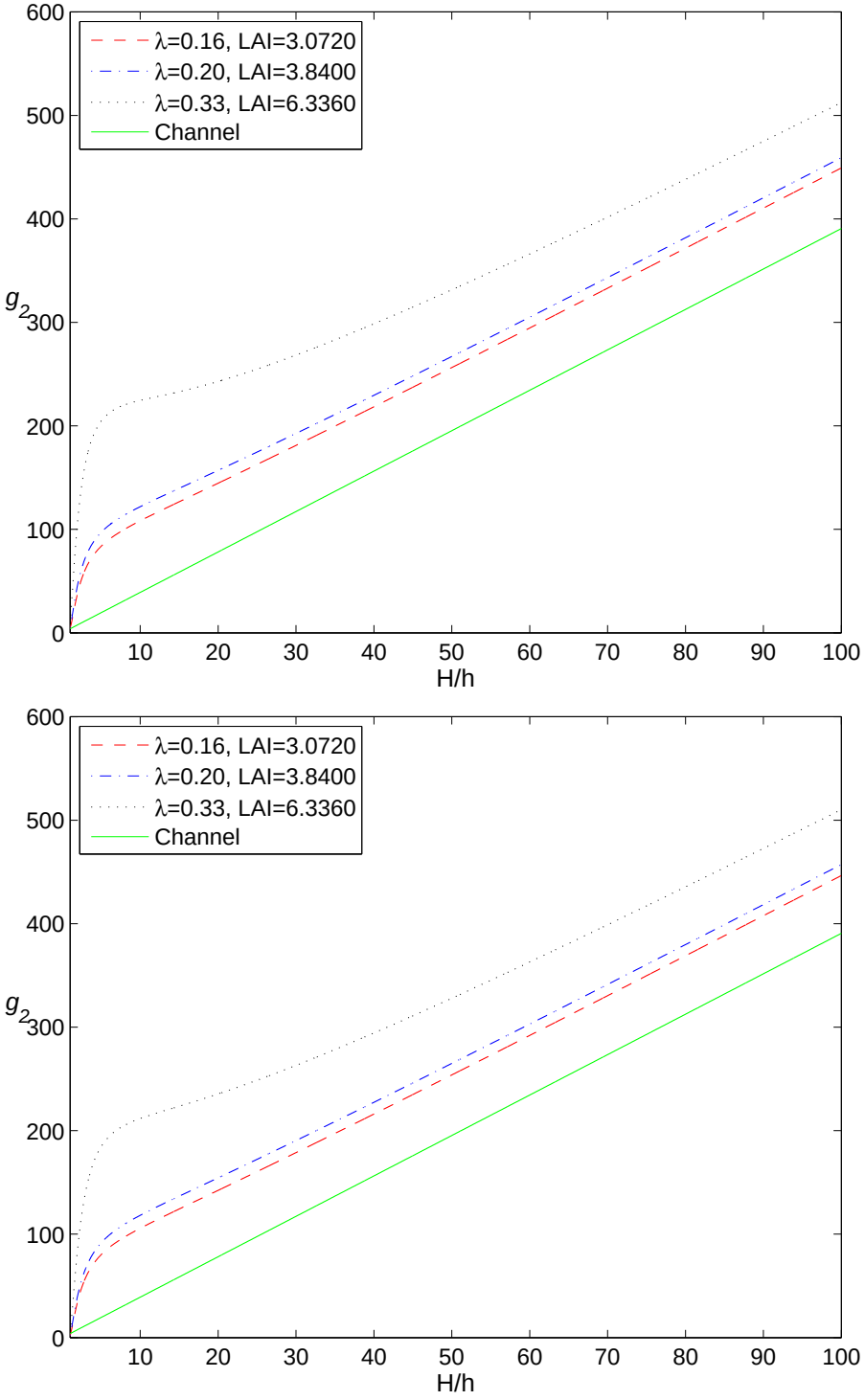

Figure 5.4 The diffusion coefficient versus total thickness for different densities of square (top) and staggered (bottom) obstacles. For the square cubes, we used the parameters $A_1 = 3.59$, $\beta = 0.55$, $u_h/u_* = 4.2$. The values $A_1 = 4.43$, $\beta = 1$, $u_h/u_* = 3.05$ are used with the staggered cubes.

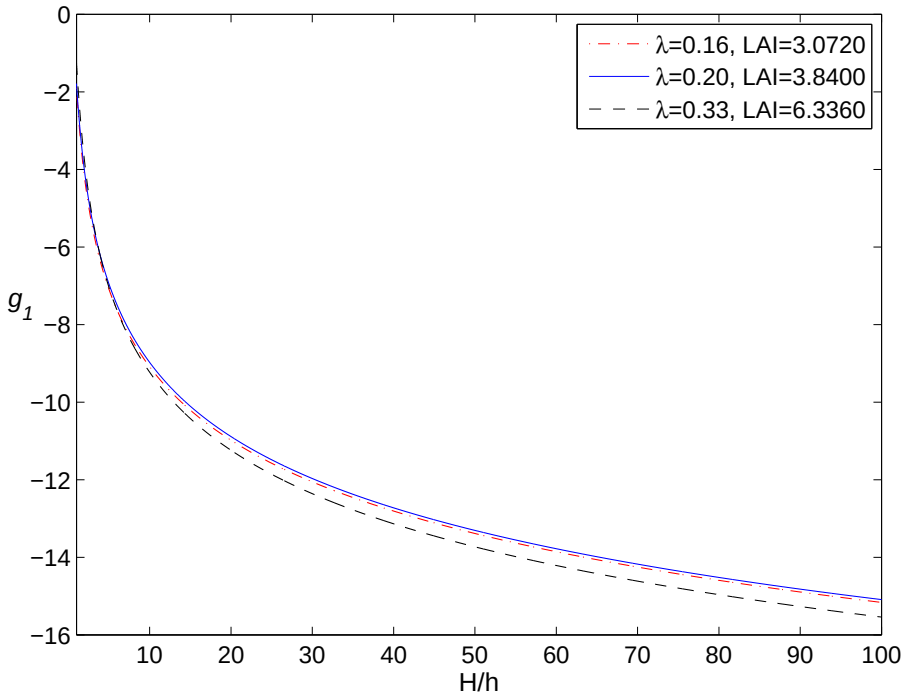

Figure 5.5 The advection coefficient for square obstacles.

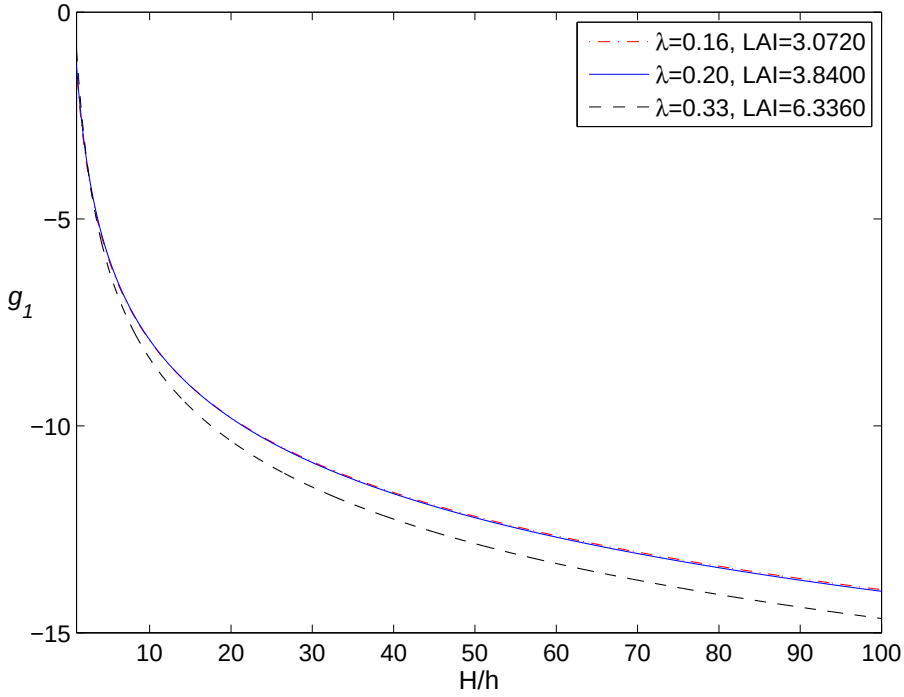

Figure 5.6 The advection coefficient for staggered obstacles.

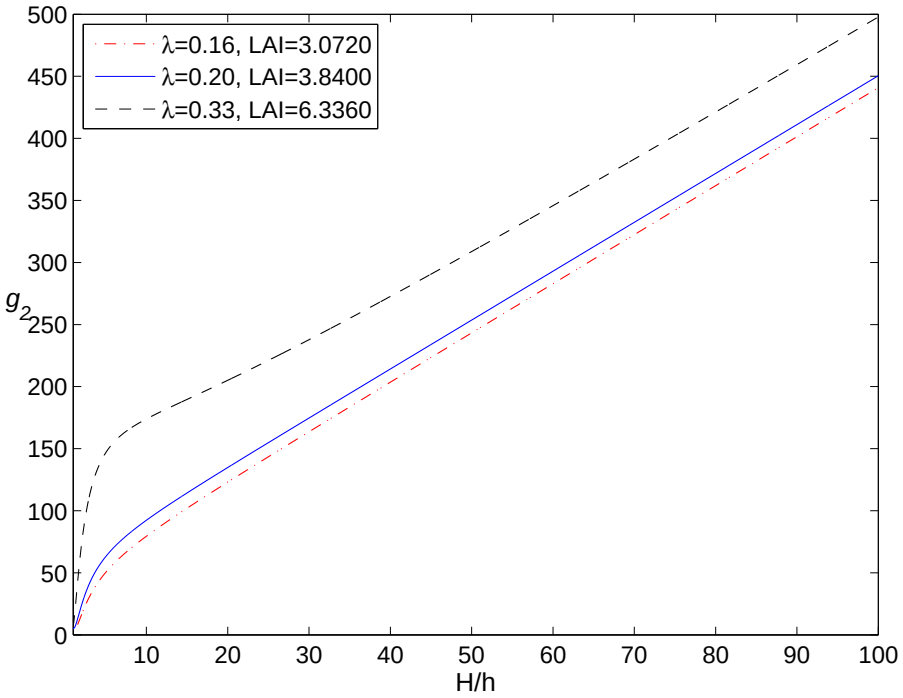

Figure 5.7 The diffusion coefficient for square obstacles.

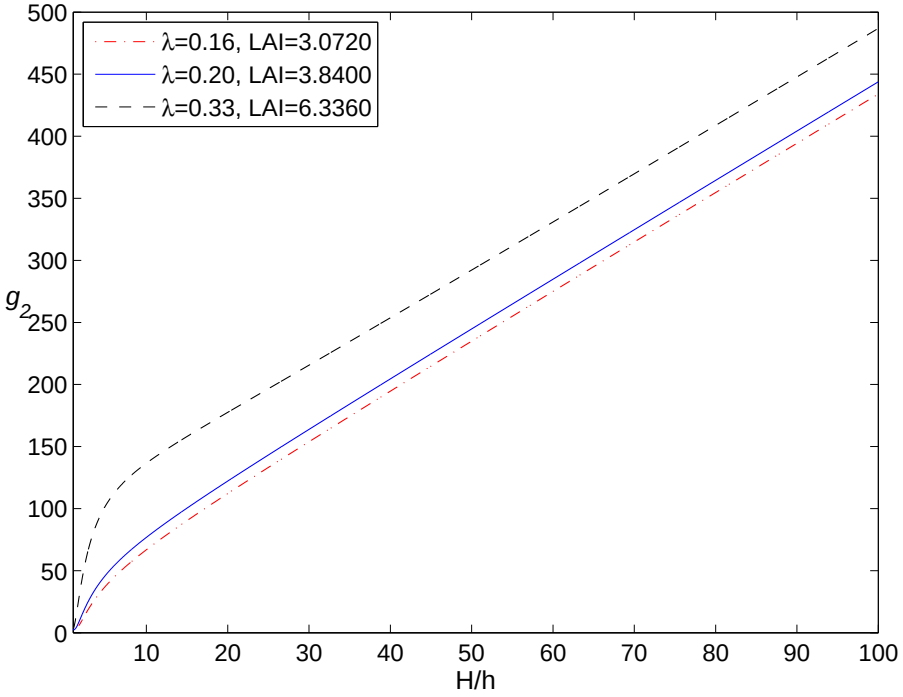

Figure 5.8 The diffusion coefficient for staggered obstacles.

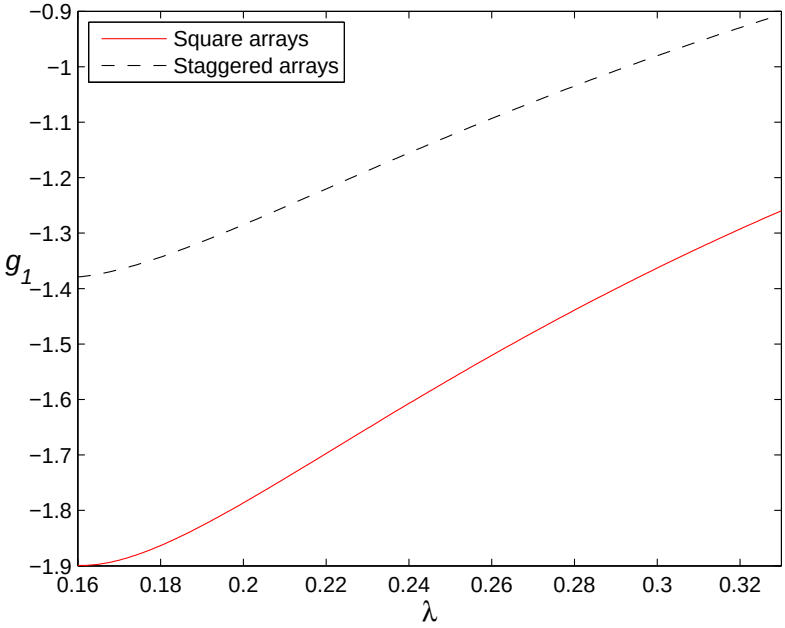

Figure 5.9 The advection coefficient for square and staggered obstacles against density for the case $H/h = 1$.

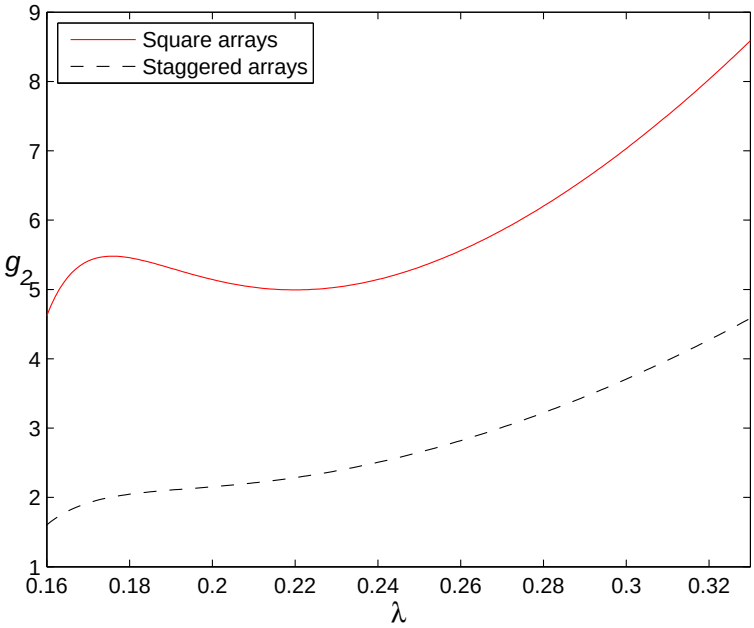

Figure 5.10 The diffusion coefficient for square and staggered obstacles against density for the case $H/h = 1$.

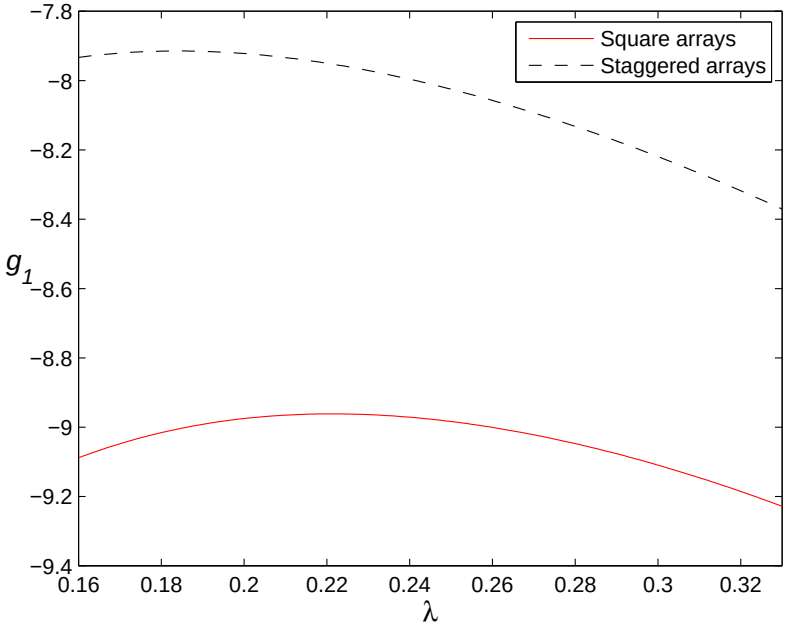

Figure 5.11 The advection coefficient for square and staggered obstacles against density for the case $H/h = 10$.

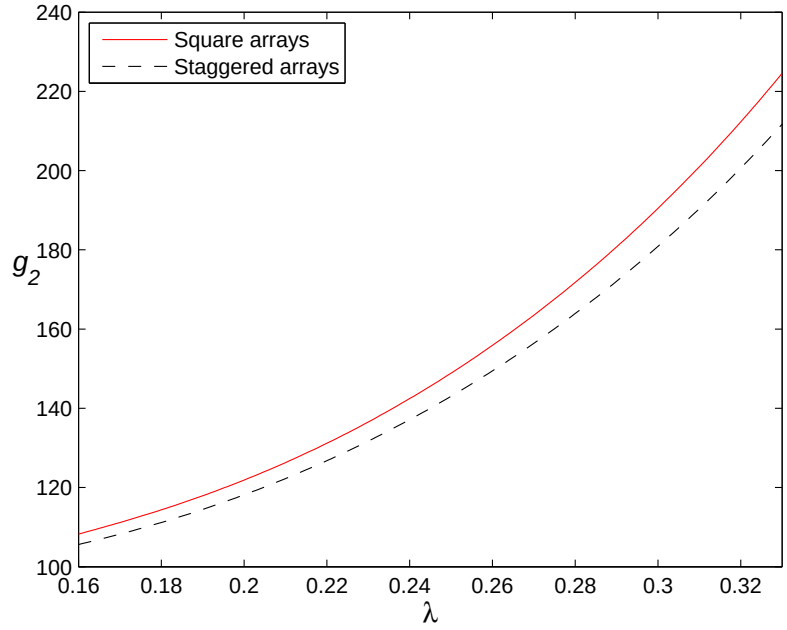

Figure 5.12 The diffusion coefficient for square and staggered obstacles against density for the case $H/h = 10$.

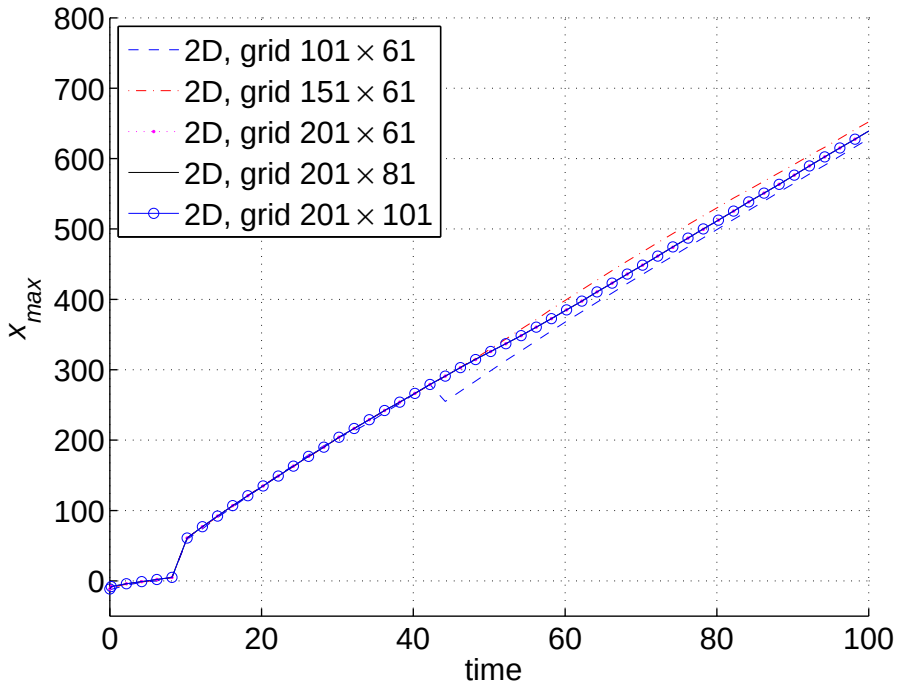

Figure 5.13 Canopy flow: the grid convergence study for 2–D analysis of the x_{max} with respect to time for $H = 4,\ \lambda = 0.16$, and using $\Delta t = 10^{-3}$.

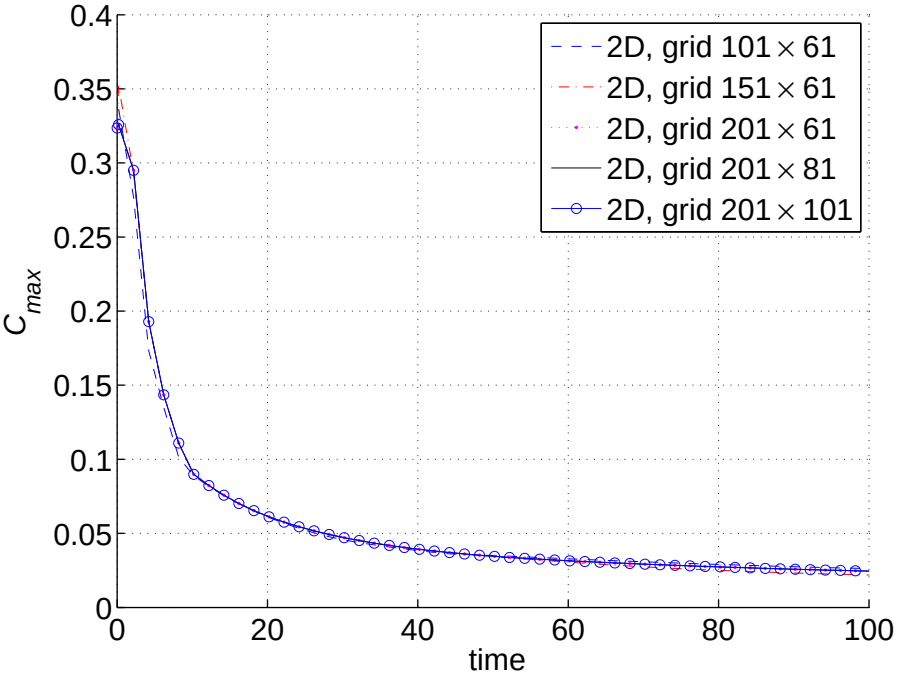

Figure 5.14 Canopy flow: the grid convergence study for 2–D analysis of the C_{max} with respect to time for $H = 4,\ \lambda = 0.16$, and using $\Delta t = 10^{-3}$.

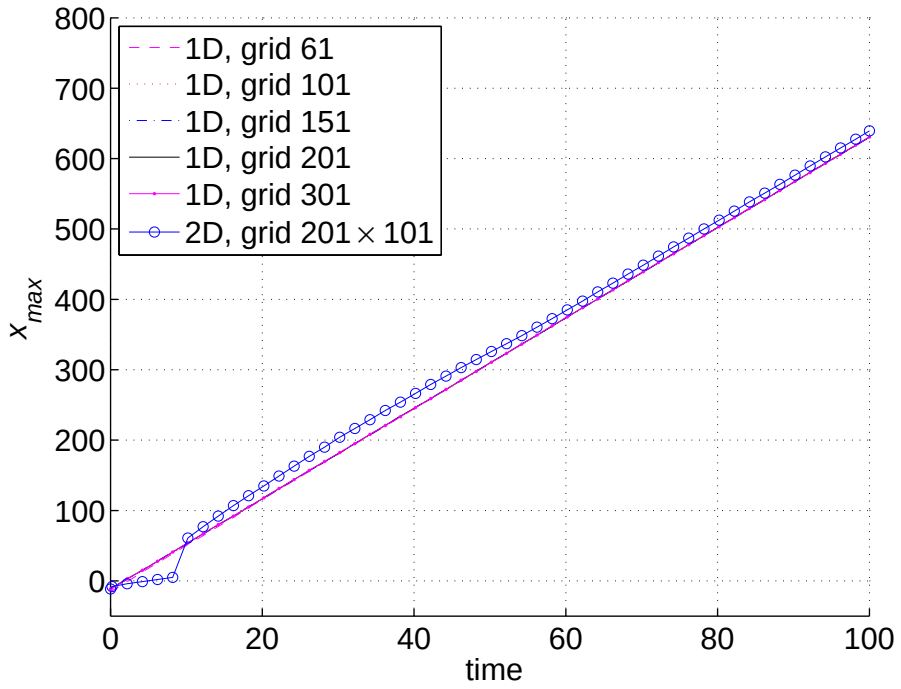

Figure 5.15 Canopy flow: the grid convergence study for 1–D analysis of the x_{max} with respect to time for $H = 4,\ \lambda = 0.16$, and using $\Delta t = 10^{-3}$.

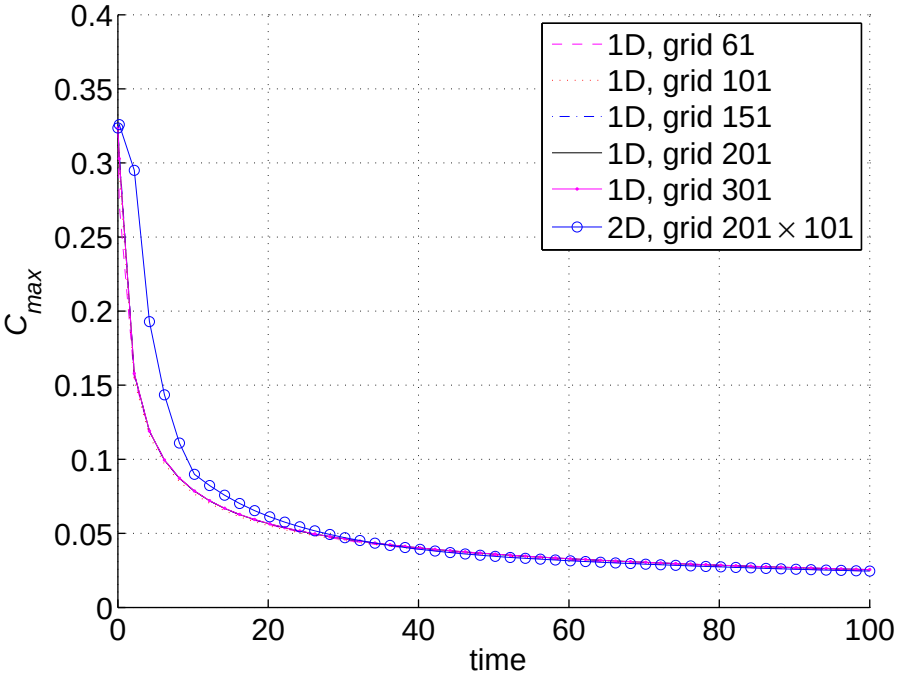

Figure 5.16 Canopy flow: the grid convergence study for 1–D analysis of the C_{max} with respect to time for $H = 4,\ \lambda = 0.16$, and using $\Delta t = 10^{-3}$.

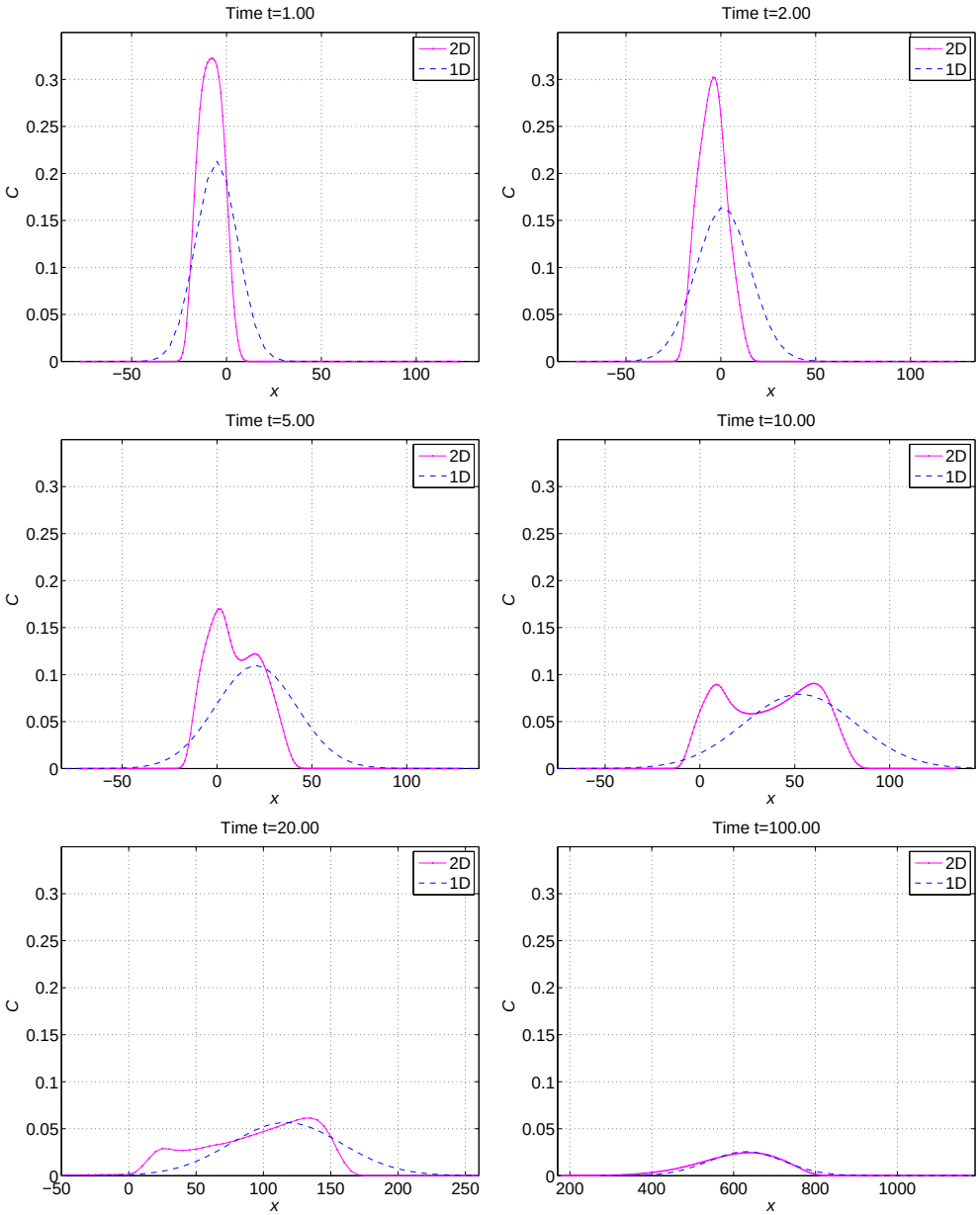

Figure 5.17 Canopy flow: averaged concentration at different times for $H = 4$, $\lambda = 0.16$, using a grid of 201×101 and $\Delta t = 10^{-3}$.

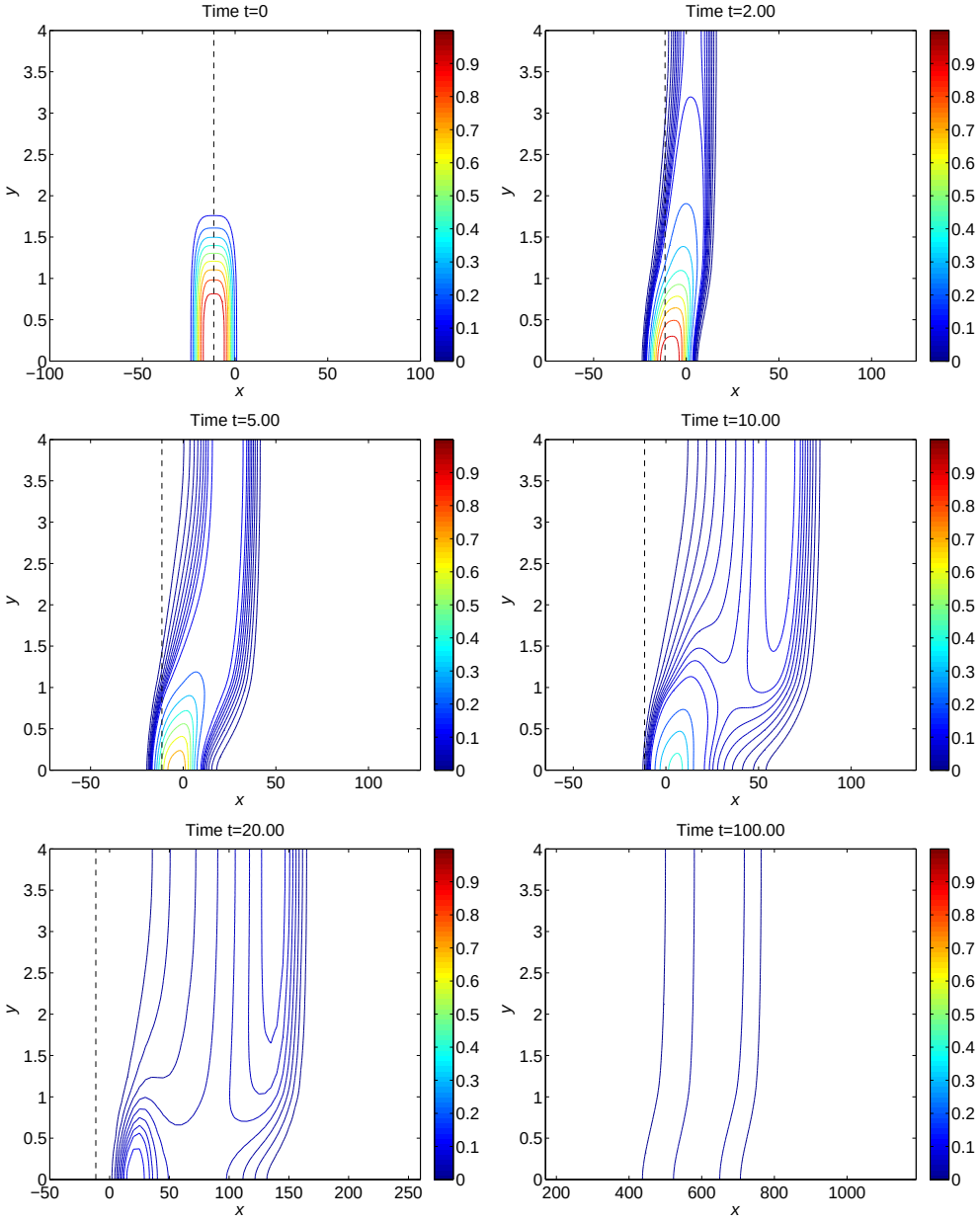

Figure 5.18 Canopy flow: concentration field at different times for $H = 4,\ \lambda = 0.16$, using a grid of 201×101 and $\Delta t = 10^{-3}$.

5.6 Concluding remarks

We constructed an averaged model of shear dispersion in the turbulent flow within and above the canopy using centre manifold approach. The core of the model is the standard advection-diffusion equation (5.3) supplemented by no-flux boundary conditions (5.4). The model contains as independent parameters the friction velocity u_*, total thickness of the flow H, height of the canopy h and frontal area density of the canopy λ. The model is reduced to the averaged form (5.1) by the centre manifold procedure. The advection and diffusion coefficients, governing the transfer of tracers of the averaged model, are found in terms of the independent parameters. The used approach required lengthy derivations and produced quite cumbersome expressions leading to the coefficients g_1 and g_2. However, we would like to put emphasis on the following aspect of the problem: the derived 1–D equation (5.1) reveals a hidden property of the transport process, namely the asymptotic 1–D law for the averaged concentration. This is an important theoretical insight into the originally 2-dimensional problem (5.3). Whether such a law existed and what form it could have was not obvious beforehand. At the same time, from practical viewpoint, our results can be useful via the simple estimates (5.2) giving the distance, travelled by the patch of the substance, and its size; of course those can only serve as a rough tool.

Chapter 6

Conclusions

The one-dimensional integrated radial basis function network 1D-IRBFN method is successfully used to verify the centre manifold approach. The 1D-RBFN has major advantages include: (i) the RBFNs have the property of universal approximation; (ii) the rectangular domain of computation is discretized using a Cartesian grid which helps reduce the computational cost; (iii) the use of integration instead of conventional differentiation to construct the RBF approximations significantly improves the stability and accuracy of the numerical solution and ensures a high convergence rate; and (iv) the 1D-IRBFN satisfies the governing differential equations together with boundary conditions in an exact manner. The centre manifold approach enables us to analytically construct an advection-diffusion equation for the depth-averaged concentration of substances in channels. The general approach laying a firm base into the averaging procedure has been proposed by Roberts and co-authors in the late 1980s. We derive the evolution partial differential equation for the depth-averaged concentration, involving first-second-and higher-order derivatives with respect to spatial coordinate. The coefficients of the equation are derived in terms of the parameters characterising the turbulent flow. The advection, diffusion and dispersion coefficients of the equation, which we calculate, help quickly estimate the dynamics and size of the clouds of contaminants in the flow. In addition, the equation represents considerable theoretical interest as a universal low-dimensional law for starting dynamics from different initial conditions. We present a direct numerical verification of this approach with examples of the dispersion in laminar and turbulent flows in an open channel with a smooth bottom. The 1D-IRBFN method is used as an approach to obtain a numerical solution for the original two-dimensional (2-D) advection-diffusion equation. The 2-D solution is depth-averaged and compared with the solution of the 1-D equation derived using the centre manifolds. The numerical results show that the 2-D and 1-D solutions are in good agreement. We also derive high-order partial differential equations governing the longitudinal dispersion of contaminants in a turbulent open channel flow. Two types of the average velocity profile are considered: the classical logarithmic profile and power profile according to a different similarity hypothesis of the flow with respect to the non-dimensional distance from the wall. The logarithmic model is Reynolds

number independent and deviates from the universal law of the wall. The power law is proposed as an alternative to the logarithmic profile based on the deviation of the later. The most recent experimental data is in support of the power profile as it gives an accurate description of the mean velocity distribution over the self-similar intermediate region adjacent to the viscous sublayer for a wide variety of boundary layer flows. The universality of the power velocity profile is guaranteed in modelling dispersion. The dispersion of contaminants for the logarithmic and power velocity profiles are separately investigated over the entire cross section of the flow. Of particular interest is the case of very large Reynolds numbers. In the two different versions, which we analyse, the layer has universal velocity structure and well-defined turbulent diffusion coefficient. We also assume that the flow is turbulent, well developed and inertial to provide a mechanism of fast distribution of contaminants across the flow. This assumption is important for the inertial layer to be treated by the centre manifold approach.

In addition to the flows above a smooth bottom, we formulated and analysed the averaged model of dispersion in turbulent canopy flows, mainly of urban or industrial nature. We showed that the coefficient values coincide with those obtained earlier for the flow over smooth bottom in the limit of large flow depth.

Appendix A

A.1 Calculating g_6 for the logarithmic velocity profile

The coefficient g_6 in (4.6) is found as follows. Substituting $n = 5$ into (4.8) leads to

$$\begin{aligned}\frac{\partial}{\partial y}\left(y\frac{\partial c_5}{\partial y}\right) = \frac{1}{4K^5\kappa^{10}}\Bigg(&\frac{51131017}{233280000} + \frac{101}{10368}y - \frac{65}{216}y^2 + \frac{29}{648}y^3 \\ &-\frac{47}{41472}y^4 + \frac{1433}{23328}\ln y + \frac{1733}{1728}y\ln y - \frac{6435}{7776}y^2\ln y \\ &+\frac{1}{12}y^3\ln y - \frac{31}{4608}y^4\ln y + \frac{3475}{10368}y\ln^2 y + \frac{103}{216}y^2\ln^2 y - \frac{19}{72}y^3\ln^2 y \\ &+\frac{59}{2592}y^4\ln^2 y + \frac{139}{432}y^2\ln^3 y - \frac{1}{18}y^3\ln^3 y \\ &+\frac{1}{1728}y^4\ln^3 y + \frac{1}{12}y^3\ln^4 y - \frac{1}{48}y^4\ln^4 y + \frac{1}{144}y^4\ln^5 y\Bigg)\,.\end{aligned} \tag{A.1}$$

Integrating (A.1) gives

$$\begin{aligned}y\frac{\partial c_5}{\partial y} = \frac{1}{4K^5\kappa^{10}}\Bigg(&\frac{36801017}{233280000}y - \frac{6721}{41472}y^2 + \frac{73}{23328}y^3 + \frac{41}{41472}y^4 \\ &+\frac{6083}{32400000}y^5 + \frac{1433}{23328}y\ln y + \frac{6923}{20736}y^2\ln y - \frac{2413}{7776}y^3\ln y \\ &+\frac{47}{1152}y^4\ln y - \frac{53707}{25920000}y^5\ln y + \frac{3475}{20736}y^2\ln^2 y + \frac{67}{1296}y^3\ln^2 y \\ &-\frac{23}{576}y^4\ln^2 y + \frac{1177}{648000}y^5\ln^2 y + \frac{139}{1296}y^3\ln^3 y - \frac{5}{144}y^4\ln^3 y \\ &+\frac{197}{43200}y^5\ln^3 y + \frac{1}{48}y^4\ln^4 y - \frac{1}{180}y^5\ln^4 y + \frac{1}{720}y^5\ln^5 y\Bigg) + B_5\,.\end{aligned} \tag{A.2}$$

The boundary condition on the bottom leads to $B_5 = 0$. Integrating (A.2) gives

$$\begin{aligned} c_5 = \frac{1}{4K^5\kappa^{10}} \Bigg(& \frac{7490339}{77760000}y - \frac{10169}{82944}y^2 + \frac{1099}{34992}y^3 - \frac{373}{165888}y^4 \\ & + \frac{33943}{648000000}y^5 + \frac{1433}{23328}y\ln y + \frac{431}{5184}y^2\ln y - \frac{2125}{23328}y^3\ln y \\ & + \frac{23}{2304}y^4\ln y - \frac{9611}{129600000}y^5\ln y + \frac{3475}{41472}y^2\ln^2 y \\ & - \frac{1}{54}y^3\ln^2 y + \frac{1}{2304}y^4\ln^2 y - \frac{689}{810000}y^5\ln^2 y + \frac{139}{3888}y^3\ln^3 y - \frac{1}{72}y^4\ln^3 y \\ & + \frac{437}{216000}y^5\ln^3 y + \frac{1}{192}y^4\ln^4 y - \frac{5}{3600}y^5\ln^4 y + \frac{1}{3600}y^5\ln^5 y \Bigg) + B_6\,. \end{aligned} \tag{A.3}$$

The integration constant B_6 is found from the condition $\int_\epsilon^1 c_5\,dy = 0$,

$$B_6 = -\frac{24941299}{279936000000K^5\kappa^{10}}\,.$$

Hereafter, (A.3) becomes

$$\begin{aligned} c_5 = \frac{1}{4K^5\kappa^{10}} \Bigg(& -\frac{24941299}{69984000000} + \frac{7490339}{77760000}y - \frac{10169}{82944}y^2 + \frac{1099}{34992}y^3 \\ & - \frac{373}{165888}y^4 + \frac{33943}{648000000}y^5 + \frac{1433}{23328}y\ln y + \frac{431}{5184}y^2\ln y - \frac{2125}{23328}y^3\ln y \\ & + \frac{23}{2304}y^4\ln y - \frac{9611}{129600000}y^5\ln y + \frac{3475}{41472}y^2\ln^2 y \\ & - \frac{1}{54}y^3\ln^2 y + \frac{1}{2304}y^4\ln^2 y - \frac{689}{810000}y^5\ln^2 y + \frac{139}{3888}y^3\ln^3 y \\ & - \frac{1}{72}y^4\ln^3 y + \frac{437}{216000}y^5\ln^3 y + \frac{1}{192}y^4\ln^4 y - \frac{5}{3600}y^5\ln^4 y + \frac{1}{3600}y^5\ln^5 y \Bigg)\,. \end{aligned} \tag{A.4}$$

The coefficient g_6 is given by

$$\begin{aligned} g_6 = -\frac{1}{4K^5\kappa^{11}}\Bigg(&\frac{24941299}{69984000000}y - \frac{8141017}{933120000}y^2 + \frac{30399}{2239488}y^3 - \frac{15845}{4478976}y^4 \\ &+ \frac{51233}{518400000}y^5 + \frac{71893}{5832000000}y^6 - \frac{24941299}{69984000000}y\ln y \\ &+ \frac{8141017}{466560000}y^2\ln y - \frac{10133}{248832}y^3\ln y + \frac{15845}{1119744}y^4\ln y - \frac{51233}{103680000}y^5\ln y \\ &- \frac{71893}{972000000}y^6\ln y + \frac{1433}{46656}y^2\ln^2 y - \frac{1}{4608}y^3\ln^2 y \\ &- \frac{2351}{186624}y^4\ln^2 y + \frac{1}{9000}y^5\ln^2 y + \frac{64303}{259200000}y^6\ln^2 y + \frac{3475}{124416}y^3\ln^3 y \\ &- \frac{211}{15552}y^4\ln^3 y + \frac{181}{57600}y^5\ln^3 y - \frac{5063}{9720000}y^6\ln^3 y \\ &+ \frac{139}{15552}y^4\ln^4 y - \frac{11}{2880}y^5\ln^4 y \\ &+ \frac{2211}{3888000}y^6\ln^4 y + \frac{1}{960}y^5\ln^5 y - \frac{1}{3600}y^6\ln^5 y + \frac{1}{21600}y^6\ln^6 y\Bigg)_{\epsilon}^{1}. \end{aligned} \tag{A.5}$$

Calculating further, we obtain

$$g_6 = -\frac{6226741}{13996800000K^5\kappa^{11}}\,.$$

A.2 Calculating g_5 and g_6 for the power velocity profile

The coefficient g_5 in (4.6) is calculated as follows. Substituting $n = 4$ into (4.8) leads to

$$\begin{aligned}\frac{\partial}{\partial y}\left(y^{1-\alpha}\frac{\partial c_4}{\partial y}\right) = {} & \frac{\alpha^2 r q^5}{6\kappa^2(2\alpha+1)^2(5\alpha+3)}y^{7\alpha+3} + \frac{\alpha^2 r q^4 g_1(3\alpha+2)}{3\kappa^2(5\alpha+3)(2\alpha+1)^2}y^{6\alpha+3} \\ & + \frac{\alpha^2 q^3 g_1^2}{2\kappa^2}\left(\frac{2r+qs}{3(\alpha+1)(4\alpha+3)} + \frac{r}{(2\alpha+1)(5\alpha+3)}\right)y^{5\alpha+3} \\ & + \frac{\alpha r b q^3}{\kappa(4\alpha+2)}y^{5\alpha+2} + \frac{\alpha^2 q^2 g_1^3}{\kappa^2(6\alpha+6)}\left(\frac{2r+qs}{4\alpha+3} + \frac{qs}{2\alpha+3}\right)y^{4\alpha+3} \\ & + \frac{\alpha r q^2(4\alpha+3)\,(g_2+bg_1)}{\kappa(4\alpha+2)}y^{4\alpha+2} + \frac{\alpha^2 s q^2 g_1^4}{\kappa(6\alpha+6)(2\alpha+3)}y^{3\alpha+3} \\ & + \frac{\alpha q\,(2r+qs)\,(2g_1g_2+bg_1^2)}{2\kappa}y^{3\alpha+2} + \frac{\alpha^2 m q^4}{\kappa^2(\alpha+1)(2\alpha+1)}y^{3\alpha+1} \\ & + \frac{\alpha s q\,(3g_1^2g_2+bg_1^3)}{2\kappa}y^{2\alpha+2} + \frac{2\alpha^2 q^3\,(g_3+bg_2+mg_1)}{\kappa^2(2\alpha+1)}y^{2\alpha+1} \\ & + \frac{\alpha^2 q^2\,(2g_1g_3+2bg_1g_2+mg_1^2+g_2^2)}{\kappa^2(\alpha+1)}y^{\alpha+1} + \frac{\alpha A_2 q^2}{\kappa}y^{\alpha} \\ & + \frac{\alpha q\,(g_4+bg_3+mg_2+A_2g_1)}{\kappa}.\end{aligned} \tag{A.6}$$

Integrating (A.6) twice gives

$$
\begin{aligned}
c_4 = & \frac{\alpha^2 r q^5}{24\kappa^2(2\alpha+1)^3(5\alpha+3)(7\alpha+4)} y^{8\alpha+4} \\
& + \frac{\alpha^2 r q^4 g_1}{6\kappa^2(2\alpha+1)^2(5\alpha+3)(7\alpha+4)} y^{7\alpha+4} \\
& + \frac{\alpha^2 q^3 g_1^2}{4\kappa^2(3\alpha+2)(5\alpha+4)} \left(\frac{2r+qs}{3(\alpha+1)(4\alpha+3)} + \frac{r}{(2\alpha+1)(5\alpha+3)} \right) y^{6\alpha+4} \\
& + \frac{\alpha r b q^3}{6\kappa(2\alpha+1)^2(5\alpha+3)} y^{6\alpha+3} + \frac{\alpha^2 q^2 g_1^3}{24\kappa^2(\alpha+1)^2(5\alpha+4)} \\
& \times \left(\frac{2r+qs}{4\alpha+3} + \frac{qs}{2\alpha+3} \right) y^{5\alpha+4} + \frac{\alpha r q^2 \left(g_2 + b g_1\right)}{2\kappa(2\alpha+1)(5\alpha+3)} y^{5\alpha+3} \\
& + \frac{\alpha^2 s q^2 g_1^4}{24\kappa^2(\alpha+1)^2(2\alpha+3)(3\alpha+4)} y^{4\alpha+4} + \frac{\alpha q \left(2r+qs\right)\left(2g_1 g_2 + b g_1^2\right)}{6\kappa(\alpha+1)(4\alpha+3)} y^{4\alpha+3} \\
& + \frac{r m q}{(4\alpha+2)} y^{4\alpha+2} + \frac{\alpha s q \left(3 g_1^2 g_2 + b g_1^3\right)}{6\kappa(\alpha+1)(2\alpha+3)} y^{3\alpha+3} + r\left(g_3 + b g_2 + m g_1\right) y^{3\alpha+2} \\
& + \frac{s\left(2g_1 g_3 + 2b g_1 g_2 + m g_1^2 + g_2^2\right)}{2} y^{2\alpha+2} + \frac{\alpha A_2 q^2}{\kappa(\alpha+1)(2\alpha+1)} y^{2\alpha+1} \\
& + \frac{\alpha q \left(g_4 + b g_3 + m g_2 + A_2 g_1\right)}{\kappa(\alpha+1)} y^{\alpha+1} + A_4 \,.
\end{aligned}
\tag{A.7}
$$

The Integration constant A_4 is found from the condition $\int_\epsilon^1 c_3\, dy = 0$,

$$
\begin{aligned}
A_4 = & -\frac{\alpha^2 r q^5}{24\kappa^2(2\alpha+1)^3(5\alpha+3)(7\alpha+4)(8\alpha+5)} \\
& - \frac{\alpha^2 r q^4 g_1}{6\kappa^2(2\alpha+1)^2(5\alpha+3)(7\alpha+4)(7\alpha+5)} \\
& - \frac{\alpha^2 q^3 g_1^2}{4\kappa^2(3\alpha+2)(5\alpha+4)(6\alpha+5)} \left(\frac{2r+qs}{3(\alpha+1)(4\alpha+3)} + \frac{r}{(2\alpha+1)(5\alpha+3)} \right) \\
& - \frac{\alpha r b q^3}{12\kappa(2\alpha+1)^2(3\alpha+2)(5\alpha+3)} - \frac{\alpha^2 q^2 g_1^3}{120\kappa^2(\alpha+1)^3(5\alpha+4)} \\
& \times \left(\frac{2r+qs}{4\alpha+3} + \frac{qs}{2\alpha+3} \right) - \frac{\alpha r q^2 \left(g_2 + b g_1\right)}{2\kappa(2\alpha+1)(5\alpha+3)(5\alpha+4)} \\
& - \frac{\alpha^2 s q^2 g_1^4}{24\kappa^2(\alpha+1)^2(2\alpha+3)(3\alpha+4)(4\alpha+5)} - \frac{\alpha q \left(2r+qs\right)\left(2g_1 g_2 + b g_1^2\right)}{24\kappa(\alpha+1)^2(4\alpha+3)} \\
& - \frac{r m q}{(4\alpha+2)(4\alpha+3)} - \frac{\alpha s q \left(3 g_1^2 g_2 + b g_1^3\right)}{\kappa(6\alpha+6)(2\alpha+3)(3\alpha+4)} - \frac{r\left(g_3 + b g_2 + m g_1\right)}{3(\alpha+1)} \\
& - \frac{s\left(2g_1 g_3 + 2b g_1 g_2 + m g_1^2 + g_2^2\right)}{2(2\alpha+3)} - \frac{\alpha A_2 q^2}{\kappa(\alpha+1)^2(4\alpha+2)} \\
& - \frac{\alpha q \left(g_4 + b g_3 + m g_2 + A_2 g_1\right)}{\kappa(\alpha+1)(\alpha+2)} \,.
\end{aligned}
\tag{A.8}
$$

The coefficient g_5 is given by

$$
\begin{aligned}
g_5 = & -\frac{\alpha^2 r q^6}{24\kappa^2(2\alpha+1)^3(5\alpha+3)(7\alpha+4)(9\alpha+5)} \\
& -\frac{\alpha^2 r q^5 g_1}{6\kappa^2(2\alpha+1)^2(5\alpha+3)(7\alpha+4)(8\alpha+5)} \\
& -\frac{\alpha^2 q^4 g_1^2}{4\kappa^2(3\alpha+2)(5\alpha+4)(7\alpha+5)}\left(\frac{2r+qs}{3(\alpha+1)(4\alpha+3)}+\frac{r}{(2\alpha+1)(5\alpha+3)}\right) \\
& -\frac{\alpha r b q^4}{6\kappa(2\alpha+1)^2(5\alpha+3)(7\alpha+4)}-\frac{\alpha^2 q^3 g_1^3}{24\kappa^2(\alpha+1)^2(5\alpha+4)(6\alpha+5)} \\
& \times\left(\frac{2r+qs}{4\alpha+3}+\frac{qs}{2\alpha+3}\right)-\frac{\alpha r q^3\left(g_2+b g_1\right)}{4\kappa(2\alpha+1)(3\alpha+2)(5\alpha+3)} \\
& -\frac{\alpha^2 s q^3 g_1^4}{120\kappa^2(\alpha+1)^3(2\alpha+3)(3\alpha+4)}-\frac{\alpha q^2\left(2r+qs\right)\left(2g_1g_2+bg_1^2\right)}{6\kappa(\alpha+1)(4\alpha+3)(5\alpha+4)} \\
& -\frac{r m q^2}{(4\alpha+2)(5\alpha+3)}-\frac{\alpha s q^2\left(3g_1^2g_2+bg_1^3\right)}{24\kappa(\alpha+1)^2(2\alpha+3)}-\frac{r q\left(g_3+bg_2+mg_1\right)}{(4\alpha+3)} \\
& -\frac{s q\left(2g_1g_3+2bg_1g_2+mg_1^2+g_2^2\right)}{(6\alpha+6)}-\frac{\alpha A_2 q^3}{\kappa(\alpha+1)(2\alpha+1)(3\alpha+2)} \\
& -\frac{\alpha q^2\left(g_4+bg_3+mg_2+A_2g_1\right)}{2\kappa(\alpha+1)^2}-\frac{A_4 q}{\alpha+1}\,.
\end{aligned}
\tag{A.9}
$$

We find the coefficient g_6 in (4.6) as follows. Substituting $n = 5$ into (4.8) leads to

$$
\begin{aligned}
\frac{\partial}{\partial y}\left(y^{1-\alpha}\frac{\partial c_5}{\partial y}\right) &= \frac{\alpha^3 r q^7}{24\kappa^3(2\alpha+1)^3(5\alpha+3)(7\alpha+4)}y^{9\alpha+4} \\
&+\frac{\alpha^3 r q^6 g_1(8\alpha+5)}{24\kappa^3(2\alpha+1)^3(5\alpha+3)(7\alpha+4)}y^{8\alpha+4} \\
&+\frac{\alpha^3 q^5 g_1^2}{12\kappa^3(3\alpha+2)(5\alpha+4)}\left(\frac{2r+qs}{(\alpha+1)(4\alpha+3)}+\frac{3r}{(2\alpha+1)(5\alpha+3)}\right)y^{7\alpha+4} \\
&+\frac{\alpha^3 r q^5 g_1^2}{6\kappa^3(2\alpha+1)^2(5\alpha+3)(7\alpha+4)}y^{7\alpha+4}+\frac{\alpha^2 r b q^5}{6\kappa^2(2\alpha+1)^2(5\alpha+3)}y^{7\alpha+3} \\
&+\frac{\alpha^3 q^4 g_1^3}{12\kappa^3}\left(\frac{2r+qs}{2(\alpha+1)^2(3\alpha+2)(4\alpha+3)}+\frac{qs}{2(\alpha+1)^2(2\alpha+3)(5\alpha+4)}\right. \\
&\left.+\frac{3r}{(2\alpha+1)(3\alpha+2)(5\alpha+3)(5\alpha+4)}\right)y^{6\alpha+4} \\
&+\frac{\alpha^2 r q^4(3\alpha+2)\left(g_2+bg_1\right)}{3\kappa^2(2\alpha+1)^2(5\alpha+3)}y^{6\alpha+3}+\frac{\alpha^3 q^3 g_1^4}{\kappa^3(\alpha+1)(5\alpha+4)} \\
&\times\left(\frac{2r+qs}{24(\alpha+1)(4\alpha+3)}+\frac{qs}{3(2\alpha+3)(3\alpha+4)}\right)y^{5\alpha+4} \\
&+\frac{\alpha^2 q^3\left(2g_1g_2+bg_1^2\right)}{2\kappa^2}\left(\frac{2r+qs}{3(\alpha+1)(4\alpha+3)}+\frac{r}{(2\alpha+1)(5\alpha+3)}\right)y^{5\alpha+3} \qquad \text{(A.10)} \\
&+\frac{\alpha r m q^3}{2\kappa(2\alpha+1)}y^{5\alpha+2}+\frac{\alpha^3 s q^3 g_1^5}{24\kappa^3(\alpha+1)^2(2\alpha+3)(3\alpha+4)}y^{4\alpha+4} \\
&+\frac{\alpha^2 q^2\left(3g_1^2g_2+bg_1^3\right)}{6\kappa^2(\alpha+1)}\left(\frac{2r+qs}{4\alpha+3}+\frac{sq}{2\alpha+3}\right)y^{4\alpha+3} \\
&+\frac{\alpha r q^2(4\alpha+3)\left(g_3+bg_2+mg_1\right)}{2\kappa(2\alpha+1)}y^{4\alpha+2}+\frac{\alpha^2 s q^2\left(4g_1^3g_2+bg_1^4\right)}{6\kappa^2(\alpha+1)(2\alpha+3)}y^{3\alpha+3} \\
&+\frac{\alpha q(2r+qs)\left(2g_1g_3+2bg_1g_2+mg_1^2+g_2^2\right)}{2\kappa}y^{3\alpha+2} \\
&+\frac{\alpha^2 A_2 q^4}{\kappa^2(\alpha+1)(2\alpha+1)}y^{3\alpha+1}+\frac{\alpha s q\left(3g_1^2g_3+3bg_1^2g_2+3g_1g_2^2+mg_1^3\right)}{2\kappa}y^{2\alpha+2} \\
&+\frac{2\alpha^2 q^3\left(g_4+bg_3+mg_2+A_2g_1\right)}{\kappa^2(2\alpha+1)}y^{2\alpha+1} \\
&+\frac{\alpha^2 q^2\left(2g_1g_4+2g_2g_3+2bg_1g_3+bg_2^2+2mg_1g_2+A_2g_1^2\right)}{\kappa^2(\alpha+1)}y^{\alpha+1}+\frac{\alpha A_4 q^2}{\kappa}y^{\alpha} \\
&+\frac{\alpha q\left(g_5+bg_4+mg_3+A_2g_2+A_4g_1\right)}{\kappa}.
\end{aligned}
$$

Integrating (A.10) twice gives

$$
\begin{aligned}
c_5 = {} & \frac{\alpha^3 r q^7}{120\kappa^3(2\alpha+1)^4(5\alpha+3)(7\alpha+4)(9\alpha+5)} y^{10\alpha+5} \\
& + \frac{\alpha^3 r q^6 g_1}{24\kappa^3(2\alpha+1)^3(5\alpha+3)(7\alpha+4)(9\alpha+5)} y^{9\alpha+5} \\
& + \frac{\alpha^3 q^5 g_1^2 \left(\frac{2r+qs}{(\alpha+1)(4\alpha+3)} + \frac{3r}{(2\alpha+1)(5\alpha+3)}\right)}{12\kappa^3(3\alpha+2)(5\alpha+4)(7\alpha+5)(8\alpha+5)} y^{8\alpha+5} \\
& + \frac{\alpha^3 r q^5 g_1^2}{6\kappa^3(2\alpha+1)^2(5\alpha+3)(7\alpha+4)(7\alpha+5)(8\alpha+5)} y^{8\alpha+5} \\
& + \frac{\alpha^2 r b q^5}{24\kappa^2(2\alpha+1)^3(5\alpha+3)(7\alpha+4)} y^{8\alpha+4} \\
& + \frac{\alpha^3 q^4 g_1^3}{12\kappa^3(6\alpha+5)(7\alpha+5)} \left(\frac{2r+qs}{2(\alpha+1)^2(3\alpha+2)(4\alpha+3)} \right. \\
& \left. + \frac{qs}{2(\alpha+1)^2(2\alpha+3)(5\alpha+4)} + \frac{3r}{(2\alpha+1)(3\alpha+2)(5\alpha+3)(5\alpha+4)} \right) y^{7\alpha+5} \\
& + \frac{\alpha^2 r q^4 \left(g_2 + b g_1\right)}{6\kappa^2(2\alpha+1)^2(5\alpha+3)(7\alpha+4)} y^{7\alpha+4} \\
& + \frac{\alpha^3 q^3 g_1^4 \left(\frac{2r+qs}{24(\alpha+1)(4\alpha+3)} + \frac{qs}{3(2\alpha+3)(3\alpha+4)}\right)}{5\kappa^3(\alpha+1)^2(5\alpha+4)(6\alpha+5)} y^{6\alpha+5} \\
& + \frac{\alpha^2 q^3 (2 g_1 g_2 + b g_1^2) \left(\frac{2r+qs}{3(\alpha+1)(4\alpha+3)} + \frac{r}{(2\alpha+1)(5\alpha+3)}\right)}{4\kappa^2(3\alpha+2)(5\alpha+4)} y^{6\alpha+4} \\
& + \frac{\alpha r m q^3}{6\kappa(2\alpha+1)^2(5\alpha+3)} y^{6\alpha+3} + \frac{\alpha^3 s q^3 g_1^5}{120\kappa^3(\alpha+1)^3(2\alpha+3)(3\alpha+4)(4\alpha+5)} y^{5\alpha+5} \\
& + \frac{\alpha^2 q^2 \left(3 g_1^2 g_2 + b g_1^3\right) \left(\frac{2r+qs}{4\alpha+3} + \frac{qs}{2\alpha+3}\right)}{24\kappa^2(\alpha+1)^2(5\alpha+4)} y^{5\alpha+4} \\
& + \frac{\alpha r q^2 \left(g_3 + b g_2 + m g_1\right)}{2\kappa(2\alpha+1)(5\alpha+3)} y^{5\alpha+3} + \frac{\alpha^2 s q^2 \left(4 g_1^3 g_2 + b g_1^4\right)}{24\kappa^2(\alpha+1)^2(2\alpha+3)(3\alpha+4)} y^{4\alpha+4} \\
& + \frac{\alpha q (2r+qs) \left(2 g_1 g_3 + 2 b g_1 g_2 + m g_1^2 + g_2^2\right)}{6\kappa(\alpha+1)(4\alpha+3)} y^{4\alpha+3} \\
& + \frac{r A_2 q}{4\alpha+2} y^{4\alpha+2} + \frac{\alpha s q \left(3 g_1^2 g_3 + 3 b g_1^2 g_2 + 3 g_1 g_2^2 + m g_1^3\right)}{6\kappa(\alpha+1)(2\alpha+3)} y^{3\alpha+3} \\
& + r \left(g_4 + b g_3 + m g_2 + A_2 g_1\right) y^{3\alpha+2} \\
& + \frac{s \left(2 g_1 g_4 + 2 g_2 g_3 + 2 b g_1 g_3 + b g_2^2 + 2 m g_1 g_2 + A_2 g_1^2\right)}{2} y^{2\alpha+2} \\
& + \frac{\alpha A_4 q^2}{\kappa(\alpha+1)(2\alpha+1)} y^{2\alpha+1} + \frac{\alpha q \left(g_5 + b g_4 + m g_3 + A_2 g_2 + A_4 g_1\right)}{\kappa(\alpha+1)} y^{\alpha+1} + A_6 \,.
\end{aligned}
\tag{A.11}
$$

The Integration constant A_6 is found from the condition $\int_\epsilon^1 c_5\, dy = 0$,

$$
\begin{aligned}
A_6 = &-\frac{\alpha^3 r q^7}{240\kappa^3(2\alpha+1)^4(5\alpha+3)^2(7\alpha+4)(9\alpha+5)} \\
&-\frac{\alpha^3 r q^6 g_1}{72\kappa^3(2\alpha+1)^3(3\alpha+2)(5\alpha+3)(7\alpha+4)(9\alpha+5)} \\
&-\frac{\alpha^3 q^5 g_1^2\left(\frac{2r+qs}{(\alpha+1)(4\alpha+3)}+\frac{3r}{(2\alpha+1)(5\alpha+3)}\right)}{24\kappa^3(3\alpha+2)(4\alpha+3)(5\alpha+4)(7\alpha+5)(8\alpha+5)} \\
&-\frac{\alpha^3 r q^5 g_1^2}{12\kappa^3(2\alpha+1)^2(4\alpha+3)(5\alpha+3)(7\alpha+4)(7\alpha+5)(8\alpha+5)} \\
&-\frac{\alpha^2 r b q^5}{24\kappa^2(2\alpha+1)^3(5\alpha+3)(7\alpha+4)(8\alpha+5)} \\
&-\frac{\alpha^3 q^4 g_1^3\left(\frac{2r+qs}{2(\alpha+1)^2(3\alpha+2)(4\alpha+3)}+\frac{qs}{2(\alpha+1)^2(2\alpha+3)(5\alpha+4)}+\frac{3r}{(2\alpha+1)(3\alpha+2)(5\alpha+3)(5\alpha+4)}\right)}{12\kappa^3(6\alpha+5)(7\alpha+5)(7\alpha+6)} \\
&-\frac{\alpha^2 r q^4\left(g_2+b g_1\right)}{6\kappa^2(2\alpha+1)^2(5\alpha+3)(7\alpha+4)(7\alpha+5)} \\
&-\frac{\alpha^3 q^3 g_1^4\left(\frac{2r+qs}{24(\alpha+1)(4\alpha+3)}+\frac{qs}{3(2\alpha+3)(3\alpha+4)}\right)}{30\kappa^3(\alpha+1)^3(5\alpha+4)(6\alpha+5)} \\
&-\frac{\alpha^2 q^3(2g_1g_2+b g_1^2)\left(\frac{2r+qs}{3(\alpha+1)(4\alpha+3)}+\frac{r}{(2\alpha+1)(5\alpha+3)}\right)}{4\kappa^2(3\alpha+2)(5\alpha+4)(6\alpha+5)} \\
&-\frac{\alpha r m q^3}{12\kappa(2\alpha+1)^2(3\alpha+2)(5\alpha+3)} \\
&-\frac{\alpha^3 s q^3 g_1^5}{120\kappa^3(\alpha+1)^3(2\alpha+3)(3\alpha+4)(4\alpha+5)(5\alpha+6)} \\
&-\frac{\alpha^2 q^2\left(3g_1^2g_2+b g_1^3\right)\left(\frac{2r+qs}{4\alpha+3}+\frac{qs}{2\alpha+3}\right)}{120\kappa^2(\alpha+1)^3(5\alpha+4)}-\frac{\alpha r q^2\left(g_3+b g_2+m g_1\right)}{2\kappa(2\alpha+1)(5\alpha+3)(5\alpha+4)} \\
&-\frac{\alpha^2 s q^2\left(4g_1^3g_2+b g_1^4\right)}{24\kappa^2(\alpha+1)^2(2\alpha+3)(3\alpha+4)(4\alpha+5)} \\
&-\frac{\alpha q(2r+qs)\left(2g_1g_3+2b g_1g_2+m g_1^2+g_2^2\right)}{24\kappa(\alpha+1)^2(4\alpha+3)}-\frac{r A_2 q}{(4\alpha+2)(4\alpha+3)} \\
&-\frac{\alpha s q\left(3g_1^2g_3+3b g_1^2g_2+3g_1g_2^2+m g_1^3\right)}{6\kappa(\alpha+1)(2\alpha+3)(3\alpha+4)}-\frac{r\left(g_4+b g_3+m g_2+A_2g_1\right)}{(3\alpha+3)} \\
&-\frac{s\left(2g_1g_4+2g_2g_3+2b g_1g_3+b g_2^2+2m g_1g_2+A_2g_1^2\right)}{2(2\alpha+3)} \\
&-\frac{\alpha A_4 q^2}{2\kappa(\alpha+1)^2(2\alpha+1)}-\frac{\alpha q\left(g_5+b g_4+m g_3+A_2g_2+A_4g_1\right)}{\kappa(\alpha+1)(\alpha+2)}\,.
\end{aligned}
\tag{A.12}
$$

The coefficient g_6 is given by

$$
\begin{aligned}
g_6 = &-\frac{\alpha^3 r q^8}{120\kappa^3(2\alpha+1)^4(5\alpha+3)(7\alpha+4)(9\alpha+5)(11\alpha+6)} \\
&-\frac{\alpha^3 r q^7 g_1}{48\kappa^3(2\alpha+1)^3(5\alpha+3)^2(7\alpha+4)(9\alpha+5)} \\
&-\frac{\alpha^3 q^6 g_1^2\left(\frac{2r+qs}{(\alpha+1)(4\alpha+3)}+\frac{3r}{(2\alpha+1)(5\alpha+3)}\right)}{36\kappa^3(3\alpha+2)^2(5\alpha+4)(7\alpha+5)(8\alpha+5)} \\
&-\frac{\alpha^3 r q^6 g_1^2}{18\kappa^3(2\alpha+1)^2(3\alpha+2)(5\alpha+3)(7\alpha+4)(7\alpha+5)(8\alpha+5)} \\
&-\frac{\alpha^2 r b q^6}{24\kappa^2(2\alpha+1)^3(5\alpha+3)(7\alpha+4)(9\alpha+5)} \\
&-\frac{\alpha^3 q^5 g_1^3\left(\frac{2r+qs}{2(\alpha+1)^2(3\alpha+2)(4\alpha+3)}+\frac{qs}{2(\alpha+1)^2(2\alpha+3)(5\alpha+4)}+\frac{3r}{(2\alpha+1)(3\alpha+2)(5\alpha+3)(5\alpha+4)}\right)}{24\kappa^3(4\alpha+3)(6\alpha+5)(7\alpha+5)} \\
&-\frac{\alpha^2 r q^5\left(g_2+b g_1\right)}{6\kappa^2(2\alpha+1)^2(5\alpha+3)(7\alpha+4)(8\alpha+5)} \\
&-\frac{\alpha^3 q^4 g_1^4\left(\frac{2r+qs}{24(\alpha+1)(4\alpha+3)}+\frac{qs}{3(2\alpha+3)(3\alpha+4)}\right)}{5\kappa^3(\alpha+1)^2(5\alpha+4)(6\alpha+5)(7\alpha+6)} \\
&+\frac{\alpha^2 q^4(2g_1g_2+b g_1^2)\left(\frac{2r+qs}{3(\alpha+1)(4\alpha+3)}+\frac{r}{(2\alpha+1)(5\alpha+3)}\right)}{4\kappa^2(3\alpha+2)(5\alpha+4)(7\alpha+5)} \\
&-\frac{\alpha r m q^4}{6\kappa(2\alpha+1)^2(5\alpha+3)(7\alpha+4)}-\frac{\alpha^3 s q^4 g_1^5}{720\kappa^3(\alpha+1)^4(2\alpha+3)(3\alpha+4)(4\alpha+5)} \\
&-\frac{\alpha^2 q^3\left(3g_1^2g_2+b g_1^3\right)\left(\frac{2r+qs}{4\alpha+3}+\frac{qs}{2\alpha+3}\right)}{24\kappa^2(\alpha+1)^2(5\alpha+4)(6\alpha+5)} \\
&-\frac{\alpha r q^3\left(g_3+b g_2+m g_1\right)}{4\kappa(2\alpha+1)(3\alpha+2)(5\alpha+3)}-\frac{\alpha^2 s q^3\left(4g_1^3g_2+b g_1^4\right)}{120\kappa^2(\alpha+1)^3(2\alpha+3)(3\alpha+4)} \\
&-\frac{\alpha q^2(2r+qs)\left(2g_1g_3+2b g_1g_2+m g_1^2+g_2^2\right)}{6\kappa(\alpha+1)(4\alpha+3)(5\alpha+4)}-\frac{r A_2 q^2}{(4\alpha+2)(5\alpha+3)} \\
&-\frac{\alpha s q^2\left(3g_1^2g_3+3b g_1^2g_2+3g_1g_2^2+m g_1^3\right)}{24\kappa(\alpha+1)^2(2\alpha+3)}-\frac{r q\left(g_4+b g_3+m g_2+A_2g_1\right)}{(4\alpha+3)} \\
&-\frac{s q\left(2g_1g_4+2g_2g_3+2b g_1g_3+b g_2^2+2m g_1g_2+A_2g_1^2\right)}{(6\alpha+6)} \\
&-\frac{\alpha A_4 q^3}{\kappa(\alpha+1)(2\alpha+1)(3\alpha+2)}-\frac{\alpha q^2\left(g_5+b g_4+m g_3+A_2g_2+A_4g_1\right)}{2\kappa(\alpha+1)^2} \\
&-\frac{A_6 q}{(\alpha+1)}\,.
\end{aligned}
\tag{A.13}
$$

Appendix B

B.1 One-dimensional radial basis function networks

In this appendix, we use

- the notation $\widehat{[\,]}$ for a vector/matrix $[\,]$ that is associated with a grid line,
- the notation $[\,]_{(\eta,\theta)}$ to denote selected rows η and columns θ of the matrix $[\,]$,
- the notation $[\,]_{(\eta)}$ to pick out selected components η of the vector $[\,]$,
- the notation $[\,]_{(:,\theta)}$ to denote all rows and selected columns θ of the matrix $[\,]$, and
- the notation $[\,]_{(\eta,:)}$ to denote all columns and selected rows η of the matrix $[\,]$.

B.1.1 Second-order 1D-IRBFN (1D-IRBFN-2 scheme)

We discuss in detail the formulation on an x-grid line and similar results can be obtained for a y-grid line.

Application of (3.7) at boundary and interior points on the grid line $[j]$ results in

$$\hat{u} = \hat{\mathbf{H}} \begin{pmatrix} \hat{w} \\ \hat{p} \end{pmatrix}, \tag{B.1}$$

where $\hat{\mathbf{H}}$ is an $N_x^{[j]} \times (N_x^{[j]} + 2)$ matrix whose entries are $\hat{H}_{ij} = H_{[0]}^{[j]}(x^{(i)})$, $\hat{u} = (u^{(1)}, u^{(2)}, ..., u^{(N_x^{[j]})})^T$, $\hat{w} = (w^{(1)}, w^{(2)}, ..., w^{(N_x^{[j]})})^T$ and $\hat{p} = (p_1, p_2)^T$. Due to the

presence of p_1 and p_2, one can add two additional equations of the form

$$\hat{f} = \hat{\mathbf{K}} \begin{pmatrix} \hat{w} \\ \hat{p} \end{pmatrix} \tag{B.2}$$

to equation system (B.1). For example, in the case of Neumann boundary conditions, this subsystem can be used to impose derivative boundary values

$$\hat{f} = \begin{pmatrix} \frac{\partial u}{\partial x}(x^{(1)}) \\ \frac{\partial u}{\partial x}(x^{(N_x^{[j]})}) \end{pmatrix}, \tag{B.3}$$

$$\hat{\mathbf{K}} = \begin{bmatrix} H_{[1]}^{(1)}(x^{(1)}) & H_{[1]}^{(2)}(x^{(1)}) & ... & H_{[1]}^{(N_x^{[j]})}(x^{(1)}) & 1 & 0 \\ H_{[1]}^{(1)}(x^{(N_x^{[j]})}) & H_{[1]}^{(2)}(x^{(N_x^{[j]})}) & ... & H_{[1]}^{(N_x^{[j]})}(x^{(N_x^{[j]})}) & 1 & 0 \end{bmatrix}. \tag{B.4}$$

The RBF coefficients including two integration constants can be transformed into the meaningful nodal variable values through the following relation

$$\begin{pmatrix} \hat{u} \\ \hat{f} \end{pmatrix} = \begin{bmatrix} \hat{\mathbf{H}} \\ \hat{\mathbf{K}} \end{bmatrix} \begin{pmatrix} \hat{w} \\ \hat{p} \end{pmatrix} = \hat{\mathbf{C}} \begin{pmatrix} \hat{w} \\ \hat{p} \end{pmatrix}, \tag{B.5}$$

or

$$\begin{pmatrix} \hat{w} \\ \hat{p} \end{pmatrix} = \hat{\mathbf{C}}^{-1} \begin{pmatrix} \hat{u} \\ \hat{f} \end{pmatrix}, \tag{B.6}$$

where $\hat{\mathbf{C}}$ is a square conversion matrix of dimension $(N_x^{[j]} + 2) \times (N_x^{[j]} + 2)$.

By substituting Eq. (B.6) into Eqs. (3.5) and (3.6), the second- and first-order derivatives of the variable u are expressed in terms of nodal variable values

$$\frac{\partial^2 u(x)}{\partial x^2} = \left(H_{[2]}^{(1)}(x), H_{[2]}^{(2)}(x), ..., H_{[2]}^{(N_x^{[j]})}(x), 0, 0 \right) \hat{\mathbf{C}}^{-1} \begin{pmatrix} \hat{u} \\ \hat{f} \end{pmatrix}, \tag{B.7}$$

$$\frac{\partial u(x)}{\partial x} = \left(H_{[1]}^{(1)}(x), H_{[1]}^{(2)}(x), ..., H_{[1]}^{(N_x^{[j]})}(x), 1, 0 \right) \hat{\mathbf{C}}^{-1} \begin{pmatrix} \hat{u} \\ \hat{f} \end{pmatrix}, \tag{B.8}$$

or

$$\frac{\partial^2 u(x)}{\partial x^2} = \bar{D}_{2x} \hat{u} + k_{2x}(x), \tag{B.9}$$

$$\frac{\partial u(x)}{\partial x} = \bar{D}_{1x} \hat{u} + k_{1x}(x), \tag{B.10}$$

where k_{1x} and k_{2x} are scalars whose values depend on x, f_1 and f_2; and $\bar{D}_{1x}$ and $\bar{D}_{2x}$ are known vectors of length $N_x^{[j]}$. Application of equation (B.9) and (B.10) to boundary and interior points on the grid line $[j]$ yields

$$\widehat{\frac{\partial^2 u^{[j]}}{\partial x^2}} = \hat{\mathbf{D}}_{2x}^{[j]} \hat{u} + \hat{k}_{2x}^{[j]}, \tag{B.11}$$

$$\widehat{\frac{\partial u^{[j]}}{\partial x}} = \hat{\mathbf{D}}_{1x}^{[j]} \hat{u} + \hat{k}_{1x}^{[j]}, \tag{B.12}$$

where $\hat{\mathbf{D}}_{1x}^{[j]}$ and $\hat{\mathbf{D}}_{2x}^{[j]}$ are known matrices of dimension $N_x^{[j]} \times N_x^{[j]}$ and $\hat{k}_{1x}^{[j]}$ and $\hat{k}_{2x}^{[j]}$ are known vectors of length $N_x^{[j]}$. Similarly, along a vertical line $[j]$ parallel to the $y-$ axis, the values of the second- and first-order derivatives of u with respect to y at the nodal points can be given by

$$\widehat{\frac{\partial^2 u^{[j]}}{\partial y^2}} = \hat{\mathbf{D}}_{2y}^{[j]} \hat{u} + \hat{k}_{2y}^{[j]}, \tag{B.13}$$

$$\widehat{\frac{\partial u^{[j]}}{\partial y}} = \hat{\mathbf{D}}_{1y}^{[j]} \hat{u} + \hat{k}_{1y}^{[j]}. \tag{B.14}$$

B.1.2 Fourth-order 1D-IRBFN (1D-IRBFN-4 scheme)

Eq. (3.14) can be written as

$$\hat{u} = \hat{\mathbf{H}} \begin{pmatrix} \hat{w} \\ \hat{p} \end{pmatrix}, \tag{B.15}$$

where $\hat{\mathbf{H}}$ is an $N_x \times (N_x + 4)$ matrix whose entries are $\hat{H}_{ij} = H_{[0]}(x^{(i)})$, $\hat{u} = (u^{(1)}, u^{(2)}, ..., u^{(N_x)})^T$, $\hat{w} = (w^{(1)}, w^{(2)}, ..., w^{(N_x)})^T$ and $\hat{p} = (p_1, p_2, p_3, p_4)^T$. In order to impose Neumann boundary conditions at both ends of the 1-D computational domain ($x = \{x^{(1)},\ x^{(N_x)}, \}$), we add two additional equations of the same form as in (B.2) to equation system (B.15). The RBF coefficients including four integration constants can be transformed into the meaningful nodal variable values through the following relation

$$\begin{pmatrix} \hat{w} \\ \hat{p} \end{pmatrix} = \hat{\mathbf{C}}^{-1} \begin{pmatrix} \hat{u} \\ \hat{f} \end{pmatrix}, \tag{B.16}$$

where $\hat{\mathbf{C}}$ is a non-square conversion matrix of dimension $(N_x+2)\times(N_x+4)$ whose inverse can be found using the singular value decomposition (SVD) technique. By substituting Eq. (B.16) into Eqs. (3.10)–(3.13), the values of derivatives of u with respect to x at the boundary and interior points on the grid line are obtained as

$$\widehat{\frac{\partial^4 u}{\partial x^2}} = \hat{\mathbf{D}}_{4x} \hat{u} + \hat{k}_{4x}, \tag{B.17}$$

$$\widehat{\frac{\partial^3 u}{\partial x^2}} = \hat{\mathbf{D}}_{3x} \hat{u} + \hat{k}_{3x}, \tag{B.18}$$

$$\widehat{\frac{\partial^2 u}{\partial x^2}} = \hat{\mathbf{D}}_{2x} \hat{u} + \hat{k}_{2x}, \tag{B.19}$$

$$\widehat{\frac{\partial u}{\partial x}} = \hat{\mathbf{D}}_{1x} \hat{u} + \hat{k}_{1x}, \tag{B.20}$$

where $\hat{\mathbf{D}}_{1x}$, $\hat{\mathbf{D}}_{2x}$, $\hat{\mathbf{D}}_{3x}$ and $\hat{\mathbf{D}}_{4x}$ are known matrices of dimension $N_x \times N_x$; and $\hat{k}_{1x}$, $\hat{k}_{2x}$, $\hat{k}_{3x}$ and $\hat{k}_{4x}$ are known vectors of length N_x.

References

Aris, R. (1956). On the Dispersion of a Solute in a Fluid Flowing Through a Tube, *Proceedings of the Royal Society of London Series A* **235**: 67–77.

Arya, S. P. (1999). *Air Pollution Meteorology and Dispersion*, Oxford University Press, New York, US.

Balakotaiah, V. and Chang, H. C. (1995). Dispersion of Chemical Solutes in Chromatographs and Reactors, *Philosophical Transactions of the Royal Society Series A* **351**: 39–75.

Barenblatt, G. I. (1993). Scalling Laws for Fully Developed Turbulent Shear Flows, *Journal of Fluid Mechanics* **248**: 513–520.

Barenblatt, G. I. (2000). Self-similar Intermediate Structure in Turbulent Boundary Layers at Large Reynolds Numbers, *Journal of Fluid Mechanics* **410**: 263–283.

Barenblatt, G. I. (2003). Transfer of A Passive Additive in A Turbulent Boundary Layer at Very Large Reynolds Numbers, *Proceedings of the National Academy of Sciences of the United State of America* **100**: 1481–1483.

Bentham, T. and Britter, R. (2003). Spatially Averaged Flow within Obstacle Arrays, *Atmospheric Environment* **37**: 2037–2043.

Bottema, M. (1996). Roughness Parameters Over Regular Rough Surfaces: Experimental Requirements and Model Validation, *Journal of Wind Engineering and Industrial Aerodynamics* **64**: 249–265.

Bottema, M. (1997). Urban Roughness Modelling in Relation to Pollutant Dispersion, *Atmospheric Environment* **31**: 3059–3075.

Bryden, M. D. and Brenner, H. (1996). Multiple-Timescale Analysis of Taylor Dispersion in Converging and Diverging Flows, *Journal of Fluid Mechanics* **311**: 343–359.

Carr, J. (1981). *Applied Mathematical Sciences, Volume 35: Applications of Centre Manifold Theory*, Springer-Verlag, New York, US.

Chatwin, P. C. (1970). The Approach to Normality of the Concentration Dispersion of a Solute Flowing Along a Straight Pipe, *Journal of Fluid Mechanics* **43**: 321–352.

Chatwin, P. C. (1971). On the Interpretation of Some Longitudinal Dispersion Experiment, *Journal of Fluid Mechanics* **48**: 689–702.

Chatwin, P. C. (1973). A Calculation Illustrating the Effects of the Viscous Sub-Layer on Longitudinal Dispersion, *Quarterly Journal of Mechanics and Applied Mathematics* **26**: 427–439.

Chen, X. L. and Morrison, P. J. (1992). Nonlinear Interactions of Tearing Modes in the Presence of Shear Flow, *AIP: Physics of Fluids Series B* **4**: 845–854.

Chikwendu, S. C. and Ojiakor, G. U. (1985). Slow-Zone Model for Longitudinal Dispersion in Two-dimensional Shear Flows, *Journal of Fluid Mechanics* **152**: 15–38.

Cionco, R. M. (1965). Mathematical Model for Air Flow in a Vegetative Canopy, *Journal of Applied Meteorology* **4**: 517–522.

Cionco, R. M. (1972). A Wind-Profile Index for Canopy Flow, *Journal of Boundary-layer Meteorol* **3**: 255–263.

Coceal, O. and Belcher, S. (2004). A Canopy Model for Mean Winds Through Urban Areas, *Quarterly Journal of the Royal Meteorological Society* **130**: 1349–1372.

Coles, D. (1956). The Law of the Wake in the Turbulent Boundary Layer, *Journal of Fluid Mechanics* **1**: 191–226.

Coullet, P. H. and Spiegel, E. A. (1983). Amplitude Equations for Systems with Competing Instabilities, *SIAM Journal on Applied Mathematics* **43**: 776–821.

Counihan, J. (1971). Wind Tunnel Determination of the Roughness Length as a Function of the Fetch and the Roughness Density of Three-Dimensional Roughness Elements, *Atmospheric Environment* **5**: 637–642.

Elder, J. W. (1959). The Dispersion of Marked Fluid in Turbulent Shear Flow, *Journal of Fluid Mechanics* **5**: 544–560.

Fischer, H. B. (1973). Longitudinal Dispersion and Turbulent Mixing in Open Channel Flow, *Annual Review of Fluid Mechanics* **5**: 59–78.

Fischer, H. B., List, E. J., Koh, R. C. Y., Imberger, J. and Brooks, N. H. (1979). *Mixing in Inland and Coastal Waters*, Academic press Inc., London.

Flesh, T. K., Wilson, J. D. and Yee, E. (1995). Backward-Time Lagrangian Stochastic Dispersion Models and Their Application to Estimate Gaseous Emissions, *Jounal of Appied Meteorology* **34**: 1320–1332.

Frankel, I. and Brenner, H. (1989). On the Foundations of Generalized Taylor Dispersion Theory, *Journal of Fluid Mechanics* **204**: 97–119.

Georgiev, D. J., Roberts, A. J. and Strunin, D. V. (2007). Nonlinear Dynamics on Centre Manifolds Describing Turbulent Floods: k-w Model, *Journal of Australian and New Zealand Industrial and Applied Mathematics,* **Supplement**: 419–428.

Gill, W. N. and Sankarasubramanian, R. (1970). Exact Analysis of Unsteady Convective Diffusion, *Proceeding of the Royal Society of London Series A* **316**: 341–350.

Gupta, V. K. and Bhattacharya, R. N. (1983). A New Derivation of the Taylor-Aris Theory of Solute Dispersion in a Capillary, *Water Resources Research* **19**: 945–951.

Hall, D. J., Macdonald, R., Walker, S. and Spanton, A. M. (1996). *Measurements of Dispersion within Simulated Urban Arrays a Small Scale Wind Tunnel Study*, Building Research Establishment, Garston Watford.

Harman, I. N. and Finnigan, J. J. (2007). A Simple Unified Theory for Flow in the Canopy and Roughness Sublayer , *Journal of Boundary-layer Meteorology* **123**: 339–363.

Ho-Minh, D., Mai-Duy, N. and Tran-Cong, T. (2012). Simulation of Viscous and Viscoelastic Flows Using a RBF-Galerkin Approach, *Australian Journal of Mechanical Engineering* **9**: 101–112.

Huffman, G. D. and Bradshaw, P. (1972). A Note on von Kármán's Constant in Low Reynolds Number Turbulent Flows, *Journal of Fluid Mechanics* **53**: 45–60.

Jackson, P. S. (1981). On the Displacement Height in the Logarithmic Velocity Profile, *Journal of Fluid Mechanics* **111**: 15–25.

Kansa, E. J. (1990a). Multiquadrics- A Scattered Data Approximation Scheme with Applications to Computational Fulid-Dynamics-I: Surface Approximations and Partial Derivative Estimates, *Computers and Mathematics with Applications* **19**: 127–145.

Kansa, E. J. (1990b). Multiquadrics - A Scattered Data Approximation Scheme with Applications to Computational Fulid-Dynamics-II: Solutions to Parabolic, Hyperbolic and Elliptic Partial Differential Equations, *Computers and Mathematics with Applications* **19**: 147–161.

Keulegan, G. H. (1938). Laws of Turbulent Flows in Open Channels, *Journal of Research of the National Bureau of Standards* **21 (6)**: 707–741.

Kutzbach, J. E. (1961). Investigations of the modification of wind profiles by artificially controlled surface roughness, *Studies of the Three Dimensional Structure of the Planetary Boundary Layer, Department of Meteorology, University of Wisconsin, Madison*, University of Wisconsin–Madison, pp. 37–96.

Landau, L. D. and Lifshitz, E. M. (1981). *Fluid Mechanics, Volume VI: Course of Theoretical Physics*, Reed Educational and Professional Publishing Ltd, UK.

Laure, P. and Demay, Y. (1988). Symbolic Computation and Equation on the Centre manifold: Application to the Couette-Taylor Problem , *Journal of Computers and Fluids* **16**: 229–238.

Le, P. B. H., Rabczuk, T., Mai-Duy, N. and Tran-Cong, T. (2010). A Moving IRBFN-Based Integration-Free Meshless Method, *CMES: Computer Modeling in Engineering and Sciences* **61**: 93–109.

Legg, B. J. (1983). Turbulent Dispersion from an Elevated Line Source: Markov Chain Simulations of Concentration and Flux Profiles, *Quarterly Journal of the Royal Meteorological Society* **109**: 645–660.

Lettau, H. (1969). Note on Aerodynamic Roughness-Parameter Estimation on the Basis of Roughness-Element Description, *Jounal of Appied Meteorology* **8**: 828–832.

Liedtke, J. (1992). *An Experimental Investigation into the Dispersion Behaviour in Neutral and Unstable Zero Pressure Gradient Boundary Layers with Different Roughness*, University of Bundeswehr, German.

Logan, J. D. (1994). *An Introduction to Nonlinear Partial Differential Equations*, John Wiley and Sons, Inc., New Yourk, US.

Lorenz, E. D. (1986). On the Existence of a Slow Manifold, *Atmospheric Sciences* **43**: 1547–1557.

Macdonald, R. W. (2000). Modeling the Mean Velocity Profile in the Urban Canopy Layer, *Journal of Boundary-layer Meteorology* **97**: 25–45.

Macdonald, R. W., Griffiths, R. F. and Hall, D. J. (1998). An Improved Method for Estimation of Surface Roughness of Obstacle Arrays, *Atmospheric Environment* **32**: 1857–1864.

Macdonald, R. W., Schofield, S. C. and Slawson, P. R. (2002). Physical Modeling of Urban Roughness Using Arrays of Regular Roughness Elements, *Water, Air, and Soil Pollution* **2**: 541–554.

Mai-Duy, N. and Tanner, R. I. (2007). A Collocation Method Based on One-Dimensional RBF Interpolation Scheme for Solving PDEs, *International Journal of Numerical Methods for Heat and Fluid Flow* **17**: 165–186.

Mai-Duy, N. and Tran-Cong, T. (2001a). Numerical Solution of Differential Equations Using Multiquadric Radial Basis Function Networks, *Neural Networks* **14**: 185–199.

Mai-Duy, N. and Tran-Cong, T. (2001b). Numerical Solution of Navier-Stokes Equations Using Multiquadric Radial Basis Function Networks, *International Journal for Numerical Methods in Fluids* **37**: 65–86.

Mai-Duy, N. and Tran-Cong, T. (2003). Approximation of Function and Its Derivatives Using Radial Basis Function Networks, *Applied Mathematical Modelling* **27**: 197–220.

Mei, Z., Roberts, A. J. and Li, Z. (2003). Modeling the Dynamics of Turbulent Floods, *SIAM Journal on Applied Mathematics* **63**: 423–458.

Mercer, G. N. and Roberts, A. J. (1990). A Centre Manifold Description of Contaminant Dispersion in Channels with Varying Flow Properties, *SIAM Journal on Applied Mathematics* **50**: 1547–1565.

Mohammed, F. J., Ngo-Cong, D., Strunin, D. V., Mai-Duy, N. and Tran-Cong, T. (2014). Modelling Dispersion in Laminar and Turbulent Flows in an Open Channel Based on Centre Manifolds Using 1D-IRBFN Method, *Journal of Applied Mathematical Modelling* **38**: 3672–3691.

Mohammed, F. J., Strunin, D. V., Ngo-Cong, D. and Tran-Cong, T. (2014). Asymptotics of Averaged Turbulent Transfer in Canopy Flows, *Journal of Engineering Mathematics, accepted* .

Monin, A. S. and Yaglom, A. M. (1975). *Statistical Fluid Mechanics, Volume II: Mechanics of Turbulence*, The MIT Press, Cambridge, US.

Ngo-Cong, D., Mai-Duy, N., Karunasena, W. and Tran-Cong, T. (2011). Free Vibration Analysis of Laminated Composite Plates Based on FSDT Using One-Dimensional IRBFN Method, *Computers and Structures* **89**: 1–13.

Ngo-Cong, D., Mai-Duy, N., Karunasena, W. and Tran-Cong, T. (2012a). A Numerical Procedure Based on 1D-IRBFN and Local MLS-1D-IRBFN Methods for Fluid-Structure Interaction Analysis, *CMES: Computer Modeling in Engineering and Sciences* **83**: 459–498.

Ngo-Cong, D., Mai-Duy, N., Karunasena, W. and Tran-Cong, T. (2012b). Local Moving Least Square-One-Dimensional Integrated Radial Basis Function Networks Technique for Incompressible Viscous Flows, *International Journal for Numerical Methods in Fluids* **70**: 1443–1474.

Ngo-Cong, D., Mohammed, F. J., Strunin, D. V., Tran-Cong, T. and Mai-Duy, N. (2013). Higher-Order Transport Equations for Turbulent Channel Flows, *Journal of Australian and New Zealand Industrial and Applied Mathematics, to appear* .

Nikuradse, J. (1932). Gesetzmassigkeiten Der Turbulenten Stromung in Glatten Rohren, *Forschung auf d. Gebiete d. Ingenieurwesens* **356**: 36 pages.

O'Loughlin, E. M. and Macdonald, E. G. (1964). Some Roughness-Concentration Effects on Boundary Resistance, *Journal of La Houille Blanche* **7**: 773–782.

Pagitsas, M., Nadim, A. and Brenner, H. (1986). Multiple Time Scale Analysis of Macrotransport Processes, *Physica Series A: Statistical Mechanics and its Applications* **135**: 533–550.

Park, J. and Sandberg, I. W. (1991). Universal Approximation Using Radial Basis-Function Networks, *Neural Computation* **3**: 246–257.

Perry, A. E. and Joubert, P. N. (1963). Rough Wall Boundary Layers in Adverse Pressure Gradients, *Journal of Fluig Mechanics* **17**: 193–211.

Petersen, L. R. (1997). A Wind Tunnel Evalution of Methods for Estimating Surface Roughness Length at Industrial Facilities, *Atmospheric Environment* **31**: 45–57.

Plate, J. E. (1995). *Urban Climates and Urban Climate Modelling: an Intoduction*, Kluwer Academic Publishers, Amsterdam.

Raupach, M. R. and Thom, A. S. (1981). Turbulence in and Above Plant Canopies, *Annual Review of Fluid Mechanics* **13**: 97–129.

Raupach, M. R., Thom, A. S. and Edwards, I. (1980). A Wind-Tunnel Study of Turbulent Flow Close to Regularly Arrayed Rough Surfaces, *Journal of Boundary-layer Meteorology* **18**: 373–397.

Renardy, Y. (1988). *A Couette-Poiseuille Flow in Two Fluids in a Channel*, Research Report, Australia National University, Canberra, Australia.

Roberts, A. J. (1985). Simple Examples of the Derivation of Amplitude Equations for Systems of Equations Possessing Bifurcations, *The Journal of the Australian Mathematical Society series B* **27**: 48–65.

Roberts, A. J. (1988). The Application of Centre-Manifold Theory to the Evolution of Systems which Vary Slowly in Space, *The Journal of the Australian Mathematical Society* **29**: 480–500.

Roberts, A. J. (1989). Appropriate Initial Conditions for Asymptotic Descriptions of the Long Term Evolution of Dynamical systems, *The Journal of the Australian Mathematical Society* **31**: 48–75.

Roberts, A. J. and Strunin, D. V. (2004). Two-zone Model of Shear Dispersion in a Channel Using Centre Manifolds , *Quarterly Journal of Mechanics and applied Mathematics* **57**: 363–378.

Sabatino, S. D., Solazzo, E., Paradisi, P. and Britter, R. (2008). A Simple Model for Satially-Averaged Wind Profiles within and Above an Uban Canopy, *Journal of Boundary-Layer Meteorology* **127**: 131–151.

Shao, Y. and Yang, Y. (2005). A Scheme for Drag Partition Over Rough Surfaces, *Atmospheric Environment* **39**: 7351–7361.

Smith, R. (1981). A Delay-Diffusion Description for Contaminant Dispersion, *Journal of Fluid Mechanics* **105**: 469–486.

Smith, R. (1982). Non-Uniform Discharges of Contaminants in Shear Flows, *Journal of Fluid mechanics* **120**: 71–89.

Smith, R. (1987). Diffusion in Shear Flows Made Easy: the Taylor Limit, *Journal of Fluid Mechanics* **175**: 201–214.

Steffler, P. M., Rajaratnam, N. and Peterson, A. W. (1985). LDA measurements in open channel, *Journal of Hydraulic Engineering* **111 (1)**: 119–130.

Stokes, A. N. and Bartonz, N. G. (1990). The Concentration Distribution Produced by Shear Dispersion of Solute in Poiseuille Flow, *Journal of Fluid Mechanics* **210**: 201–221.

Strunin, D. V. (2011). Universality of Turbulent Dispersion in a Steady Flow in an Open Channel, *Quarterly Journal of Mechanics and applied Mathematics* **64**: 197–214.

Strunin, D. V. and Mohammed, F. J. (2012). Numerical analysis of an averaged model of turbulent transport near a roughness layer, *Journal of Australian and New Zealand Industrial and Applied Mathematics* **53**: C142–C154.

Strunin, D. V. and Roberts, A. J. (2009). Low-Dimensional Boundary-Layer Model of Turbulent Dispersion in a Channel, *Proceeding of the World Congress on Engineering Vol. II, Imperial College, London, UK*, Newswood Ltd, International Association of Engineers, pp. 1230–1234.

Syare, W. W. and Chang, F. M. (1968). *A Laboratory Investigation of the Open Channel Dispersion Process for Dissolved, Suspended, and Floating Dispersants*, U. S. Geological Survey Professional Paper 433-E.

Taylor, G. (1953). Dispersion of Soluble Matter in Solvent Flowing Slowly Through A Tube, *Proceedings of the Royal Society of London Series A* **219**: 186–203.

Taylor, G. (1954). The Dispersion of Matter in Turbulent Flow Through a Pipe, *Proceedings of the Royal Society of London Series A* **223**: 446–468.

Tennekes, H. and Lumley, J. L. (1972). *A First Course in Turbulence*, Massachusetts Institute of Technology, United State of America.

Thacker, W. C. (1976). A Solvable Model of "Shear Dispersion", *Journal of Physics Oceanography* **6**: 66–75.

Theurer, W. (1973). *Dispersion of Ground-Level Emissions in Complex Built-up Areas*, University of Karlsruhe, German.

Thom, A. S. (1971). Momentum Absorption by Vegetation, *Quarterly Journal of the Royal Meteorological Society* **97**: 414–428.

Tran, C.-D., Mai-Duy, N., Le-Cao, K. and Tran-Cong, T. (2012). A Continuum-Microscopic Method Based on IRBFs and Control Volume Scheme for Viscoelastic Fluid Flows, *CMES: Computer Modeling in Engineering and Sciences* **85**: 499–519.

Watt, S. D. and Roberts, A. J. (1995). The Accurate Dynamic Modelling of Contaminant Dispersion in Channels, *SIAM Journal on Applied Mathematics* **55**: 1016–1038.

Watt, S. D. and Roberts, A. J. (1996). The Concentration of the Zonal Models of Dispersion in Channels via Matching Centre Manifolds, *Journal of Australian Mathematical Society* **38**: 101–125.

Wieringa, J. (1993). Representative Roughness Parameters for Homogeneous Terrain, *Journal of Boundary-Layer Meteorology* **63**: 323–363.

Wooding, R. A., Bradley, E. F. and Marshall, J. K. (1973). Drag Due to Regular Arrays of Roughness Elements of Varying Geometry, *Journal of Boundary-Layer Meteorology* **5**: 285–308.

Yi, C. (2008). Momentum Transfer within Canopies, *Jounal of Applied Meteorology and Climatology* **47**: 262–275.

Yi, C., Monson, R. K., Zhai, Z., Anderson, D. E., Lamb, B., Allwine, G., Turnipseed, A. A. and Burns, S. P. (2005). Modeling and Measuring the Nocturnal Drainage Flow in a High-Elevation, Subalpine Forest with Complex Terrain, *Journal of Geographical Research* **110**: D22303, doi:10.1029/2005JD006282.